234

Advances in Polymer Science

Advances in Polymer Science

Recently Published and Forthcoming Volumes

Chemical Design of Responsive Microgels
Volume Editors: Pich, A., Richtering, W.
Vol. 234, 2010

Hybrid Latex Particles
Volume Editors: van Herk, A.M., Landfester, K.
Vol. 233, 2010

Biopolymers
Volume Editors: Abe, A., Dušek, K., Kobayashi, S.
Vol. 232, 2010

Polymer Materials
Volume Editors: Lee, K.-S., Kobayashi, S.
Vol. 231, 2010

Polymer Characterization
Volume Editors: Dušek, K., Joanny, J.-F.
Vol. 230, 2010

Modern Techniques for Nano- and Microreactors/-reactions
Volume Editor: Caruso, F.
Vol. 229, 2010

Complex Macromolecular Systems II
Volume Editors: Müller, A.H.E., Schmidt, H.-W.
Vol. 228, 2010

Complex Macromolecular Systems I
Volume Editors: Müller, A.H.E., Schmidt, H.-W.
Vol. 227, 2010

Shape-Memory Polymers
Volume Editor: Lendlein, A.
Vol. 226, 2010

Polymer Libraries
Volume Editors: Meier, M.A.R., Webster, D.C.
Vol. 225, 2010

Polymer Membranes/Biomembranes
Volume Editors: Meier, W.P., Knoll, W.
Vol. 224, 2010

Organic Electronics
Volume Editors: Meller, G., Grasser, T.
Vol. 223, 2010

Inclusion Polymers
Volume Editor: Wenz, G.
Vol. 222, 2009

Advanced Computer Simulation Approaches for Soft Matter Sciences III
Volume Editors: Holm, C., Kremer, K.
Vol. 221, 2009

Self-Assembled Nanomaterials II
Nanotubes
Volume Editor: Shimizu, T.
Vol. 220, 2008

Self-Assembled Nanomaterials I
Nanofibers
Volume Editor: Shimizu, T.
Vol. 219, 2008

Interfacial Processes and Molecular Aggregation of Surfactants
Volume Editor: Narayanan, R.
Vol. 218, 2008

New Frontiers in Polymer Synthesis
Volume Editor: Kobayashi, S.
Vol. 217, 2008

Polymers for Fuel Cells II
Volume Editor: Scherer, G.G.
Vol. 216, 2008

Polymers for Fuel Cells I
Volume Editor: Scherer, G.G.
Vol. 215, 2008

Photoresponsive Polymers II
Volume Editors: Marder, S.R., Lee, K.-S.
Vol. 214, 2008

Photoresponsive Polymers I
Volume Editors: Marder, S.R., Lee, K.-S.
Vol. 213, 2008

Chemical Design of Responsive Microgels

Volume Editors: Andrij Pich
Walter Richtering

With contributions by

K. Albrecht · K.-F. Arndt · M. Ballauff · J. Groll · F. Krahl
K. Landfester · Y. Lu · M. Moeller · A. Musyanovych
A. Pich · W. Richtering · N. Welsch

Springer

Editors
Prof. Andrij Pich
DWI an der RWTH Aachen e.V.
Pauwelsstraße 8
52056 Aachen
Germany
pich@dwi.rwth-aachen.de

Prof. Walter Richtering
RWTH Aachen
Inst. Physikalische Chemie
Landoltweg 2
52056 Aachen
Germany
richtering@rwth-aachen.de

ISSN 0065-3195 e-ISSN 1436-5030
ISBN 978-3-642-16378-4 e-ISBN 978-3-642-16379-1
DOI 10.1007/978-3-642-16379-1
Springer Heidelberg Dordrecht London New York

Library of Congress Control Number: 2010936633

Cover design: WMXDesign GmbH, Heidelberg

Printed on acid-free paper

Springer is part of Springer Science+Business Media (www.springer.com)

Volume Editors

Prof. Andrij Pich
DWI an der RWTH Aachen e.V.
Pauwelsstraße 8
52056 Aachen
Germany
pich@dwi.rwth-aachen.de

Prof. Walter Richtering
RWTH Aachen
Inst. Physikalische Chemie
Landoltweg 2
52056 Aachen
Germany
richtering@rwth-aachen.de

Editorial Board

Advances in Polymer Sciences
Also Available Electronically

Advances in Polymer Sciences is included in Springer's eBook package *Chemistry and Materials Science*. If a library does not opt for the whole package, the book series may be bought on a subscription basis. Also, all back volumes are available electronically.

For all customers who have a standing order to the print version of *Advances in Polymer Sciences*, we offer free access to the electronic volumes of the Series published in the current year via SpringerLink.

If you do not have access, you can still view the table of contents of each volume and the abstract of each article by going to the SpringerLink homepage, clicking on "Browse by Online Libraries", then "Chemical Sciences", and finally choose *Advances in Polymer Science*.

You will find information about the

- Editorial Board
- Aims and Scope
- Instructions for Authors
- Sample Contribution

at springer.com using the search function by typing in *Advances in Polymer Sciences*.

Color figures are published in full color in the electronic version on SpringerLink.

Aims and Scope

The series *Advances in Polymer Science* presents critical reviews of the present and future trends in polymer and biopolymer science including chemistry, physical chemistry, physics and material science. It is addressed to all scientists at universities and in industry who wish to keep abreast of advances in the topics covered.

Review articles for the topical volumes are invited by the volume editors. As a rule, single contributions are also specially commissioned. The editors and publishers will, however, always be pleased to receive suggestions and supplementary information. Papers are accepted for *Advances in Polymer Science* in English.

In references *Advances in Polymer Sciences* is abbreviated as *Adv Polym Sci* and is cited as a journal.

Special volumes are edited by well known guest editors who invite reputed authors for the review articles in their volumes.

Impact Factor in 2009: 4.600; Section “Polymer Science”: Rank 4 of 73

Preface

Modern concepts in polymer chemistry are based on complex molecular architectures. In this way, some new functions such as self-organisation, adaptability and self-healing can be realised in synthetic materials of different dimensions and complexity. Colloidal polymer networks (nano- or microgels) are unique 3-D polymer structures with tuneable properties and enormous application potential.

The term microgels has been mentioned in the literature already in the 1930 by Hermann Staudinger and mainly discussed for rubber gel particles. The recent developments indicate that the majority of the currently investigated microgel systems are operating in aqueous phase. The progress in chemical design and understanding of physico-chemical properties of microgels resulted in numerous chemical, medical and technical applications such as catalyst supports, delivery vehicles, adhesives, flocculants, sequestrants and sensors.

The major purpose of this book is to give a description of the advances made during the past two decades in the synthesis of aqueous microgels. The chemical design of microgel particles from molecular building blocks is the key for their functionalization and finally for successful application in different systems.

This volume is primarily concerned with the synthetic techniques for the preparation of aqueous polymer microgels having different architecture, chemical composition, size, surface charge and swelling but also demonstrates how sophisticated techniques enable the analysis of the complex structure of functional microgels.

Summer 2010

Andrij Pich
Walter Richtering

Contents

Adv Polym Sci (2010) 234: 1–37
DOI:10.1007/12_2010_70

Published online: 28 May 2010

Microgels by Precipitation Polymerization: Synthesis, Characterization, and Functionalization

Andrij Pich and Walter Richtering

Abstract This chapter reviews recent work on the synthesis of aqueous microgel particles by precipitation polymerization. Precipitation polymerization allows flexible control over important physicochemical properties of aqueous microgels, such as size distribution, surface charge, chemical composition, and microstructure. The microgel systems discussed in this review are mainly based on poly(*N*-isopropyl acrylamide) and poly(*N*-vinylcaprolactam) due to their ability to react to external stimuli such as the pH or temperature of the surrounding medium. We discuss synthetic routes to obtain microgels based on homo- or copolymers as well as colloids with complex core–shell morphology. The functionalization of microgels is of crucial importance from the application point of view. Different routes for incorporation of functional groups, synthetic polymers, proteins, or nanoparticles in microgel structures are discussed.

Keywords Microgels · Precipitation polymerization · Sensitivity · Swelling

Contents

A. Pich (✉)
Functional and Interactive Polymers, DWI RWTH Aachen University, 52056 Aachen, Germany
e-mail: pich@dwi.rwth-aachen.de

W. Richtering (✉)
Institute of Physical Chemistry, RWTH Aachen University, 52074 Aachen, Germany
e-mail: richtering@rwth-aachen.de

Abbreviations

AAc	Acrylic acid
AAEM	Acetoacetoxyethyl methacrylate
AEP	Aminoethyl phosphate
AMPA	2,2′-Azobis(2-methylpropyonamidine) dihydrochloride
BIS	*N*,*N*-methylene bisacrylamide
DEAEMA	2-(Diethylamino)ethyl methacrylate
DLS	Dynamic light scattering
EDOT	Ethylenedioxythiophene
EDX	Energy dispersive X-ray
EGMAP	Ethyleneglycol methacrylate phosphate
GMA	Glycidyl methacrylate
HAp	Hydroxyapatite
IR	Infrared
LCST	Lower critical solution temperature
MAAc	Methacrylic acid
MMA	Methyl methacrylate
NIPAAm	*N*-Isopropylacrylamide
NPs	Nanoparticles
PCS	Photon correlation spectroscopy
PEGMA	Poly(ethylene glycol) methacrylate
PEGMEMA	Poly(ethylene glycol) methacrylester
PSD	Particle size distribution
PVA	Polyvinyl alcohol
R_g	Radius of gyration
R_h	Hydrodynamic radius
SEM	Scanning electron microscopy
SLS	Static light scattering
STEM	Scanning transmission electron microscopy
TEM	Transmission electron microscopy
UV	Ultraviolet
VCL	*N*-Vinylcaprolactam
VIm	Vinylimidazole
VPTT	Volume phase transition temperature

1 Introduction

Aqueous colloidal microgels are an important subdivision of polymer colloids. Microgels find useful applications in different areas such as coatings, agriculture, and medicine. In the last decade, numerous microgel systems have been developed. The preparation and characterization of microgel particles has been described in the reviews of Park and Hoffman [1], and of Pelton [2]. These papers give an excellent overview of the microgel field as well as a basic understanding of the microgel particles, and their synthesis and behavior in dispersed media. Recently, numerous reviews on microgel synthesis [3], characterization [4, 5], and modification [6, 7], and on their application in drug delivery [8], design of biomaterials [9], and development of sensors [10] have been published, thus showing the potential of the microgels in different fields of science and technology.

There is no universal definition of microgels; however, some special properties can be described. Aqueous microgels are mostly spherical particles with average diameter of 50–10 µm and, similarly to latex particles, can be characterized by a certain particle size distribution (PSD). Similarly to latex particles, microgels are stabilized in continuous medium and form stable dispersions. Another characteristic feature of microgels is the average crosslink density and degree of swelling. The swelling degree depends upon the interplay between polymer–polymer and polymer–water interactions and, additionally, numerous factors such as temperature, pH, and ionic strength influence the behavior of polymer chains inside the microgel. By taking into account these features, aqueous microgels can be considered as porous crosslinked polymeric particles that swell in water and adjust their dimensions, density, and related properties according to the surrounding conditions (Fig. 1).

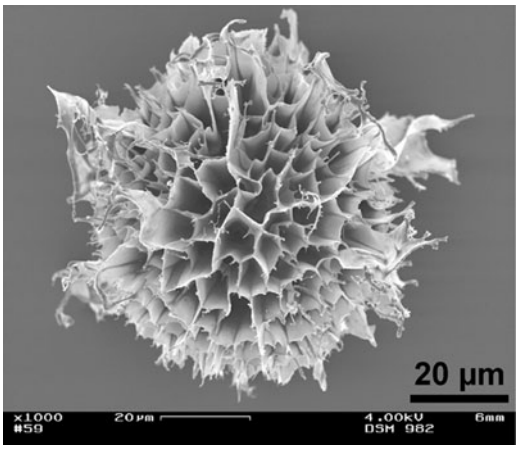

Fig. 1 SEM image of single PNIPAAm microgel particle

The application of stimuli-sensitive polymers in the design of microgels is quite interesting from an application point of view. One of the widely studied stimuli-sensitive polymers is poly(*N*-isopropylacrylamide) (PNIPAAm) [11]. This polymer exhibits endothermic entropy-driven phase transition in water [12]. PNIPAAm forms hydrogen bonds to water through the amide side chains. At the same time, the isopropyl group induces hydrophobic structuring of the water and this leads to entropy-controlled polymer–polymer interactions. If the solvent–polymer interactions are stronger than the polymer–polymer interactions, the PNIPAAm chains exhibit a random-coil structure. If the hydrogen bonds to water break (due to temperature increase), the release of structured water takes place and polymer–polymer interactions become dominant, leading to coil–globule transition. The temperature at which the phase separation takes place is called the lower critical solution temperature (LCST). The microgels consisting of crosslinked PNIPAAm chains exhibit thermoresponsive behavior and a volume phase transition temperature (VPTT) close to the LCST of non-crosslinked PNIPAAm chains [13]. PNIPAAm-based microgels swell if the temperature is below VPTT and shrink if the temperature increases above VPTT. In this fashion, stimuli-sensitive microgels can be prepared in which the solvation of polymer chains can be reversibly triggered by influencing the balance between solvent–solvent, solvent–polymer, and polymer–polymer interactions due to the change of temperature, pH, ionic strength, solvent composition, etc.

2 Microgel Synthesis

Present and future microgel applications require a high degree of control over microgel properties. Basically, the techniques used for the preparation of "bulk hydrogels" can be applied to microgel synthesis. However, in the case of microgels some special aspects play important roles. It is of interest to control the size and PSD of microgel particles during the preparation process. The colloidal stability of microgel systems is important, and microgels should be effectively stabilized in aqueous medium to avoid aggregation and precipitation. Finally, selective incorporation of functional groups in the microgel core or corona is a big challenge. To give a brief overview of available techniques for microgel synthesis we will summarize the existing methods for the preparation of microgels.

2.1 Synthetic Routes

The various synthetic strategies for the preparation of aqueous microgels can be divided into three groups: (1) physical self-assembly or crosslinking of prepolymers in homogeneous phase or in microdroplets; (2) polymerization of monomers in homogeneous phase or in microdroplets; and (3) photolithographic techniques.

The homogeneous gelation method was used for the preparation of chitosan-based microgels in water. Reversible physical crosslinking of chitosan and

polyethyleneimine [14] or tripolyphosphate [15–17] based on electrostatic interactions led to formation of pH-sensitive microgels. The carbodiimide coupling reaction between chitosan and poly(ethylene glycol) (PEG) dicarboxylic acid resulted in formation of chemically crosslinked microgels with a diameter of 50–120 nm [18].

The physical or chemical crosslinking of polymers can be also realized in water-in-oil (W/O) emulsion systems. In this case, aqueous droplets of prepolymers are stabilized by oil-soluble surfactants in a continuous oil phase. Hyaluronan-based microgels were prepared by crosslinking of carboxylic units of hyaluronan with adipic dihydrazide in aqueous droplets [19]. Chitosan-based microgels were prepared by crosslinking of chitosan chains with glutaraldehyde in aqueous droplets [20–25].

Membrane emulsification techniques allow preparation of highly monodisperse microgel particles. The Shirasu porous glass (SPG) membrane with a pore size of 0.1–18 μm was used to prepare uniformly sized water droplets containing chitosan in organic solvent, and polymer chains were crosslinked by glutaraldehyde [26].

Microfluidic techniques have been recently used for the synthesis of microgel particles with dimensions of 1–30 μm. In these methods, microfluidic devices are used that provide emulsification of polymer solutions followed by physical [27, 28] or chemical [29] crosslinking.

Microgels can be prepared by heterophase polymerization (free radical or controlled radical) of monomers in the presence of a crosslinking agent in aqueous phase. Heterophase polymerization techniques suitable for microgel synthesis are precipitation polymerization and inverse mini- and microemulsion.

During precipitation polymerization, all ingredients are dissolved in a solvent (water) to form a homogeneous mixture in which initiation of polymerization takes place. The formed polymers are transformed into a collapsed state because the reaction temperature is far above VPTT (for example in the case of PNIPAAm) and become crosslinked by crosslinker molecules to form a colloidal polymer network or microgel. This technique has been widely used for the synthesis of thermosensitive PNIPAAm [30–35] and poly(*N*-vinylcaprolactam) (PVCL) [36] microgels.

The W/O emulsion methods involve polymerization of monomers in the presence of crosslinker in aqueous droplets. In the case of miniemulsion polymerization, aqueous droplets are generated by sonication of the two-phase mixture and become stabilized in organic solvent by oil-soluble surfactants. The kinetically stable emulsion is usually formed at a surfactant concentration below or near its critical micellar concentration (CMC). This technique has been successfully used for the preparation of hollow PNIPAAm microspheres [37], or PNIPAAm microgels functionalized by acrylic acid [38]. The size of the microgels varied between 150 and 300 nm. By inverse microemulsion polymerization, thermodynamically stable emulsions are formed. This requires use of a large amount of oil-soluble surfactant in a continuous organic medium. Usually, microgels prepared by this technique have a diameter of less than 100 nm. Microemulsion polymerization was used to prepare PNIPAAm [39, 40], polyacrylamide (PAAm) [41–43], or poly(vinylpyrolidone) (PVP) [44, 45] microgels. Microgel preparation by polymerization of monomers can

be also realized in aqueous droplets prepared by use of membrane emulsification or microfluidic devices, as mentioned above. Alternatively, microgel formation in W/O systems can also be realized by polyaddition reactions between reactive multifunctional prepolymers [46]. In this case, the use of crosslinker is not required.

Recently it has been shown that hydrogel layers of variable thickness can be prepared on solid substrates by photolithographic technique [47]. The technique called "PRINT" (particle replication in non-wetting templates) [48, 49] utilizes elastomeric molds from a low surface energy perfluoropolyether network. The molds prevent the formation of an interconnecting film between molded objects and allow production of monodisperse microgel particles of different sizes, shapes, compositions, and surface functionalities.

2.2 Precipitation Polymerization

Precipitation polymerization is probably the most frequently used technique for microgel synthesis. This method is very powerful for the preparation of thermosensitive microgels. In such systems, all ingredients are dissolved in water, including the monomer(s), crosslinker, and initiator. The formation of microgel particles occurs by a homogeneous nucleation mechanism. At polymerization temperature (50–70°C), water-soluble initiator (peroxide- or azo-based compound) decomposes to produce free radicals. In the case of persulfate, initiator decomposition leads to the formation of sulfate radicals that attack water-soluble monomers followed by radical propagation and chain growth. If NIPAAm or VCL are used, the growing polymer chains collapse if they reach a critical length and form precursor particles. This occurs because the polymerization temperature is far above the LCST of formed polymers.

The precursor particles can grow by different mechanisms. Precursor particles can (1) aggregate to form a large colloidally stable polymer particle; (2) deposit on the surface of existing polymer particles; or (3) grow by addition of monomers or macroradicals. Once microgel particles reach the critical size they become stabilized by an electrostatic stabilization mechanism. The charges originate from the initiator fragments (sulfate groups) incorporated into polymer chains during the nucleation and growth process. At this stage, microgel particles are in a collapsed state but still contain a lot of water. This is a principal difference between precipitation polymerization and classical emulsion polymerization of water-insoluble monomers like styrene or butyl acrylate, where latex particles with compact structure are formed during the polymerization process [50]. When the polymerization is completed and the reaction mixture cools down to room temperature, microgel particles swell (temperature below VPTT of polymer chains) and develop a "hairy" morphology. At temperatures below VPTT, microgels are stabilized by steric mechanisms due to the formation of hydrogen bonds between polymer segments and water molecules. Figure 2 shows a simplified mechanism for precipitation polymerization.

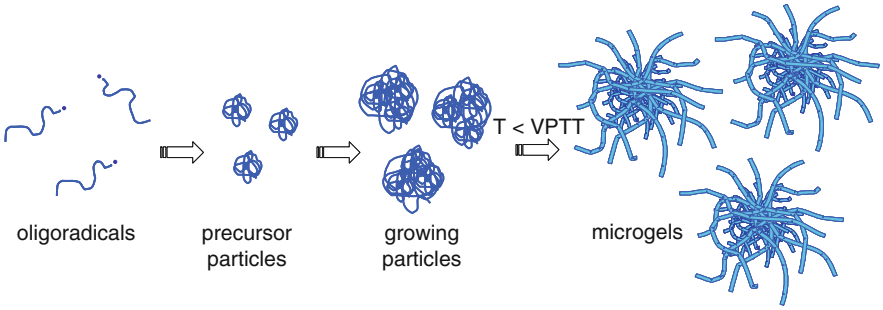

Fig. 2 Microgel formation by precipitation polymerization

The precipitation polymerization technique was first utilized by Philip Chibante in 1978 for preparation of PNIPAAm microgels [2, 51, 52]. In the case where NIPAAm or VCL are used, the use of crosslinking agent is necessary to prevent the microgel from dissolving in water at low temperatures. However, several reports indicate that PNIPAAm chains can undergo "self-crosslinking" by chain-transfer reactions and that microgels can be prepared without use of crosslinking agent [53, 54]. During precipitation polymerization of hydrophilic monomers such as NIPAAm or VCL, a significant amount of non-crosslinked polymer chains can be formed. Additional cleaning of microgel samples by dialysis, centrifugation, and redispergation in water helps to remove the sol fraction.

The precipitation polymerization is a versatile technique and offers several advantages for the preparation of aqueous microgels:

1. The polymerization process can be carried out as a batch, semibatch, or continuous process. This offers the possibility to optimize reaction conditions and obtain microgels with desired properties.
2. Microgel size can be controlled over a broad range (from 100 nm to 3 μm) by the use of surfactants or co-monomers.
3. Microgel particles with narrow PSD can be obtained.
4. Different co-monomers can be integrated into the microgel network during the polymerization process.
5. Hybrid colloids can be prepared by encapsulation of nanoparticles (NPs) during microgel formation.

However, precipitation polymerization has some limitations:

1. Due to the high polymerization temperature, only thermostabile materials can be used; therefore the incorporation of biomacromolecules is not possible.
2. It is difficult to prepare very small microgels (nanogels) with size below 50 nm without use of additional stabilizing agents.
3. Formation of sol fraction during the polymerization process can be a problem.

2.2.1 Homopolymer-Based Microgels

Surfactant-Free Synthesis

The surfactant-free synthesis of aqueous temperature-sensitive microgels was pioneered by the Pelton's group [52]. Monodisperse PNIPAAm microgels were obtained by using persulfate initiator and N,N'-methylene bisacrylamide (BIS) as crosslinker. Freitag and coworkers reported surfactant-free synthesis of thermoresponsive poly(N,N'-diethylacrylamide) (PNDEAm) microgels [55]. In their study, the influence of the stirring rate on the microgel size was investigated. The microgel size decreased with increased stirring rate for the reference PNIPAAm system (from 1110 to 886 nm); however, no significant effect was detected for the PNDEAm system (microgel size around 870 nm).

Imaz et al. [56] reported surfactant-free synthesis of PVCL microgels in aqueous phase in the presence of persulfate as initiator. The authors reported that the microgel particles possessed a size of 350 nm in swollen state below VPTT.

The variation of the crosslinker type used for the synthesis of temperature-sensitive microgels gives an additional possibility for influencing their size and swelling properties under surfactant-free conditions. Helweg and coworkers reported preparation of PNIPAAm microgels in a surfactant-free system by using different crosslinkers with ethyleneglycol dimethacrylate (EGDMA) and triethyleneglycol dimethacrylate (TREGDMA) [57]. Conventional crosslinker BIS was used as a reference. The obtained microgel particles were of hydrodynamic radius (R_h) 273, 356, and 444 nm for BIS-, EGDMA-, and TREGDMA-crosslinked microgels, respectively. The authors noticed significantly lower polydispersity and larger swelling degree in the case of microgels prepared with ethylene-glycol-based crosslinkers. The authors explain the difference in size and stronger swelling of microgels by the higher flexibility of ethylene-glycol-based crosslinkers compared to BIS.

Elaissari and coworkers reported synthesis of poly(N-ethylmethacrylamide) (PNEMAM) microgels by using various crosslinkers exhibiting different solubility in water, namely tetraethylene glycol dimethacrylate (TEGMA) (41 mmol L^{-1}), EGDMA (5.441 mmol L^{-1}), 1,3-butanediol dimethacrylate (1,3-BDDMA) (0.8 mmol L^{-1}), and 1,4-butanediol dimethacrylate (1,4-BDDMA) (0.441 mmol L^{-1}) [58]. The authors reported that the VPTT of obtained microgels was not influenced by the crosslinker type, but that the R_h of colloids increased with the water-solubility of the crosslinker (320, 350, 370, and 430 nm for TEGDMA-, EGDMA-, 1,3-BDDMA-, and 1,4-BDDMA microgels, respectively).

Hydrophilic crosslinking agents glycerol dimethacrylate (GDMA), pentaerythritol triacrylate (PETA), and pentaerythritol propoxylate triacrylate (PEPTA) were used for synthesis of submicron PNIPAAm microgels [59]. Both the average size and swelling degree of microgel particles were lower in the case of crosslinking agents having three acrylate units than with GDMA.

A new synthetic protocol for the synthesis of large diameter (2.5–5 μm), temperature-, and pH-responsive microgels via aqueous surfactant-free radical

precipitation copolymerization was presented by Lyon's group [60]. It has been reported that in the size range, which is not typically attainable using traditional dispersion polymerization approaches, excellent monodispersity and size control are achieved when the synthesis employs a programmed temperature ramp from 45°C to 65°C during the nucleation stage of the polymerization. Combined kinetic and thermodynamic hypotheses for large particle formation under these conditions were described. The obtained microgels exhibited similar behavior (temperature and pH sensitivity) to particles prepared via more conventional routes.

Surfactant-Stabilized Microgels

In the case of temperature-sensitive microgels based on PNIPAAm or PVCL, the surfactant-free method is limited in the sense of particle size variation. To prepare small microgels, the growing precursor particles must be effectively stabilized at early stages of the polymerization process. The stabilization provided by ionic initiator residues incorporated into polymer chains is not sufficient to stabilize the extremely large surface area of small precursor particles. In this case, a surfactant can be added to the reaction mixture to stabilize precursor particles and minimize their growth by aggregation. This leads finally to the reduction of microgel size.

Pelton and coworkers showed that the size of PNIPAAm microgels decreases by a factor of 10 if sodium dodecyl sulfate (SDS) is used in the polymerization procedure [61]. Lyon's group used SDS for stabilization of PNIPAAm microgels prepared with PEG diacrylates of different PEG chain length [62]. To investigate the influence of polymerization conditions on internal structure of PNIPAAm microgels, SDS was used in batch and semibatch polymerization processes [63].

Boyko and coworkers reported use of poly(vinyl alcohol) (PVA) with different molecular weights for steric stabilization of PVCL microgels [64]. In this system, the R_h of temperature-sensitive PVCL microgels decreased from 280 to 180 nm with increased PVA concentration in the reaction system from 2 to 10 g L^{-1} (Fig. 3). The colloidal stability of the PVCL microgels was improved with PVA of lower molecular weight and lower degree of hydrolysis.

2.2.2 Copolymer-Based Microgels

A good alternative to the use of stabilizers (LMM surfactants or polymeric tensides) during preparation of aqueous microgels is the use of reactive functional co-monomers in combination with NIPAAm or VCL. The reactive co-monomers participate in the polymerization process and become covalently attached to the polymer chains of microgel network. The co-monomers can improve colloidal stability of the microgels and help to regulate microgel size. Finally, co-monomers can be used to incorporate functional groups into microgel structures. The co-monomers used for the preparation of aqueous microgels can be low molecular mass functional hydrophilic monomers or macromonomers.

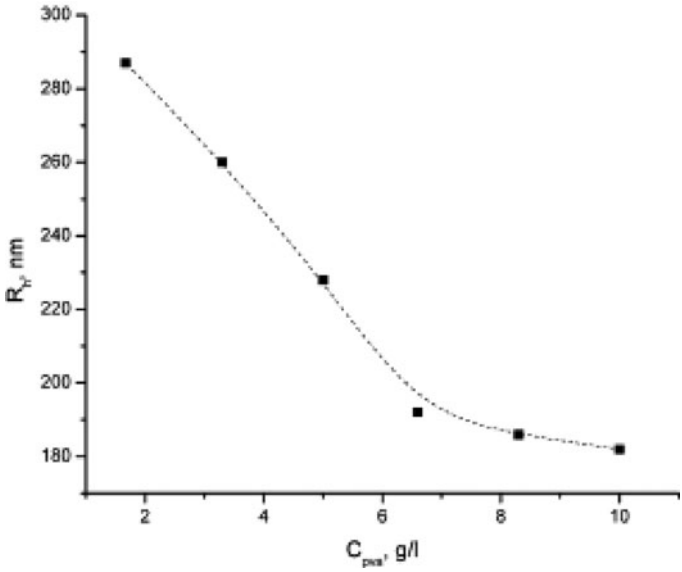

Fig. 3 Hydrodynamic radius (R_h) of PVCL microgels as a function of PVA concentration (C_{PVA}) in aqueous phase (PVA: $M_w = 14{,}000\,g\,mol^{-1}$; hydrolysis degree 99%; $T = 15°C$). Taken from [64], with permission of Springer

Different ionic monomers were copolymerized with NIPAAm or VCL to obtain pH- and temperature-sensitive microgels. Snowden et al. [65] reported preparation of aqueous microgels by copolymerization of NIPAAm and acrylic acid (AAc) in a precipitation polymerization process. The AAc content was 5 wt%. Obtained microgels displayed pH and electrolyte sensitivity, as well as temperature sensitivity.

Kratz et al. [66] reported synthesis of a series of PNIPAAm/PAAc microgels with variable contents of AAc. The size of the microgel particles as well as their deswelling ratio increased significantly with introduction of charged acrylic acid groups into the polymer network. For the charged microgels in salt-free solutions, the shift of the VPTT occurs at higher temperatures.

Saunders and coworkers prepared pH-responsive microgels by copolymerization of methyl methacrylate (MMA), ethyl acrylate (EA), or butyl methacrylate (BA) [67]. The crosslinking monomers were either butanediol diacrylate (BDDA) or EGDMA. The microgel particles swelled significantly at pH values greater than approximately 6.0. It was shown that EA-based microgels swelled more strongly than polyMMA-based microgels. Furthermore, greater swelling occurred for particles prepared using EGDMA than using BDDA.

Monodisperse microgels based on poly(acrylamide-methacrylic acid) copolymer [P(AAm-*co*-MAAc)] crosslinked by BIS with a sharp pH-induced volume transition were prepared in ethanol [68]. Osmotic pressure and deformation of crosslinked polymer network were considered to be the two dominant factors influencing the

characteristics of the pH-induced volume transition. High content of MAAc and high degree of crosslinking increased the osmotic pressure, thereby moving the onset of the volume transition to a higher pH. Association/dissociation of PMAAc segments in the domains contributed to the free energy of hydrogel–solvent mixing. As soon as the pH was high enough to overcome the osmotic pressure, the dissociated PMAAc segments simultaneously decreased the osmotic pressure and free energy of hydrogel–solvent mixing, thereby allowing the sharp and large volume transition. As a result, [P(AAm-*co*-MAAc)] microgels change their volume by factor of 12 upon variation of pH by 0.5.

Hoare and McLean [69] developed a kinetic model for the copolymerization of up to four co-monomers to predict both chain and radial distributions of carboxylic groups in PNIPAAm-based microgels. The model can accurately predict the experimentally observed radial distributions of functional monomers with significantly different hydrophobicities, copolymerization kinetics, and reactivities.

Elaissari and coworkers prepared cationic microgels by copolymerization of NIPAAM and aminoethyl methacrylate hydrochloride (AEMH) in the presence of cationic water-soluble initiator [70]. The presence of the hydrophilic co-monomer AEMH increases the solubility of the thermally sensitive polymer domains, thus showing higher VPTT compared to anionic microgel prepared with persulfate as initiator without AEMH. The presence of AEMH induced a decrease in the microgel size due to the more effective stabilization of growing precursors during the nucleation step.

Copolymer microgel systems based on VCL were reported recently. Peng and Wu [71] reported synthesis of poly(*N*-vinylcaprolactam-*co*-sodium acrylate) microgels and Boyko et al. [72] synthesized microgels based on poly(*N*-vinylcaprolactam-*co*-*N*-vinylpyrrolidone).

Lyon's group prepared aqueous microgels by copolymerization of NIPAAm with hydrophobic [*tert*-butyl acrylamide (TBAm)] and pH-sensitive acrylic acid monomers [73].

As the amount of TBAm increases, the VPTT as well as initial and final microgel radii decrease (Fig. 4a). These experimental results indicate that, due to the hydrophobic character of TBAm, its incorporation in polymer network results in microgels possessing VPTTs much lower than those of the native PNIPAAm particles (Fig. 4b). Due to the incorporation of AAc units, the phase transitions of microgel particles can be modulated by pH. As shown in Fig. 4b, at pH 8 the phase transitions are shifted and occur at much higher temperatures due to the deprotonation of carboxylic groups.

Rictering's group reported synthesis of copolymer microgels based on mono- and disubstituted acrylamides [74, 75]. For copolymer microgels consisting of NIPAAm and *N*,*N*-diethylacrylamide (DEAAM), or *N*-isopropylmethacrylamide (NIPMAAm) and DEAAM, the transition temperature depends on the composition and substitution pattern of monomers, and thus on the ability to build intra- and intermolecular hydrogen bonds between the monomer units. The additional α-methyl group of the NIPMAAm backbone restricts the flexibility of the entire

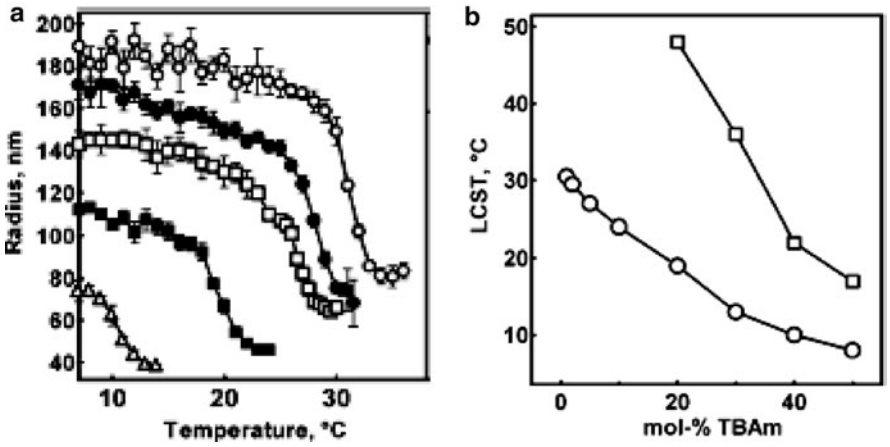

Fig. 4 (**a**) Hydrodynamic radii of: *open circles* 1, *filled circles* 5, *open squares* 10, *filled squares* 20, and *triangles* 40 mol% TBAm copolymer microgels as a function of temperature at pH 3.5. (**b**) Dependence of the volume phase transition temperature on the mol% of TBAm in copolymer microgels at pH 3.5 (*circles*) and pH 8 (*squares*). Reprinted from [73] with permission. Copyright 2003 American Chemical Society

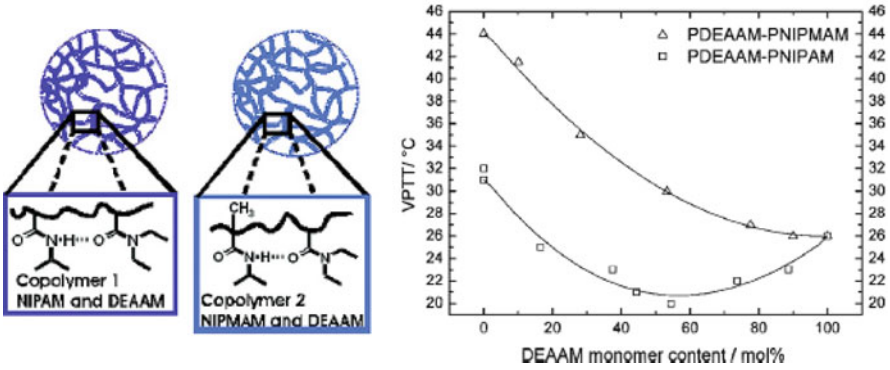

Fig. 5 Influence of composition on the phase transition temperature (VPTT) of two different copolymer microgel series. Reprinted from [74] with permission. Copyright 2008 American Chemical Society

copolymer system and thus hinders the formation of the intramolecular hydrogel bonds. Consequently, the VPTT of the NIPMAAm-based microgels occurs at higher temperatures than in NIPAAm systems (Fig. 5).

The copolymerization of different functional monomers during precipitation polymerization can be used for design of amphoteric aqueous microgels [76–82]. Amphoteric microgels were prepared by copolymerization of NIPAAm with acrylic acid and vinylimidazole (VIm) [76–80]. Alternatively, Tan and coworkers prepared amphoteric colloids by copolymerization of acrylic acid, 2-(diethylamino)ethyl

methacrylate (DEAEMA) and poly(ethylene glycol) methyl ether methacrylate in aqueous phase [81]. Kawaguchi and coworkers used acrylamide, MAAc and DEAEMA to prepare amphoteric microgels by semicontinuous precipitation polymerization in ethanol [82].

Interesting microgel systems have been prepared by application of reactive macromonomers. Armes and coworkers used the reactive macromonomers monomethoxy-capped poly(ethylene glycol) methacrylate (PEGMA), styrene-capped poly[2-(dimethylamino)ethyl methacrylate] ($PDMA_{50}$-styrene), and partially quaternized styrene-capped poly[2-(dimethylamino)ethyl methacrylate] (10q $PDMA_{50}$-styrene) to prepare colloidally stable pH-sensitive microgels based on poly[2-(dimethylamino)ethyl methacrylate] (PDEA) [83]. The average size of microgel particles ranged from 250 to 700 nm. In a recent paper, the authors explored the use of the microgels deposited onto silica substrates for pH-triggered capture and release of pyrene dye [84]. PEGMA macromonomer was used by the same group for preparation of microgel particles based on poly(2-vinylpyridine) (P2VP) [85, 86]. The mean diameters of microgels ranged from 390 to 970 nm.

PVCL microgels with grafted amphiphilic chains were prepared by using reactive macromonomer consisting of a hydrophobic hydrocarbon segment and hydrophilic PEO segment [87]. Due to the amphiphilic character of the macromonomer and its ability to form micelles in water (CMC value was $0.25\,g\,L^{-1}$ at 20°C), the obtained microgels exhibited a small size (73 nm at 20°C) and narrow size distribution. Microgel samples prepared with macromonomer showed discontinuous thermal transition at 35°C, whereas in the case of microgels prepared with SDS as stabilizer the collapse transition occurs over a broad temperature range.

Pich and coworkers synthesized microgels by free-radical co-polymerization of vinyl caprolactam and acetoacetoxyethyl methacrylate (AAEM) in the presence of methoxy-capped PEGMA macromonomers [88]. It has been reported that variation of the amount of PEG macromonomer or the length of the PEG chain provides effective control of the microgel diameter in the range 60–220 nm (Fig. 6).

The presence of the grafted PEG chains improves the colloidal stability of the microgels. The incorporation of the PEG macromonomers into the microgel structure decreases the swelling degree and induces a shift of the VPTT to higher temperatures.

Figure 7 shows SEM (scanning electron microscopy) images of microgel particles prepared with different macromonomers. The decrease in the microgel size with increase in macromonomer concentration is obvious in the case of PEGMEMA1100 and PEGMEMA2080 systems. However, the results in Fig. 7 indicate that PEGMEMA1100- and PEGMEMA2080-modified microgels became irregularly shaped above a critical macromonomer concentration. In the case of PEGMEMA2080 macromonomer, the appearance of 10 nm secondary particles is clearly visible in Fig. 7. Both effects are attributed to the increase in water-solubility of the precursor particles due to the hydrophilic macromonomers used in the polymerization recipe.

A synthetic scheme involving chemical protection/deprotection to combine interfering functional groups on the same microgel particle has been developed

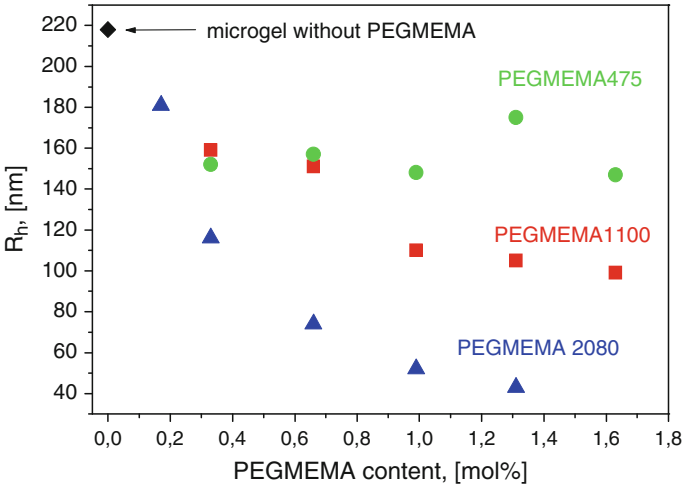

Fig. 6 Hydrodynamic radii (R_h) of PVCL/PAAEM microgel particles as a function of PEGMEMA content ($T = 20°C$). Taken from [88]

[89]. The synthesis of amine-containing PNIPAAm nanogels was carried out via free-radical precipitation polymerization by incorporating a Fmoc-protected amine-PEG macromonomer. The Fmoc (9*H*-fluoren-9-ylmethoxycarbonyl) group was then removed to obtain free amines, which were shown to be available for conjugation with biomacromolecules. The introduction of protected amine-PEG into P(NIPAAm-*co*-AAc) nanogels resulted in formation of zwitterionic colloids.

2.2.3 Core–Shell Structures

Precipitation polymerization allows preparation of microgel particles with a core–shell structure. This can be achieved by using monomers of different reactivity or hydrophilicity in a batch polymerization process. Alternatively, core–shell microgels can be prepared by seed polymerization techniques or by stepwise addition of co-monomers to the reaction mixture.

The core–shell microgel system has been prepared by copolymerization of VCL and AAEM in the aqueous phase by using cationic initiator and a crosslinker under surfactant-free conditions [36]. At the first stage, a water-soluble cationic radical initiates mainly polymerization of water-soluble AAEM and BIS monomers. When the polymer chains reach a critical length, they precipitate to become precursor particles. These precursor particles create nuclei for PVCL growing chains, which collapse on the nuclei surface at the polymerization temperature of 70°C. This is far above their LCST and the chains become additionally crosslinked. The growing VCL/AAEM microgel particles are stabilized by steric mechanisms, and partial electrostatic stabilization is provided by the charged groups of the cationic initiator.

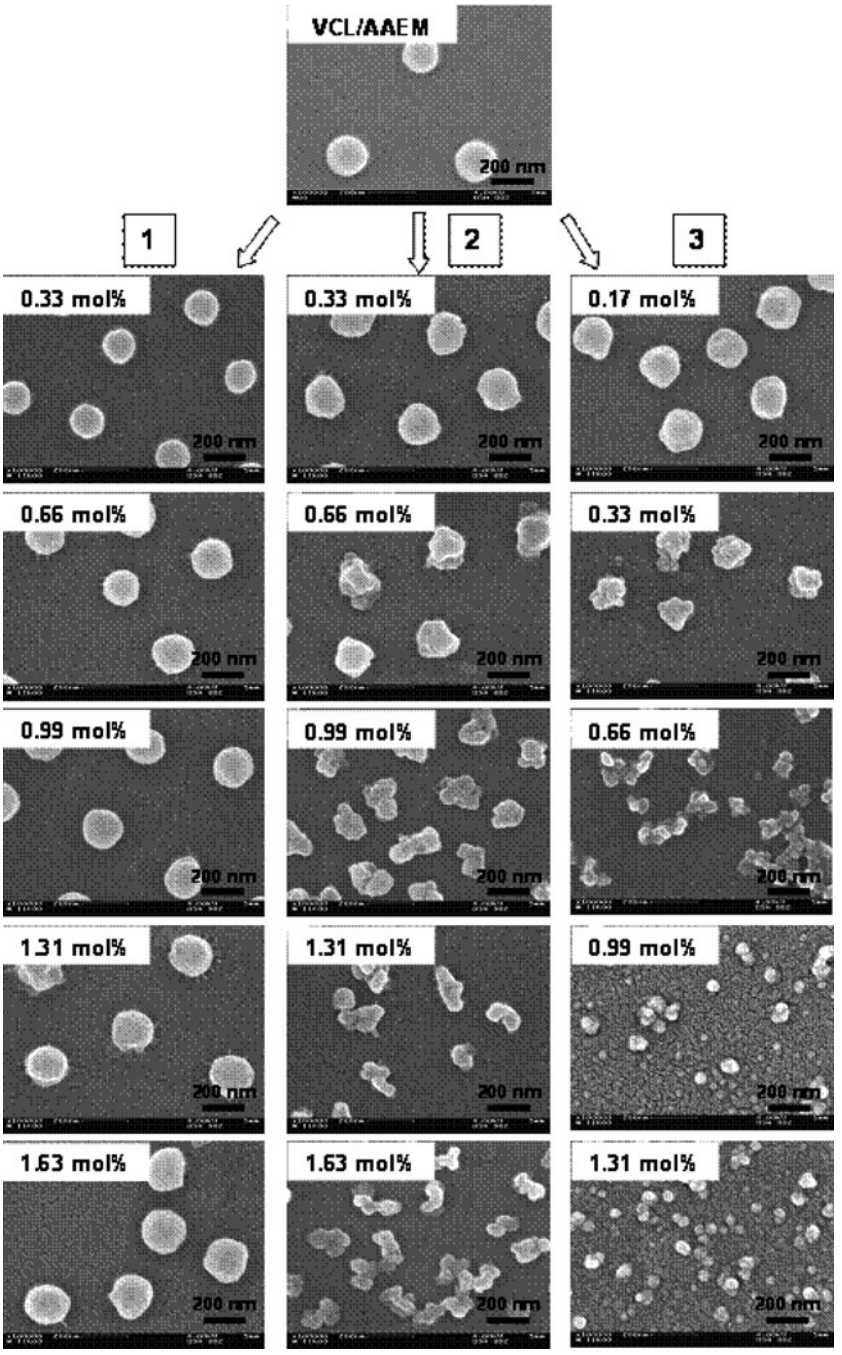

Fig. 7 SEM images of VCL/AAEM/PEGMEMA microgels: *column 1* PEGMEMA475, *column 2* PEGMEMA1100, and *column 3* PEGMEMA2080. Taken from [88]

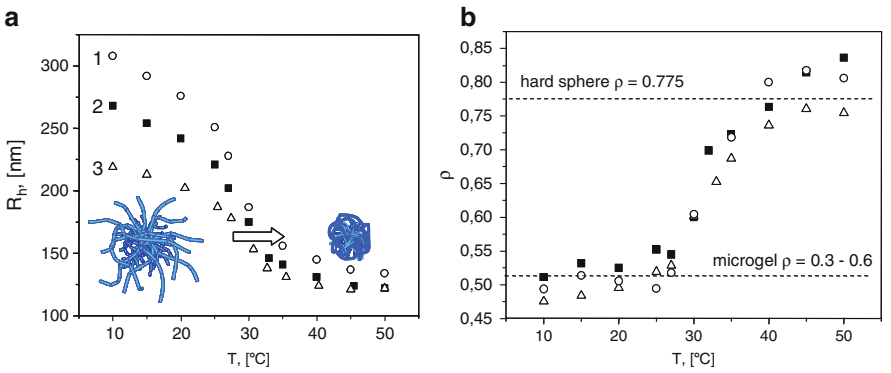

Fig. 8 (**a**) Hydrodynamic radii (R_h) and (**b**) ratio $\rho = R_g/R_h$ as a function of the temperature for VCL/AAEM microgels with different composition: *circles* 4, *squares* 6.5, and *triangles* 15 mol% AAEM. Reprinted from [36], Copyright 2003 with permission of Elsevier

The resulting particles have a core–shell structure due to fast consumption of highly reactive AAEM during the first stage of reaction. Therefore, the microgel particles consist of a PAAEM-rich core and PVCL-rich shell, which consists mainly of covalently bonded PVCL chains. The variation of monomer ratio allows tuning of the size of formed particles and regulation of the swelling degree of the microgels. Figure 8 demonstrates the thermosensitive properties of VCL/AAEM microgels. For microgel samples with different compositions, a broad continuous decrease in R_h was detected, and the transition temperature shifted slightly to 28°C in comparison to the reported 32°C for linear PVCL. It can also be seen that all microgels shrink to approximately the same size, although the difference in swelling is significant (Fig. 8a). The combination of dynamic and static light scattering gives the possibility to calculate the $<R_g>/<R_h>$ ratio (ρ), which reflects the conformation of a polymer chain or the density distribution of a particle and thus gives valuable information about the internal structure of microgels. Figure 8b shows that, at low temperatures, the ρ values for microgels are in the range 0.3–0.6. The temperature increase induces a decrease in the mobility of the PVCL chains and a compact structure without internal motion is formed. Therefore, ρ increases rapidly close to the critical temperature and finally approaches the theoretically predicted ρ value for the homogeneous sphere (0.775). At high temperatures, microgels exhibit hard sphere behavior (deviations from theoretical value are within experimental error).

In a different system, VCL was copolymerized with AAEM and VIm by a simple batch polymerization procedure in aqueous medium, leading to the formation of colloidally stable pH- and temperature-sensitive core–shell microgel particles [90]. Figure 9a shows the influence of VIm content on the particle size of microgels at pH 6 and 20°C. Figure 9a indicates that the R_h of microgels increase linearly if larger VIm amounts are introduced into the microgel structure. At the same time, the polydispersity index (PDI) of obtained microgels remains unaltered, which indicates that introduction of VIm does not induce the formation of secondary particles

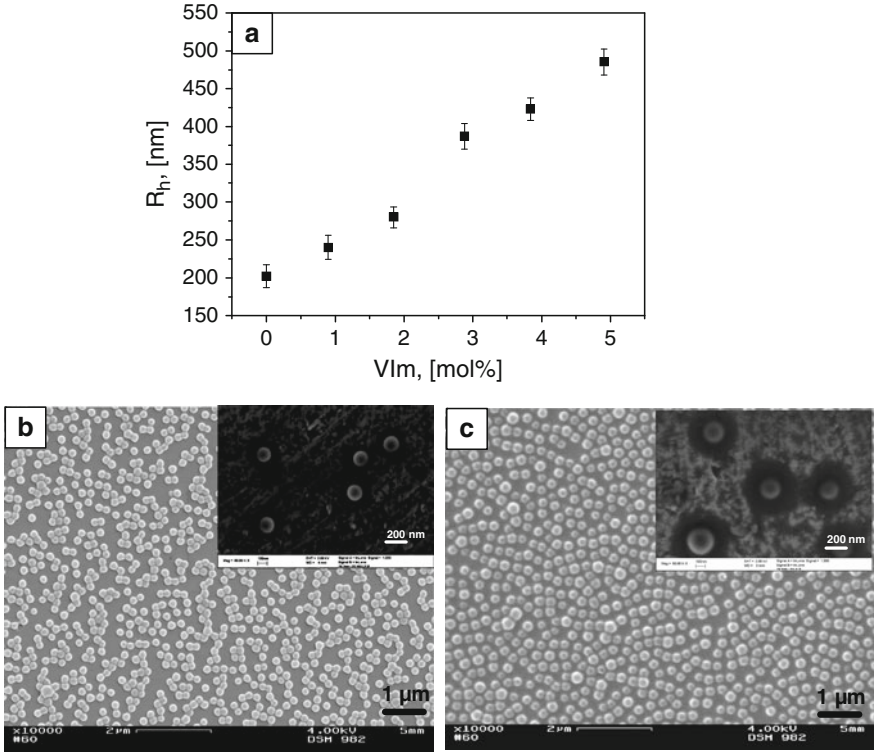

Fig. 9 (**a**) Hydrodynamic radii (R_h) of microgel particles prepared at different VIm contents ($T = 20°C$, pH 6). SEM images of (**b**) VCL/AAEM and (**c**) VCL/AAEM/VIm(2.9%) microgels. *Insets* show high-magnification field-emission SEM images. Reprinted from [90] with permission. Copyright 2006 American Chemical Society

in the aqueous phase. These observations lead to the conclusion that incorporation of small amounts of VIm strongly increase the hydrophilicity of the particles, leading to better solvation by water molecules and higher swelling in continuous medium. This results finally in the increase of R_h of microgels with gradual increase in VIm content. SEM images presented in Fig. 9b, c indicate that VCL/AAEM/VIm(2.9%) particles are larger than VCL/AAEM microgels, which supports light scattering measurements. Field-emission SEM images indicate that VCL/AAEM/VIm(2.9%) microgels exhibit a much thicker corona-like shell than VCL/AAEM particles.

Glycidyl methacrylate (GMA) was selected as co-monomer for the precipitation polymerization of VCL to obtain temperature-sensitive microgels functionalized by epoxy groups [91]. The attractiveness of GMA is related to its versatility in functionalization. GMA can react with amino groups that are suitable for covalent binding of proteins [92] as well as for grafting [93] and crosslinking reactions [94]. The mechanism of the particle nucleation in this system is similar to VCL/AAEM microgels. Due to the large reactivity difference between VCL and GMA [95] and

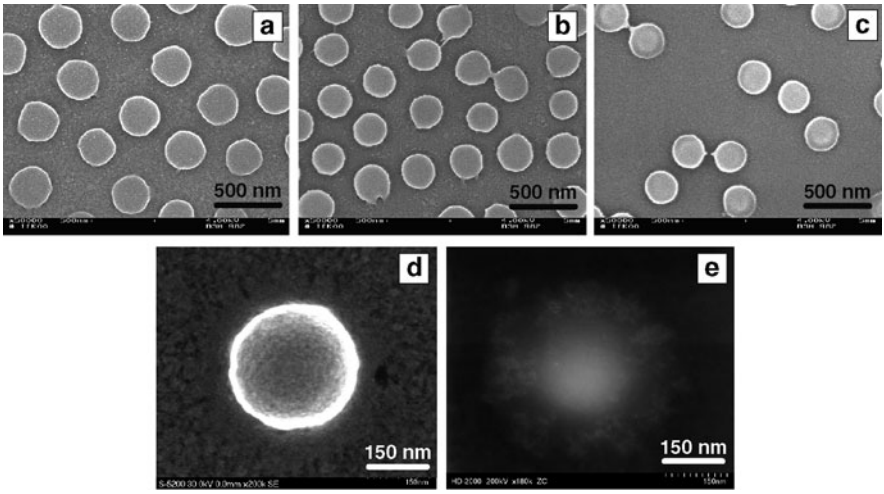

Fig. 10 SEM images of VCL/GMA microgel samples containing (**a**) 4.8, (**b**) 9.1, and (**c**) 16.7 mol% GMA. High-resolution (**d**) SEM and (**e**) STEM of a single microgel particle containing 16.7 mol% GMA. Reprinted from [91] with permission. Copyright 2007 American Chemical Society

the more hydrophobic nature of PGMA, we expect to obtain microgel particles with a heterogeneous structure, e.g., reactive PGMA-rich core and temperature-sensitive PVCL-rich shell. This microgel architecture will ensure the localization of the highly reactive GMA units in the microgel interior, providing the possibility of further functionalization. SEM images in Fig. 10a–c show that the size of microgels decreases with increasing GMA content due to the more hydrophobic nature of PGMA compared to PVCL. Figure 10d, e present high-magnification SEM and TEM (transmission electron microscopy) images of a single microgel particle with high GMA content. Both images indicate clearly the core–shell structure of the microgel, where the more compact GMA-rich core is surrounded by a soft VCL-rich shell.

The seed polymerization technique has been used by many groups to generate microgels with core–shell architecture. Recently, Kawaguchi's group reported synthesis of GMA/NIPAAm core–shell microgels [96–98]. The authors used a feed technique to generate the desired particle morphology. At the initial stage, NIPAAm was copolymerized with GMA in the presence of crosslinker to form seed particles. At the second stage, NIPAAm was added to seed microgels and shell polymerization took place.

Lapeyre et al. [99] prepared aqueous microgels consisting of thermoresponsive PNIPAAm core and thermo- and glucose-responsive poly(NIPAAm-*co*-acrylamidophenylboronic acid) shell. The radius of the core in the collapsed state (40°C) was 65 nm. By variation of the monomer concentrations added during the second polymerization step from 20 to 80 mM, the shell thickness increased from 15 to 38 nm.

Li et al. [100] synthesized core–shell microgels with temperature-sensitive PNIPAAm core and pH-sensitive poly(4-vinylpyridine) (P4VP) shell. Narrowly distributed microgel particles with core diameter of 95 nm and shell thickness of approximately 30 nm were obtained.

Vincent's group reported synthesis of PVP core and PNIPAAm shell by a seed-feed polymerization process [101]. At the first stage, the polymerization of 2VP in the presence of crosslinker was performed to obtain PVP seed colloids. Then, a small amount of cationic surfactant was added (surfactant concentration was kept below its CMC) to enhance colloidal stability in the subsequent shell growing stage. For the shell formation, two separate feed solutions were prepared (feed 1: NIPAAm, BIS, and water; feed 2: initiator and water) and added to PVP seed dispersion (feed 1, and after 30 min feed 2). The authors suggested that during shell addition, feed 1 is commenced before the initiator feed 2, so that initially NIPAAm is grown on the living ends of still-growing PVP chains and forms a chemical bond between the PVP core and PNIPAAm shell.

Richtering's group reported synthesis of doubly temperature-sensitive core–shell microgels [102–104]. The microgels were composed of a core of crosslinked PNIPAAm and a shell of crosslinked PNIPMAAm. Due to the fact that the polymers exhibit LCSTs at 34°C and 45°C (for PNIPAAm and PNIPMAAm, respectively), the authors reported that the core–shell microgels display a temperature-dependent two-step shrinking behavior. By varying the amount of NIPMAAm added during the second polymerization step, the authors prepared a series of microgels with different shell thicknesses (Fig. 11). The same group designed microgels with a core of crosslinked PNIPMAAm and a shell of crosslinked PNIPAAm [105]. In this case, a doubly temperature-sensitive core–shell microgel was prepared, which at intermediate temperatures reveals a shell with a higher segment density than the core. The temperature dependence of the R_h demonstrated that the shell restricts the core swelling at temperatures between the LCSTs of core and shell. Using different temperature-sensitive polymers, a core–shell microgel was prepared, which at intermediate temperatures has a shell with a higher segment density than the core (see radial density profiles in Fig. 12).

Temperature- and pH-sensitive core–shell microgels consisting of a PNIPAAm core crosslinked with BIS and a polyvinylamine (PVAm) shell were synthesized by graft copolymerization in the absence of surfactant and stabilizer [106] The core–shell morphology of the microgels was confirmed by TEM and zeta-potential measurements. Other examples of core–shell microgel systems are PNIPAAm-*g*-P(NIPAM-*co*-styrene) colloids [107] or PS(core)-*g*-PNIPAAm (shell) particles [108].

2.2.4 Hybrid Microgels

Precipitation polymerization can be used for integration of inorganic NPs into microgel structures. An interesting approach for the preparation of the hybrid microgels is encapsulation of the NPs during precipitation polymerization. To demonstrate the efficiency of this method, LaF_3:Eu NPs modified with a mixed

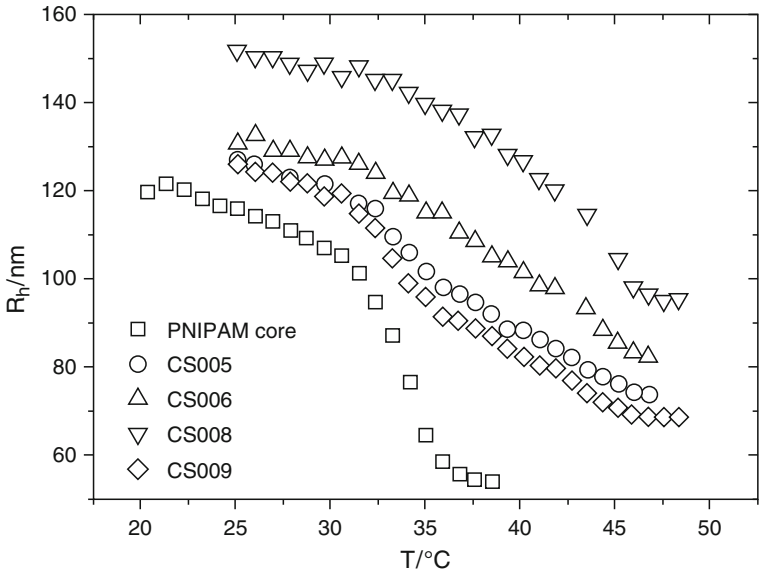

Fig. 11 Hydrodynamic radius vs. temperature of core–shell microgels with different shell thickness at shell crosslinker content of 9.0 mol%. The parent PNIPAAm core is shown for comparison. Reprinted from [102] with permission. Copyright 2003 American Chemical Society

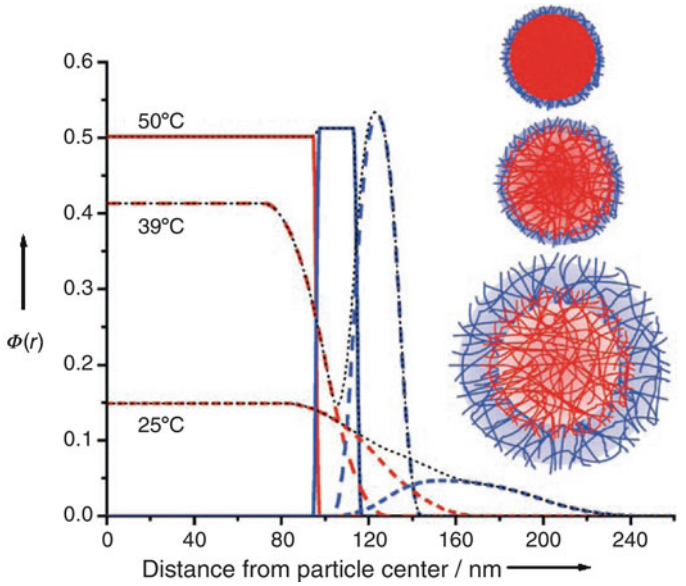

Fig. 12 Radial density $\varphi(r)$ profiles calculated from the modeling procedure at 25, 39, and 50°C for core (*red*) and shell (*blue*); *black dotted lines* show total density. At the intermediate temperature, the shell has a higher density than the swollen core. Also shown are schematic pictures of the density of the core–shell microgels at temperatures of 50, 39, and 25°C (*top to bottom*). Taken from [105], Copyright Wiley-VCH. Reproduced with permission

ligand [aminoethyl phosphate (AEP) and ethyleneglycol methacrylate phosphate (EGMAP) in molar ratio 3:1] have been used [109]. In this system, AEP provides stabilization of NPs in water and the introduction of EGMAP provides incorporation of the double bond, which ensures covalent fixation of the NPs in the microgel.

The presence of reactive LaF_3:Eu NPs in the reaction mixture has several important consequences with respect to the formation of microgel particles during the precipitation polymerization process. First, the reactive NPs participate in the initial polymerization step by being integrated into growing polymer chains and forming the nuclei that grow to form the composite microgel particles (see Fig. 13). Second, the incorporation of the NPs during early stages of polymerization ensures their localization in the microgel interior. Third, the NP incorporation is essentially quantitative. This is an advantage over methods based on NP diffusion, where incorporation efficiencies of $<50\%$ are common.

Figure 14a shows the R_h (at 20°C) for microgels prepared at different NP concentrations. The increase of the NP concentration in the reaction mixture reduces the size of the microgel considerably (from 220 to 80 nm). However, as indicated in

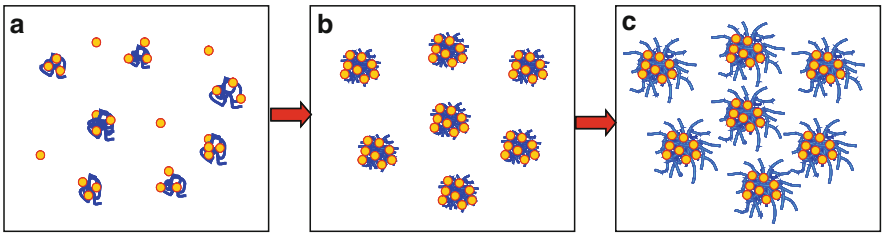

Fig. 13 Different stages of the heterophase polymerization process: (**a**) homogeneous distribution of NPs in a reaction mixture containing monomers, crosslinker and initiator before polymerization; (**b**) early stages of the nucleation process indicating incorporation of NPs into the growing polymer particles; and (**c**) final NP-containing microgel particles

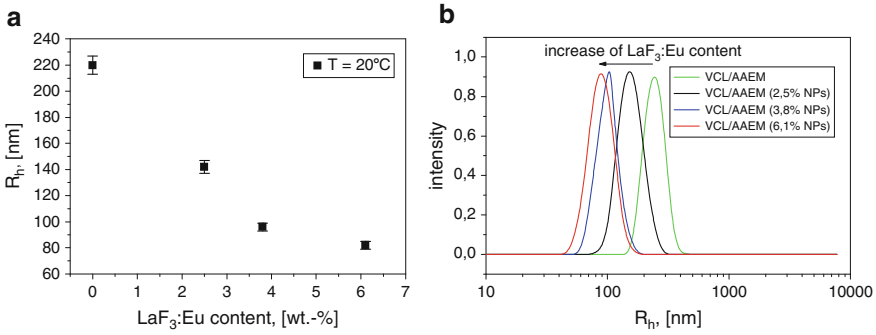

Fig. 14 (**a**) Hydrodynamic radii and (**b**) size distribution curves of the hybrid microgels. Taken from [109], Copyright Wiley-VCH. Reproduced with permission

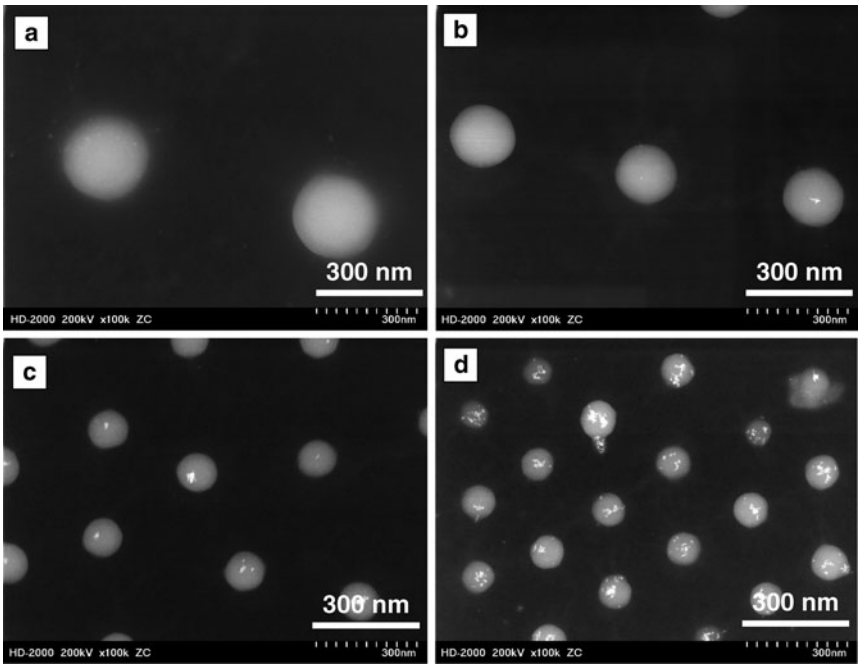

Fig. 15 STEM images of hybrid microgels: (**a**) no NPs, (**b**) 2.5, (**c**) 3.8, and (**d**) 6.1 wt% NPs. Taken from [109], Copyright Wiley-VCH. Reproduced with permission

Fig. 14b, the PSD remains unaltered and no free NPs could be detected. The reason for the decrease in the particle size is the ability of the NPs used in present study to act as nucleation centers.

Scanning transmission electron microscopy (STEM) images in Fig. 15 indicate that the NPs are located mostly in the microgel core. Very few of them can be found in the shell region, suggesting that integration of the NPs into microgel occurs during the early nucleation stage.

In several reports, the encapsulation of non-reactive NPs into microgels was reported. Zhang et al. [110] reported synthesis of hybrid PNIPAAm-based microgels by using inorganic clay (hectorite) as crosslinker. The authors reported significant reduction of the microgel size to 322 nm (microgel prepared without clay displayed a diameter of 808 nm) when clay NPs were present in the reaction mixture. The authors suggest that polymer chains of the microgel network are attached to the clay surface by ionic or polar interactions. X-ray diffraction indicated that clay platelets are in an exfoliated state, forming an organic–inorganic network structure within microgels.

Pich et al. [111] reported synthesis of microgel–clay composite particles by one-step surfactant-free precipitation polymerization (unpublished results). Laponite NPs present in the reaction mixture become encapsulated during the microgel

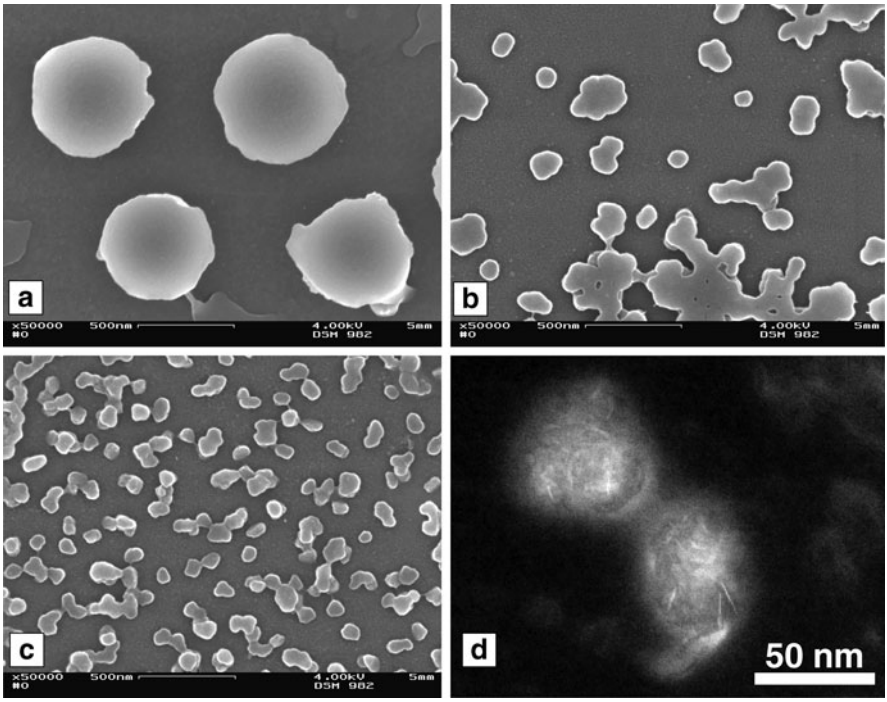

Fig. 16 SEM images of microgel particles: (**a**) no clay, (**b**) 2.3, and (**c**) 8.8 wt% clay. (**d**) STEM image of microgel particles (9.7 wt% clay). Taken from [111]

formation process. Microgel samples based on poly(*N*-vinylcaprolactam-*co*-acetoacetoxyethyl methacrylate) containing different amount of incorporated clay NPs were synthesized. The clay content was varied from 2 to 18 wt%. Fig. 16a–c shows SEM images of microgel samples in a dehydrated state. The use of clay NPs during the polymerization process decreases the size of microgel particles. TEM images show needle-like laponite nanocrystals in the microgel interior (Fig. 16d).

3 Postmodification of Microgels

The preparation of aqueous microgels by precipitation polymerization cannot fulfill all requirements in the sense of desired functionalization, which is extremely important for certain applications. Not all functional units can be integrated into microgels during the polymerization step. This is caused by limited availability of functional water-soluble monomers or thermal instability of some functional groups or proteins during the polymerization process. In some cases, different reactivity ratios of monomers do not allow the design of microgel particles with desired localization

of the functional groups. In many cases, postpolymerization modification of the microgels with small molecules, synthetic polymer, or proteins was used to introduce desired functionalities in polymer colloids.

3.1 Incorporation of Small Molecules, Synthetic Polymers, and Biomacromolecules

A convenient approach to the modification of microgel particles is postmodification by using polymer–analog transformations. Recently, Kawaguchi's group reported synthesis of GMA/NIPAAm core–shell microgels and their use for targeted deposition of gold NPs [92]. In their work, epoxy groups have been used for the targeted modification with thiol-containing compounds to selectively load inorganic NPs in the microgel particles. Häntzschel et al. [112] reported postmodification of VCL/GMA microgels by reaction with thioethanamine in order to incorporate amino groups into microgel structures.

Garcia et al. [113] reported synthesis of photo-, thermo-, and pH-responsive microgels. The authors modified NIPAAm/allylamine copolymer microgels with carboxy-functionalized spiropyran photochrome. In this manner, the functionalized spyropyrane was coupled to the microgel by an amide bond. This postmodification of aqueous microgels resulted in photo-sensitive colloids: The microgels shrunk upon irradiation with visible light because spyropyrane changed from the polar merocyanine form to the nonpolar spiro form.

Pelton's group reported synthesis of amine-functionalized PNIPAAm microgels [114]. Microgels were prepared by the precipitation copolymerization of NIPAAm and *N*-vinylformamide (NVF). The obtained microgels were hydrolyzed at 70°C and pH 1.5 to transform formamide into amine groups. Later, oligo(NVF) (prepared in a separate step) was attached to the microgel surface at pH 9 and 25°C. Finally, the formamide groups were hydrolyzed in acidic medium at 70°C and microgel particles with PNIPAAM core and amine-rich shell were obtained.

Recently, it has been shown that functional molecules can be integrated into aqueous microgels by formation of intermolecular complexes [115]. A simple route for the design of hydrophilic microgels comprising inner hydrophobic nanodomains has been developed based on postmodification of microgels by complexation of wedge-shaped amphiphilic molecules with complementary functional groups (Fig. 17). Aqueous microgels with imidazole groups integrated into the network were transferred into an organic medium, where they were neutralized by water-insoluble wedge-shaped molecules bearing a sulfonic acid group at the tip of the wedge and a large hydrocarbon body [115]. After redispersion of the modified microgel particles into the aqueous phase, wedge-shaped amphiphiles ionically attached to the polymer chains self-assembled into discrete nanodomains in the interior of the polymer colloids due to the hydrophobic attraction force. The loading of the wedge-shaped molecules into microgels can be controlled by variation of the amount of imidazole groups integrated into the microgel network as well as the neutralization degree.

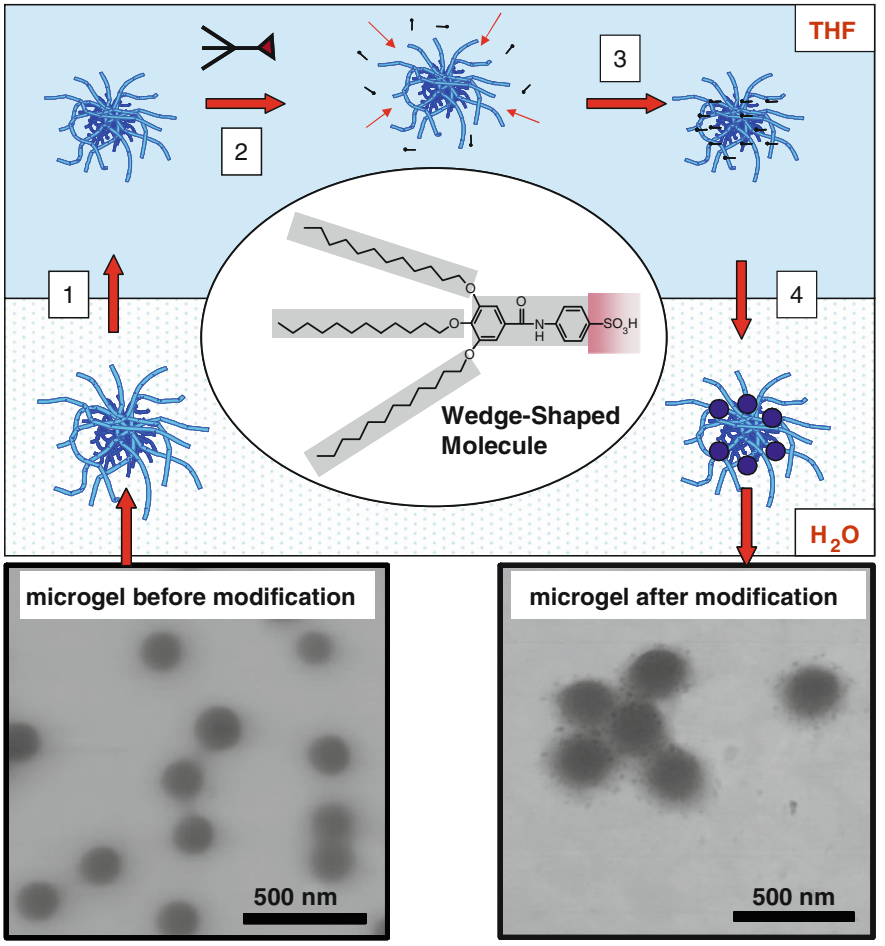

Fig. 17 Preparation of complexes of wedge-shaped sulfonic acid molecules (TDBBSA) and PVCL/AAEM/VIm microgels by the reversible transfer from water to THF: (*1*) transfer of the aqueous microgel to THF by solvent exchange; (*2*) addition of TDBBSA molecules to the microgel suspension in THF and diffusion of wedge-shaped molecules into porous polymer colloids; (*3*) fixation of TDBBSA within microgels by complexation; and (*4*) transfer of the modified microgel to the aqueous phase by solvent exchange. TEM images of the microgels are shown. Taken from [115]

The experimental results suggested that incorporation of hydrophobic domains into hydrophilic colloids induced dramatic changes in their properties, such as swelling degree, surface charge, and responsiveness to temperature and pH.

Richtering's group reported that the polyelectrolyte adsorption on charged microgel particles is a promising approach for design of new microgel architectures [116]. The adsorption of poly(diallyldimethylammonium chloride) (PDADMAC) on PNIPAAm-*co*-MAAc microgels was studied with regard to different ratios

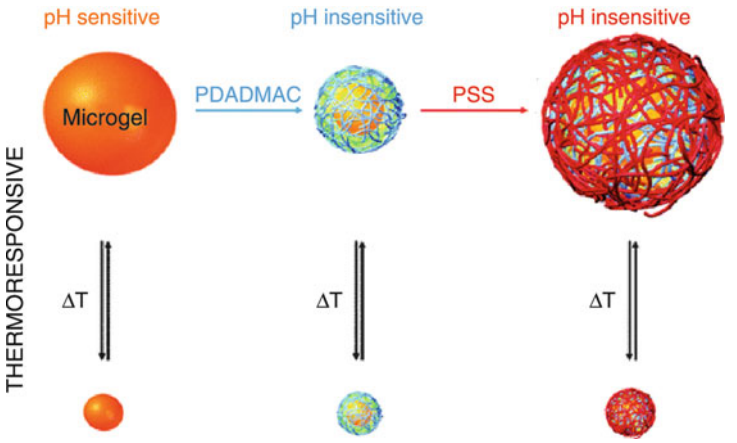

Fig. 18 Microgel design by layer-by-layer deposition of polyelectrolytes. Reprinted from [118] with permission. Copyright 2008 American Chemical Society

between the positive charges of PDADMAC and the negative charges originating from MAAc units [117]. The authors reported that the adsorption of the polyelectrolyte on the microgel surface leads to a decrease in the microgel size. The light scattering experiments performed at different temperatures indicated that at temperatures above VPTT, the microgel/polyelectrolyte complexes cannot collapse completely due to additional physical crosslinking and enhanced stiffness of the surface layer. The layer-by-layer technique was used by the same group to design complex microgel colloids (Fig. 18) [118].

The alternating adsorption of PDADMAC and poly(sodium styrenesulfonate) (PSS) on the surface of PNIPAAm-*co*-MAAc microgels was investigated. The microgels coated with polyelectrolyte multilayers retained their temperature sensitivity and displayed a reversible swelling/deswelling process. The deposition of polyelectrolyte layers did not hinder the colloidal stability of microgels. The authors reported that PSS-terminated microgels exhibit a higher degree of swelling compared to PDADMAC-terminated microgels. After deposition of rigid polyelectrolyte layers, composite microgels lose their pH sensitivity.

Free-radical RAFT polymerization was used to graft linear PNIPAAm chains onto PNIPAAm-*co*-acrylic acid 2-hydroxyethyl ester (HEA) microgels [119]. P(NIPAAm-*co*-HEA) microgels repaired by precipitation polymerization were modified by initiator fragments by addition of α-butyl acid dithiobenzoate in THF solution. Finally, the RAFT polymerization of NIPAAm was initiated, leading to controlled growth of linear PNIPAAm chains from the microgel surface. The authors reported that the obtained microgels display two different kinds of temperature-induced transitions related to the grafted PNIPAAm layer. In the temperature range 25–32°C the layer thickness decreased due to the coil-to-globule transition of grafted linear PNIPAAm chains. At higher temperatures 32–35°C, the layer thickness increased linearly due to the repulsion among the grafted chains on the surface, which was related to globule-to-brush transition of the collapsed PNIPAAm chains.

Su et al. [120] reported modification of PNIPAAm microgels with antibody or with a DNA aptamer. The PNIPAAm microgels carrying carboxyl groups were prepared as the first step. During the second step, microgels were modified with streptavidin in the presence of *N*-ethyl-*N*′-(3-dimetylaminopropyl)carbodiimide hydrochloride (EDC) in 2-(*N*-morpholino)ethanesulfonic acid buffer. Finally, anti-rabbit IgG biotin conjugate or aptamer-biotin conjugate were covalently attached to the microgel particles through the streptavidin–biotin coupling reaction. The authors reported that antibodies and aptamers retained their recognition activities when coupled to microgels.

Delair et al. [121] immobilized DNA on the surface of PNIPAAm microgels. The amino groups integrated into PNIPAAm microgels were reacted with single-stranded DNA containing a terminal isocyanate groups.

3.2 Incorporation of Nanoparticles

The potential use of aqueous microgels as templates or microreactors for synthesis, storage, and transport of different nanostructured materials has been recently demonstrated by different research groups. On the basis of typical microgel properties, one can predict the following advantages when using them as microreactors or carriers compared to other template systems: easy preparation; variable size and flexible functionalization by reactive groups; highly porous structure with adjustable crosslinking degree; enhanced colloidal stability; and stimuli-responsive change of the microgel dimension (temperature and pH sensitivity). With regard to those features, the preparation of different materials in the form of NPs inside the microgels can offer controlled NP synthesis in microgels (localization of reactive sites and controlled growth, homogeneous distribution within microgel); adjustable NP properties (particle size and morphology control; separation and stabilization in polymer network); NP accessibility (high surface area, no diffusion limitation); control of the distance between NPs by swelling or collapse of microgel in response to environmental conditions; and high colloidal stability provided by microgel particles. However, one should be aware of some undesired effects that can be expected at high microgel loading by another material. The specific interactions between NPs and polymer chains within the microgel can lead to reduction of the chain mobility and a shift of the phase transition temperature, as well as colloidal destabilization.

Two rather distinct approaches have been taken for loading different nanomaterials into microgel particles. The first utilizes the microgel as a template for in situ preparation of nanoscale materials such as inorganic NPs. In this case, the NPs are trapped in the microgel interior by hydrophobic forces, hydrogen bonding, or electrostatic interactions. This approach has been realized for both aqueous microgels [122] and microgels dispersed in organic solvents [123, 124]. The attractive features of this approach are the effective control of the NP dimensions within the microgel, and flexibility in control of the NP loading.

The second approach involves filling the microgels by diffusion of preformed NPs into the microgel, accompanied by trapping due to the electrostatic interactions or hydrogen bonding with polymer chains [125, 126]. This technique offers some important advantages in terms of the simplicity of the process and independent adjustment of the NP properties. This approach, however, has been employed primarily in aqueous media and has limited utility for incorporation of inorganic nanocrystals synthesized in organic solutions. In both of these approaches, the microgel network serves not only as a container for transporting the NPs, but also as a functional unit that can be attached to substrates or respond to stimuli such as changes in temperature or pH. By using the two methods described above, a variety of composite microgel particles have been prepared, containing NPs of conducting polymers [127–132], noble metals [133–139], metal oxides [140, 141], metal sulfides [142, 143], and biominerals [144–146]. In most cases, the composite microgels preserve the colloidal stability and maintain the stimuli-responsiveness of the pure microgels. At the same time, the NPs carried by the composite exhibit the typical physical and chemical properties of the nanomaterials themselves.

The incorporation of poly(ethylenedioxy thiophene) (PEDOT) into microgels has been performed in two steps [147]. In the first step, EDOT was added to microgel dispersion. In the second step, the addition of oxidant ($FeCl_3$) starts the oxidative polymerization of EDOT in the system. Figure 19a shows a TEM image of VCL/AAEM microgel particles filled with PEDOT nanorods. The dark spherical areas in Fig. 19a correspond to the microgel core and PEDOT nanorods are located in the microgel shell (light grey regions). The swollen microgel shell provides optimal conditions for the growth of PEDOT nanorods and provides efficient stabilization for the composite microgel particles in continuous medium. The EDX analysis confirmed the presence of sulfur in the microgel shell originating from the PEDOT nanorods (Fig. 19b). The amount of PEDOT nanorods can be increased up to 15 wt%.

The unique property of conjugated polymers to uptake/release the anions upon transformation from oxidized to reduced state can be used for the targeted deposition of NPs. To demonstrate the principal viability of such approach, VCL/AAEM/PEDOT microgels have been used as templates for the incorporation of AuNPs [148]. Figure 20 shows the procedure of AuNP deposition into microgels filled with PEDOT nanorods.

Figure 21 shows STEM images of VCL/AAEM and VCL/AAEM/PEDOT microgels after deposition of AuNPs. Comparing the microscopy images of the two microgel samples, it is obvious that in the case of VCL/AAEM microgel AuNPs are randomly distributed within microgel shell, but in the VCL/AAEM/PEDOT sample AuNPs are located predominantly on the surface of PEDOT nanorods. It is also interesting that the size of the AuNPs is different (3 ± 0.5 nm and 10 ± 1 nm for the VCL/AAEM and VCL/AAEM/PEDOT samples, respectively), which can be explained by the "concentration" of the $[AuCl_4]^-$ anions close to the PEDOT nanorod surface. The inset in Fig. 21d shows an ultrahigh resolution TEM image indicating the alignment of AuNPs on the PEDOT nanorod surface. It can be assumed that the efficient fixation of the metal NPs on the PEDOT nanorods is due to the presence of sulfur in the thiophene ring, famous for its strong affinity to Au^0.

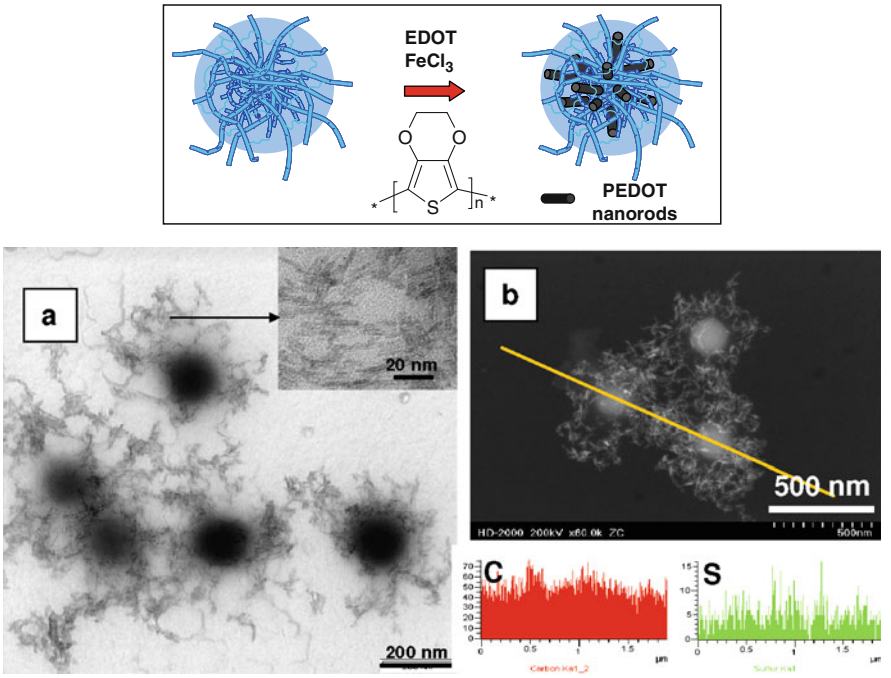

Fig. 19 *Top*: Process of PEDOT incorporation into microgel. (**a**) TEM image of microgel particles filled by PEDOT nanorods. *Inset* shows high-magnification image of PEDOT nanorods embedded into microgel network. (**b**) STEM image of microgel/PEDOT composite particles. *Line* indicates the EDX scan trace. The distribution of C and S along the EDX scan is shown in graphs below. Taken from [147], Copyright Wiley-VCH. Reproduced with permission

Aqueous microgels were modified by hydroxyapatite (HAp) nanocrystals [149]. During the first step, an appropriate amount of $Ca(NO_3)_2$ was dissolved in microgel dispersion and the pH value adjusted to 10 by addition of 25% NH_4OH. In a separate flask, an appropriate $(NH_4)_2HPO_4$ amount was dissolved in water and pH adjusted to 10 by addition of 25% NH_4OH. The $(NH_4)_2HPO_4$ solution was then added under continuous stirring to the microgel dispersion containing dissolved $Ca(NO_3)_2$.

Figure 22a–d shows TEM images of VCL/AAEM/VIm-HAp hybrid microgels containing different amounts of HAp. The HAp needles (aspect ratio 12:15) are located predominantly in the microgel shell and their amount increases with increased HAp content. The incorporation of VIm units into microgel leads to controlled growth of HAp within the microgel, and well-defined hybrid particles can be obtained. The results of EDX line scan presented in Fig. 22e indicate presence of Ca and P in the microgel outer layer, which confirms the effective deposition of HAp.

Gorelikov et al. [150] demonstrated a way to provoke photothermally modulated volume transitions in microgel particles in the near-IR spectral range. Gold nanorods with different aspect ratios (from 2 to 6) stabilized by cationic surfactant were inte-

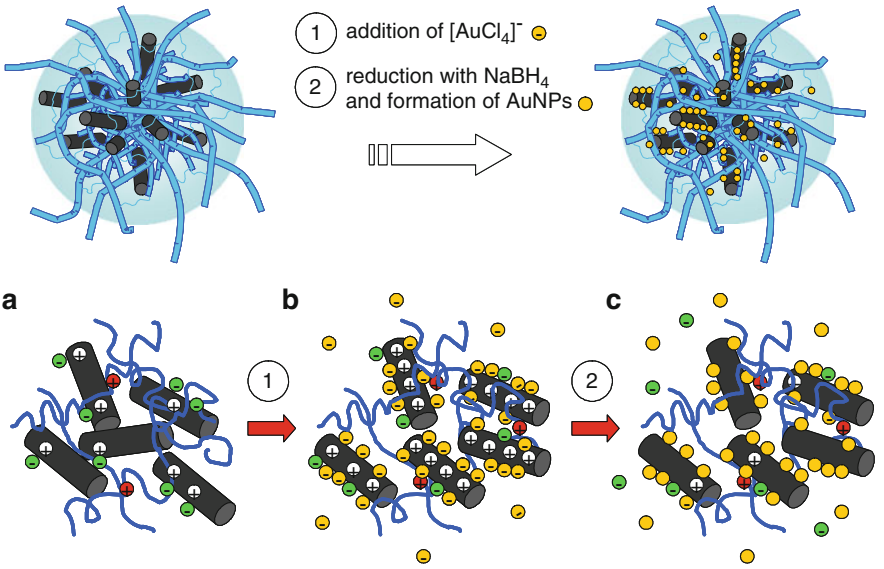

Fig. 20 Selective AuNPs deposition on PEDOT nanorods in microgel structures: (**a**) PEDOT nanorods are not fully oxidized and attract a small amount of counterions (*green circles*). The small amount of positively charged groups (*red circles*) are due to the incorporation of initiator residues into polymer chains of microgel. (**b**) After addition of H^+, $[AuCl_4]^-$ PEDOT nanorods become oxidized in acidic pH and $[AuCl_4]^-$ anions (*yellow circles*) are drawn into the microgel to compensate for a charge on the nanorod surface (*white circles*). (**c**) After addition of $NaBH_4$ and a reduction process, AuNPs are predominantly formed on the PEDOT nanorod surface. Taken from [148], Copyright Wiley-VCH. Reproduced with permission

grated into negatively charged PNIPAAm microgels (the negative charge originated from carboxylic groups) and fixed by electrostatic attraction forces (Fig. 23).

The gold nanorods can absorb near-IR light and the wavelength of their longitudinal surface plasmon can be accurately controlled by altering their aspect ratio. So, when the hybrid microgel was irradiated by laser at wavelength 810 nm, a strong photothermally induced decrease in microgel volume was observed, and the authors demonstrated that this process could be repeated several times by switching the laser on and off.

Surface-modified negatively charged magnetic NPs with grafted PAAc layer were adsorbed on the surface of PNIPAAm microgels modified by adsorbtion of polycations (PDADMAC) [151]. This new hybrid core–shell microgel possesses a unique combination of thermoresponsivity and magnetism that could open up novel prospects for remotely controlled drug carriers.

The methods for the preparation of composite microgels described above require the adjustment of the microgel and NPs (or their syntheses) to the nature of the medium, whether water or an organic solvent. The medium in which the composite microgels are formed using these strategies is normally the only medium in which they are stable and can be employed. This limitation can be overcome by the

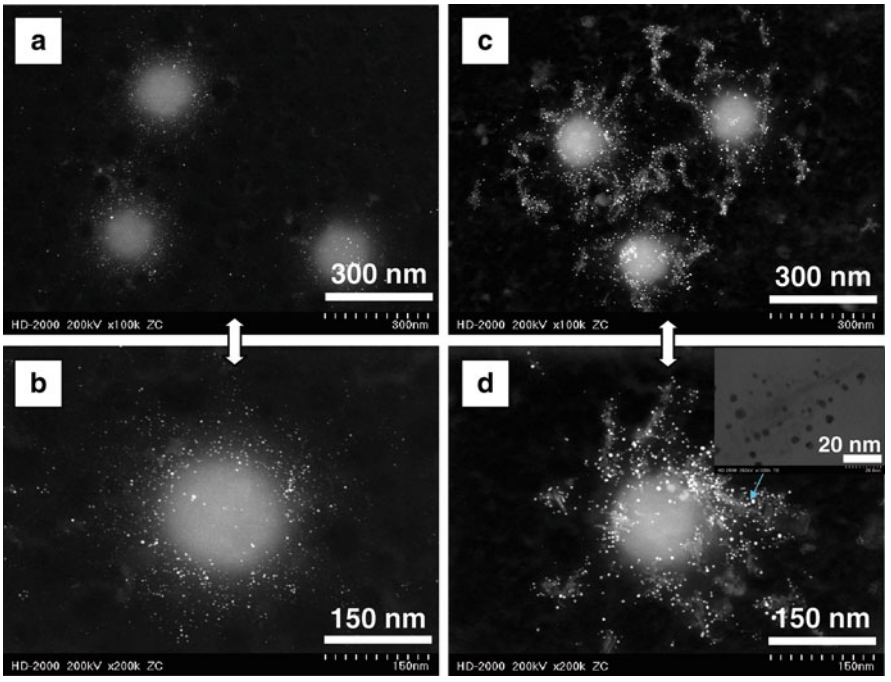

Fig. 21 (**a–b**) STEM images of VCL/AAEM (3 wt% Au) and (**c–d**) VCL/AAEM/PEDOT (9.3 wt% Au) microgels modified with AuNPs (the $HAuCl_4$ to microgel weight ratio was 1:10, solvent water). Taken from [148], Copyright Wiley-VCH. Reproduced with permission

consideration of one important property of the microgel itself, which has not been exploited for microgel–NP composites: the ability of many kinds of microgels to form stable colloidal solutions in solvents of very different polarity. Some authors have noted the nearly universal ability of microgels to form emulsions [152–156] or colloidal solutions in mixed solvents [157]. Little attention has been paid, however, to the possibility of transferring microgels from water to organic solvents or from organic solvents to aqueous media.

Winnik's group [158] demonstrated preparation of inorganic-NP composite microgels based on the reversible transfer of microgels between water and THF as the organic solvent. The working hypothesis was that appropriately chosen microgels can be synthesized to contain functional groups that can serve as surface ligands for the TOPO-stabilized CdSe NPs (quantum dots, QDs). These microgels can capture QDs via a ligand exchange process in an organic medium, where the QDs form colloidal solutions. Then, the composite microgels can be transferred into water, in which the microgel is also able to provide colloidal stability. The authors employed the imidazole group as an amine-based ligand and examined two different polymer microgel compositions as the carriers: PNIPAAm and VCL/AAEM. Both types of microgels were synthesized in the presence of different amounts of VIm (1–5 mol%) as the functional co-monomer.

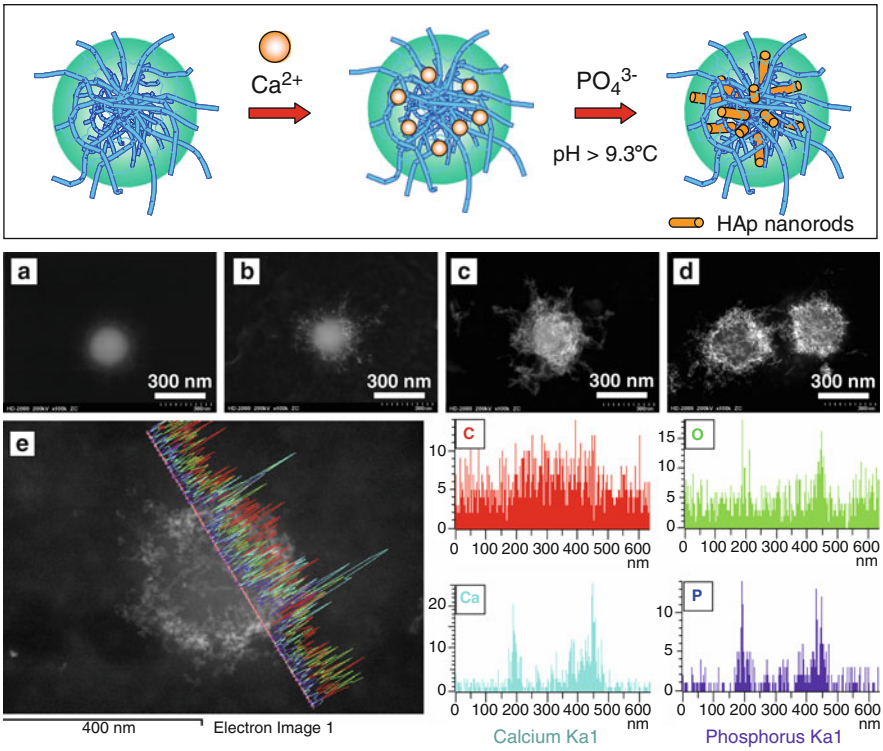

Fig. 22 *Top*: Modification of aqueous microgels by hydroxyapatite (HAp) nanocrystals. (**a–d**) TEM images of VCL/AAEM/VIm-HAp hybrid microgels containing different amounts of HAp: (**a**) 0, (**b**) 7.9, (**c**) 34.2, and (**d**) 52.2 wt%. (**e**) EDX line scan of single microgel containing 52.2 wt% HAp with element distribution curves. *Color of the lines* in (**e**) corresponds to the color in the element distribution spectra. Reprinted from [149] with permission. Copyright 2008 American Chemical Society

The process of QD loading into microgel particles has been monitored by light scattering measurements to check the change in microgel size and size distribution. Figure 24 shows size distribution curves of NIPAAm/VIm and VCL/AAEM/VIm microgels containing similar amount of VIm units. The light scattering results presented in Fig. 24 indicate that no aggregation of the microgel particles occurs during the transfer to THF, NP loading, and transfer back to water. The STEM images in Fig. 24 show the morphology of VCL/AAEM/VIm microgels before and after the NP loading procedure. STEM images indicate homogeneous distribution of NPs within microgel particles after the modification process.

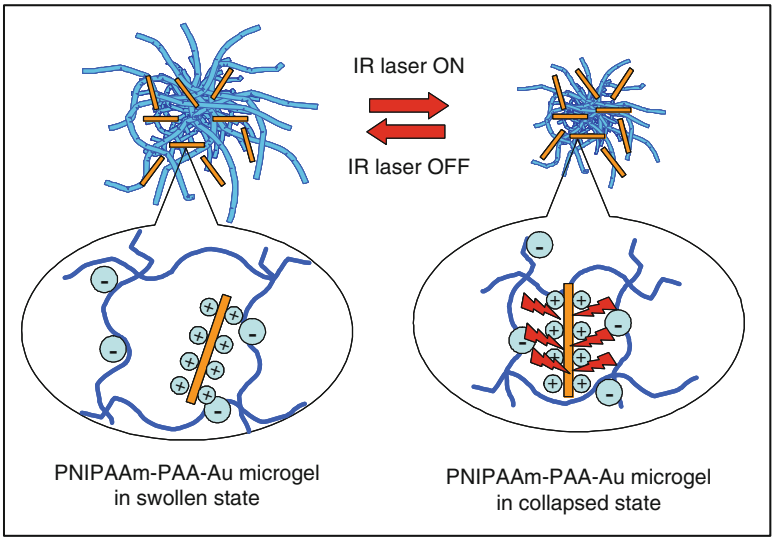

Fig. 23 Photoresponsive hybrid microgels filled with Au-nanorods. Reprinted with permission from [150], Copyright 2004 American Chemical Society

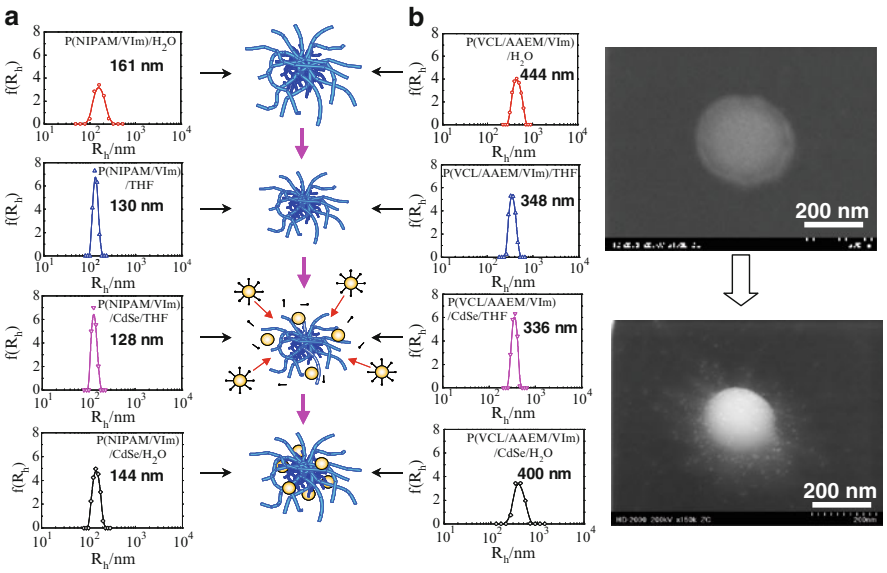

Fig. 24 Hydrodynamic radius distributions $f(R_h)$ of different microgels in each step of the incorporation of TOPO-stabilized CdSe NPs into microgel: *column* (**a**) NIPAM/VIm(2.78%), *column* (**b**) VCL/AAEM/VIm(2.88%). *Right*: TEM images of single VCL/AEM/VIm(2.88%) microgel particle before and after loading with QDs. Taken from [158]

4 Conclusions

The results reviewed herein demonstrate that precipitation polymerization is a powerful technique for the preparation of aqueous microgel particles with defined properties. Precipitation polymerization allows design of microgel particles with controlled size, narrow size distribution, and enhanced colloidal stability. Additionally, a wide range of functional groups can be integrated into the microgel structure. Aqueous microgels synthesized by precipitation polymerization can display sensitivity to temperature, pH, light, ionic strength, etc. Postpolymerization modification reactions allow incorporation of small organic molecules, synthetic polymers, biopolymers, or inorganic NPs into the microgel network.

Acknowledgment The authors thank the Deutsche Forschungsgemeinschaft and VolkswagenStiftung for financial support of their research.

References

1. Park TG, Hoffman AS (1992) J Polym Sci 30:505
2. Pelton R (2000) Adv Colloid Interface Sci 85:1
3. Tauer K, Gau D, Schulze S, Volkel A, Dimova R (2009) Colloid Polym Sci 287:299
4. Hoare T, Pelton R (2008) Curr Opin Colloid Interface Sci 13:413
5. Tan BH, Tam KC (2008) Adv Colloid Interface Sci 136:25
6. Zhang J, Xu S, Kumacheva E (2004) J Am Chem Soc 126:7908
7. Pich A, Adler HJ (2007) Polym Int 56:291
8. Oh JK, Drumright R, Siegwart DJ, Matyjaszewski K (2008) Prog Polym Sci 33:448
9. Saunders BR, Laajam N, Daly E, Teow S, Hu X, Stepto R (2009) Adv Colloid Interface Sci. 147–148:251
10. Nayak S, Lyon LA (2005) Angew Chem Int Ed Engl 44:7686
11. Liu R, Fraylich M, Saunders BR (2009) Colloid Polym Sci 287:627
12. Heskins M, Guillet JE (1968) J Macromol Sci Chem 2:1441
13. Shibayama M, Tanaka T (1993) Adv Polym Sci 109:1
14. Zhou X, Liu B, Yu X, Zha X, Zhang X, Chen Y (2007) J Control Release 121:200
15. Ko JA, Park HJ, Hwang SJ, Park JB, Lee JS (2002) Int J Pharm 249:165
16. Shu XZ, Zhu KJ (2000) Int J Pharm 201:51
17. Xu Y, Du Y (2003) Int J Pharm 250:215
18. Bodnar M, Hartmann JF, Borbely J (2006) Biomacromolecules 7:3030
19. Yun YH, Goetz DJ, Yellen P, Chen W (2004) Biomaterials 25:147
20. Kumbar SG, Kulkarni AR, Aminabhavi TM (2002) J Macroencapsul 19:173
21. Denkbas EB, Seyyal M, Piskin E (1999) J Macroencapsul 16:741
22. Al-Helw AA, Al-Angary AA, Mahrous GM, Al-Dardari MM (1998) J Macroencapsul 15:373
23. Thanoo BC, Sunny MC, Jayakrishnan A (1992) J Pharm Pharmacol 44:283
24. Sankar C, Rani M, Srivastava AK, Mishra B (2001) Pharmazie 56:223
25. Jameela SR, Kumary TV, Lal AV, Jayakrishnan A (1998) J Control Release 52:17
26. Wang LY, Gu YH, Zhou QZ, Ma GH, Wan YH, Su ZG (2006) Colloids Surf B Biointerfaces 50:126
27. Xu S, Nie Z, Seo M, Lewis P, Kumacheva E, Stone HA (2005) Angew Chem Int Ed Engl 44:724
28. Berli CLA, Quemada D, Parker A (2003) Colloids Surf A Physicochem Eng Asp 215:201
29. De Geest BG, Urbanski JP, Thorsen T, Demeester J, De Smedt SC (2005) Langmuir 21:10275

30. Duracher D, Elaissari A, Pichot C (1999) J Polym Sci A Polym Chem 37:1823
31. Hazot P, Chapel JP, Pichot C, Elaissari A, Delair T (2002) J Polym Sci A Polym Chem 40:1808
32. Huang G, Gao J, Hu Z, St John JV, Ponder BC, Moro D J (2004) J Control Release 94:303
33. Hoare T, Pelton R (2004) Langmuir 20:2123
34. Leobandung W, Ichikawa H, Fukumori Y, Peppas NA (2003) J Appl Polym Sci 87:1678
35. Berndt I, Pedersen JS, Lindner P, Richtering W (2006) Langmuir 22:459
36. Boyko V, Pich A, Lu Y, Richter S, Arndt KF, Adler HJ (2003) Polymer 44:7821
37. Sun Q, Deng Y (2005) J Am Chem Soc 127:8274
38. Dowding PJ, Vincent B, Williams E J (2000) Colloid Interface Sci 221:268
39. Braun O, Selb J, Candau F (2001) Polymer 42:8499
40. Fernandez VVA, Tepale N, Sanchez-Diaz JC, Mendizabal E, Puig JE, Soltero JFA (2006) Colloid Polym Sci 284:387
41. Juranicova V, Kawamoto S, Fujimoto K, Kawaguchi H, Barton J (1998) Angew Makromol Chem 258:27
42. Barton J (2002) Macromol Symp 179:189
43. Renteria M, Munoz M, Ochoa JR, Cesteros LC, Katime I (2005) J Polym Sci A Polym Chem 43:2495
44. Gaur U, Sahoo SK, De TK, Ghosh PC, Maitra A, Ghosh PK (2000) Int J Pharm 202:1
45. Bharali DJ, Sahoo SK, Mozumdar S, Maitra A (2003) J Colloid Interface Sci 258:415
46. Groll J, Singh S, Albrecht K, Moeller M J Polym Sci A Polym Chem 47:5543
47. Kuckling D (2009) Colloid Polym Sci 287:881
48. Rolland JP, Maynor BW, Euliss LE, Exner AE, Denison GM, De Simone JM (2005) J Am Chem Soc 127:10096
49. Rolland JP, Hagberg EC, Denison GM, Carter KR, De Simone JM (2004) Angew Chem Int Ed 43:5796
50. Tauer K, Hernandez H, Kozempel S, Lazareva O, Nazaran P (2008) Colloid Polym Sci 286:499
51. Wu X, Pelton RH, Hamjelec AE, Woods DR (1994) Colloid Polym Sci 272:467
52. Pelton RH, Chibante P (1986) Colloids Surf 20:247
53. Gao J, Frisken BJ (2003) Langmuir 19:5212
54. Gao J, Frisken BJ (2003) Langmuir 19:5217
55. Panayiotou M, Pöhner C, Vandevyver C, Wandrey C, Hilbrig F, Freitag R (2007) React Funct Polym 67:807
56. Imaz A, Miranda JI, Ramos J, Forcada J (2008) Eur Polym J 44:4002
57. Kratz K, Lapp A, Eimer W, Helweg T (2002) Colloids Surf A Physicochem Eng Asp 197:55
58. Hazot P, Delair T, Pichot C, Chapel JP, Elaissari A (2003) C R Chimie 6:1417
59. Elmas B, Tuncel M, Senel S, Patir S, Tuncel A (2007) J Colloid Interface Sci 313:174
60. Meng ZY, Smith MH, Lyon LA (2009) Colloid Polym Sci 287:277
61. McPhee W, Tam KC, Pelton R (1993) J Colloid Interface Sci 156:24
62. Nolan CM, Reyes CD, Debord JD, Garcia AJ, Lyon LA (2005) Biomacromolecules 6:2032
63. Meyer S, Richtering W (2005) Macromolecules 38:1517
64. Boyko V, Richter S, Pich A, Arndt KF (2003) Colloid Polym Sci 282:127
65. Snowden MJ, Chowdry BZ, Vincent B, Morris GE (1996) J Chem Soc Faraday Trans 92:5013
66. Kratz K, Helweg T, Eimer W (2000) Colloids Surf A Physicochem Eng Asp 170:137
67. Lally S, Bird R, Freemont TJ, Saunders BR (2009) Colloid Polym Sci 287:335
68. Ni H, Kawaguchi H, Endo T (2007) Colloid Polym Sci 285:819
69. Hoare T, McLean D (2006) J Phys Chem B 110:20327
70. Lpez-Len T, Ortega-Vinuesa JL, Bastos-Gonzlez D, Elaissari A (2006) J Phys Chem B 110:4629
71. Peng S, Wu C (2001) Macromolecules 34:568
72. Boyko V, Richter S, Burchard W, Arndt KF (2007) Langmuir 23:776
73. Debord JD, Lyon LA (2003) Langmuir 19:7662
74. Keerl M, Smirnovas V, Winter R, Richtering W (2008) Macromolecules 41:6830
75. Keerl M, Richtering W (2007) Colloid Polym Sci 285:471

76. Ito S, Ogawa K, Suzuki H, Wang B, Yoshida R, Kokofuta E (1999) Langmuir 15:4289
77. Ogawa K, Nakayama A, Kokufuta E (2003) Langmuir 19:3178
78. Ogawa K, Nakayama A, Kokufuta E (2003) J Phys Chem B 107:8223
79. Nayak SP, Lyon LA (2003) Polymer Prepr 44:679
80. Das M, Kumacheva E (2006) Colloid Polym Sci 284:1073
81. Tan BH, Ravi P, Tam KC (2006) Macromol Rapid Commun 27:522
82. Ni H, Kawaguchi H, Endo T (2007) Macromolecules 40:6370
83. Amalvy JI, Wanless EJ, Li Y, Michailidou V, Armes SP, Duccini Y (2004) Langmuir 20:8992
84. FitzGerald PA, Amalvy JI, Armes SP, Wanless EJ (2008) Langmuir 24:10288
85. Dupin D, Fujii S, Armes SP, Reeve P, Baxter SM (2006) Langmuir 22:3381
86. Yin J, Dupin D, Li J, Armes SP, Liu S (2008) Langmuir 24:9334
87. Laukkanen A, Hietala S, Maunu SL, Tehnu H (2000) Macromolecules 33:8703
88. Pich A, Berger S, Ornatsky O, Baranov V, Winnik MA (2009) Colloid Polym Sci 287:269
89. Singh N, Lyon LA (2008) Colloid Polym Sci 286:1061
90. Pich A, Teissier A, Boyko V, Lu Y, Adler HJ (2006) Macromolecules 39:7701
91. Häntzschel N, Zhang F, Eckert F, Pich A, Winnik MA (2007) Langmuir 23:10793
92. Xu FJ, Cai QJ, Li YL, Kang ET, Neoh KG (2005) Biomacromolecules 6:1012
93. Virtanen J, Baron C, Tenhu H (2000) Macromolecules 33:336
94. Yin X, Stöver HDH (2003) Macromolecules 36:9817
95. Qui X, Sukhishvili S (2006) J Polym Sci A Polym Chem 44:183
96. Suzuki D, Kawaguchi H (2005) Langmuir 21:8175
97. Suzuki D, Kawaguchi H (2005) Langmuir 21:12016
98. Suzuki D, Kawaguchi H (2006) Colloid Polym Sci 284:1443
99. Lapeyre V, Ancla C, Catargi B, Rivaine V (2008) J Colloid Interface Sci 327:316
100. Li X, Guo Y, Yuan X (2004) Macromolecules 37:10042
101. Bradley M, Vincent B (2008) Langmuir 24:2421
102. Berndt I, Richtering W (2003) Macromolecules 36:8780
103. Berndt I, Pedersen JS, Richtering W (2005) J Am Chem Soc 127:9372
104. Berndt I, Popescu C, Wortmann FJ, Richtering W (2006) Angew Chem Int Edit Engl 45:1081
105. Berndt I, Pedersen JS, Richtering W (2006) Angew Chem Int Ed Engl 45:1737
106. Chen Q, Xu K, Zhang W, Song C, Wang P (2009) Colloid Polym Sci 287:1339
107. Guo XY, Lu TH, Huang XH (2008) Colloid Polym Sci 286:469
108. Crassous JJ, Wittemann A, Siebenburger M, Schrinner M, Drechsler M, Ballauff M (2008) Colloid Polym Sci 286:805
109. Pich A, Zhang F, Shen L, Berger S, Ornatsky O, Baranov V, Winnik MA (2008) Small 4:2171
110. Zhang Q, Zha L, Ma J, Liang B (2007) Macromol Rapid Commun 28:116
111. Pich A, Berger S, Singh R, Sudha JD, Adler H-J Polymer (submitted)
112. Häntzschel N, Schrinner M, Hund H, Hund RD, Lück C, Pich A (2009) Macromol Biosci. 9:444
113. Garcia A, Marques M, Cai T, Rosario R, Hu Z, Gust D, Hayes M, Vail SA, Park CD (2007) Langmuir 23:224
114. Xu J, Pelton R (2004) J Colloid Interface Sci 276:113
115. Cheng C, Zhu X, Pich A, Möller M (2010) Langmuir 26:4709
116. Greinert N, Richtering W (2004) Colloid Polym Sci 282:1146
117. Wong JE, Diez-Pascual AM, Richtering W (2009) Macromolecules 42:1229
118. Kleinen J, Richtering W (2008) Macromolecules 41:1785
119. Hu T, You Y, Pan C, Wu C (2002) J Phys Chem B 106:6659
120. Su S, Monsur ali Md, Filipe CDM, Li Y, Pelton R (2008) Biomacromolecules 9:935
121. Delair T, Meunier F, Elaissari A, Charles MH, Pichot C (1999) Colloids Surf A Physicochem Eng Asp 153:341
122. Zhang J, Xu S, Kumacheva E (2004) J Am Chem Soc 126:7908
123. Antonietti M, Grohn F, Hartmann J, Bronstein L (1997) Angew Chem Int Ed Engl 36:2080
124. Biffis A, Orlandi N, Corain B (2003) Adv Mater 15:1551
125. Kuang M, Yang D, Bao H, Gao M, Möhwald H, Jiang M (2005) Adv Mater 17:267
126. Gong Y, Gao M, Wang D, Möhwald H (2005) Chem Mater 17:2648

127. Mrkic J, Saunders BR (2000) J Colloid Interface Sci 222:75
128. Pich A, Lu Y, Adler HP, Schmidt T, Arndt K (2002) Polymer 43:5723
129. Pich A, Lu Y, Boyko V, Arndt KF, Adler HJP (2003) Polymer 44:7651
130. Pich A, Lu Y, Boyko V, Richter S, Arndt K, Adler HP (2004) Polymer 45:1079
131. Lopez-Cabarcos E, Mecerreyes D, Sierra-Martin B, Romero-Cano MS, Strunz P, Fernandez-Barbero A (2004) Phys Chem Chem Phys 6:1396
132. Rubio Retama J, Lopez Cabarcos E, Mecerreyes D, Lopez-Ruiz B (2004) Biosens Bioelectron 20:1111
133. Sharma G, Ballauff M (2004) Macromol Rapid Comm. 25:547
134. Mei Y, Sharma G, Lu Y, Ballauff M, Drechsler M, Irrgang T, Kempe R (2005) Langmuir 21:12229
135. Lu Y, Mei Y, Drechsler M, Ballauff M (2006) Angew Chem Int Ed Engl 45:813
136. Suzuki D, Kawaguchi H (2005) Langmuir 21:12016
137. Zhang J, Xu S, Kumacheva E (2005) Adv Mater 17:2336
138. Pich A, Karak A, Lu Y, Ghosh A, Adler HJP (2006) Macromol Rapid Commun 27:344
139. Biffis A, Orlandi N, Corain B (2003) Adv Mater 15:1551
140. Gao M, Peng X, Shen J (1994) Thin Solid Films 248:106
141. Menager C, Sandre O, Mangili J, Cabuil V (2004) Polymer 45:2475
142. Bai C, Fang Y, Zhang Y, Chen B (2004) Langmuir 20:263
143. Pich A, Hain J, Lu Y, Boyko V, Prots Y, Adler H (2005) Macromolecules 38:6610
144. Nassif N, Gehrke N, Pinna N, Shirshova N, Tauer K, Antonietti M, Cölfen H (2005) Angew Chem 117:6158
145. Zhang G, Wang D, Gu Z, Hartmann J, Möhwald H (2005) Chem Mater 17:5268
146. Zhang G, Wang D, Gu Z, Möhwald H (2005) Langmuir 21:9143
147. Hain J, Eckert F, Pich A, Adler HJ (2008) Macromol Rapid Commun 29:472
148. Hain J, Lu Y, Schrinner M, Pich A (2008) Small 4:2016
149. Schachschal S, Pich A (2008) Langmuir 24:5129
150. Gorelikov I, Field LM, Kumacheva E (2004) J Am Chem Soc 126:15938
151. Wong JE, Gaharwar AK, Muller-Schulte D, Bahadur D, Richtering W (2007) J Magn Magn Mater 311:219
152. Fujii S, Read E S, Binks BP, Armes S P (2005) Adv Mater 17:1014
153. Ngai T, Behrens SH, Auweter H (2005) Chem Commun 3:331
154. Ngai T, Behrens SH, Auweter H (2006) Macromolecules 39:8171
155. Fujii S, Armes S P, Binks BP, Murakami R (2006) Langmuir 22:6818
156. Koh AYC, Saunders BR (2005) Langmuir 21:6734
157. Crowther HM, Vincent B (1998) Colloid Polym Sci 276:46
158. Shen L, Pich A, Fava D, Wang M, Kumar S, Wu C, Scholes GD, Winnik MA (2008) J Mater Chem 18:763

Adv Polym Sci (2010) 234: 39–63
DOI:10.1007/12_2010_68

Published online: 17 June 2010

Hydrogels in Miniemulsions

Katharina Landfester and Anna Musyanovych

Abstract In the last decade, the synthesis of polymeric materials that respond to specific environment stimuli by changing their size has attracted widespread interest in both fundamental and applied areas of research. Hydrogels in dispersions are composed of randomly oriented, physically or chemically crosslinked hydrophilic or amphiphilic polymer chains. The synthesis of these gels at the nanoscale (nanogels or microgels) is especially of great importance for their application in drug delivery and controlled release systems, and in biomimetics, biosensing, tissue regeneration, heterogeneous catalysis, etc. The focus of this review is to present the versatility of the miniemulsion process for the formation of monodisperse nanogels from synthetic and natural polymers. Several applications of the obtained microgels are briefly described.

Keywords Confined reaction environment · Heterophase polymerization · Microgels · Miniemulsion · Nanocapsules · Nanoparticles

Contents

K. Landfester (✉) and A. Musyanovych
Max Planck Institute for Polymer Research, Ackermannweg 10,
55128 Mainz, Germany
e-mail: landfester@mpip-mainz.mpg.de; musyanovych@mpip-mainz.mpg.de

1 Miniemulsion Polymerization

"Miniemulsion" generally implies a method that allows one to create small stable droplets in a continuous phase by applying high shear stress [1]. Under high shear, e.g. ultrasonication or high-pressure homogenization, broadly distributed (macro)droplets are broken into narrowly distributed, defined small nanodroplets in the size range between 50 and 500 nm. The size of the droplets mainly depends on the type and the amount of the emulsifier used in the particular system. The idea of miniemulsion polymerization is to initiate the polymerization in each of the small stabilized droplets, meaning that polymerization takes place in small nanodroplets. To prevent the degradation of miniemulsion through coalescence or Ostwald ripening, an efficient surfactant and a costabilizer that is highly soluble in the dispersed phase, but insoluble in the continuous phase, should be employed in order to prevent Ostwald ripening. Typically, long-chain alkanes and alcohols as (ultra)hydrophobes have been used a costabilizers for direct (oil-in-water) miniemulsion. In Fig. 1 the process of direct (oil-in-water) miniemulsion polymerization is presented.

The principle of miniemulsion may also be extended to the inverse (water-in-oil) case, in which the Ostwald ripening is suppressed by an agent that is insoluble in the continuous oily phase, a so-called lipophobe. Ionic compounds (e.g., salts or sugars) show a low solubility in organic solvents and can be used as lipophobes,

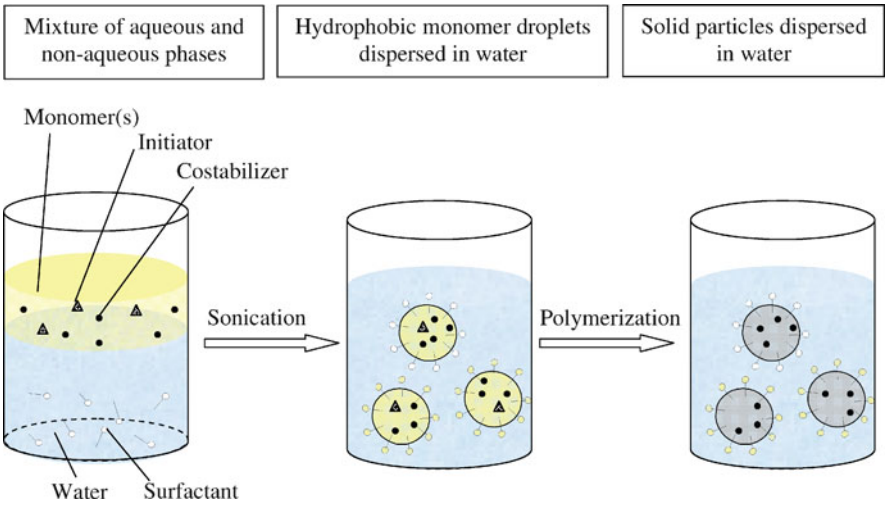

Fig. 1 Synthesis of polymeric nanoparticles from hydrophobic monomers(s) via the direct miniemulsion process

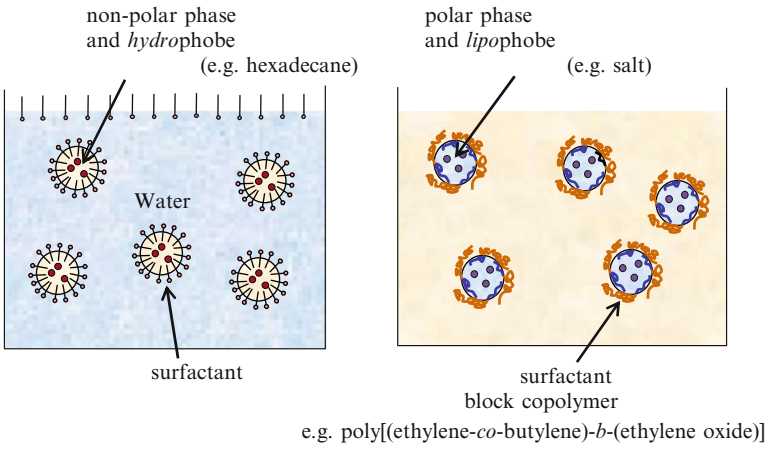

Fig. 2 Comparison between direct (*left*) and inverse (*right*) miniemulsion

and therefore act as costabilizers in water-in-oil miniemulsions [2]. Due to the change of the continuous phase from hydrophilic to hydrophobic, surfactants with low hydrophilic–lipophilic balance (HLB) values are required. Owing to the polymeric and steric-demanding nature, the nonionic block copolymer stabilizers, like poly(ethylene-*co*-butylene)-*b*-poly(ethylene oxide) [P(E/B-*b*-EO)], (which consists of hydrophilic and hydrophobic blocks), are the most efficient [2]. They provided maximal steric stabilization, which is the predominant mechanism in inverse emulsions. In the case of CO_2 miniemulsions, block copolymers with a hydrophilic block and a fluoro- or silicon-containing block like poly(1,1-dihydroperfluorooctyl methacrylate)-*b*-poly(ethylene oxide) (PFOMA-*b*-PEO) have to be utilized [3]. Figure 2 compares direct and inverse miniemulsion systems.

2 Polymerization of Hydrophilic Monomers in Inverse Miniemulsion

In inverse (water-in-oil) miniemulsions, hydrophilic monomers can easily be polymerized. Here, the monomer or the monomer solution is miniemulsified in a continuous hydrophobic phase. The polymerization can be initiated either from the droplet or from the continuous phase. Using crosslinking agent(s) in the monomer mixture leads to the formation of microgel nanoparticles after polymerization, keeping their identity after transferring them into water as continuous phase. This way, nanoparticles based on acrylic acid, acrylamide (AAm) and HEMA could successfully be obtained (see Fig. 3) [2].

As a new approach to the preparation of water-soluble polymers in inverse miniemulsions, a redox initiation system consisting of ceric ions and carbohydrate-based surfactant Span 60 as a reducing agent has been successfully used for the

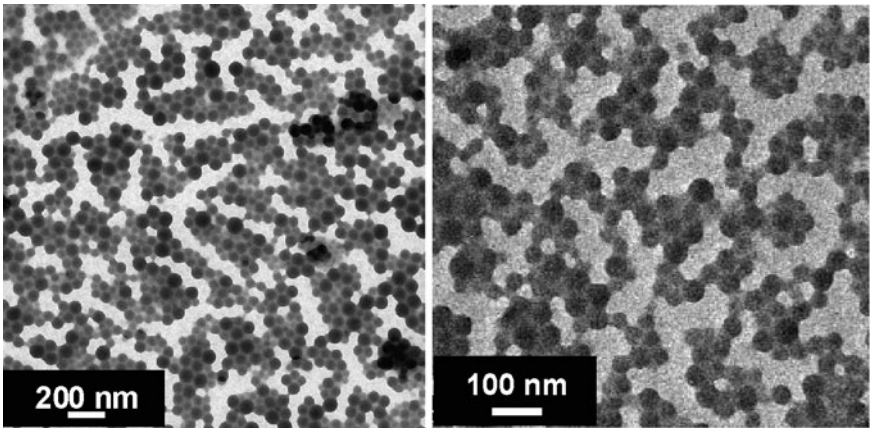

Fig. 3 TEM micrograph of polyacrylamide (*left*) and poly(acrylic acid) (*right*) nanoparticles as obtained by the inverse miniemulsion process

polymerization of AAm. Such an initiation system provides chain nucleation and growth near to interfacial boundaries. As a result, stable uniform polyacrylamide (PAAm) latexes with particle radius of about 50–70 nm are obtained. The prepared PAAm has rather high M_w of up to about 2×10^6 Da. A homogeneous crosslinking, and therefore the formation of microgel nanoparticles, can be obtained by using 2 mol% of N,N'-methylene-bis-acrylamide as a crosslinking agent.

3 Gelatin Nanoparticles

As a different approach, preformed hydrophilic polymers in aqueous solution can also be used for the miniemulsification process. In this case, the formulation process should be carried out in an inverse miniemulsion with a hydrophobic continuous phase. In order to obtain microgel nanoparticles, the polymer chains have to be crosslinked in the inverse miniemulsion prior to the transfer to an aqueous continuous phase. As a nice example, gelatin has been used for the formation of microgel nanoparticles [4].

Gelatin is a proteinaceous polyampolytic gel obtained by the partial hydrolysis (acidic or basic) of collagen. Depending on the process used, gelatin is produced as type-A or type-B gelatin. Whereas the acidic treatment yields type-A gelatin with an isoelectric point (pI) around 9 and a broad molecular weight profile, the alkaline hydrolysis yields type-B gelatin with a pI of around 5 [5, 6]. Due to its chemical and physical nature, gelatin is often used as drug carrier system. By changing the pH or the temperature, the phase behavior of gelatin in solution changes significantly. At low temperatures (around 20°C) and pH 7, the gelatin chains are physically crosslinked, leading to a gel. At high temperature (above 40°C) and pH above 7, the

physical crosslinks break and the gelatin becomes soluble in water. However, chemical crosslinkage results in the formation of a temperature- and pH-independent material, and therefore enables the formation of a microgel.

The different functional groups in the chain allow the incorporation of more functionalities and the introduction of modifications by chemical derivatization. Poly(ethylene glycol)-modified gelatin [7, 8], thiolated derivatives of gelatin [9, 10], chitosan-conjugated gelatin [11], and poly(D,L-lactide)-grafted gelatin [12], have been reported as gelatin-based derivatives for potential pharmaceutical applications. Gelatin-DNA nanospheres as gene delivery vehicles have also been reported [13]. Gelatin can also be used as a matrix for mineralization processes in tissue engineering [14]. The use of gelatin nanoparticles as microgel reactors allows potential application for the release of a variety of different components. However, for this purpose, the gelatin has to be crosslinked chemically in order to keep the nanoparticulate structure at elevated temperature or at low pH.

Several techniques have been used to synthesize gelatin nanoparticles from gelatin and gelatin derivatives. Well-established techniques are desolvation [15–19], coacervation [20–22], and water-in-oil emulsion techniques [23–25]. The flexibility offered by these techniques in tailoring the properties of the nanoparticles is limited. With increasing gelatin concentration and by using a gelatin having a broad molecular weight distribution, it is not possible to effectively and uniformly achieve high gelatin content within the particles. In the desolvation technique, the final particle yield constitutes about only 70–75% of the original amount of gelatin used. As much as 40% of free gelatin chains were still present, irrespective of the amount of crosslinker used [16]. The coacervation and desolvation techniques are both based on phase separation during the preparation step; the crosslinking step is performed after phase separation, when the nanoparticles are already formed and gelatin chains are no longer in the dissolved state. Due to problems with diffusion of the crosslinker molecules into the interior of the nanoparticles, crosslinking only occurs at the surface, and the chains in the interior are not crosslinked. This results in inhomogeneous crosslinking of the nanoparticles with free polymer chains. Among the water-in-oil emulsion techniques, the emulsifier-free water-in-oil approach leads to relatively large particles with an average size of 840 nm [23]. The use of the water-in-oil microemulsion approach in order to obtain smaller particles, however, demands a large excess of surfactant – the ratio of gelatin to surfactant can be as high as 1:1600 [25]. The degree of crosslinking with increasing gelatin concentration and scalability to industrial production are often limited.

In order to overcome the aforementioned problems in producing uniformly glutaraldehyde-crosslinked gelatin nanoparticles with high degrees of crosslinking, a convenient synthetic route based on the concept of nanoreactors (individual nanosized homogeneous entities) using the miniemulsion technique has been used [1, 26].

The miniemulsion technique is here a straightforward approach because it does not rely on phase separation and offers the flexibility of easily varying the gelatin content and the degree of crosslinking using small amounts of surfactant [4]. For the preparation of homogeneously crosslinked nanoparticles, a gelatin solution is

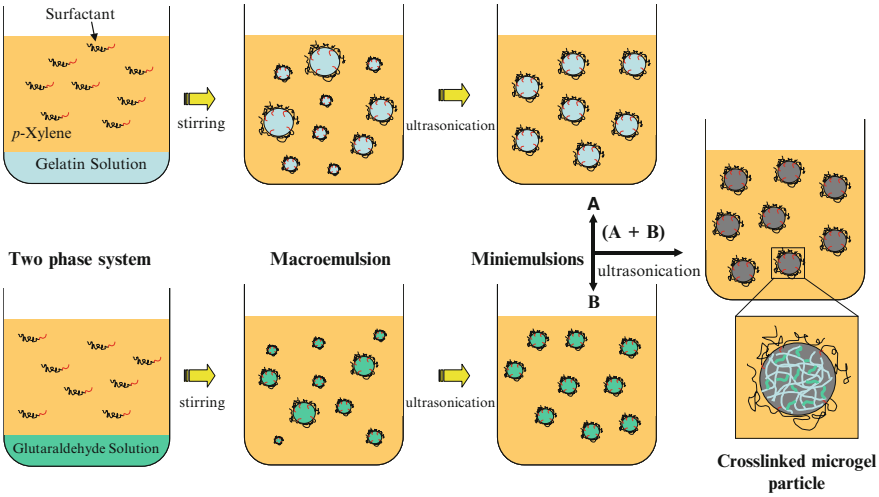

Fig. 4 The inverse miniemulsion process for synthesis of crosslinked gelatin nanoparticles (for details see text) [4]

miniemulsified at elevated temperature in a hydrophobic continuous phase, resulting in a stable inverse miniemulsion [4]. By adding a second inverse miniemulsion consisting of droplets with the crosslinking agent glutaraldehyde, the crosslinking reaction can be performed by a fission and fusion process between the different droplet species (see Fig. 4). The technique allows one to use different types of gelatin without purification or fractionation, and the amount of the gelatin in the droplet and the degree of crosslinking can be varied over a wide range. However, it is of interest to use a minimum concentration of crosslinking agent, at which all chains are crosslinked and no free chains are left behind within the particles. It has been demonstrated that, independent of the molecular weight distribution of the gelatin used, stable nanoparticles can be produced with a small amount of surfactant (see Fig. 4 left). After the synthesis, the organic solvent can be removed and the particles transferred to an aqueous continuous phase. The stability of the dispersion, particle size, and the efficiency of crosslinking (by analyzing the non-crosslinked free chains) have been studied in detail. As gelatin can undergo the volume transition induced by temperature, the swelling behavior of the gelatin particles can be seen when the nanoparticles in water are subjected to a thermal cycle in which the temperature changes between 20°C and 45°C. At 20°C, swollen hydrogel with water present in the channels/pores between the networks is detected. Increasing the temperature to 45°C leads to a loss of the physical crosslinks, resulting in an increase in particle size.

Such microgel nanoparticles with varying gelatin concentration and crosslinking density have a high potential for use in drug delivery applications. The gelatin nanoparticles can also be used as template particles for the formulation of apatite

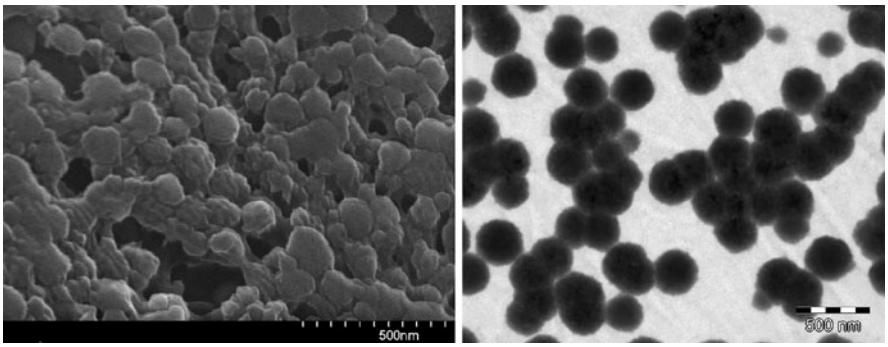

Fig. 5 Air-dried gelatin particles using HRSEM (*left*) [4]. Bright field TEM image of hybrid gelatin nanoparticles (*right*) [27]

nanocrystals [27]. Here, it could be shown that the nano-environment promotes a different growth environment for the crystal due to the confinement inside the hydrogel particle. The formation of hydroxyapatite (HAP) inside the particles follows Ostwald's rule of stages. At first an amorphous phase is formed, which itself has a great potential to be used as a resorbable bone substitute. This further transforms into single crystalline HAP via an octacalcium phosphate intermediate. The solution-mediated transformation into the HAP phase without any calcination step has been studied in detail using transmission electron microscopy (TEM) (see Fig. 5 right) and X-ray diffraction (XRD) measurements.

4 Gels for Release

Smart or stimulus-responsive polymer gels undergo sharp, often jump-wise, volumetric transitions under small changes of external conditions, such as ionic strength, pH, temperature, the action of electric current, mechanical force, etc. [28–30]. These features of smart gels make them increasingly attractive for biotechnology and medicine, as well as for the development of new devices, for example, artificial muscles [31]. The incorporation of diverse particles in the gels often imparts new properties. Gels with entrapped magnetic particles are responsive to a magnetic field [32], and gels containing clays have improved mechanical and adsorption properties [33, 34]. Gels having isolated pores filled with water effectively trap linear macromolecules [35] and low molecular weight multicharged ions [36].

A series of gels with incorporated emulsions have been obtained recently [37]. These gels were used for the preparation of polyelectrolyte gels containing voids [36], in particular, gels with voids having charged walls [38]. It was demonstrated that composite gels that contain entrapped emulsions are effective absorbers of oil-soluble organic substances [39]. Such gels are expected to be of significant practical interest as effective drug delivery systems. The polymer matrix of

similar composite gels can be formed either by the network of crosslinked synthetic polymers (e.g., PAAm [36]) or by physical gels (e.g., agarose-based gels [39]). It was shown that such composites containing entrapped emulsions of water-insoluble hydrocarbons like tetradecane (TD) are very stable and do not release the "oily phase" for at least several months. However, PAAm- and agarose-based gels are not "smart" in the sense that they do not markedly change their swelling degree under changed external conditions, as do poly(*N*-isopropylacrylamide) (PNIPAM) gels. "Smart" thermo-responsive composite PNIPAM gels and cryogels, both containing entrapped TD emulsions, were prepared by three-dimensional free-radical copolymerization of NIPAM and *N*,*N*′-methylene-bis-acrylamide or bis(acryloyl)cystamine, respectively, in the presence of a dispersion of TD stabilized with sodium dodecyl sulfate (SDS). The polymerization of PNIPAM gels was carried out at room temperature, and cryogels were fabricated in a moderately frozen reaction system below the water crystallization temperature. The latter technique is known to produce macroporous gels with labyrinth-like interconnected gross pores [40]. Both composite gels and cryogels thus obtained were capable of heat-induced collapse at certain critical temperatures. It was found that the extent of the collapse of the composite gel prepared at room temperature was much smaller and without visible squeezing of the liquid lipophilic phase out of the shrunk gel.

5 Hyperbranched Polymers in Miniemulsion

As a basis for hydrogels, hyperbranched polymers [41] can also be used. These polymers can be connected by "click" chemistry in miniemulsion droplets in order to obtain hyperbranched polyglycerol (HPG)-based particles. Such materials are of great interest for drug release because they are nontoxic [42, 43] and show similar behavior to poly(ethylene glycol)s.

Due to the inherent dendritic topology, hyperbranched polymers are of interest for a wide range of optical [44], medical [45–47], materials, and reagent immobilization applications [48]. Compared to perfect dendrimers, the synthesis of hyperbranched polymer is much easier to achieve. The first HPGs were reported by Vandenberg in the 1980s. He used the anionic polymerization of glycidol, resulting in relatively monodisperse, highly branched products with a controlled molecular weight in the range of a few thousand Daltons [49, 50]. Recently, Brooks extended this approach to HPGs with up to 1 MDa molecular weight by conducting the polymerization in bulk heterophase using a nonsolvent (dioxane) as an emulsifying agent [51]. The resulting HPGs are very compact and have spherical conformations in water with a diameter in the order of about 10 nm.

By utilizing polymerization in the miniemulsion system, larger HPG analogues can be created by linking several HPG units to a nanoparticle in order to obtain an optimum diameter of 50 nm [116]. This size range is considered to be ideal for drug delivery carriers that may accumulate in tumors or inflamed tissue by the enhanced permeation and retention effect (EPR) [52].

The majority of reported miniemulsion reactions are between low molecular weight monomers, giving rise to linear polymers via radical or polyaddition processes. The crosslinking of the hyperbranched polymer represents an approach to the crosslinking of existing (2–3 nm diameter, $M_n \approx 5$ KDa) HPG dendritic macromonomers to higher homologues, using the "nanoreactor" template to control size. For this, as facile crosslinking "click" reaction, the Huisgen alkyne/azide cycloaddition was used [53–56]. A similar approach has been reported recently with miniemulsion atom transfer radical polymerization (ATRP) crosslinking of macromoners by Oh et al. [57]. The Huisgen reaction has been used in macroemulsion to crosslink dextran macromonomers, but this approach has not yet been realized in miniemulsion [58]. Therefore, the "click" chemistry concept has been utilized in order to polymerize highly branched polyvalent macromonomers in miniemulsion, resulting in dendritic nanoparticle covalent aggregates. Dynamic light scattering (DLS) and TEM characterize the formation of HPG-based particles with a narrow size distribution that is tunable between 25 and 85 nm diameter.

For the formulation of hydrophobic nanoparticles, hydrophobic HPG was dissolved in chloroform and then this solution was miniemulsified in water using SDS as surfactant (see Fig. 6a). The crosslinking reaction was performed by $CuSO_4$ and sodium ascorbate. Hydrophilic nanoparticles of the hyperbranched polymer were obtained in an inverse miniemulsion system by dissolving the polymer in DMF and miniemulsifying the solution in cyclohexane using the block copolymer P(E/B-*b*-EO) as surfactant (see Fig. 6b). After the crosslinking reaction performed at 80°C, the obtained particles could be transferred into an aqueous phase.

Due to the presence of the "click" substrates on the particle surface it is possible to perform further functionalization directly on the surface.

6 Amphiphilic Copolymers

The formation of amphiphilic copolymers consisting of hydrophilic and hydrophobic monomer units leads to hydrogel structures. Amphiphilic copolymers consist of polar and nonpolar monomeric units and are able to stabilize diverse interfaces in aqueous systems. Due to the different polarities, such systems are, however, not easy to make and it is still a great challenge to control the relative incorporation of each monomer in the resulting polymer chain, as well as the homogeneity of the obtained structures. Radical copolymerization reactions in solvents like dimethyl formamide or butanone allows the preparation of some amphiphilic copolymers that can also be suitable for the formation of hydrogels [59, 60]. However, due to solubility problems, the limited range of accessible polymers and control of the monomer sequence are major problems.

Therefore, another idea is the synthesis of amphiphilic systems via radical polymerization using a two-phase or heterophase starting situation. In principle, these techniques allow the kinetic control of the copolymer structures or monomer sequence of the polymer chain. The final polymer chain is not only defined by the

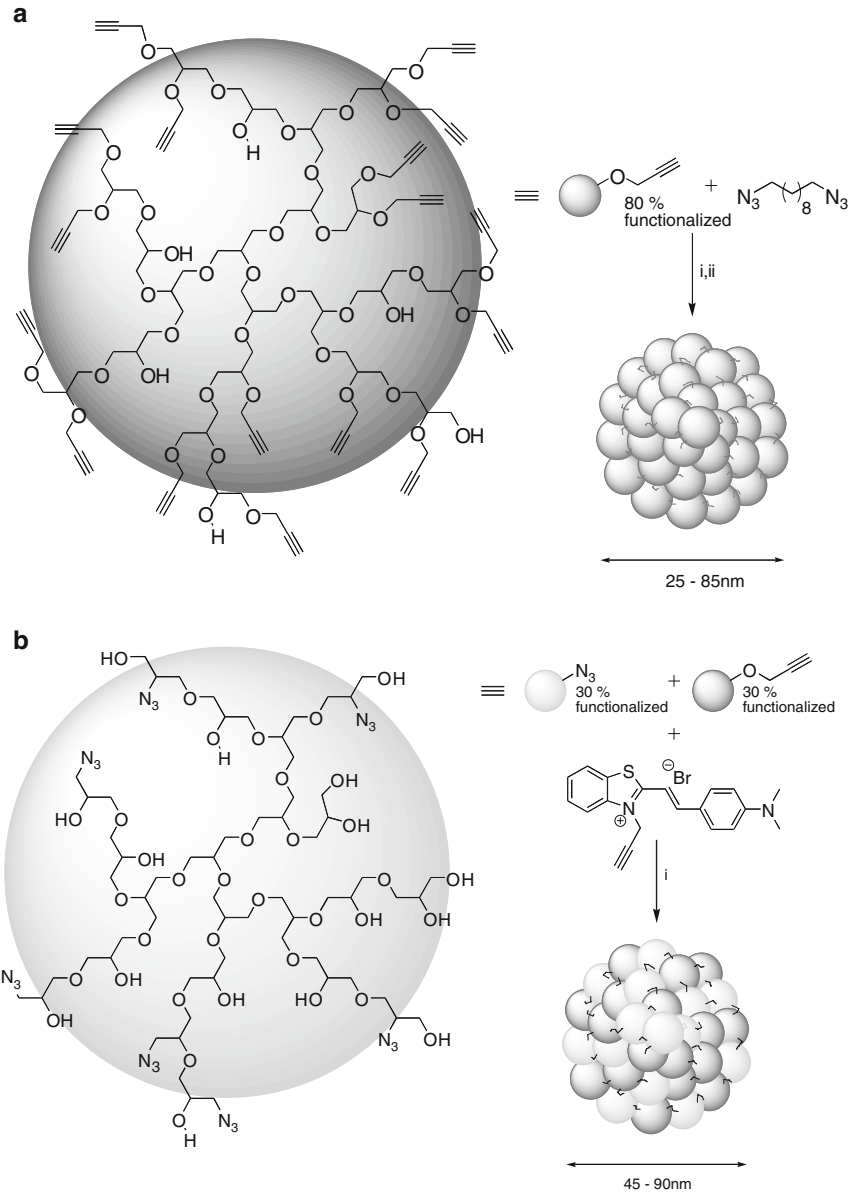

Fig. 6 (**a**) Procedure employed for the formation of hydrophobic nanoparticles carried out in direct miniemulsion: (*i*) the hyperbranched polymer dissolved in $CHCl_3$ is miniemulsified in continuous phase consisting of H_2O and SDS, (*ii*) catalytic amounts of $CuSO_4$ or sodium ascorbate are added, and the reaction mixture stirred for 3 h at 60°C, followed by reaction for 16 h at room temperature. (**b**) Procedure employed for the formation of hydrophilic nanoparticles carried out in inverse miniemulsion: (*i*) the hyperbranched polymer dissolved in DMF is miniemulsified in a continuous phase consisting of cyclohexane and P(E/B-*b*-EO) as surfactant, followed by reaction at 80°C for 16 h [116]

copolymerization parameters, but also by the locus of polymerization and its change throughout the reaction. Using the techniques of microemulsion and micellar polymerization, one creates a large interface area between the hydrophobic and the hydrophilic sites where polymerization between two polarities can occur. The most remarkable effect of copolymerizations in microemulsions is the improvement of structural homogeneity, even for monomers that are not suitable for copolymerization in solution or emulsion. Monomers of very different hydrophilicities can now be successfully copolymerized. With higher amounts of the hydrophilic monomer, hydrogel materials could be obtained. In microemulsion, the comonomers are preferably oriented towards the water–oil interface, and charge effects are shielded that way. Kaler et al. [61] studied the copolymerization of styrene and acrylic acid in a cationic microemulsion. In this case, isolated acrylic acid units were randomly distributed among polystyrene blocks.

To synthesize water-soluble or swellable copolymers, inverse heterophase polymerization processes are of special interest. The inverse macroemulsion polymerization is only reported for the copolymerization of two hydrophilic monomers. Hernandez-Barajas and Hunkeler [62] investigated the copolymerization of AAm with quaternary ammonium cationic monomers in the presence of block copolymeric surfactants by batch and semi-batch inverse emulsion copolymerization. Glukhikh et al. [63] reported the copolymerization of AAm and methacrylic acid using an inverse emulsion system. Amphiphilic copolymers from inverse systems are also successfully obtained in microemulsion polymerization. For example, Vaskova et al. [64–66] copolymerized the hydrophilic AAm with more hydrophobic methyl methacrylate (MMA) or styrene in a water-in-oil microemulsion initiated by radical initiators with different solubilities in water. However, not only copolymer, but also homopolymer was formed. The total conversion of MMA was rather limited ($<10\%$) and the composition of the copolymer was almost independent of the comonomer ratio. This was probably due to a constant molar ratio of the monomers in the water phase or at the interface as the possible locus of polymerization. Also, in the case of styrene copolymerizing with AAm, the molar fraction of AAm in homopolymer compared to copolymer is about 45–55 wt% [67], which is still too high for a meaningful technical application.

Corpart and Candau [68, 69] described the formulation of polyampholytes containing both positive and negative charges in inverse microemulsions. The copolymers can show very different behaviors in the aqueous solution, ranging from insoluble, water-swollen hydrogels to water-soluble compounds, depending on the monomer composition. For polyampholytes with balanced stoichiometry, the polymer behavior is controlled by attractive electrostatic forces. The compound is usually insoluble in water, but becomes soluble upon the addition of salt.

It could be shown that miniemulsion polymerization is a very suitable method for synthesis of amphiphilic copolymer of high homogeneity and for control of the primary sequence [117]. Both direct and inverse miniemulsions can be formed by placing the same monomers in the dispersed or continuous phase, reciprocally. The high interfacial area of miniemulsions is expected to stimulate the change of the growing radical from one phase to the other and, therefore, the formation of copoly-

mers is possible. Finally, in comparison to microemulsion, miniemulsion can be formed with much less surfactant, which is of high interest for the direct application of the resulting copolymers. This is what also makes miniemulsions very promising for the generation of amphiphilic copolymers.

The polymerization process of two monomers with different polarities was carried out in direct or inverse miniemulsions using the monomer systems AAm/MMA and acrylamide/styrene (AAm/Sty). The monomer, which is insoluble in the continuous phase, is miniemulsified in the continuous phase water or cyclohexane in order to form stable and small droplets with a low amount of surfactant. The monomer with the opposite hydrophilicity dissolves in the continuous phase (and not in the droplets). Starting from those two dispersion situations, the locus of initiation (in one of the two phases or at the interface) was found to have a great influence on the reaction products and on the quality of the obtained copolymers, which can act as hydrogels.

In the AAm/MMA system, the best copolymer with respect to low content of homopolymers, low blockiness, and good redispersibility in polar and nonpolar solvents was obtained in inverse miniemulsion with initiation in the continuous phase cyclohexane (see Fig. 7). In this case, the MMA chains grow in the continuous phase until they become insoluble and precipitate onto the AAm droplets, which enable the radicals to cross the interface. AAm units can then be added to the polymer chain.

In the AAm/Sty system, the best copolymer was also obtained in the inverse miniemulsion process, but using interfacial initiation. This leads to almost homopolymer-free copolymer samples with low blockiness, indicating a fast change of the growing radical between the phases in order to add Sty and AAm units. A copolymerization in the direct miniemulsion with water as continuous phase, using the interfacial initiator PEGA200, results in a higher homo-AAm content. This can be attributed to the fact that the initiator, due to its hydrophilicity, has a slightly higher tendency to be in the water phase, where AAm units can be captured.

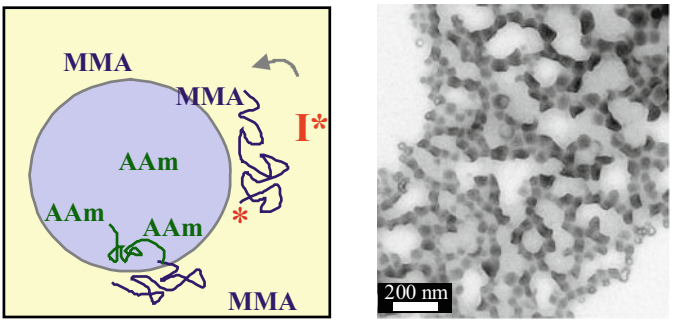

Fig. 7 Copolymerization of hydrophobic (MMA) and hydrophilic (AAm) monomers in inverse miniemulsions with MMA dissolved in the continuous phase in order to obtain a copolymer with low content of homopolymers, low blockiness, and good redispersibility in polar and nonpolar solvents (*left*). I^* and $*$ signifies a free radical at the initiator molecule and in the end of the polymeric chain, respectively. TEM image of the copolymer nanoparticles (*right*) [117]

7 Hydrogel Formation at the Particle Surface

7.1 Copolymers with Hydrophilic Functional Monomers

As shown above, the miniemulsion is a very efficient system for production of copolymer particles from hydrophobic and hydrophilic monomers. In the case of direct (oil-in water) miniemulsion, if the hydrophilic monomer is used in smaller quantities, there is a possibility to form an amphiphilic copolymers close to the interface of the nanoparticles. This shell region of the polymeric particle can be considered as a hydrogel shell. The structure of the hydrogel shell mainly depends on the monomer(s) concentration, reactivity ratios of the monomers, their solubility in water, and the type of surfactant used.

Recently, carboxyl- and amino-functionalized polystyrene latex particles were synthesized by the miniemulsion copolymerization of styrene and acrylic acid or 2-aminoethyl methacrylate hydrochloride (AEMH) [70, 71]. The reaction was started by using an oil-soluble initiator, 2,2′-azobis(2-methylbutyronitrile) (V-59). Two types of surfactant, i.e., ionic negatively charged SDS or positively charged CTMA-Cl, and nonionic Lutensol AT50 (which is a PEO hexadecyl ether with an EO block length of about 50 units) were used to stabilize the initial droplets and final particles.

From the particle size measurements it was found that, in the case of carboxyl-functionalized samples stabilized with SDS, the particle size is relatively constant (around 100 nm) until 10 wt% of added acrylic acid. At higher amounts of acrylic acid, the diameter sharply increased, reaching an average value of 140 nm. The increase in particle size with increased amount of acrylic acid was explained by the formation of a "hairy" layer around the particle, which is mainly composed of the hydrophilic poly(acrylic acid) units. In contrast, the size of the amino-functionalized particles is not strongly dependent on the initial amount of functional monomer and was in the range 110–130 nm. This was expected because, in contrast to acrylic acid, the AEMH ($pK_\alpha = 8.5$) is completely water-soluble at the experimental pH below 3.5. Moreover, AEMH is very reactive and shows strong chain-transfer behavior [72, 73], and therefore the surface layer mainly consists of short chains.

Determining the amount of surface carboxyl groups as a function of the surfactant, it was shown that the dense monolayer of carboxylic groups (0.68 nm^2 per COOH; 1.47 groups per nm^2) on the particles prepared with nonionic surfactant was almost achieved with 3 wt% of acrylic acid. More than 10 wt% of acrylic acid was required in the case of SDS-stabilized particles. TEM images of carboxyl-functionalized polystyrene particles stabilized with nonionic (Lutensol AT50) and ionic (SDS) surfactant are presented in Fig. 8.

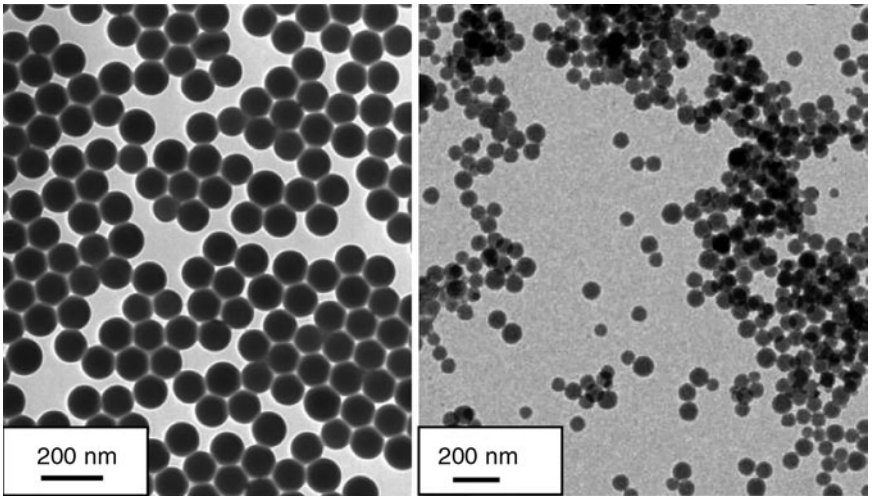

Fig. 8 TEM images of carboxyl-functionalized polystyrene particles: with 3 wt% of acrylic acid and stabilized with Lutensol AT50 (*left*); or with 15 wt% of acrylic acid and stabilized with SDS (*right*)

7.2 Nanoparticles Surface as Templates

The use of polymeric nanoparticles as templates for the crystallization of inorganic materials is an intriguing approach because it offers the feasibility of synthesizing organic/inorganic hybrid materials for a broad spectrum of applications. Besides surfactant assemblies [74–76], hydrogels [77, 78], block copolymers [79, 80], polyelectrolytes [81], self-associated nanogels [82], emulsions, and microemulsions [83–85], there have also been reports of biomimetic routes for the mineralization of calcium phosphates (apatites) employing biodegradable synthetic polymers [86, 87], collagen [88, 89], and gelatin [90, 91]. The synthesis of hybrid particles by the encapsulation of preformed inorganic materials within a polymeric matrix has also been reported [92]. However, the in-situ formation of inorganic materials allows varying several parameters and offers better organic–inorganic interface integrity. Because the compatibility of the inorganic component with the organic matrix plays a crucial role in the encapsulation efficiency, very often an additional coating of the inorganic material with a polymer or a surfactant (in this case as a surface modifier as well as to separate individual entities to ease encapsulation) is a prerequisite. Moreover, the inorganic component is encapsulated very often within the matrix. For applications involving the inorganic materials outside of the nanoparticle matrix, the synthesizing possibilities are very much limited.

Surface-functionalized nanoparticles are very good candidates as templates for crystallization on the outside surface of the particles owing to their monodisperse size and large surface area. The use of such nanoparticles for biomimetic HAP

deposition is interesting for applications involving bioimplants. For example, implants made of titanium and its alloys can be coated with HAP in order to eliminate the failure of the implant owing to poor osteoconductive properties, and to impart better osteointegration and bonding between implant and bone [93–95]. In order to take advantage of the biocompatibility of HAP as well as the mechanical properties of the underlying metallic substrate, it is necessary to optimize the coating possibilities of implants with complex shapes. One of the excellent options for enhancing the surface-coating possibilities is to use HAP-coated nanoparticles. The presence of HAP on the surface of the nanoparticles offers several advantages: it allows the implant material to adapt to the surrounding tissues; it can act as a scaffold for nucleation and growth of new bone materials; and it can impart nanoscaled features on the surface, thereby modifying the surface topography and influencing the physicochemical properties as well as the biochemistry at the surface [96]. Above all, a valuable aspect is that these nanoparticles can also act as carriers of biomolecules and drugs.

Surface-functionalized nanoparticles can be very well exploited as templates for the growth of HAP crystals on the polymeric nanoparticle surface. Tamai and Yasuda [97] have reported HAP-coated polymer particles by employing Pd^0-immobilized poly(styrene-*co*-acrylic acid) copolymer particles synthesized using emulsifier-free emulsion polymerization. Later, the formation of HAP nanocrystals on the surface of β-diketone-functionalized polymeric nanoparticles employing styrene and acetoacetoxyethyl methacrylate (AAEM) obtained by emulsifier-free emulsion polymerization was reported [98]. The carboxylated polystyrene latex particles have also been used previously for the preparation of other inorganic materials like Ag/AgO [99]. However, in these studies the amount of functional groups was always fixed and the amount of inorganic material precipitated was controlled by controlling either the reaction parameters [97, 99] or the amount of added salts [98]. The synthesis of functionalized polystyrene particles by miniemulsion polymerization has been well studied and documented [71]. The miniemulsion technique allows the synthesis of amino- or carboxyl-functionalized polystyrene particles with different amounts of bound surface charge groups by varying the amount of functional comonomer such as amine ethyl methacrylate or acrylic acid, respectively [70, 71].

In the previous studies using self-assembled monolayers (SAMs) with several functional groups (–OH, $–SO_3H$, $–PO_4H_2$, –COOH) on Ti wafers, the –COOH functional group has been proven to be an optimal endgroup for producing highly crystalline and thick layers of HAP [100]. Thus, the use of carboxyl-functionalized polystyrene particles synthesized via the miniemulsion polymerization as templates seems to be a practical way to synthesize hybrid colloids with highly crystalline HAP. These hybrid particles could be used for the coating of implants in order to make them more osteoconductive as well as for the preparation of scaffolds for tissue engineering.

Recently, surface-functionalized particles with covalently bound carboxyl groups were prepared using an ionic as well as a nonionic surfactant as templates to perform crystallization on the surface of the particles [101]. This approach of crystallization outside of the particle (Fig. 9a) is in contrast to a previous report [27], where the

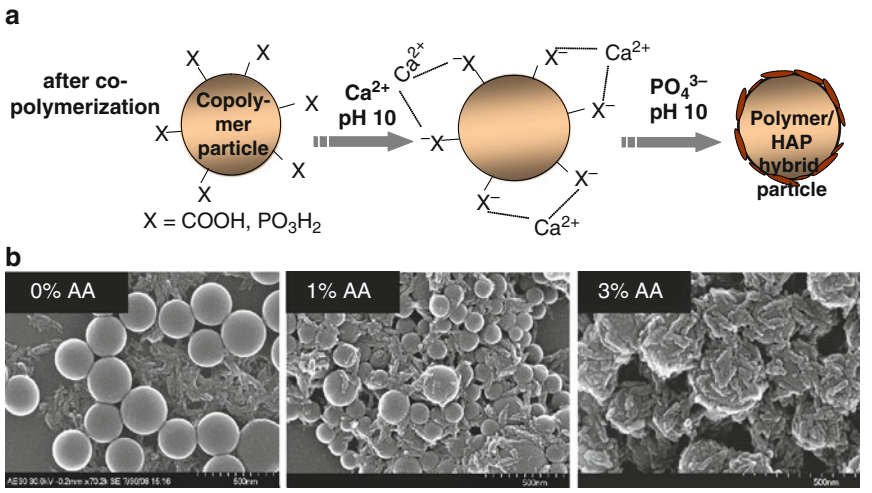

Fig. 9 (**a**) Surface-functionalized nanoparticles as templates for biomineralization. (**b**) TEM micrographs of carboxylated nanoparticles with hydroxyapatite nanocrystals [101]

crystallization was performed inside gelatin nanoparticles that served as a confined reaction environment. The influence of the type of surfactant with respect to particle size, density of functional surface groups, and HAP formation were studied in detail using high-resolution scanning electron microscopy (HRSEM), TEM, and XRD. TEM micrographs of carboxylated nanoparticles with HAP nanocrystals as a function of the initial amount of acrylic acid are presented in Fig. 9b.

It was shown that for a fixed concentration of Ca^{2+} and PO_4^{3-} ions added, the amount of HAP formed on the particle surface increases with the increase in the concentration of acrylic acid added during synthesis of nanoparticles. The absence of HAP on latexes prepared with 0 wt% acrylic acid for both ionic and nonionic surfactant types confirms that the amount of HAP formed depends only on the amount of carboxyl groups present on the surface. HAP formation was pronounced for particles prepared with nonionic surfactant, which is in agreement with the high amount of –COOH groups as compared to the latexes prepared with SDS as anionic surfactant. However, to obtain high HAP nanocrystal formation it was also found that, in addition to high carboxyl functionalization on the surface of the particles, it is absolutely necessary to have an optimum surfactant concentration for particles prepared with nonionic surfactant [101].

8 Microgel Nanocapsules

Not only solid particles can be built up by using hydrogel as shell material, but also capsules. Over the past two decades, the encapsulation of materials has become an extensive area of research activity owing to their utilization as submicrome-

ter containers for the encapsulation of biologically active substances. The main advantage of nanocapsules for drug delivery is the efficient protection of therapeutic agents against degradation or oxidation. It is possible to achieve durability, compatibility, and controlled release of the ingredients. Weidenheimer et al. altered the formulation for the synthesis of soft gelatin capsules by adding plasticizing agents such as formamide, acetamide, lactamide, mannitol, or glycerine [102]. Starch as a native polymer and modified starches are now established for the microencapsulation of, e.g., fragrances [103, 104] or drugs [105].

The suspension polymerization process allowed the formation of capsules of 1–30 µm consisting of migrin oil as core and polyurea as wall material. The latter was formed by interfacial polycondensation reactions between different diisocyanates and emulsified ethylenediamine [106].

The synthesis of nanocapsules can best be obtained in miniemulsion using different approaches [107]. One possibility is based on the phase separation process within a droplet during the polymerization [108]. Here, vinyl monomers were polymerized in the presence of a hydrophobic oil. During the polymerization, the polymer becomes insoluble in the oil, leading to a phase separation. With properly chosen physicochemical properties of monomer and encapsulated material, a polymeric shell surrounding the liquid core can be formed.

In another approach, the polymer is precipitated from the continuous phase onto on stable nanodroplets in an inverse miniemulsion [109]. In this case, a miniemulsion with the liquid core material is formed in a continuous phase that consists of a mixture of a solvent and a nonsolvent for the polymer. That way, PMMA nanocapsules encapsulating an antiseptic agent could be produced.

As a third possibility, nanocapsules in a miniemulsion system could be achieved using different interfacial reactions in inverse miniemulsions. The formation of polyurea, polythiourea, and polyurethane nanocapsules synthesized through the polyaddition reaction has been described in detail [110–112]. The size of the nanocapsules could be controlled by the amount of surfactant used and the addition time of the diisocyanate. The wall thickness was adjusted by the amount of employed monomers. dsDNA molecules were successfully encapsulated into polybutylcyanoacrylate (PBCA) nanocapsules by anionic polymerization, which took place at the interface between the miniemulsion droplets and the continuous phase [113].

The crosslinking of starch at the droplet interface in inverse miniemulsion leads to the formation of hydrogels. The formulation process for the preparation of crosslinked starch capsules in inverse miniemulsion is schematically shown in Fig. 10. The influence of different parameters such as the amount of starch, surfactant P(E/B-*b*-EO), and crosslinker (2,4-toluene diisocyanate, TDI) on the capsule size and stability of the system were studied. The obtained capsules were in a size range of 320–920 nm. Higher amounts of starch and surfactant result in a smaller capsule size. The TEM images of crosslinked starch capsules prepared with different amount of crosslinker (TDI) are presented in Fig. 11. The nanocapsules can be employed as nanocontainers for the encapsulation of dsDNA molecules with different lengths [114] and for the encapsulation of magnetite nanoparticles.

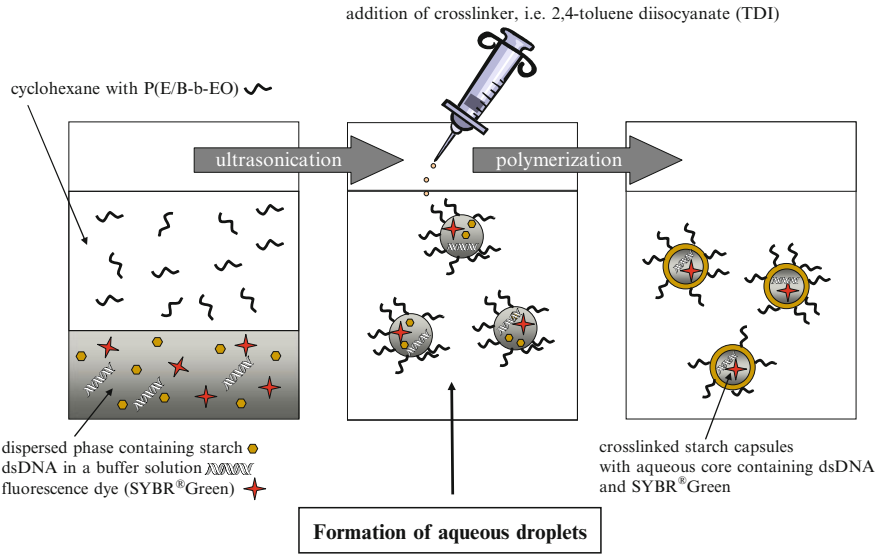

Fig. 10 Preparation of crosslinked starch capsules in an inverse miniemulsion

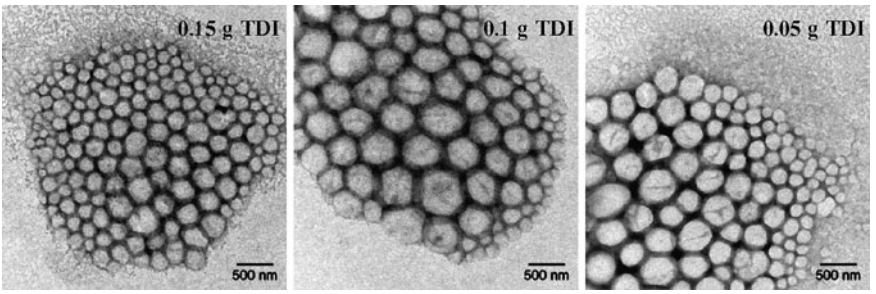

Fig. 11 TEM images of starch-based hydrogels in cyclohexane using different amounts of TDI [114]

9 Molecular Imprinting

The preparation of noncovalent molecularly imprinted particles consisting of EGDMA as crosslinker and methacrylic acid as functional monomer was described using the process of miniemulsion polymerization [115]. The obtained particles were in a size range of 185–220 nm. A high amount of crosslinking agents leads to the formation of microgel particles and therefore enables the polymer network to be maintained during dissolving the template. In this specific case, hydrogel nanoparticles were not prepared, but microgel nanoparticles that can swell in organic solvents. The preparation of molecularly imprinted particles and their utilization for molecular recognition are schematically presented in Fig. 12. Different kinds of particles

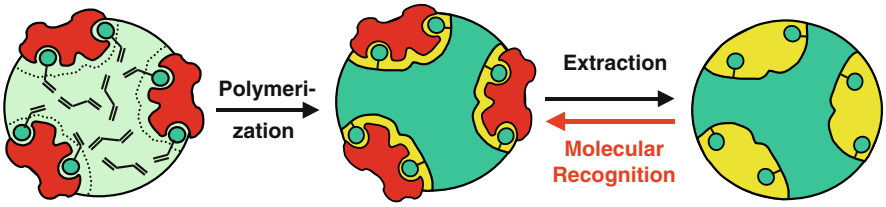

Fig. 12 Preparation of molecularly imprinted particles and their use for molecular recognition: Template molecules induce the formation of binding sites during the miniemulsion polymerization. The templates are extracted from the highly crosslinked particles and are molecularly recognized by the selective binding sites on the nanospheres [114, 115]

were synthesized by varying the molar ratio of monomer to crosslinker and in the presence or absence of a chiral template, i.e., L- or D-Boc-phenylalanine anilid. A protected amino acid, L- and D-Boc-phenylalanine anilid (BFA), were chosen as model templates SDS was used as surfactant and hexadecane as hydrophobic agent to prevent Ostwald ripening of the miniemulsion. The efficiency of the molecular imprinting effect was examined by binding experiments and quantified by UV. It was found that the best enantioselective molecular recognition properties were for particles with a molar ratio of the monomer to crosslinker (MAA:EGDMA) of 0.25:1. The preparation of molecularly imprinted polymers using the miniemulsion polymerization approach is highly efficient in regard to the yield of useful particles as well as in recycling of the templates [115].

10 Concluding Remarks

In summary, the formation of various gel-type materials using different synthetic routes has been described in this contribution. The advantages of the miniemulsion technique include its versatility in terms of the materials used and the reaction conditions, simplicity of formulation, and high reproducibility. The miniemulsion technique allows one to produce nanoparticles with controlled size and surface properties, which are very important parameters for further application in the area of nanotechnology.

References

1. Landfester K (2006) Synthesis of colloidal particles in miniemulsions. Annu Rev Mater Res 36:231–279
2. Landfester K, Willert M, Antonietti M (2000) Preparation of polymer particles in nonaqueous direct and inverse miniemulsions. Macromolecules 33(7):2370–2376
3. Dickson JL, Psathas PA, Salinas B, Ortiz-Estrada C, Luna-Barcenas G, Hwang HS, Lim KT, Johnston KP (2003) Formation and growth of water-in-CO_2 miniemulsions. Langmuir 19(12):4895–4904

4. Ethirajan A, Schoeller K, Musyanovych A, Ziener U, Landfester K (2008) Synthesis and optimization of gelatin nanoparticles using the miniemulsion process. Biomacromolecules 9(9):2383–2389
5. Courts A (1954) The N-terminal amino acid residues of gelatin. 2. Themal degradation. Biochem J 58(1):74–79
6. Schrieber R, Garies H (2007) Gelatine handbook: theory and industrial practice. Wiley-VCH, Weinheim
7. Kaul G, Amiji M (2002) Long-circulating poly(ethylene glycol)-modified gelatin nanoparticles for intracellular delivery. Pharm Res 19(7):1062–1068
8. Kushibiki T, Matsuoka H, Tabata Y (2004) Synthesis and physical characterization of poly(ethylene glycol)-gelatin conjugates. Biomacromolecules 5(1):202–208
9. Coester C, Kreuter J, Von Briesen H, Langer K (2000) Preparation of avidin-labelled gelatin nanoparticles as carriers for biotinylated peptide nucleic acid (PNA). Int J Pharm 196(2): 147–149
10. Weber C, Reiss S, Langer K (2000) Preparation of surface modified protein nanopartiles by introdction of sulfhydryl groups. Int J Pharm 211(1–2):67–78
11. Chen T, Embree HD, Wu LQ, Payne GF (2002) In vitro protein-polysaccharide conjugation: tyrosinase-catalyzed conjugation of gelatin and chitosan. Biopolymers 64(6):292–302
12. Ma J, Cao H, Li Y, Li Y (2002) Synthesis and characterization of poly(DL-lactide)-grafted gelatin chains as bioabsorbable amphiphilic polymers. J Biomater Sci Polymer Ed 13(1): 67–80
13. Truong-Le VL, Walsh SM, Schweibert E, Mao HQ, Guggino WB, August JT, Leong KW (1999) Gene transfer by DNA-gelatin nanospheres. Arch Biochem Biophys 361(1):47–56
14. Busch S, Schwarz U, Kniep R (2003) Chemical and structural investigations of biomimetically grown fluorapatite-gelatin composite aggregates. Adv Funct Mater 13:189–198
15. Marty JJ, Oppenheim RC, Speiser P (1978) Nanoparticles – a new colloidal drug delivery system. Pharm Acta Helv 53(1):17–23
16. Balthasar S, Michaelis K, Dinauer N, Briesen HV, Kreuter J, Langer K (2005) Preparation and characterisation of antibody modified gelatin nanoparticles as drug carrier system for uptake in lymphocytes. Biomaterials 26(15):2723–2732
17. Coester CJ, Langer K, Von Briesen H, Kreuter J (2000) Gelatin nanoparticles by two step desolvation – a new preparation method, surface modifications and cell uptake. J Microencapsul 17(2):187–193
18. Azarmi S, Huang Y, Chen H, McQuarrie S, Abrams D, Roa W, Finlay WH, Miller GG, Löbenberg R (2006) Optimization of a two-step desolvation method for preparing gelatin nanoprticles and cell uptake studies in 143B osteosarcoma cancer cells. J Pharm Pharmaceut Sci 9(1):124–132
19. Farrugia CA, Groves MJ (1999) Gelatin behaviour in dilute aqueous solution: designing a nanoparticulate formulation. J Pharm Pharmacol 51(6):643–649
20. Leong KW, Mao HQ, Truong-Le VL, Roy K, Walsh SM, August JT (1998) DNA-polycation nanospheres as non-viral gene delivery vehicles. J Control Release 53:183–193
21. Leo E, Vandelli MA, Cameroni R, Forni F (1997) Doxorubicin-loaded gelatin nanoparticles stabilized by glutaraldehyde: involvement of the drug in the cross-linking process. Int J Pharm 155(1):75–82
22. Oppenheim RC, Stewart NF (1979) The manufacture and tumor cell uptake of nanoparticles labelled with fluorescein isothiocyanate. Drug Dev Ind Pharm 5(6):563–572
23. Li JK, Wang N, Wu XS (1998) Gelatin nanoencapsulation of protein/peptide drugs using an emulsifier-free emulsion method. J Microencapsul 15(2):163–172
24. Cascone MG, Lazzeri L, Carmignani C, Zhu ZH (2002) Gelatin nanoparticles produced by a simple W/O emulsion as delivery system for methotrexate. J Mater Sci Mater Med 13(5): 523–526
25. Gupta AK, Gupta M, Yarwood SJ, Curtis ASG (2004) Effect of cellular uptake of gelatin nanoparticles on adhesion, morphology and cytoskeleton organisation of human fibroblasts. J Control Release 95(2):197–207

26. Landfester K (2009) Miniemulsion polymerization and the structure of polymer and hybrid nanoparticles. Angew Chem Int Ed Engl 48(25):4488–4507
27. Ethirajan A, Ziener U, Chuvilin A, Kaiser U, Cölfen H, Landfester K (2008) Biomimetic hydroxyapatite crystallization in gelatin nanoparticles synthesized via miniemulsion process. Adv Funct Mater 18(15):2221–2227
28. Tanaka T (1978) Collapse of gels and critical endpoint. Phys Rev Lett 40(12):820–823
29. Khokhlov AR, Starodubtsev SG, Vasilevskaya VV (1993) Conformational transitions in polymer gels: theory and experiment. In: Dusek K (ed) Responsive gels: volume transitions I, vol 109. Springer, Heidelberg, pp 123–171
30. Shibayama M, Tanaka T (1993) Volume phase transition and related phenomena of polymer gels. In: Dusek K (ed) Responsive gels: volume transitions I, vol 109. Springer, Heidelberg, pp 1–62
31. Galaev IY (1999) 'Smart' polymers and what they could do in biotechnology and medicine. Trends Biotechnol 17(8):335–340
32. Zrinyi M, Szabo D, Genoveva F, Feher J (2002) Electrical and magnetic field-sensitive smart polymer gels. In: Osada Y, Khokhlov AR (eds) Polymer gels and networks. Marcel Dekker, New York, pp 309–356
33. Churochkina NA, Starodubtsev SG, Khokhlov AR (1998) Swelling and collapse of the gel composites based on neutral and slightly charged poly(acrylamide) gels containing Na-montmorillonite. Polym Gels Networks 6(3–4):205–215
34. Starodubtsev SG, Churochkina NA, Khokhlov AR (2000) Hydrogel composites of neutral and slightly charged poly(acrylamide) gels with incorporated bentonite. Interaction with salt and ionic surfactants. Langmuir 16(4):1529–1534
35. Liu L, Li PS, Asher SA (1999) Entropic trapping of macromolecules by mesoscopic periodic voids in a polymer hydrogel. Nature 397(6715):141–144
36. Komarova GA, Starodubtsev SG, Khokhlov AR (2005) Synthesis and properties of polyelectrolyte gels with embedded voids. Macromol Chem Phys 206(17):1752–1756
37. Komarova GA, Starodubtsev SG, Lozinsky VI, Kalinina EI, Landfester K, Khokhlov AR (2008) Intelligent gels and cryogels with entrapped emulsions. Langmuir 24:4467–4469
38. Starodubtsev SG, Khokhlov AR (2004) Synthesis of polyelectrolyte gels with embedded voids having charged walls. Macromolecules 37(6):2004–2006
39. Komarova GA, Starodubtsev SG, Khokhlov AR (2007) Reactivity of mercapto groups in cationic micelle solutions and gel-embedded emulsions. Dokl Phys Chem 416:253–255
40. Lozinsky VI (2002) Cryogels on the basis of natural and synthetic polymers: preparation, properties and application. Uspekhi Khimii 71(6):559–585
41. Gao C, Yan D (2004) Hyperbranched polymers: from synthesis to applications. Prog Polym Sci 29(3):183–275
42. Kainthan RK, Brooks DE (2007) In vivo biological evaluation of high molecular weight hyperbranched polyglycerols. Biomaterials 28(32):4779–4787
43. Kainthan RK, Hester SR, Levin E, Devine DV, Brooks DE (2007) In vitro biological evaluation of high molecular weight hyperbranched polyglycerols. Biomaterials 28(31):4581–4590
44. Lo SC, Burn PL (2007) Development of dendrimers: macromolecules for use in organic light-emitting diodes and solar cells. Chem Rev 107(4):1097–1116
45. Lee CC, MacKay JA, Frechet JMJ, Szoka FC (2005) Designing dendrimers for biological applications. Nat Biotechnol 23(12):1517–1526
46. Haag R, Kratz F (2006) Polymer therapeutics: concepts and applications. Angew Chem Int Ed Engl 45(8):1198–1215
47. Siegers C, Biesalski M, Haag R (2004) Self-assembled monolayers of dendritic polyglycerol derivatives on gold that resist the adsorption of proteins. Chem Eur J 10(11):2831–2838
48. Haag R (2001) Dendrimers and hyperbranched polymers as high-loading supports for organic synthesis. Chem Eur J 7(2):327–335
49. Vandenberg EJ (1985) Polymerization of glycidol and its derivatives – a new rearrangment polymerization. J Polym Sci Polym Chem Ed 23(4):915–949

50. Sunder A, Hanselmann R, Frey H, Mülhaupt R (2006) Controlled synthesis of hyperbranched polyglycerols by ring-opening multibranching polymerization. Macromolecules 32(13):4240–4246
51. Kainthan RK, Muliawan EB, Hatzikiriakos SG, Brooks DE (2006) Synthesis, characterization, and viscoelastic properties of high molecular weight hyperbranched polyglycerols. Macromolecules 39(22):7708–7717
52. Maeda H, Wu J, Sawa T, Matsumura Y, Hori K (2000) Tumor vascular permeability and the EPR effect in macromolecular therapeutics: a review. J Control Release 65(1–2):271–284
53. Kolb HC, Finn MG, Sharpless KB (2001) Click chemistry: diverse chemical function from a few good reactions. Angew Chem Int Ed Engl 40(11):2004–2021
54. Moses JE, Moorhouse AD (2007) The growing applications of click chemistry. Chem Soc Rev 36(8):1249–1262
55. Huisgen R (1968) Cycloadditions-definition, classification and characterization. Angew Chem Int Ed Engl 7(5):321–406
56. Fournier D, Hoogenboom R, Schubert US (2007) Clicking polymers: a straightforward approach to novel macromolecular architectures. Chem Soc Rev 36(8):1369–1380
57. Oh JK, Siegwart DJ, Lee HI, Sherwood G, Peteanu L, Hollinger JO, Kataoka K, Matyjaszewski K (2007) Biodegradable nanogels prepared by atom transfer radical polymerization as potential drug delivery carriers: synthesis, biodegradation, in vitro release, and bioconjugation. J Am Chem Soc 129(18):5939–5945
58. De Geest BG, Van Camp W, Du Prez FE, De Smedt SC, Demeester J, Hennink WE (2008) Biodegradable microcapsules designed via "click" chemistry. Chem Commun 2:190–192
59. Srinivasulu P, Raghunath Rao P, Sundaram EV (1991) Synthesis and characterization of ethyl methacrylate-acrylamide copolymers. J Appl Polym Sci 43(8):1521–1525
60. Sanayei RA, O'Driscoll KF, Klumperman B (1994) Pulsed laser copolymerization of styrene and maleic anhydride. Macromolecules 27(20):5577–5582
61. Puig JE, Corona-Galvan S, Maldonado A, Schulz PC, Rodriguez BE, Kaler EW (1990) Microemulsion copolymerization of styrene and acrylic acid. J Colloid Interface Sci 137(1): 308–310
62. Hernández-Barajas J, Hunkeler DJ (1997) Inverse-emulsion copolymerization of acrylamide and quaternary ammonium cationic monomers with block copolymeric surfactants: copolymer composition control using batch and semi-batch techniques. Polymer 38(2):449–458
63. Glukhikh V, Graillat C, Pichot C (1987) Inverse emulsion polymerization of acrylamide. II. Synthesis and characterization of copolymers with methacrylic acid. J Polym Sci Polym Chem Ed 25(4):1127–1161
64. Vasková V, Hlousková Z, Barton J, Juranicová V (1992) Polymerization in inverse microemulsions, 4 locus of initiation by ammonium peroxodisulfate and 2,2-azoisobutyronitrile. Macromol Chem 193(3):627–637
65. Vasková V, Juranicová V, Barton J (1990) Polymerization in inverse microemulsions, 1. Homopolymerizations of water- and oil-soluble monomers in inverse microemulsions. Macromol Chem 191(3):717–723
66. Vasková V, Juranicová V, Barton J (1991) Polymerization in inverse microemulsions, 3. Copolymerization of water- and oil-soluble monomers initiated by radical initiators. Macromol Chem 192(6):1339–1347
67. Barton J (1992) Copolymerization of polar and nonpolar monomers in direst and inverse emulsion systems. Makromol Chem Macromol Symp 53:289–306
68. Corpart JM, Candau F (1993) Formulation and polymerization of microemulsions containing a mixture of cationic and anionic monomers. Colloid Polym Sci 271(11):1055–1067
69. Corpart JM, Candau F (1993) Aqueous solution properties of ampholytic copolymers prepared in microemulsions. Macromolecules 26(6):1333–1343
70. Musyanovych A, Rossmanith R, Tontsch C, Landfester K (2007) Effect of hydrophilic comonomer and surfactant type on the colloidal stability and size distribution of carboxyl- and amino-functionalized polystyrene particles prepared by miniemulsion polymerization. Langmuir 23(10):5367–5376

71. Holzapfel V, Musyanovych A, Landfester K, Lorenz MR, Mailänder V (2005) Preparation of fluorescent carboxyl and amino functionalized polystyrene particles by miniemulsion polymerization as markers for cells. Macromol Chem Phys 206(24):2440–2449
72. Musyanovych A, Adler H-JP (2005) Grafting of amino functional monomer onto initiator-modified polystyrene particles. Langmuir 21(6):2209–2217
73. Duracher D, Sauzedde F, Elaissari A, Perrin A, Pichot C (1998) Cationic amino-containing *N*-isopropylacrylamide–styrene copolymer latex particles: 1-particle size and morphology vs. Polymerization process. Colloid Polym Sci 276(3):219–231
74. Welzel T, Meyer-Zaika W, Epple M (2004) Continuous preparation of functionalised calcium phosphate nanoparticles with adjustable crystallinity. Chem Commun 10:1204–1205
75. Fowler CE, Li M, Mann S, Margolis HC (2005) Influence of surfactant assembly on the formation of calcium phosphate materials – A model for dental enamel formation. J Mater Chem 15(32):3317–3325
76. Sarda S, Heughebaert M, Lebugle A (1999) Influence of the type of surfactant on the formation of calcium phosphate in organized molecular systems. Chem Mater 11(10):2722–2727
77. Schachschal S, Pich A, Adler H-JP (2008) Aqueous microgels for the growth of hydroxyapatite nanocrystals. Langmuir 24(9):5129–5134
78. Schnepp ZAC, Gonzalez-McQuire R, Mann S (2006) Hybrid biocomposites based on calcium phosphate mineralization of self-assembled supramolecular hydrogels. Adv Mater 18(14):1869–1872
79. Antonietti M, Breulmann M, Goltner CG, Cölfen H, Wong KKW, Walsh D, Mann S (1998) Inorganic/organic mesostructures with complex architectures: precipitation of calcium phosphate in the presence of double-hydrophilic block copolymers. Chem Eur J 4(12):2493–2500
80. Kakizawa Y, Miyata K, Furukawa S, Kataoka K (2004) Size-controlled formation of a calcium phosphate-based organic-inorganic hybrid vector for gene delivery using poly(ethylene glycol)-*block*-poly(aspartic acid). Adv Mater 16(8):699–702
81. Shchukin DG, Sukhorukov GB, Möhwald H (2003) Smart inorganic/organic nanocomposite hollow microcapsules. Angew Chem Int Ed Engl 42(37):4472–4475
82. Sugawara A, Yamane S, Akiyoshi K (2006) Nanogel-templated mineralization: polymer-calcium phosphate hybrid nanomaterials. Macromol Rapid Commun 27(6):441–446
83. Walsh D, Hopwood JD, Mann S (1994) Crystal tectonics: construction of reticulated calcium phosphate frameworks in bicontinuous reverse microemulsions. Science 264(5165): 1576–1578
84. Lim GK, Wang J, Ng SC, Gan LM (1999) Formation of nanocrystalline hydroxyapatite in nonionic surfactant emulsions. Langmuir 15(22):7472–7477
85. Perkin KK, Turner JL, Wooley KL, Mann S (2005) Fabrication of hybrid nanocapsules by calcium phosphate mineralization of shell cross-linked polymer micelles and nanocages. Nano Lett 5(7):1457–1461
86. Rezwan K, Chen QZ, Blaker JJ, Boccaccini AR (2006) Biodegradable and bioactive porous polymer/inorganic composite scaffolds for bone tissue engineering. Biomaterials 27(18):3413–3431
87. Kretlow JD, Mikos AG (2007) Review: mineralization of synthetic polymer scaffolds for bone tissue engineering. Tissue Eng 13(5):927–938
88. Olszta MJ, Cheng XG, Jee SS, Kumar R, Kim YY, Kaufman MJ, Douglas EP, Gower LB (2007) Bone structure and formation: a new perspective. Mater Sci Eng R Rep 58(3–5): 77–116
89. Bradt JH, Mertig M, Teresiak A, Pompe W (1999) Biomimetic mineralization of collagen by combined fibril assembly and calcium phosphate formation. Chem Mater 11(10):2694–2701
90. Bigi A, Panzavolta S, Rubini K (2004) Setting mechanism of a biomimetic bone cement. Chem Mater 16(19):3740–3745
91. Rosseeva EV, Buder J, Simon P, Schwarz U, Frank-Kamenetskaya OV, Kniep R (2008) Synthesis, characterization, and morphogenesis of carbonated fluorapatite-gelatine nanocomposites: a complex biomimetic approach toward the mineralization of hard tissues. Chem Mater 20(19):6003–6013

92. Qiu XY, Han YD, Zhuang XL, Chen XS, Li YS, Jing XB (2007) Preparation of nano-hydroxyapatite/poly(L-lactide) biocomposite microspheres. J Nanopart Res 9(5):901–908
93. Ducheyne P, Beight J, Cuckler J, Evans B, Radin S (1990) Effect of calcium phosphate coating characteristics on early post-operative bone tissue ingrowth. Biomaterials 11(8):531–540
94. Campbell AA, Fryxell GE, Linehan JC, Graff GL (1996) Surface-induced mineralization: a new method for producing calcium phosphate coatings. J Biomed Mater Res 32(1):111–118
95. Cook SD, Thomas KA, Kay JF, Jarcho M (1988) Hydroxyapatite-coated titanium for orthopedic implant applications. Clin Orthop Relat Res 232:225–243
96. Mendonca G, Mendonca DBS, Aragao FJL, Cooper LF (2008) Advancing dental implant surface technology – from micron- to nanotopography. Biomaterials 29(28):3822–3835
97. Tamai H, Yasuda H (1999) Preparation of polymer particles coated with hydroxyapatite. J Colloid Interface Sci 212(2):585–588
98. Schachschal S, Pich A, Adler H-JP (2007) Growth of hydroxyapatite nanocrystals on polymer particle surface. Colloid Polym Sci 285(10):1175–1180
99. Zhang RW, Zhang D, Mao H, Song WL, Gao G, Liu FQ (2006) Preparation and characterization of Ag/ago nanoshells on carboxylated polystyrene latex particles. J Mater Res 21(2):349–354
100. Liu DP, Majewski P, O'Neill BK, Ngothai Y, Colby CB (2006) The optimal SAM surface functional group for producing a biomimetic HA coating on Ti. J Biomed Mater Res A 77A(4):763–772
101. Ethirajan A, Ziener U, Landfester K (2009) Surface-functionalized polymeric nanoparticles as templates for biomimetic mineralization of hydroxyapatite. Chem Mater 21(11): 2218–2225
102. Weidenheimer JF, Callahan FM (1956) Soft gelatine encapsulation. US2770553A1
103. Soottitantawat A, Bigeard F, Yoshii H, Furuta T, Ohkawara M, Linko P (2005) Influence of emulsion and powder size on the stability of encapsulated D-limonene by spray drying. Innovat Food Sci Emerg Tech 6(1):107–114
104. Brückner M, Bade M, Kunz B (2007) Investigations into the stabilization of a volatile aroma compound using a combined emulsification and spray drying process. Eur Food Res Tech 226:137–146
105. Liu C-S, Desai KGH, Meng X-H, Cheng X-G (2007) Sweet potato starch microparticles as controlled drug release carriers: preaparation and in vitro drug release. Drying Technol 25:689–693
106. Hong K, Park S (2000) Polyurea microcapsules with different structures: preparation and properties. J Appl Polym Sci 78(4):894–898
107. Landfester K, Musyanovych A, Mailänder V (2010) From polymeric particles to multifunctional nanocapsules for biomedical applications using the miniemulsion process. J Polym Sci Polym Chem Ed 48(3):493–515
108. Tiarks F, Landfester K, Antonietti M (2001) Preparation of polymeric nanocapsules by miniemulsion polymerization. Langmuir 17(3):908–918
109. Paiphansiri U, Tangboriboonrat P, Landfester K (2006) Polymeric nanocapsules containing an antiseptic agent obtained by controlled nanoprecipitation onto water-in-oil miniemulsion droplets. Macromol Biosci 6(1):33–40
110. Crespy D, Stark M, Hoffmann-Richter C, Ziener U, Landfester K (2007) Polymeric nanoreactors for hydrophilic reagents synthesized by interfacial polycondensation on miniemulsion droplets. Macromolecules 40(9):3122–3135
111. Jagielski N, Sharma S, Hombach V, Mailänder V, Rasche V, Landfester K (2007) Nanocapsules synthesized by miniemulsion technique for application as new contrast agent materials. Macromol Chem Phys 208:2229–2241
112. Rosenbauer E-M, Landfester K, Musyanovych A (2009) Surface-active monomer as a stabilizer for polyurea nanocapsules synthesized via interfacial polyaddition in inverse miniemulsion. Langmuir 25(20):12084–12091
113. Musyanovych A, Landfester K (2008) Synthesis of poly(butylcyanoacrylate) nanocapsules by interfacial polymerization in miniemulsions for the delivery of DNA molecules. Prog Colloid Polym Sci 134:120–127

114. Baier G, Musyanovych A, Dass M, Theisinger S, Landfester K (2010) Crosslinked starch capsules prepared in inverse miniemulsion as “nanoreactors” for dsDNA and polymerase chain reaction. Biomacromolecules 11:960–968
115. Vaihinger D, Landfester K, Kräuter I, Brunner H, Tovar GEM (2002) Molecularly imprinted polymer nanospheres as synthetic affinity receptors obtained by miniemulsion polymerisation. Macromol Chem Phys 203(13):1965–1973
116. Sisson A, Papp I, Landfester K, Haag R (2009) Functional nanoparticles from dendritic precursors: hierarchical assembly in miniemulsion. Macromolecules 42:556–559
117. Willert M, Landfester K (2002) Amphiphilic copolymers from miniemulsified systems. Macromol. Chem. Phys. 203:825–836

Adv Polym Sci (2010) 234: 65–93
DOI:10.1007/12_2010_69

Published online: 17 June 2010

Nano- and Microgels Through Addition Reactions of Functional Oligomers and Polymers

Krystyna Albrecht, Martin Moeller, and Juergen Groll

Abstract Nano- and Microgels are predominantly prepared using radical polymerization techniques. This chapter reviews alternative approaches to microgel preparation based on addition reactions of functional oligomers and polymers. This allows preparation of microgels under physiological conditions and in the presence of biologically active molecules without affecting their function. This method is therefore predominantly used to synthesize microgels for biomedical applications. Different crosslinking chemistries that have been used in this context are presented and discussed with regard to reaction conditions and stability of the reaction product. Microgels that have been prepared by these techniques are divided into two groups. Natural polymers used for the preparation of microgels are described first, followed by artificial prepolymers that are suitable for the preparation of microgels. The different preparation methods as well as the resulting microgels and their properties are presented and discussed.

Keywords Addition reactions · Disulfide bridges · Drug delivery · Michael addition · Microgel · Prepolymers

Contents

K. Albrecht, M. Moeller, and J. Groll (✉)
DWI e.V. and Institute of Technical and Macromolecular Chemistry, RWTH Aachen University, Pauwelsstr. 8, 52056 Aachen, Germany
e-mail: albrecht@dwi.rwth-aachen.de; moeller@dwi.rwth-aachen.de; groll@dwi.rwth-aachen.de

Abbreviations

BBMEC	Bovine brain microvessel endothelial cell lines
BSA	Bovine serum albumin
CDI	*N*,*N*′-Carbonyldiimidazole
CHP	Cholesterol-bearing PuL
CHPNG	Cholesterol-bearing PuL nanogels
CL	Cellulose
CS	Chitosan
DDC	*N*,*N*′-Dicyclohexylcarbodiimide
DLS	Dynamic light scattering
DMSO	Dimethyl sulfoxide
DSP	Dithiobis(succinimidyl propionate)
DTBP	Dimethyl 3, 3′-dithiobispropionimidate
DTME	Dithio-bis-maleimidoethane
DTT	Dithiothreitol
DVS	Divinyl sulfone
ECM	Extracellular matrix
EDC	1-Ethyl-3-(3-dimethylaminopropyl)carbodiimide hydrochloride
EDTADA	Ethylenediaminetetraacetic dianhydride
FATP	5-Fluoroadenine arabinoside
GSH	Glutathione
HA	Hyaluronan
HPC	Hydroxypropylcellulose
LCST	Lower critical solution temperature
NAC	*N*-Acetylcysteine
ODN	Oligonucleotide
PASP	Poly(aspartic acid)
PEG	Poly(ethylene glycol)
PEG-OVS	Poly(ethylene glycol)-octavinylsulfone

PEI	Poly(ethylene imine)
PG	Poly(glycidol)
PNIPAM	Poly(*N*-isopropylacrylamide)
p-NPC	*p*-Nitrophenylcarbonate
PuL	Pullulan
RAFT	Reversible addition-fragmentation chain transfer polymerization
SEM	Scanning electron microscopy
SFM	Scanning force microscopy
STS	Sulfanyl thiocarbonyl sulfanyl
TEM	Transmission electron microscopy
TPP	Tripolyphosphate

1 Introduction

Microgels and nanogels, three-dimensionally crosslinked hydrophilic polymer networks with finite dimensions in the micro- and submicrometer range, have raised considerable attention over the last decade. They combine the characteristics of hydrogels, like high water content, diffusion processes into and through the network, as well as tunable chemical and mechanical properties, with the features of colloids such as high surface area [1, 2]. Traditionally, microgels are prepared by free-radical precipitation polymerization, a technique that is reviewed in the chapter by Pich and Richtering [3]. Methods that have been used for the preparation of microgels comprise photolithography, micromolding, microfluidics, spray-drying, homogeneous phase crosslinking and inverse emulsion techniques [4], the latter being reviewed in detail in the chapter contributed by Landfester and Musyanovych [5].

An alternative concept for the preparation of microgels is based on crosslinking of well-defined macromolecular building blocks, either by direct interaction between the (pre-)polymers or by the use of low molecular weight crosslinkers [6–8]. Such a prepolymer condensation concept allows the use of building blocks with predefined tailored properties and the choice of crosslinking chemistries that tolerate functional groups that interfere with radical polymerization, like thiols. Furthermore, crosslinking can be performed under application-relevant conditions such as physiological temperature, ion strength and pH. For these reasons, micro- and especially nanogels prepared by this method are particularly suitable for biomedical applications such as targeted delivery of low molecular weight drugs, siRNA, proteins, peptides, or plasmids into cells.

Nanogels from functional macromers can generally be prepared either by chemical covalent crosslinking through addition reactions or radical polymerization or by physical non-covalent crosslinking. The latter includes crosslinking by ionic interaction and polyelectrolyte complexation (coacervation) as well as self-assembly of hydrophobically modified polymers. This chapter particularly focuses on the formation of covalently crosslinked microgels through addition reaction, either directly between polymers and prepolymers or by the use of low molecular weight crosslinkers.

Radical polymerization techniques that are for example used for the crosslinking of methacrylate-modified polysaccharides [9] are not included in this chapter. Prepolymer crosslinking through radical polymerization techniques as well as noncovalent microgel formation has recently been reviewed in a number of excellent review articles [2, 4, 10–14] and is thus not discussed within this chapter.

In the following section, the chemistries used for crosslinking are presented in more detail. Microgels prepared from biopolymers and synthetic prepolymers will subsequently be addressed in Sects. 3 and 4, respectively.

2 Crosslinking Mechanisms

2.1 Disulfide Bond Formation

The reversible reaction between two thiol (sulfhydryl) groups that form a disulfide bridge under oxidative conditions, which is rapidly cleaved back to free thiols under reductive conditions [15, 16] (Scheme 1), has widely been used for the preparation of hydrogels and microgels.

Because deprotonation of thiol to thiolate is the first step in disulfide formation, acidic conditions stabilize free thiols, whereas disulfide formation is fast under neutral and basic conditions. For reduction of disulfides to thiols in an aqueous environment, dithiothreitol (DTT), 2-thioethanol, triscarboxyethylphosphin (TCEP), or glutathione (GSH) are commonly used as reduction reagents. GSH is a tripeptide (Glu-Cys-Gly) with an unusual peptide linkage between the γ-carboxy group of glutamate and the amino group of cysteine [17, 18]. It is present in the cytosol of mammalian cells with a concentration in the range of 0.5–10 mM and acts as major protection against oxidants such as reactive oxygen species. When reacting with oxidants, GSH itself is oxidized and forms disulfides (GSSG). In a healthy cell, 90% of GSH is present in the reduced form. In contrast to the fluid inside cells, the concentration of GSH in blood and the extracellular matrix (ECM) is lower than 20 μM. This high redox potential difference between the neutral or oxidizing extracellular space and the reducing intracellular space makes disulfide-crosslinked nano- and microgels especially attractive as drug delivery systems due to the possibility of controlled biodegradation of the crosslinked network, and thus quantitative drug release in the cytosol [19, 20].

Disulfides form spontaneously by autoxidation of thiols upon exposure to air. This process is, however, relatively slow and not useful for most microgel preparation techniques. Thus, oxidizing catalysts such as diamide [21], peroxides [22], and sodium tetrathionate [23], or a catalyst based on Fenton chemistry [24], are often applied in order to shorten the oxidation time.

Scheme 1 Disulfide formation by oxidation of thiols

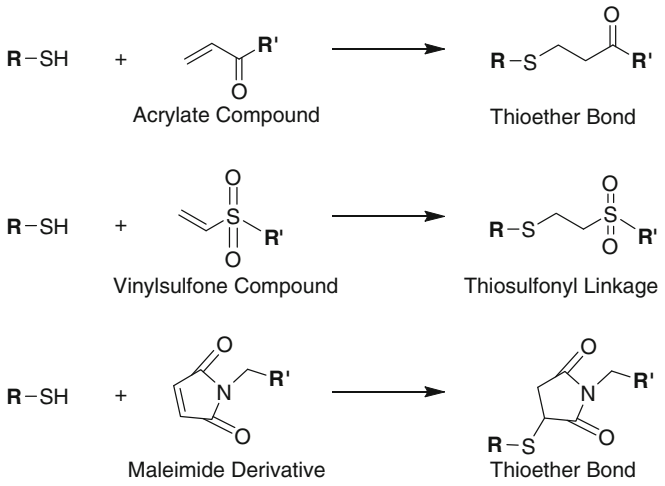

Scheme 2 Michael addition reaction of acrylates, vinylsulfones, and maleimides with thiol

2.2 Michael Addition

Michael addition is a facile reaction between nucleophiles and activated olefins and alkynes in which the nucleophile adds across a carbon–carbon multiple bond [25]. For the preparation of hydrogels, the hydroxyl, thiol or amine functionalities have been reacted with vinyl sulfones [26–28], acrylates [29–31], acrylamides [32], and maleimides [33, 34] (Scheme 2).

As electron-rich olefins are more reactive, vinyl-sulfones are the most reactive species and are capable of reacting with thiols, amines, and even with small nucleophilic alcohol groups. Less reactive are acrylamides and acrylates, which are reactive towards amines and thiols. Maleimides are the least reactive of the mentioned species and allow selective addition of thiols in the presence of amines in the pH range 6.5–7.5. However, hydrolysis of the imide, especially at elevated pH values [35], may be a concern for certain applications. The mentioned Michael addition reactions do not require organic solvents and can be carried out at physiological temperature and pH [36]. In acidic conditions, the reaction is either very slow or does not proceed because protonation removes the nucleophilic form in the case of amines, and the thiolate anion is usually the active species in Michael additions involving thiols [25].

2.3 Condensation Reactions

A condensation reaction is a chemical reaction in which two molecules or functional groups combine to form a single molecule, accompanied by the loss of a small

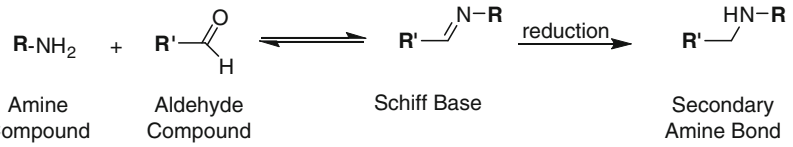

Scheme 3 Reaction between primary amine and aldehyde

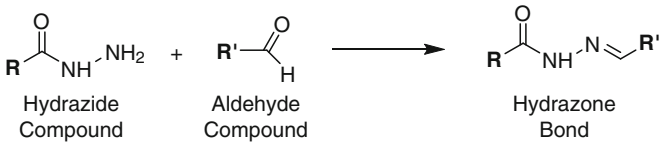

Scheme 4 Synthesis of hydrazone linkages from hydrazide and aldehyde compounds

molecule. Such reactions have been widely applied for the preparation of microgels (Schemes 3–8). An excellent detailed overview of different conjugation routes and the advantages and disadvantages of the different approaches can be found in [37].

A great deal of work has been done on microgel preparation through reaction between aldehydes and primary amines to Schiff bases (Scheme 3). These are unstable in aqueous solution and can be reversibly hydrolyzed to the initial compounds. Thus, reduction of the Schiff base, for example using sodium cyanoborohydride, is often used as a second step that results in highly stable alkylamine bonds [37]. Aldehyde groups can also spontaneously react with hydrazide compounds leading to the formation of hydrazone linkages – a special type of Schiff base that is more stable in aqueous conditions (Scheme 4). However, its stability can be further increased by the reduction of the double bonds.

Carbodiimides are widely used as mediating agents in the reactions between carboxylates and amines or hydroxyl groups, resulting in the formation of amide and ester bonds, respectively. They are very popular zero-length crosslinkers for conjugation of biomolecules such as protein, peptide, or oligonucleotide, for coupling of biomolecules to surfaces, and for conjugation of synthetic molecules [38, 39]. Two commonly used carbodiimides are the water-soluble 1-ethyl-3-(3-dimethylaminopropyl)carbodiimide hydrochloride (EDC) and the water insoluble N,N'-dicyclohexylcarbodiimide (DDC) (Scheme 5). They both react with the carboxyl group to form active acylisourea intermediates. Upon conjugation with amines or hydroxyl compounds, isourea byproducts are formed.

Homobifunctional NHS esters and imidoester crosslinkers are widely used for the crosslinking of amine-containing compounds. They can both contain disulfide bridges that, upon crosslinking, lead to the formation of redox-sensitive particles [40, 41]. NHS ester reaction with primary or secondary amines leads to stable amide and imide linkages, respectively (Scheme 6). The NHS esters can also react with thiol and hydroxyl functionalities; however, this leads to thioester and ester linkages that are susceptible to hydrolysis and thus not stable in aqueous environments, especially in slightly basic physiological conditions.

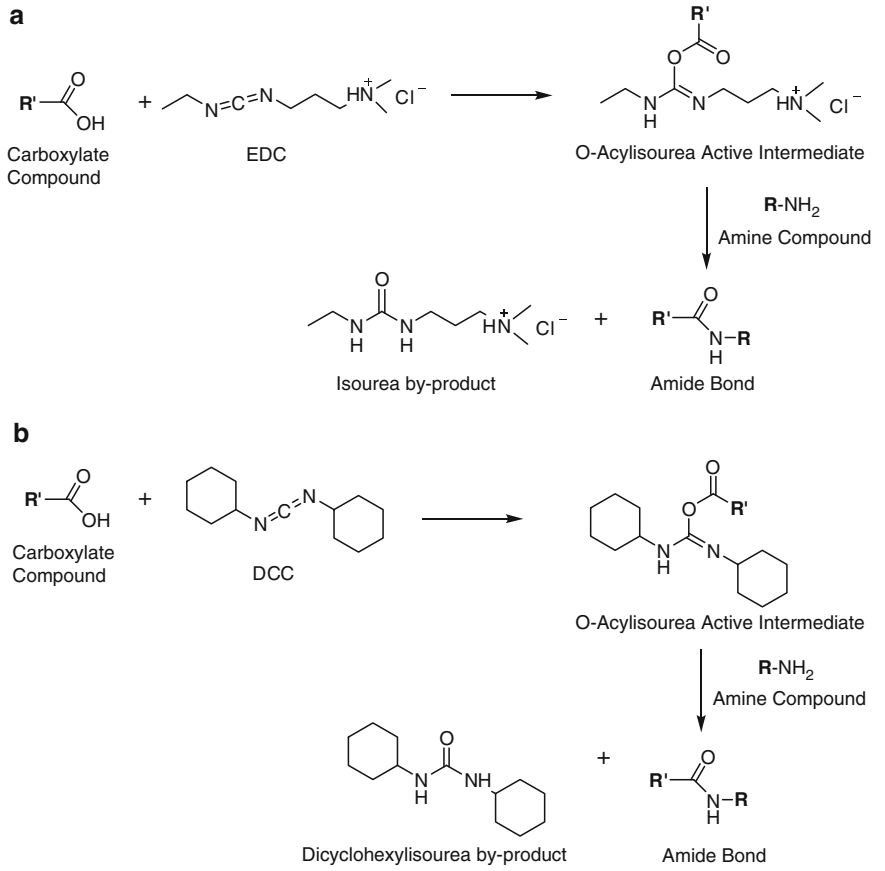

Scheme 5 Carbodiimide-mediated coupling between carboxyl and amine functionalities with (**a**) EDC and (**b**) DCC couplers

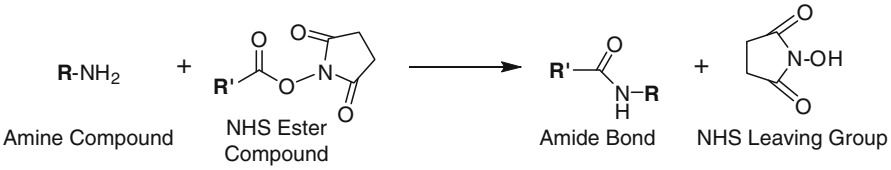

Scheme 6 Reaction between primary amine and NHS ester compound

Imidoesters react with primary amino groups to form amidine bonds (Scheme 7). The amidine bonds are protonated and carry a positive charge at neutral and physiological pH. In addition, they are relatively stable at low pH but prone to hydrolysis at elevated pH.

N,*N*′-Carbonyldiimidazole (CDI) is a highly reactive carbonylating agent that is used for activation of carboxyl or hydroxyl groups for conjugation to amines

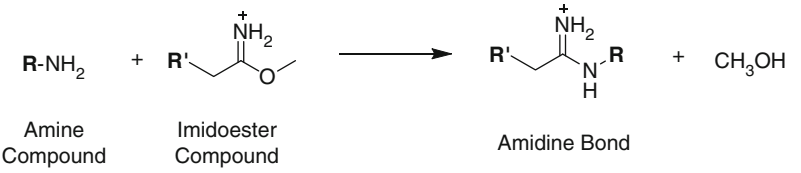

Scheme 7 Reaction between primary amine and imidoester compound

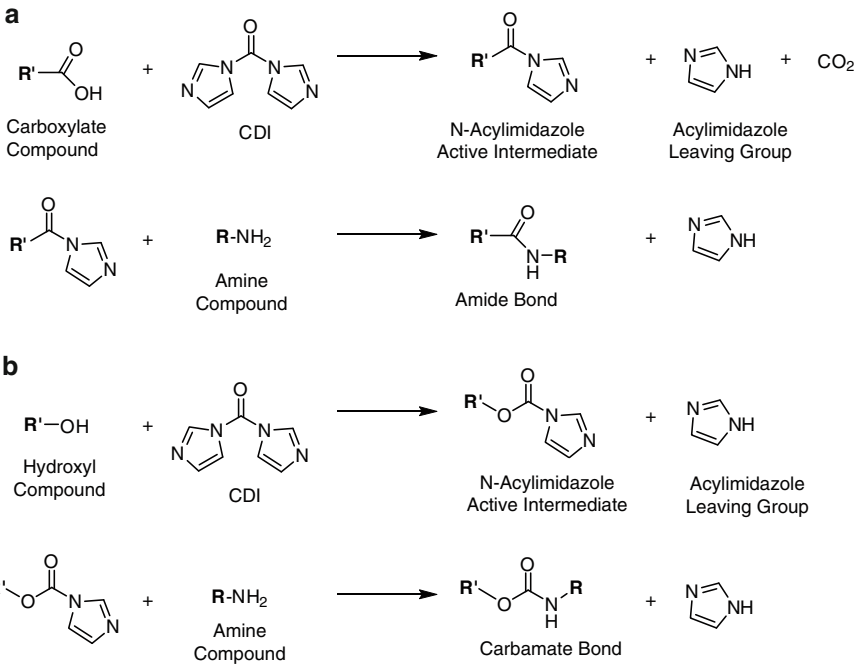

Scheme 8 CDI-mediated reaction between amine compounds with (**a**) carboxyl and (**b**) hydroxyl functionalities

[37, 42]. Similarly to carbodiimide-mediated conjugation, the coupling reaction is a two-step process (Scheme 8). First, an active intermediate imidazole derivative is generated, followed by the formation of an amide bond in the case of carboxyl groups, or a carbamate linkage in the case of a hydroxyl derivative conjugation.

2.4 Other Mechanisms

Isocyanates react rapidly with thiol, amine, or hydroxyl groups resulting in thiourea, urea, and carbamate linkages, respectively (Scheme 9). Without the use of catalysts, the reaction is fastest for thiols that are most nucleophilic, followed by amines and alcohols.

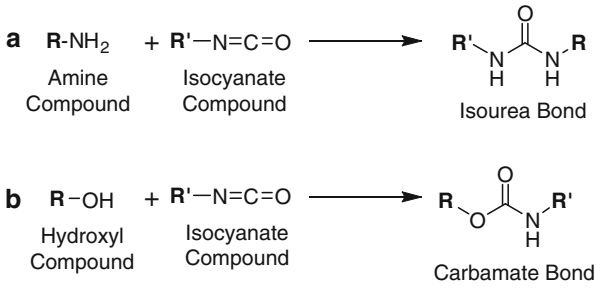

Scheme 9 Reaction between (**a**) amines or (**b**) hydroxyl compounds with isocyanates

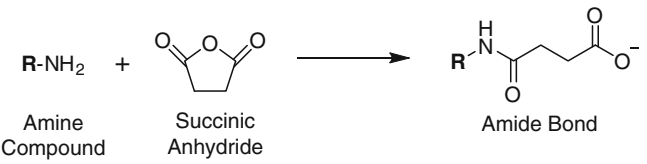

Scheme 10 Reaction between amine and anhydride functionalities

When primary aliphatic isocyanates that show the lowest reactivity compared to secondary or aromatic isocyanates are used in combination with hydrophilic (pre-) polymers, crosslinking may be performed in aqueous solution without the use of additional crosslinkers. At neutral pH, hydrolysis of isocyanates to carbaminic acid with subsequent decarboxylation yields amines. These amines react much more rapidly than water with isocyanates, resulting in crosslinking if the functionality per macromolecule is more than two [43]. This crosslinking reaction can be quenched by adjustment of the pH value. At pH values above 10, carbamate formation is faster than decarboxylation, whereas at pH values below 3 an almost quantitative protonation of the formed amino groups results in the formation of ammonium. In both cases, chemical crosslinking is prevented.

Anhydrides are also highly reactive toward nucleophiles; however, only the reaction with amines towards amide linkages results in products that are stable against hydrolysis [44] (Scheme 10). In contrast, the reaction with both thiol and hydroxyl functionalities leads to the formation of unstable thioesters and esters, respectively.

3 Biopolymer Micro- and Nanogels

3.1 Biopolymers

Hydrogel micro- and nanoparticles composed of biopolymer matrixes have gained a lot of attention in recent years due to their application in drug delivery and tissue engineering [10, 14, 45–47]. The biopolymers used for these purposes are nontoxic,

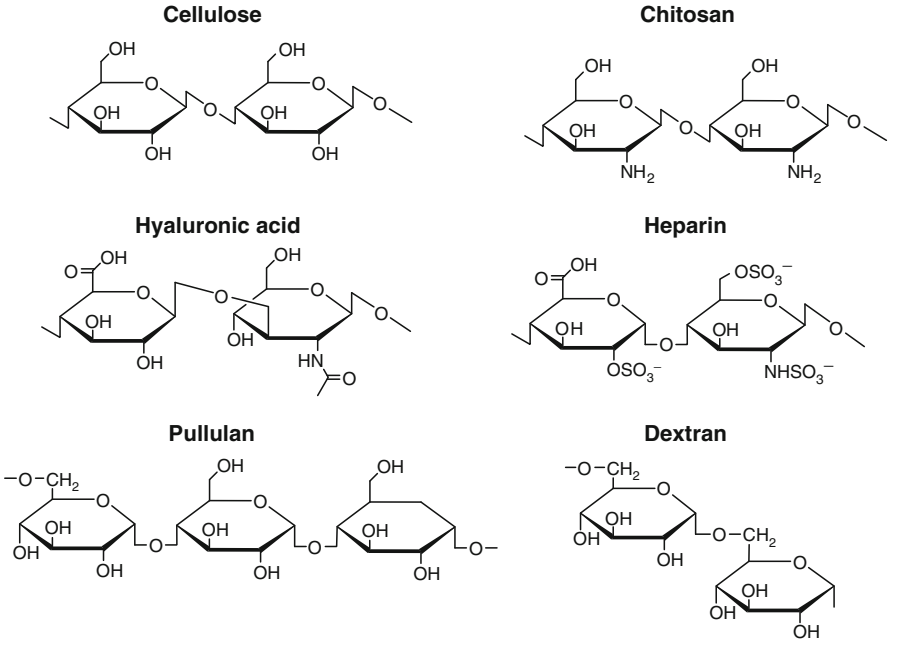

Scheme 11 Most prominently used biopolymers for nano- and microgels

biodegradable, abundant in nature, frequently cheaper than synthetic polymers and, in addition, many of them show a number of interesting physicochemical properties that make them especially interesting for drug delivery applications. They posses a high content of functional groups including hydroxyl, amino, and carboxylic functionalities that can be used both for the crosslinking reactions as well as for the conjugation of bioactive compounds [48–50].

The typical biopolymers used for the preparation of micro- and nanogels are polysaccharides (Scheme 11): cellulose (CL), chitosan (CS), hyaluronan (HA), heparin, pullulan (PuL), dextran, and gelatin – a proteinaceous polyamolytic gel obtained by partial hydrolysis of collagen. Gelatine microgels are addressed by Landfester and Musyanovych in another chapter of this issue [5] and will thus not be discussed further here.

CL is a β-(1→4)-linked homopolymer of D-glucose. It is the most abundant polysaccharide in nature and the major building element of plants. CS is a polysaccharide obtained by deacetylation of chitin, which is similar in structure to CL as they are both composed of linear β-(1→4)-linked monosaccharides. However, CS is different to CL in that it is composed of 2-amino-2-deoxy-β-D-glucan combined with glycosidic linkages [51]. Primary amine groups render special properties that make CS very useful in biomedical applications. Compared to many other natural polymers, CS has a positive charge and is mucoadhesive [52]. Therefore, it is used extensively in drug delivery applications. An additional benefit is the antibacterial effect of CS.

HA is an unsulfated glycosaminoglycane composed of repeating disaccharide units of D-glucuronic acid and *N*-acetylglucosamine linked α-(1→4) and β-(1→3), respectively. HA has special importance because it is a component of the ECM [53] in the soft tissues of mammals, where it mainly ensures water retention [54]. This enables the transport of nutrients to, and removal of waste from, cells that do not have a direct blood supply, such a cartilage cells. Moreover, HA is present in the synovial joint fluid, the vitreous humor of the eye, cartilage, blood vessels, and the unbilical cord. More detailed information about the biological functions and physicochemical properties of HA can be found elsewhere [55, 56].

Heparin is a linear polymer consisting of repeating units of 1→4-linked pyranosyluronic acid and 2-amino-2-deoxyglucopyranose (glucosamine) residues. It has the highest negative charge density of any known biological molecule. Heparin is a well-known anticoagulant that, in addition, is involved in diverse physiological processes through interaction with a number of proteins having heparin-binding domains [57].

PuL is a linear bacterial homopolysaccharide originating from *Aureobasidium pullulans*. Its backbone is formed by glycosidic linkages of α-(1→6) D-glucopyranose and α-(1→4) D-glucopyranose units in a 1:2 ratio. It has a number of applications in the food and beverage industry, in pharmaceuticals, and in manufacturing and electronics [49].

Dextrans are glucose homopolysaccharides that have a considerable number of consecutive α-(1→6) linkages in their major chains, usually more than 50% of the total linkages. These α-D-glucans also possess side-chains stemming from α-(1→2), α-(1→3), or α-(1→4) branch linkages.

3.2 Disulfide Bond Formation

The group of Bernkop-Schnürch describes the preparation of thiolated CS microparticles loaded with insulin as a potential carrier for nasal delivery. For thiolation, 2-iminothiolane (Traut's reagent) was covalently linked to CS via amidine bonds, leading to the formation of CS-4-thiobutylamidine. These polymers show higher mucoadhesive and permeation-enhancing properties than unmodified CS [58–60], which makes them ideal precursors for nasal or oral drug delivery systems. Microgels were prepared either by water-in-oil (w/o) emulsification solvent evaporation [61] or by a precipitation–micronization technique [62]. Both preparation methods resulted in comparable average particle diameters: $18.7 \pm 0.3\,\mu m$ for the w/o particles and $18.0 \pm 0.7\,\mu m$ for the precipitation–micronization technique. This diameter is in the right range for application in nasal drug delivery since particles greater than $10\,\mu m$ are mainly deposited in the nasal cavity. Thiolated CS/DNA complexes with a mean diameter of 125 nm have been prepared in aqueous solution [63]. The decrease in the number of thiol groups was measured in order to prove disulfide bond formation. In comparison to the particles prepared by complexation of DNA with thiol-free CS, the oxidized particles with DNA showed an

increased stability to artificial intestinal fluid, a triggered release in a reducing environment, and improved transfection efficiency. Chitosan-*N*-acetylcysteine (NAC) nanoparticles were investigated as a nonviral gene carrier [64]. Coupling of the *N*-acetylcysteine to CS was mediated through the carbodiimide reaction. The CS–NAC/DNA particles have been prepared in water and the oxidation of free thiol groups was catalyzed by the addition of hydrogen peroxide. The resulting oxidized nanogels had a mean diameter of 73 nm. They showed enhanced stability in comparison to the non-crosslinked particles against polyanionic heparin as well as alkaline pH. The same thiolation of CS was applied by Atyabi et al. [65]. Subsequently, amikacin-loaded nanoparticles with an average diameter of 280 nm were prepared by tripolyphosphate (TPP) gelation, in which disulfide bond formation was achieved by time-dependent oxidation.

Lee at al. describe the preparation of thiolated CS/pDNA nanocomplexes using an aqueous homogeneous chemical gelation process [66]. The thiolated 33 kDa CS derivative was synthesized by a carbodiimide-mediated reaction with thioglycolic acid. During particle preparation, the content of the free thiol groups decreased constantly, indicating the formation of inter- and intramolecular disulfide bonds. Whereas coacervate complexes of unmodified and thiolated CS with pDNA were 120 ± 7 nm and 113 ± 7 nm in diameter, respectively, the crosslinked particles showed a diameter of 220 ± 16 nm (as determined by DLS). Although the non-crosslinked thiolated CS provided higher transfection efficiency in vitro, the disulfide-crosslinked complexes showed a more sustained pDNA release profile and significantly higher gene expression in comparison to non-crosslinked systems, especially at 14 days post-intranasal administration in a mouse model.

Another strategy was pursued by Shu et al., who prepared CS-based disulfide solidified polyelectrolyte nanogels through mild ionic gelation [67]. In this procedure, 50 kDa CS dissolved in acetic acid was added dropwise to an aqueous solution of polyaspartic acid functionalized with cysteamine (PASP-CA). The resulting coacervates were covalently fixed by chloramine-T-mediated disulfide formation between the PASP-CA chains. Such nanogels were successfully loaded with insulin and showed a pH-dependent size variation, with shrinkage to 127.2 ± 1.9 nm at pH 1.2 and expansion to 172.8 ± 2.4 nm at pH 6.8, indicating a suitability of these particles for oral drug delivery applications (Fig. 1).

Preparation of erythropoietin (EPO)-loaded HA microgels was described by Hahn et al. [68]. Therefore, thiolated 200 kDa HA was synthesized by adding Traut's reagent to HA grafted with adipic acid dihydrazine. Under addition of sodium tetrathionate as a specific crosslinking reaction accelerator, microgels with a diameter of 2.3 µm were prepared by spray drying. Lee et al. prepared thiolated 132 kDa HA by mixing HA in PBS with an excess of EDC and HOBt prior to addition of cysteamine dihydrochloride [69]. Subsequently, the disulfide bonds in the conjugated cysteamine were cleaved by DTT. The resulting thiol-HA was used for the preparation of disulfide-crosslinked nanogels with physically entrapped green fluorescence protein siRNA by an inverse w/o emulsion approach. A 1:1 mixture of Span80 and Tween80 surfactants resulted in nanogels with a hydrated diameter of ca. 200 nm. These nanogels effectively protected the encapsulated siRNA from enzymatic degradation, and the release of the siRNA from the nanogels was

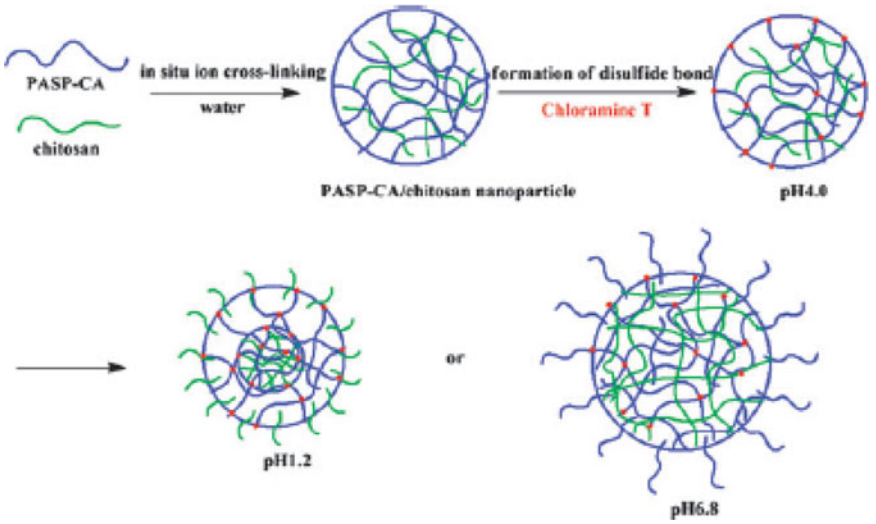

Fig. 1 Representation of the pH-responsive characteristics of PASP–CA–CS NPs in different pH environments. Reprinted from [67] with permission. Copyright 2009 Royal Society of Chemistry

dependent on the concentration of GSH. The siRNA/HA nanoparticles showed a considerable gene silencing effect in serum conditions. The same group prepared disulfide-crosslinked HA microgels (average diameter of $16.2 \pm 8.3\,\mu m$) from thiolated 17 kDa HA by a w/o suspension preparation with hydrogen peroxide as oxidation catalyst. These microgels were used as templates for the preparation of shell crosslinked HA/polylysine layer-by-layer polyelectrolyte microcapsules through layer-by-layer deposition onto the microgels and final removal of the reducible HA microgel cores with DTT [70].

Recently, dual stimuli-responsive disulfide-crosslinked nanogels were prepared by covalently linking sulfanylthiocarbonylsulfanyl (STS) to 100 kDa PuL and subsequent grafting of short PNIPAM chains through reversible addition-fragmentation chain transfer (RAFT) polymerization of NIPAM [71]. Aminolysis of the STS functionalities at the PNIPAM chain ends with isopropylamine yields thiol groups. Upon temperature increase of an aqueous polymer solution to 50°C, the PNIPAM chains collapse and nanogels result from a process of thiol conversion to disulfides through exposure to a flow of air for 24 h. The crosslinked particles retained their integrity also at temperatures below the lower critical solution temperature (LCST) of the PNIPAM chains and displayed a hydrodynamic radius of ~87 nm at 25°C, indicating the formation of disulfide crosslinks in the nanogel matrixes (Fig. 2). Reheating the nanogel solution to 40°C led to a sharp decrease in the nanogel size ($R_h = 54.5$ nm). DLS analysis confirmed cleavage of the disulfide crosslinks to free thiols upon addition of a reductive agent, demonstrating that these nanogels are both redox- and temperature-sensitive.

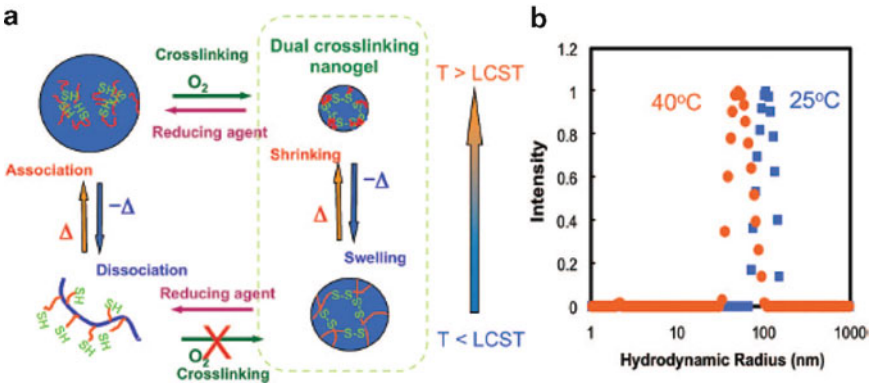

Fig. 2 (**a**) Temperature- and redox-responsive disulfide-crosslinked PNIPAM-g-PuL nanogels. (**b**) Hydrodynamic radius of the dual-responsive nanogels in water below and above LCST. Reprinted from [71] with permission. Copyright 2008 American Chemical Society

Disulfide-crosslinked heparin nanogels were prepared for efficient cellular uptake of heparin in order to induce apoptotic cell death [72]. Thiol-functionalized heparin was synthesized by selective oxidation of the D-glucuronic acid residues of heparin with sodium periodate, followed by the addition of cysteamine hydrochloride. Nanogels were prepared in a two-step procedure. In the first step, thiolated heparin and poly(ethylene glycol) (PEG) were dissolved in DMSO, leading to spontaneous physical complexation. Subsequently, disulfide bond formation between adjacent heparin molecules was induced by sonication. The obtained stable nanogels, with an average diameter of 250 nm in water, rapidly disintegrated and released free heparin upon reduction with GSH. These nanogels enhanced the internalization of heparin and, in addition, significantly reduced the proliferation of mouse melanoma cells.

3.3 Michael Addition

Divinyl sulfone (DVS) is a homobifunctional crosslinker that reacts rapidly with nucleophiles including hydroxyl, amine, and thiol functionalities through Michael addition. The stability of the crosslinked products strongly depends on the pH and on the reactant. Products resulting from addition of hydroxyl groups are unstable above pH 9, and reaction between DVS and amines yield products that are unstable above pH 8 [73]. In a series of publications, Hu et al. presented the use of DVS for the preparation hydroxypropylcellulose (HPC) nanogels [74–76]. These particles were synthesized in aqueous solution in a two-step process. First, the association of HPC above its LCST (~41°C) led to metastable aggregates, followed by crosslinking through addition of DVS. The size of the particles was dependent on the temperature, according to the temperature sensitivity and LCST of HPC. HA

hydrogel particles with a diameter of 900 nm were synthesized by DVS crosslinking in inverse microemulsion [77]. The particles were further modified with aldehyde functionalities by oxidizing the –OH groups with sodium periodate. The aldehyde-functionalized HA nanogels were used for a second crosslinking with HA derivative containing hydrazide groups, which resulted in three-dimensional hydrogels for soft tissue regeneration.

As DVS is highly cytotoxic, and the use of biocompatible crosslinkers with similar reactivity but based on PEG have been intensively studied. Eight-arm, star-shaped PEG with vinyl sulfone endgroups (PEG-octavinylsulfone, PEG-OVS) was used as a crosslinking agent for preparation of bovine serum albumin (BSA) microgels [78]. In this reaction, microgels were formed upon Michael-type conjugation between amine functionalities of BSA and vinyl sulfone groups of PEG-OVS. The particles were prepared in aqueous solution by mixing BSA and PEG-OVS and maintained at 37°C until the desired mean effective diameters were reached. Subsequently, the particles with diameters of ca. 100 nm were used for preparation of thin, biologically active hydrogel coatings through Michael addition covalent conjugation between PEG-OVS and thiol-functionalized substrates. These coatings showed reduced protein adsorption and cell adhesion.

Well-ordered, raspberry-like assemblies of cholesterol-bearing PuL (CHP) particles were prepared by Michael addition of acrylate-group-modified CHP nanogels with four-arm star-shaped PEG bearing thiol groups at the terminus (PEGSH; Fig. 3) [79].

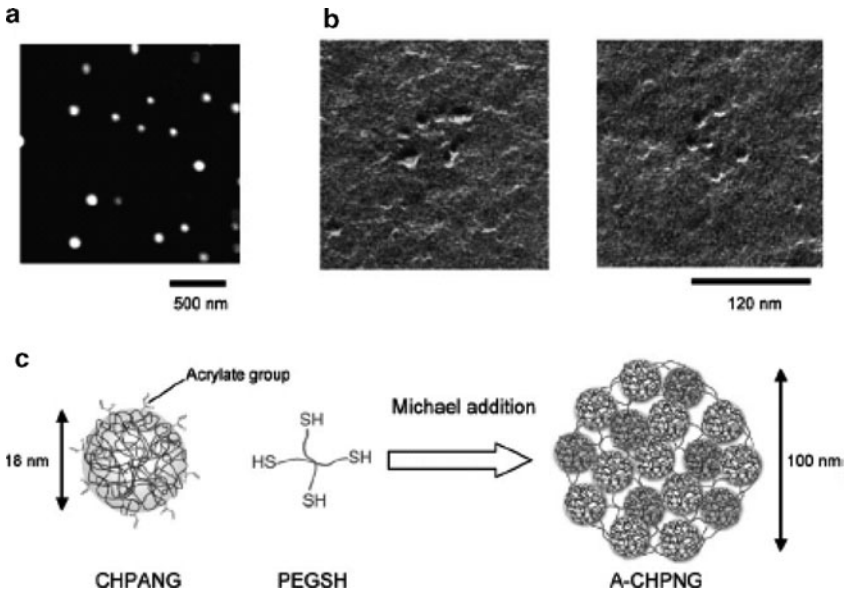

Fig. 3 Characterization of the assembly of nanogels (A-CHPNG). (**a**) SFM image of A-CHPNG. (**b**) TEM images of A-CHPNG. (**c**) Formation of A-CHPNG. Reprinted from [79] with permission. Copyright 2009 Elsevier

CHP bearing acryloyl groups (CHPA) was synthesized by acrylic acid esterification mediated with DCC. CHPA nanogels (CHPANG) with a diameter of 18 nm were prepared by self-assembly of CHPA in PBS. Subsequently, PEGSH was added with a molar ratio of acrylate to thiol groups of 1:1. Depending on the concentration of CHPANG and PEGSH, the size of the resulting particles was in the range of 40–120 nm.

3.4 Condensation Reactions

Glutaraldehyde has been mainly used as an effective crosslinker for the preparation of CS particles. It reacts with the primary amine groups of CS to form Schiff bases [80]. Several reports deal with glutaraldehyde-crosslinked CS particles prepared through w/o emulsion. Various drugs including 5-fluorouracil, phenobarbitone, theophylline, aspirin, griseofulvin, and progesterone were loaded into such particles of sizes in the range 30–450 µm [81–84]. Kumbar et al. prepared CS particles loaded with diclofenac sodium using three different crosslinking mechanisms: glutaraldehyde, sulfuric acid, and heat treatment [85]. Among those, glutaraldehyde-crosslinked microspheres showed the slowest drug release, indicating the highest degree of crosslinking. Mitra et al. describe glutaraldehyde-crosslinked CS nanoparticles encapsulating doxorubicin–dextran conjugate [86]. Nanogels were prepared by a reverse micellar method that resulted in spherical, highly monodispersed hydrogel nanoparticles with a diameter of 100 ± 10 nm.

Spray drying is another method that has been used for preparation of crosslinked CS microspheres with sizes in the range 3–13 µm. Upon increasing the amount of crosslinker (glutaraldehyde or formaldehyde) added, the resulting particles are less irregular and their size decreased [87, 88]. A membrane emulsification method has been applied for the preparation of glutaraldehyde-crosslinked CS particles loaded with BSA as a model drug. The diameter of the particles depended on the membrane pore size and was in the range of 0.65–26.06 µm [89]. Alternatively, the CS microspheres were solidified by a two-step crosslinking method. As first step, a TPP solution was dropped gradually into the emulsion. TPP caused physical crosslinking of CS by diffusion into the droplets, generating microgels. In the second step, an adequate amount of glutaraldehyde was added for covalent crosslinking [90]. It was found that glutaraldehyde-crosslinked CS microspheres are autofluorescent due to presence of C=N bonds from the Schiff base and the C=C linkages from the α,β-unsaturated aldehyde polymers formed by the condensation and dehydration of glutaraldehyde monomers. The particles remained autofluorescent after the reduction of the Schiff base due to C=C linkages [91]. Unfortunately, the cytotoxicity of glutaraldehyde limits its application in the field of drug delivery, and the use of more biocompatible crosslinkers is thus of advantage.

CS nanogels were synthesized by carbodiimide coupling of CS with an oligo(ethylene glycol) dicarboxylic acid crosslinker in an aqueous homogeneous chemical gelation process [92]. The hydrodynamic diameter of the resulting

particles was in the range between 60 and 98 nm, depending on the ratio of crosslinking agent to CS. Aggregates of the nanogels with sizes up to 340 nm, which originated from secondary interactions between the single particles and intermolecular crosslinking reactions, were found in all cases [93]. HA-DNA microspheres for sustained gene delivery were prepared in w/o emulsion using adipic-dihydrazide-mediated crosslinking chemistry. The resulting particles with diameters of 5–20 µm showed release of the encapsulated DNA that could be sustained for about 2 months and was capable of transfection both in vitro and in vivo [94].

HA-based microgels for vocal fold regeneration were prepared by in situ crosslinking of HA derivatives carrying hydrazine (HAADH) and aldehyde (HAALD) functionalities via inverse emulsion [95]. Alternatively, PEG dialdehyde ($M_w = 3400\,g\,mol^{-1}$) was employed instead of HAALD. The size of the resulting microgels was in the range of 10–12 µm. The microgels prepared from the HA derivatives only were more resistant to enzymatic degradation than those crosslinked with PEG dialdehyde. In addition, the former particles were nontoxic whereas the PEG-crosslinked particles showed adverse effects in cell culture at higher concentrations. The residual functionalities of the particles were used for further crosslinking with reactive HA, which resulted in the formation of double crosslinked networks [95].

3.5 Other Mechanisms

Ethylenediaminetetraacetic dianhydride (EDTADA) was used as a crosslinker by Shen et al. for the preparation of CS-based nanogels [96]. The hydrodynamic diameter of the particles was 80 and 74 nm at pH 2 and 11, respectively. These stable CS-EDTADA nanogels showed a pH-dependent switch character that enables a reversible change of their surface charge to be positive at pH < 4.8 and negative at pH > 5.2 (Fig. 4).

4 Nanogels Prepared from Synthetic Polymers

4.1 Suitable Prepolymers

As mentioned above, the preparation of nanogels by addition reactions of functional macromolecular precursors is mainly used for biomedical applications. Thus, the choice of synthetic precursors for microgel formation is restricted to biocompatible materials. Moreover, as most applications are in drug delivery, the molecular weight of the gel precursors should be below the threshold for renal clearance, a value that depends on the molecular architecture and chemical nature of the polymer but that is usually smaller than 30 kDa, which is set as the limit for linear PEG [97]. Polymers that are mostly used and thus presented in more detail here are PEG, poly(glycidol) (PG), and poly(ethylene imine) (PEI).

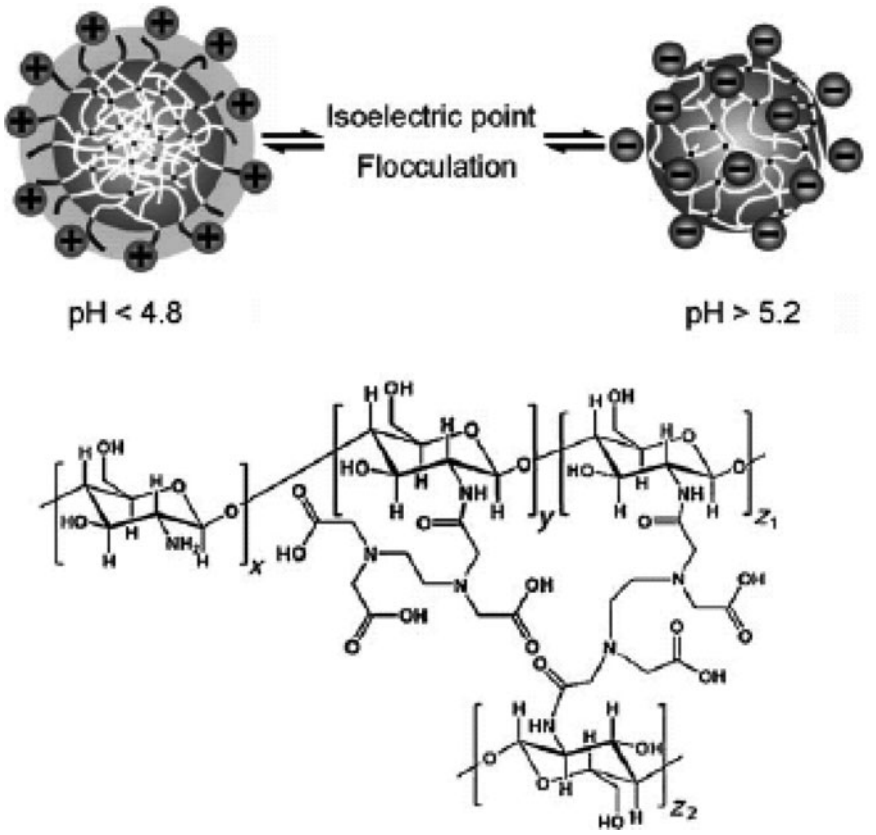

Fig. 4 *Top*: Surface switch of the nanogel triggered by pH changes. *Bottom*: Chemical structure of the CS-EDTADA nanogel. Reprinted from [96] with permission. Copyright 2007 Wiley

PEG is a hydrophilic, uncharged, biocompatible, and FDA-approved polymer that has been used for decades for biomedical applications [98]. It is produced by anionic ring-opening polymerization of ethylene oxide (oxiran), which results in linear polymer chains. Surfaces that are coated with PEG show remarkable minimization of protein adsorption [99, 100]. For particles, modification of the surface with PEG chains (PEGylation) increases circulation times in blood (Stealth effect), therefore both PEGylated liposomes (e.g., Doxil) and PEGylated drugs (e.g., Neulasta) are clinically used. However, one drawback of PEG is the lack of functionality because functional groups can only be present at the chain ends. This has been addressed by the use of multifunctional initiators for polymerization, resulting in star-like polymers with an increased amount of functional groups. While linear PEG is commonly used for PEGylation or as crosslinking agent, star-shaped PEG is additionally used for coating systems that comprise intermolecular crosslinking and one-step functionalization [43], the generation of hydrogels [101–103] and, as discussed in more detail below, microgels.

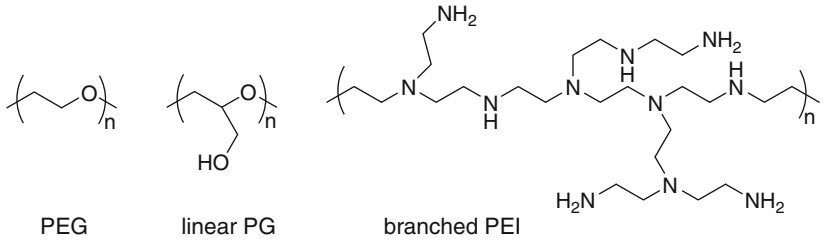

Scheme 12 Overview of the most prominently used synthetic polymers for nano- and microgels

PG is a polymer that has raised increasing attention in recent years. PG is also produced through anionic polymerization of the monomer. If glycidol (2,3-epoxy-1-propanol) is used as monomer, the ring opening by the attacking anion generates a second alcohol group in the molecule, so that subsequent initiation may occur from both. Thus, branched structures are obtained by the polymerization of unprotected glycidol [104, 105]. For the production of linear polymers, the primary alcohol group of the glycidol-monomer has to be protected [106]. After polymerization and deprotection, a linear polymer is obtained with a backbone identical to PEG but with a hydroxymethylene side-chain at each repeating unit. Thus, PG can be seen as the functional analog of PEG. Moreover, if orthogonally removable protective groups are used, functionalization of the deprotected alcohol groups can be done in a controlled manner, in terms of both amount and localization along the polymer chain [107]. Also, multifunctional initiators may be used for the production of star-shaped molecular architectures [108]. Finally, the biocompatibility of linear and branched PG has been demonstrated [109], which makes these polymers a highly attractive alternative to PEG (Scheme 12).

Branched PEI is one of the most frequently employed cationic gene-delivery carriers and has been used as a gene-delivery vector since 1995 [110, 111]. It has a high density of primary, secondary, and tertiary amine groups in a ratio of 1:2:1 of which two thirds are protonated in a physiological milieu [112]. The unprotonated groups provide a buffering effect over a wide range of pH. This unique property of PEI makes it a strong "proton sponge," a concept introduced by Behr et al. and applied to polymers that can buffer the endosome and induce its rupture, thus enabling escape of endosomal content [110, 113]. Both gene transfection efficiency and cytotoxicity are strongly related to the molecular weight of PEI. High molecular weight PEI showed superior transfection efficiency in comparison to low molecular weight oligomer. However, the former is cytotoxic, whereas the latter shows no cytotoxic effects. One of the possibilities for reducing cytotoxicity and enhancing the transfection efficiency is the formation of small crosslinked PEI particles or polymers.

Generally, DNA complexation to such particles can be performed either by direct crosslinking of PEI/DNA polyplexes with chosen amine-reactive crosslinkers or by complexing the oligonucleotides or DNA by pre-crosslinked PEI particles. It is important to mention that the latter method often yields low molecular weight

crosslinked PEI polymers (2–30 kDa), too small to be considered as nanogel particles. These polymers can be prepared by oxidation of thiol-modified polymers [114], Michael addition reactions with the diacrylate crosslinkers [115, 116], condensation reactions with redox-sensitive disulfide crosslinkers like dimethyl 3,3′-dithiobispropionimidate (DTBP) and dithiobis(succinimidylpropionate) (DSP) [116–118]], or by other amine-active crosslinkers [12]. Degradability of the disulfide-containing polymer carriers with the condensed DNA in the reductive environment was proven by the addition of reductive agents. The types of the oligoamine and crosslinker influenced DNA binding, haemolytic and endosomolytic membrane activity, transfection efficiency, and the cytotoxicity of the carrier [116]. For crosslinked polymers prepared by Michael addition, the biodegradability was assured through the presence of the ester bonds. Ethylene glycol bis(succinimidylsuccinate) and disuccinimidyl suberate crosslinkers were applied by Klibanov et al. [119]. The in vitro and in vivo gene delivery by these crosslinked small molecular weight PEI was enhanced by up to 550- and 80-fold, respectively, without a cytotoxicity increase. All these crosslinking routes can be also applied for the micro- and nanogels preparation from PEI or other amine-functional oligomers and polymers. A detailed overview on PEI and other nonviral gene delivery vectors can be found in recent reviews [120–124].

4.2 Disulfide Bond Formation

Aliyar et al. describe nanogels prepared by intramolecular crosslinking of high molecular weight polyacrylamide [125]. Thiol-functional polyacrylamide was synthesized by copolymerization of acrylamide and *N*,*N*′-bisacryloylcystamine, and subsequent reduction of the obtained gel using DTT. Dissolution of the thiomer in water at very low concentrations followed by air oxidation at pH 7.5 resulted in crosslinked particles. Diluted solution conditions favored the formation of intramolecular crosslinks so that mainly single-chain nanogel particles were obtained. Recently, we published a report on nanogels prepared from star-shaped poly(ethylene oxide-*stat*-propylene oxide) [sP(EO-*stat*-PO)] or from linear PG [126]. Both precursors were functionalized with thiol groups through carbodiimide-mediated Steglich esterification between the free hydroxyl groups of the polymers and the disulfide-containing dicarboxy acid. This reaction yielded hydrogels that were subsequently reduced by cleaving the disulfide crosslinks to thiol groups. Nanogels were prepared in inverse miniemulsion and the disulfide bond formation was accelerated by addition of catalytic amounts of the hydrogen peroxide. Cryo-scanning electron microscopy (cryo-SEM) and DLS were applied to characterize the size of the nanogel particles in water (i.e., in the swollen state), and SFM was used as a characterization technique for dry particles (Fig. 5).

The z-average particle diameter determined by DLS was 380 and 330 nm for sP(EO-*stat*-PO) and PG nanogels, respectively. Based on the SFM analysis, the diameter of the sP(EO-*stat*-PO) nanogels in the dry state was determined to be

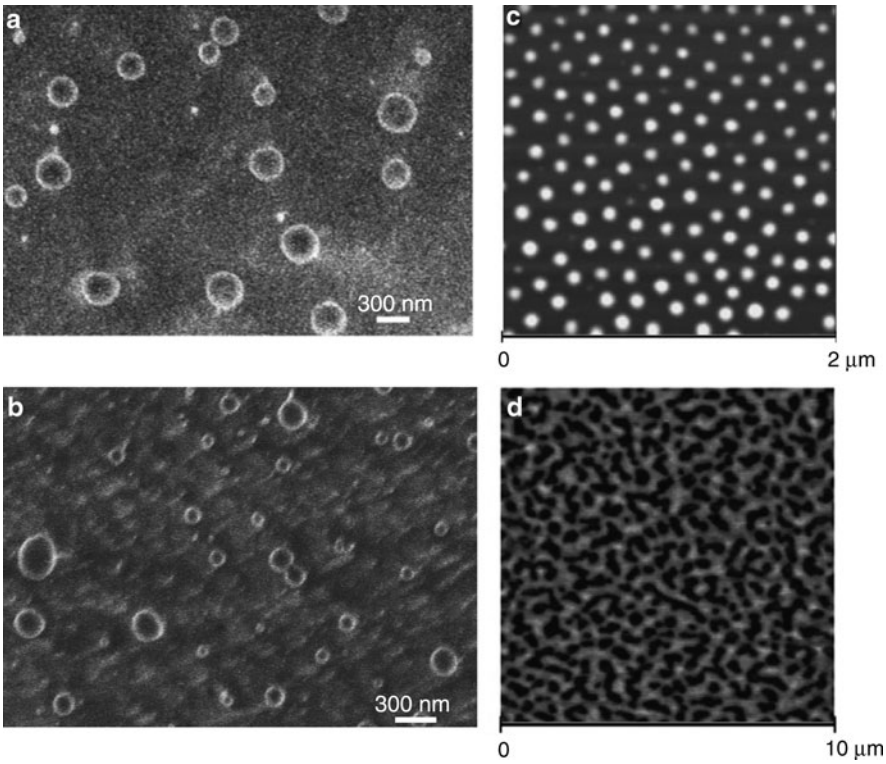

Fig. 5 Cryo-SEM images of nanogels prepared from thiol-functional (**a**) sP(EO-*stat*-PO) and (**b**) PG. SFM images of sP(EO-*stat*-PO) nanogels (**c**) before and (**d**) after reduction with GSH. Reprinted from [126] with permission. Copyright 2009 Wiley

70 ± 5nm. By comparing this value with the size in aqueous environment, determined from cryo-SEM and DLS, a strong swelling ability of the nanogels in water with an estimated swelling ratio of 3.5–5 was observed.

4.3 Michael Addition

Despite the increasing application of Michael addition reactions for the preparation of bulk hydrogels, to the best of our knowledge there are only two reports dealing with nanogels prepared exclusively from synthetic polymers crosslinked by this mechanism. Nanogels with average diameter of ca. 100 nm synthesized by crosslinking PEG-OVS with eight-arm amine-terminated PEG-octamine (PEG-OA) have been prepared by Elbert et al. according to the procedure described earlier in Sect. 3.3 [78]. The same prepolymers were used to fabricate microspheres in order to exploit the LCST behavior of PEG particles in aqueous sodium sulfate

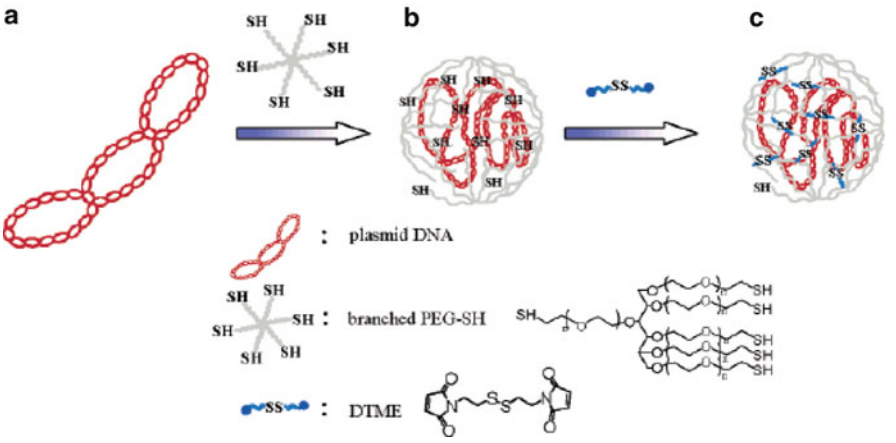

Fig. 6 PEG-assisted DNA solubilization in DMSO and preparation of PEG/DNA nanogels: (**a**) Plasmid DNA in water, (**b**) PEG/DNA nanocomplex in DMSO, and (**c**) stable DTME-crosslinked PEG/DNA nanogel in water. Reprinted from [128] with permission. Copyright 2006 American Chemical Society

solutions [127]. During a "pre-reaction" in PBS below the cloud point, particles with an average diameter of 100 nm were obtained. Subsequently, the solutions were diluted with sodium sulfate solution at room temperature, followed by an increase of temperature to 37°C in order to induce phase segregation. In this process, depending on the pH and the reaction time, particles with a size of 1–100 µm were obtained.

The preparation of disulfide-stabilized nanogel PEG/DNA complexes with a diameter of around 100 nm was reported by Mok et al. [128]. A thiol-functionalized six-arm branched PEG was used for DNA solubilization in DMSO, which led to spontaneous PEG/DNA nanocomplex formation. Subsequent addition of the thiol-reactive dithio-bis-maleimidoethane (DTME) disulfide crosslinker led to stabilized nanogels (Fig. 6) that showed high gene transfection efficiency.

4.4 Condensation Reactions

Chemically crosslinked nanogels based on PEG-*cl*-PEI were introduced by Kabanov et al. in 1999 [129]. The nanogels exhibit the combined properties of swollen polyelectrolyte and hydrophilic nonionic networks in which the PEI chains bind oppositely charged macromolecules, leading to collapse of the network. Nonionic PEG fragments prevent precipitation and stabilize the nanogels in aqueous dispersions [130]. The particles were prepared by crosslinking branched PEI with bis-carbonyldiimidazole-activated PEG using emulsion techniques, followed by evaporation of the solvent, maturation of the nanogels in aqueous solution and final fractionation of the obtained particles by gel-permeation chromatography. Due to

the positive charge of PEI, the nanogels can bind and encapsulate spontaneously negatively charged molecules such as short oligomeric parts of DNA (oligodeoxyribonucleic acid, ODN; usually called oligonucleotides), resulting in the formation of stable polyelectrolyte complexes. Upon loading with 20-mer antisense phosphorothioate ODN, the diameter of the nanogels was reduced from 120 to 80 nm, together with a decrease of the zeta potential value due to the neutralization of the PEI charges by ODN. The particles were stable in solution and no aggregation was observed over an extended period of time. In vitro studies showed that the uptake of the ODN-loaded nanogels by multidrug-resistant human oral epidermoid carcinoma cells was increased in comparison to free ODN [129]. Formation of hydrophobic domains in such nanogels was achieved by complexation of the particles with anionic surfactants. Incorporation of surfactants such as sodium tetradecyl sulfate had an onset at the "critical association concentration" which was two orders of magnitude lower than the critical micelle concentration of the surfactant alone. Interestingly, the dramatic decrease in nanogel diameter from 300 nm before to 50 nm after complexation was observed. The hydrophobic pockets in the nanogels served as reservoirs for water-insoluble molecules. The nanogel/surfactant dispersions containing hydrophobic dyes or poorly water-soluble biologically active molecules such as retinoic acid and indomethacin remained stable for several days [131]. PEI/PEG nanogels with a diameter of 100 nm were also used as a carrier for ODN transport across the blood–brain barrier (BBB) [132]. In vitro studies performed with bovine brain microvessel endothelial cell lines (BBMEC) that served as a BBB model demonstrated effective transport across cellular monolayers in vitro. The permeability was further increased after modification of the nanogel surface with insulin or bovine transferrin, proteins that target specific receptors at the blood side of the brain epithelium. Remarkably, after transport through the BBB model, the ODN remained mostly incorporated in the nanogel network and showed only little degradation in comparison to free ODN. In vivo biodistribution studies in a mouse model showed 15-fold higher accumulation of the nanogel-bound ODN in the brain and a twofold decrease in liver and spleen compared to free ODN 1 h after intravenous injection. A subsequent study confirmed the transport of such nanogels, this time loaded with valproic acid, across a BBB model in vitro and explained the 70% increased transport over the cellular monolayer despite permanent integrity of the cell layer as being due to specific transcytosis of the drug-loaded nanogels [133]. PEI/PEG nanogels were also studied as a potential drug carrier for the delivery of nucleoside analog 5′-triphosphates, an active form of cytotoxic anticancer drug [134, 135]. The polyplexes formed spontaneously by mixing nanogels with 5′-triphosphate of cytotoxic 5-fluoroadenine arabinoside (FATP). FATP encapsulated in the nanogel was well protected from in vitro enzymatic degradation during the first 60 min of incubation. Remarkably, the drug–nanogel formulation showed increased cytotoxicity in cultured cancer cells in comparison to the free drug. Attaching folate to the nanogels as a targeting molecule resulted in a tenfold increase in nanogel internalization in human breast carcinoma cells [134]. Alternatively, the PEI/PEG nanogels were prepared by PEI crosslinking with PEG-bis (*p*-nitrophenylcarbonate) (*p*-NPC). The size of the particles was dependent on the

molecular weight of PEG as well as on the crosslinking density. The PEI-PEG nanogels were 16-fold more efficient as transferring agent than PEI itself [136].

Several small molecular weight homobifunctional crosslinker systems have been used for the preparation of PEI particles. Nanogels solidified by crosslinking through carbodiimide-mediated reaction with adipic acid as well as by dialdehyde crosslinkers are described by Swami et al. [137]. Their size was dependent on the crosslinking density and the crosslinker used and was in the range of 80–210 nm. As an alternative to thiol oxidation, redox-sensitive particles can be also obtained through crosslinking functional polymers with low molecular weight disulfide crosslinkers. This way, redox-sensitive PEI/PEG nanogels were prepared by DTBP crosslinking. Subsequently, they were loaded with 5′-triphosphorylated Ribavirin, a drug used for treatment of many respiratory infections including influenza A virus. These biodegradable particles could easily be cleaved in the reductive environment of the cytosol [138].

So far, all the described PEI gene carriers were prepared for ODN or DNA complexation by crosslinked PEI particles. Kissel et al. compared the DNA polyplexes prepared either by the method described above or by addition of the DSP crosslinker in DMSO to a buffered aqueous solution of the PEI/DNA polyplexes, and thus by covalent crosslinking after complexation [139]. Only the latter method yielded small polyplexes with particle sizes of 100–300 nm, for 0.05 and 0.30 crosslinking degrees, respectively. In addition, pre-crosslinked PEIs showed decreased plasmid compaction and stabilization properties, resulting most probably from incomplete caging of the DNA (Fig. 7). In vivo studies in mice showed that introduction of the crosslinks after polyplex formation makes these polyplexes relatively stable in the circulation, and their transfection efficiency after intravenous administration is retained [140].

Recently, studies performed in DMSO revealed that it is crucial to remove traces of both carbon dioxide and water in the crosslinking of PEI with DSP. In addition, the DSP adding rate as well as its amount is important for the preparation of low toxicity and high efficiency gene transfection vectors [141]. Super-expandable nanogels that undergo nano- to microscale volume transition in response to

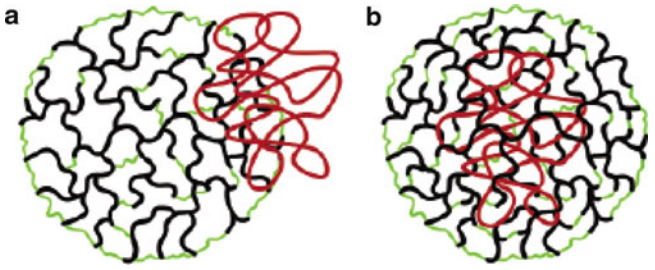

Fig. 7 Comparison of DNA complexation and caging for pre-crosslinked PEI nanogels (**a**) and crosslinking of the gels after complexation (**b**). Reprinted from [139] with permission. Copyright 2006 American Chemical Society

temperature were described by Lee et al. [142]. The particles were prepared in o/w emulsion by chemical crosslinking between *p*-NPC terminally activated oligo(L-lactic acid)-*block*-poly(ethylene oxide)-*block*-poly(propylene oxide)-*block*-poly(ethylene oxide)-*block*-oligo(L-lactic acid) penta-*block*-copolymer and the amine groups of poly(ethylene oxide)-grafted poly(L-lysine). They exhibited a dramatic and reversible volume transition from 150 nm at 37°C to around 1.4 µm upon cooling to 15°C.

4.5 Other Mechanisms

Hydrogel microspheres from isocyanate-terminated sP(EO-*stat*-PO) [NCO-sP(EO-*stat*-PO)] with an overall molecular weight of between 3 and 18 kDa were prepared by homogeneous chemical gelation in aqueous solution. As the isocyanate group at the distal ends of the star-shaped polymers originates from isophorone diisocyanate, the molecules possess amphiphilic character with hydrophilic backbones and hydrophobic end groups. Thus, in aqueous solution, the hydrophilic backbone makes the molecules soluble, but the endgroups cause a driving force for aggregate formation [143]. In addition, hydrolysis of the isocyanate groups leads to formation of carbaminic acid, which, at neutral pH, instantly decarboxylates to form amine groups. These amines react with unreacted isocyanate groups to form urea bridges. Since the kinetics of amine addition to isocyanate is much faster than hydrolysis, formation of urea bridges occurs preferentially until steric restrictions significantly lower the reaction probability [144]. The microgel diameter increases with the concentration of the prepolymers and was in the range 3.7–8.1 µm.

5 Conclusions

This chapter presents the different approaches for covalent microgel preparation based on addition reactions of functional oligomers and polymers. Different crosslinking mechanisms, mainly Michael-type addition, disulfide formation from thiols, and condensation reactions have been presented and compared. This set of different mechanisms allows a proper application-dependent choice. As the possibility to use most of these mechanisms in the presence of biologically active molecules without affecting their function and in physiological conditions is one major advantage of this approach to microgel preparation, most studies are focused on biomedical applications. Thus, either biopolymers or biocompatible artificial gel precursors, predominantly PEI, PEG, or PG, have been used for microgel preparation. The summarized studies show that microgels prepared by addition reactions possess high potential, especially for controlled and targeted drug delivery.

References

1. Peppas NA, Hilt JZ, Khademhosseini A, Langer R (2006) Adv Mater 18:1345
2. Kabanov AV, Vinogradov SV (2009) Angew Chem Int Ed Engl 48:5418
3. Pich A, Richtering W (2010) Adv Polym Sci doi: 10.1007/12_2010_70
4. Oh JK, Drumright R, Siegwart DJ, Matyjaszewski (2008) Prog Polym Sci 33:448
5. Landfester K, Musyanovych A (2010) Adv Polym Sci doi: 10.1007/12_2010_68
6. Hennik WE, van Nostrum CF (2002) Adv Drug Deliv Rev 54:13
7. van Tomme SR, Storm G, Hennink WE (2008) Int J Pharm 355:1
8. Hoare TR, Kohane DS (2008) Polymer 49:1993
9. De Geest BG, Dejugnat C, Sukhorukov GB, Braeckmans K, De Smedt SC, Demeester J (2005) Adv Mater 17:2357
10. Oh JK, Lee DI, Park JM (2009) Prog Polym Sci 34:1261
11. Raemdonck K, Demeester J, De Smedt S (2009) Soft Matter 5:707
12. Soussan E, Cassel S, Blanzat M, Rico-Lattes I (2009) Angew Chem Int Ed Engl 48:274
13. Rivest C, Morrison DWG, Ni B, Rubin J, Yadav V, Mahdavi A, Karp JM, Khademhosseini A (2007) J Mech Mater Struct 2:1103
14. Liu Z, Jiao Y, Wang Y, Zhou C, Zhang Z (2008) Adv Drug Deliv Rev 60:1650
15. Voet D, Voet JG (2005) Biochemistry, 3rd edn. Wiley, New York
16. Gilbert HF (1995) Meth Enzymol 251:8
17. Meister A, Anderson ME (1983) Annu Rev Biochem 52:711
18. Wu G, Fang Y-Z, Yang S, Lupton JR, Turner ND (2004) J Nutr 134:489
19. Saito G, Swanson JA, Lee K-D (2003) Adv Drug Deliv Rev 55:199
20. Meng F, Hennink WE, Zhong Z (2009) Biomaterials 30:2180
21. Kosower NS, Kosower EM (1995) Meth Enzymol 251:123
22. Shu XZ, Liu Y, Luo Y, Roberts MC, Prestwich GD (2002) Biomacromolecules 3:1304
23. Hahn SK, Park JK, Tomimatsu T, Shimobouji T (2007) Int J Biol Macromol 40:374
24. Goessl A, Tirelli N, Hubbell JA (2004) J Biomater Sci Polym Ed 15:895
25. Mather BD, Viswanathan K, Miller KM, Long TE (2006) Prog Polym Sci 31:487
26. Qiu B, Stefanos S, Ma J, Lalloo A, Perry BA, Leibowitz MJ, Sinko PJ, Stein S (2003) Biomaterials 24:11
27. Hiemstra C., van der Aa LJ, Zhong Z, Dijkstra PJ, Feijen J (2007) Macromolecules 40:1165
28. Gehrke SH, Uhden LH, McBride JF (1998) J Control Release 55:21
29. Lutolf MP, Tirelli N, Cerritelli S, Cavalli L, Hubbell JA (2001) Bioconjug Chem 12:1051
30. Metters A, Hubbell J (2005) Biomacromolecules 6:290
31. Kim M-S, Choi Y-J, Noh I, Tae G (2007) J Biomed Mater Res A 83A:674
32. Han S-C, He W-D, Li J, Li L-Y, Sun X-L, Zhang B-Y, Pan T-T (2009) J Polym Sci A Polym Chem 47:4074
33. Yamaguchi N, Kiick KL (2005) Biomacromolecules 6:1921
34. Schultz KM, Baldwin AD, Kiick KL, Furst EM (2009) Macromolecules 42:5310
35. Kratz F, Warnecke A, Riebeseel K, Rodrigues PCA (2002) In: Dumitriu S (ed) Polymeric biomaterials. Marcel Dekker, New York, p 859
36. van Dijk M, Rijkers DTS, Liskamp RM, van Nostrum CF, Hennink WE (2009) Bioconjug Chem 20:2001
37. Hermanson GT (2008) Bioconjugate techniques, 2nd edn. Elsevier, Amsterdam
38. Hoare DG, Koshland DE (1966) J Am Chem Soc 88:2057
39. Kunkel GR, Mehrabian M, Martinson HG (1981) Mol Cell Biol 34:3
40. Lomant AJ, Fairbanks G (1976) J Mol Biol 104:243
41. Wang K, Richards F (1974) J Biol Chem 249:8005
42. Paul R, Anderson GW (1960) J Am Chem Soc 82:4596
43. Gasteier P, Reska A, Schulte P, Salber J, Offenhäusser A, Moeller M, Groll J (2007) Macromol Biosci 7:1010
44. Smyth DG (1967) J Biol Chem 242:1592
45. Janes KA, Calvo P, Alonso MJ (2001) Adv Drug Deliv Rev 47:83

46. Agnihotri SA, Mallikarjuna NN, Aminabhavi TM (2004) J Control Release 100:5
47. Prabaharan M, Mano JF (2005) Drug Deliv 12:41
48. Hoffman AS (2002) Adv Drug Deliv Rev 54:3
49. Coviello T, Matricardi P, Marianecci C, Alhaique F (2007) J Control Release 119:5
50. Lee KY, Mooney DJ (2001) Chem Rev 101:1869
51. Payne GF, Raghavan SR (2007) Soft Matter 3:521
52. Illum L (1998) Pharm Res 15:1326
53. Fraser JRE, Laurent TC, Laurent UBG (1997) J Intern Med 242:27
54. Asari A (2004) In: Garg HG, Hales CA (eds) Chemistry and biology of hyaluronan. Elsevier, Amsterdam, pp 457–468
55. Leach JB, Schmidt C (2004) In: Wnek GE, Bowlin GL (eds) Encyclopedia of biomaterials and biomedical engineering. Marcel Dekker, New York, pp 779–788
56. Phillips GO (1992) In: Glasser WG, Hatakayma H (eds) Viscoelasticity of biomaterials. ACS symposium series, vol 489. American Chemical Society, Washington DC, p 168
57. Capila I, Linhardt RJ (2002) Angew Chem Int Ed Engl 41:390
58. Bernkop-Schnürch A, Schwarz V, Steininger S (1999) Pharm Res 16:876
59. Bernkop-Schnürch A, Hornof M, Pinter Y (2003) Int J Pharm 260:229
60. Bernkop-Schnürch A, Guggi D, Pinter Y (2004) J Control Release 94:177
61. Krauland AH, Guggi D, Bernkop-Schnürch A (2006) Int J Pharm 307:270
62. Krauland AH, Leitner VM, Grabovac V, Bernkop-Schnürch A (2006) J Pharm Sci 95:2463
63. Schmitz T, Bravo-Osuna I, Vauthier C, Ponchel G, Loretz B, Bernkop-Schnürch A (2007) Biomaterials 28:524
64. Loretz B, Thaler M, Bernkop-Schnürch A (2007) Bioconjug Chem 18:1028
65. Atyabi F, Talaie F, Dinarvand R (2009) J Nanosci Nanotechnol 9:4593
66. Lee D, Zhang W, Shirley SA, Kong X, Hellermann GR, Lockey RF, Mohapatra SS (2007) Pharm Res 24:157
67. Shu S, Wang X, Zhang X, Zhang, X, Wang Z, Li C (2009) New J Chem 33:1882
68. Hahn SK, Kim JS, Shimobouji T (2006) J Biomed Mater Res 80A:916
69. Lee, H, Mok H, Lee S, Oh Y-K, Park TG (2007) J Control Release 119:245
70. Lee, H, Jeong Y, Park TG (2007) Biomacromolecules 8:3705
71. Morimoto N, Qui X-P, Winnik FM, Akiyoshi K (2008) Macromolecules 41:5985
72. Bae KH, Mok H, Park TG (2008) Biomaterials 29:3376
73. Wong SS (1991) Chemistry of protein conjugation and cross-linking. CRC, Boca Raton
74. Gao J, Haidar G, Lu X, Hu Z (2001) Macromolecules 34:2242
75. Xia X, Tang S, Lu X, Hu Z (2003) Macromolecules 36:3695
76. Cai T, Hu Z (2004) Langmuir 20:7355
77. Jha AK, Hule RA, Jiao T, Teller SS, Clifton RJ, Duncan RL, Pochan DJ, Jia X (2009) Macromolecules 42:537
78. Scott EA, Nichols, MD, Cordova, LH, George BJ, Jun Y-S, Elbert DL (2008) Biomaterials 29:4481
79. Hasegawa U, Sawada S-I, Shimizu T, Kishida T, Otsuji E, Mazda O, Akiyoshi K (2009) J Control Release 140:312
80. Monteiro OAC, Airoldi C (1999) Int J Biol Macromol 26:119
81. Denkbas EB, Seyyal M, Piskin E (1999) J Microencapsul 16:741
82. Al-Helw AA, Al-Angary AA, Mahrous GM, Al-Dardari MM (1998) J Microencapsul 15:373
83. Thanoo BC, Sunny MC, Jayakrishnan A (1992) J Pharm Pharmacol 44:283
84. Jameela SR, Kumary TV, Lal AV, Jayakrishnan A (1998) J Control Release 52:17
85. Kumbar SG, Kulkarni A, Aminabhavi TM (2002) J Microencapsul 19:173
86. Mitra A, Gaur U, Ghosh PC, Maitra AN (2001) J Control Release 74:317
87. He P, Davis SS, Illum L (1998) Int J Pharm 166:75
88. He P, Davis SS, Illum L (1999) Int J Pharm 187:53
89. Wang L-Y, Ma G-H, Su Z-G (2005) J Control Release 106:62
90. Wang L-Y, Gu Y-H, Zhou Q-Z, Ma G-H, Wan Y-H, Su Z-G (2006) Colloids Surf B Biointerfaces 50:126

91. Wei W, Wang L-Y, Yuan L, Wei Q, Yang X-D, Su Z-G, Ma G-H (2007) Adv Funct Mater 17:3153
92. Bodnar M, Hartmann JF, Borbely J (2005) Biomacromolecules 6:2521
93. Bodnar M, Hartmann JF, Borbely J (2006) Biomacromolecules 7:3030
94. Yun YH, Goetz DJ, Yellen P, Chen W (2004) Biomaterials 25:147
95. Jia X, Yeo Y, Clifton RJ, Jiao T, Kohane DS, Kobler JB, Zeitels SM, Langer R (2006) Biomacromolecules 7:3336
96. Shen X, Zhang L, Jiang X, Hu Y, Guo J (2007) Angew Chem Int Ed Engl 46:7104
97. Yamaoka T, Tabata Y, Ikada Y (1994) J Pharm Sci 83:601
98. Harris JM, Zalipsky S (eds) (1997) Poly(ethylene glycol): chemistry and biological applications. American Chemical Society, Washington DC
99. Prime KL, Whitesides GM (1993) J Am Chem Soc 115:10714
100. Leckband D, Sheth S, Halperin A (1999) J Biomater Sci Polym Ed 10:1125
101. Oral E, Peppas NA (2004) J Biomed Mater Res 68A:439
102. Lutolf MP, Hubbell JA (2003) Biomacromolecules 4:713
103. Dhanasingh A, Salber J, Moeller M, Groll J (2010) Soft Matter. 6:618
104. Vandenberg EJ (1985) J Polym Sci A Polym Chem 23:915
105. Sunder A, Hanselmann R, Frey H, Mülhaupt R (1999) Macromolecules 32:4240
106. Dworak A, Baran G, Trzebicka B, Wałach W (1999) React Funct Polym 42:31
107. Erberich M, Keul H, Möller M (2007) Macromolecules 40:3070
108. Keul H, Möller M (2009) J Polym Sci A Polym Chem 47:3209
109. Kainthan RK Janzen J, Levin E, Devine DV, Brooks DE (2006) Biomacromolecules 7:703
110. Boussif O, Lezoualc'h F, Zanta MA, Mergny MD, Scherman D, Demeneix B, Behr J-P (1995) Proc Natl Acad Sci USA 92:7297
111. Pack DW, Hoffman AS, Pun S, Stayton PS (2005) Nat Rev Drug Discov 4:581
112. Garnett MC (1999) Crit Rev Ther Drug Carrier Syst 16:147
113. Behr J-P (1997) Chimia 51:34
114. Peng Q, Zhong Z, Zhuo R (2008) Bioconjug Chem 19:499
115. Forrest ML, Koerber JT, Pack DW (2003) Bioconjug Chem 14:934
116. Kloeckner J, Wagner E, Ogris M (2006) Eur J Pharm Sci 29:414
117. Gosselin MA, Guo W, Lee RJ (2001) Bioconjug Chem. 12:989
118. Wang Y, Chen P, Shen J (2006) Biomaterials 27:5292
119. Thomas M, Ge Q, Lu JJ, Chen J, Klibanov A (2005) Pharm Res 22:373
120. Schmidt-Wolf GD., Schmidt-Wolf, IGH (2003) Trends Mol Med 9:67
121. Park TG, Jeong JH, Kim SW (2006) Adv Drug Deliv Rev 58:467
122. Bauhuber S, Hozsa C, Breunig M, Göpferich A (2009) Adv Mat 21:3286
123. Luten J, van Nostrum CF, De Smedt SC, Hennink WE (2008) J Control Release 126:97
124. Jere D, Jiang HL, Arote R, Kim YK, Choi YJ, Cho MH, Akaike T, Cho CS (2009) Expert Opin Drug Deliv 6:827
125. Aliyar HA, Hamilton PD, Remsen EE, Ravi N (2005) J Bioact Compat Polym 20:169
126. Groll J, Singh S, Albrecht K, Moeller M (2009) J Polym Sci A Polym Chem 47:5543
127. Nichols MD, Scott EA, Elbert DL (2009) Biomaterials 30:5283
128. Mok H, Park TG (2006) Bioconjug Chem 17:1369
129. Vinogradov S, Batrakova E, Kabanov A (1999) Colloids Surf B Biointerfaces 16:291
130. Vinogradov SV, Bronich TK, Kabanov AV (2002) Adv Drug Deliv Rev 54:135
131. Bronich TK, Vinogradov SV, Kabanov AV (2001) Nano Lett 1:535
132. Vinogradov SV, Batrakova EV, Kabanov AV (2004) Bioconjug Chem 15:50
133. Vinogradov SV (2006) Curr Pharm Res 12:4703
134. Vinogradov SV, Zeman AD, Batrakova EV, Kabanov AV (2005) J Control Release 107:143
135. Vinogradov SV, Kohli E, Zeman AD (2006) Pharm Res 23:920
136. Nimesh S, Goyal A, Pawar V, Jayaraman S, Kumar P, Chandra R, Singh Y, Gupta KC (2006) J Control Release 110:457
137. Swami A, Goyal R, Tripathi SK, Singh N, Katiyar N, Mishra AK, Gupta KC (2009) Int J Pharm 374:125
138. Kohli E, Han H-Y, Zeman AD, Vinogradov SV (2007) J Control Release 121:19

139. Neu M, Sitterberg J, Bakowsky U, Kissel T (2006) Biomacromolecules 7:3428
140. Neu M, Germerhaus O, Mao S, Voigt KH, Behe M, Kissel T (2007) J Control Release 118:370
141. Deng R, Yue Y, Jin F, Chen Y, Kung H-F, Lin MCM, Wu C (2009) J Control Release 140:40
142. Lee Y, Park SY, Kim C, Park TG (2009) J Control Release 135:89
143. Dalton PD, Hostert C, Albrecht K, Moeller M, Groll J (2008) Macromol Biosci 8:923
144. Caraculacu AA, Coseri S (2001) Prog Polym Sci 26:799

Adv Polym Sci (2010) 234: 95–128
DOI:10.1007/12_2010_76

Published online: 28 May 2010

Synthesis of Microgels by Radiation Methods

Franziska Krahl and Karl-Friedrich Arndt

Abstract The key features of applying radiation techniques to synthesize microgels is the additive-free initiation and an easy process control. Therefore, radiation methods are very suitable for applications in biosciences. Microgels with desired dimensions can be obtained simply by varying the experimental parameters such as concentration, radiation dose, or radiation temperature. By intramolecular cross-linking of single polymer chains even nanogels with diameters smaller than 0.1 µm can be synthesized. Examples of microgels based on different polymers are summarized in this article. The structure of various polymeric architectures such as micelles or interpolymer complexes can be fixed by irradiation to form microgels with specific properties. Their huge application potential as well as selective examples are described.

Keywords Intramolecular cross-linking · Nanogels · Radiation cross-linking · Responsive polymers · Sensitive microgels

Contents

F. Krahl (✉) and K.-F. Arndt
Department of Chemistry, Physical Chemistry of Polymers,
Technische Universität Dresden, 01069 Dresden, Germany
e-mail: franziska.krahl@tu-dresden.de; karl-friedrich.arndt@chemie.tu-dresden.de

Abbreviations

CMC	Critical micelle concentration
CP	Cloud point
DLS	Dynamic light scattering
FESEM	Field emission scanning electron microscopy
Gy	Gray ($1\,\mathrm{Gy} = 1\,\mathrm{J\,kg^{-1}}$)
HPC	Hydroxypropyl cellulose
MWD	Most-probable molecular weight distribution
PAA	Poly(acrylic acid)
PAAm	Polyacrylamide
PEO	Poly(ethylene oxide)
PI	Polyisoprene
PPO	Poly(propylene oxide)
PPy	Polypyrrole
PVME	Poly(vinyl methyl ether)
PVP	Poly(vinyl pyrrolidone)
Py	Pyrrole
SEM	Scanning electron microscopy
SLS	Static light scattering

Symbols

D	Dose
D_g	Gelation dose
D_V	Virtual dose
g	Gel fraction
g'	Viscosity branching parameter
G_s	Radiation yield of chain scission
G_x	Radiation yield of cross-linking
M_n	Number-averaged molecular weight
M_w	Weight-averaged molecular weight
p_0	Degradation density
q_0	Cross-linking density
R_g	Radius of gyration
R_h	Hydrodynamic radius

s	Sol content
T_c	Phase transition temperature
$u_{2,0}$	Weight-averaged degree of polymerization before irradiation

1 Introduction

Radiation can contribute to biotechnology and bioengineering by various chemical and physical means (polymerization, grafting, etching, cross-linking, etc.). Radiation cross-linking of polymers is a very attractive production process for various materials, including improved insulating wires and cables, heat-shrinkable materials, adhesives, interpenetrating polymer networks, and polymeric foams. There is an increasing interest in radiation-induced polymerization and cross-linking in polymeric hydrogels. Radiation is used advantageously for the control of cross-linking because the properties of hydrogels are strongly affected by cross-linking density and structure. A hydrogel is often introduced into a structural part of a functional material. Radiation grafting, radiation lithography, and track etching technology are used for modification of a material surface with a hydrogel.

The history of radiation chemistry of polymers started in the early 1950s [9, 11]. Poly(*N*-vinyl pyrrolidone) (PVP) was and still is often applied in medicine and pharmacy as a polymer and as a hydrogel. In 1955, Charlesby and Alexander first reported on cross-linking of PVP [11]. Since then, various other water-soluble polymers have been radiochemically treated and cross-linked, even as one step in the preparation of novel polymeric biomaterials for diagnostic and therapeutic devices, instruments, or implants [23]. The radiation technique has already become one of the standard methods for formation of hydrogels. The methods applied are usually based on the irradiation of monomer or polymer solutions with a sufficient dose. Besides the synthesis of macroscopic "wall-to-wall" hydrogels, there is an interest in the formation of gels, especially of smart gels, in the micrometer or nanometer range. Examples are thin layers on different substrates, smart coatings, patterned structures for application in microsystems (sensors, actuators), etc., and gel particles with dimensions in the micrometer range (microgels) and submicrometer range (nanogels) [18, 35].

Typically, micro- and nanogels are synthesized by combined polymerization and cross-linking, e.g., in emulsion. A disadvantage of this procedure is the necessity of applying further treatments to purify the gels, especially when the products are designed for biomedical application. Unreacted monomers, cross-linker, initiator, stabilizer, etc., are potentially harmful substances. Radiation cross-linking is a way to a "clean" product. The first radiochemical synthesis of a microgel was done by Schnabel and Borwardt in 1969. A low concentration aqueous solution of poly(ethylene oxide) (PEO) was irradiated by γ-rays from a ^{60}Co source [44]. Different water-soluble polymers were cross-linked by irradiation in dilute solutions to form microgels and nanogels.

This report gives an overview on:

- Irradiation parameters; Sect. 2.1
- Irradiation mechanisms; Sect. 2.2
- Radiation sources; Sect. 2.3
- Examples of inter- and intramolecular cross-linked microgels; Sects. 3.1 and 3.2
- Characterization methods for radiation cross-linked polymers; Sect. 4.1
- Applications of microgels obtained by radiation cross-linking; Sect. 4.2

2 Radiation and Polymers

High energy radiation splits covalent bonds into unpaired radicals, which can then recombine randomly. Depending upon the relative rates of recombination and scission, an irradiated polymer can be cross-linked or it degrades into low molecular weight fragments. The influence of irradiation on polymers depends on their chemical structure:

- For polymers with quaternary C-atoms in the backbone, chain scission will occur
- Aromatic groups in the polymer chain reduce the influence of radiation
- Unsaturated bonds reinforce the tendency to cross-linking

Cross-linking also depends on the irradiation conditions, like atmosphere (influence of oxygen) and temperature (glass transition temperature). Polymers that cross-link under inert atmosphere might degrade under oxygen atmosphere. The mobility of the polymer chains is hindered at a temperature lower than the glass transition temperature and cross-linking might be suppressed. Table 1 gives an overview of the influence of high-energy radiation on different polymers.

Table 1 Influence of high-energy radiation on polymers under inert atmosphere (according to [18])

Polymers prone to scission	Polymers prone to cross-linking
Poly(isobutylene)	Poly(ethylene)
Poly(tetrafluoroethylene)	Poly(styrene)
Poly(methyl methacrylate)	Poly(vinyl alcohol)
Poly(acrylnitrile)	Poly(butadiene)
Poly(methacrylamide)	Poly(acrylates)
Cellulose and derivatives	Poly(acrylamide)
Poly(α-methylstyrene)	Poly(dimethylsiloxane)
Poly(vinylidene fluoride)	Poly(urethanes)
–[CH_2–CR′R″]–	Natural rubber
	–[CH_2–CHR]–

2.1 Gelation Dose, Sol–Gel Analysis

The formation of a polymer networks starts with an increase in molecular weight and formation of branched structures. At a typical extent of reaction, the gelation point is that point at which a network is first formed. The extent of reaction as well as the cross-linking density in radiation-induced cross-linking processes is determined by the radiation dose. The term "dose" means the quantity of radiation applied to or absorbed accidentally by a given volume or mass of sample. The absorbed dose is measured in Gray (Gy), $1\,\mathrm{Gy} = 1\,\mathrm{J\,kg^{-1}}$. Therefore, the formation of a polymeric network needs a certain dose, the gelation dose D_g, which can be determined by "sol–gel analysis."

Typically, a cross-linked polymer is insoluble. During the cross-linking reaction, the amount of polymer chains being connected by chemical bonds increases. The determination of the insoluble fraction (gel) and the soluble fraction (sol) of a polymer is done by the sol–gel analysis. In general, the cross-linking density increases and the sol content decreases with increasing dose. But, it is necessary to determine these correlations for each polymer at the conditions during irradiation.

Sol–gel analysis is an important tool for distinguishing between polymers that can be cross-linked by irradiation and polymers that are not cross-linkable by radiation techniques. These experiments are typically done for "wall-to-wall" gels and offer the possibility to determine the irradiation conditions for microgel formation. Charlesby and Pinner first obtained a simple expression relating the soluble part of a polymer sample, the sol fraction (s) or sol content (in contrast to the insoluble part, the gel fraction (g) or gel content) to the absorbed dose D of radiation [10, 12].

$$s + \sqrt{s} = \frac{p_0}{q_0} + \frac{2}{q_0 u_{2,0} D}, \tag{1}$$

where p_0 is the degradation density, i.e., the average number of main chain scissions per monomer unit and per unit dose; q_0 is the cross-linking density, i.e., proportion of monomer units cross-linked per unit dose; and $u_{2,0}$ is the weight-averaged degree of polymerization of the polymer before irradiation. This equation was derived from an example of a polymer with a most-probable molecular weight distribution (MWD) and with $M_\mathrm{w} = 2\,M_\mathrm{n}$, where M_n is the number-averaged molecular weight and M_w the weight-averaged molecular weight.

The sum of s and g amounts to unity.

$$s = 1 - g. \tag{2}$$

Plotting $s + \sqrt{s}$ against the reciprocal value of the dose D gives a straight line. The value q_0 can be calculated from its slope and the ratio p_0/q_0 from the intercept at $1/D = 0$. Values of p_0/q_0 above unity mean that degradation is preferred, whereas values smaller than unity reveal that cross-linking is preferred.

The gelation dose D_g can be determined at $s = 1$ or $s + \sqrt{s} = 2$, with $1/D = 1/D_g$. If the absorbed dose D is smaller than the gelation dose ($D < D_g$), then no cross-linking occurs. If the absorbed dose equals the gelation dose, then a network is formed for the first time. For $D > D_g$, the amount of polymer chains that have reacted with the network increases, and therefore the gel fraction increases and the sol fraction decreases.

Often, the experimental data do not fit the straight line predicted by Charlesby and Pinner. Deviations from the simple Charlesby–Pinner equation cannot be ascribed to structural effects of the polymer, but rather to the deviation of the real MWD of the polymer from the most-probable MWD and to other relationships between M_n and M_w. A modified equation, first reported by Rosiak, often named the Charlesby–Pinner–Rosiak equation [36], is:

$$s + \sqrt{s} = \frac{p_0}{q_0} + \left(2 - \frac{p_0}{q_0}\right)\left(\frac{D_V + D_g}{D_V + D}\right), \tag{3}$$

where D_g is a so-called virtual dose. The virtual dose is required for changing the MWD of the polymer in such a way that $M_w = 2\,M_n$. If the investigated polymer has a broader distribution, then $D_V > 0$, or if it has a narrower distribution, then $D_V < 0$.

If M_n and M_w of the investigated polymer are known, D_V can be calculated from the following equation:

$$D_V = \frac{4}{3q_0}\left(\frac{1}{2M_n} - \frac{1}{M_w}\right). \tag{4}$$

Otherwise, a fit of measured sol fraction in dependence on dose D enables the calculation of D_V, D_g, and p_0/q_0.

Another manner of considering dose requirements is to express the average energy input (e.g., in electron volts) needed to promote a certain reaction. So-called G-values are reported (e.g., [31]) for different radiochemical yields (yield of free radicals, yield of cross-links, yield of main chain scission, yield of product molecules) at defined conditions (temperature, atmosphere, radiation source). They are defined as the yield of individual atomic or molecular events for 100 eV (or per joule) of energy absorbed by the system. Following the changes in molecular weight of an irradiated polymer (sol–gel analysis and determination of molecular weights of the sol content) allows calculation of the radiation yield of cross-linking (G_x in moles per joule) and of chain scission (G_s in moles per joule) [10]:

$$G_x - G_s = \frac{c}{D\rho}\left(\frac{1}{M_{n,0}} - \frac{1}{M_n}\right). \tag{5}$$

For a most-probable MWD and $M_w/M_n = 2$ it follows that:

$$4G_x - G_s = \frac{2c}{D\rho}\left(\frac{1}{M_{w,0}} - \frac{1}{M_w}\right), \tag{6}$$

where M_n and M_w are the number and weight average molecular weights of the irradiated polymer, respectively; D is the absorbed dose (in Gray); ρ is the density of the polymer in the irradiated solution (in grams per cubic centimeter); and c its concentration (in grams per cubic decimeter). The subscript 0 denotes the molecular weights before irradiation. M_w is infinite at the gel point. The number of moles of cross-linking bonds G_x per Joule of a dry polymer (under the assumption $G_s = 0$) can be calculated from D_g (in Gray):

$$G_x = \frac{0.5 \times 10^{-3}}{M_{w,0} D_g}. \tag{7}$$

From experiments, it follows that D_g depends on concentration of polymer in an irradiated solution in such a manner that the higher the polymer concentration, the higher the $D_g$value [e.g., for poly(vinyl methyl ether) (PVME): 2% w/w, 6.2 kGy; 5% w/w, 10.1 kGy; bulk, 48.5 kGy. The G_x ranges from 0.3×10^{-7} to 2.2×10^{-7} mol J^{-1}. For details see [26]].

2.2 Processes and Procedures

Hydrogels can be synthesized in different ways, starting from either monomers or polymers:

- Starting from monomers: Monomers in bulk or in solution are irradiated. Polymerization takes place as the first stage of reaction. The polymer chains are then cross-linked. It is frequent practice to add bifunctional monomers to increase the efficiency of cross-linking. Typically, this procedure is used for synthesis of "wall-to-wall" hydrogels or microspheres. For biomedical use of the formed gels, all non-reacted monomers and residues have to be extracted.
- Starting from polymers: It is possible to cross-link polymers in the dry state, e.g., thin polymer layers ([8] PVP, [19] HPC, [5, 42] patterning, [20] PVME), films, coatings, or polymer objects of technical interests. The dimension and structure of the formed polymeric gel depend on the concentration of the macromolecules and on conditions during the irradiation. At low polymer concentrations (low regarding the overlap concentration) the formation of a "wall-to-wall" gel is not possible. The single macromolecules are separated. It is well-known that the most water-soluble polymers are not monodisperse when dissolved. They tend to form supermolecular structures, even at low concentrations. The radiochemical approach offers possibilities for fixing the polymeric structures that are formed in solution at low concentrations, e.g., complexes, aggregates, micelles.

The irradiation of a low concentration aqueous solution (e.g., degassed or saturated with inert gases to prevent the disturbing influence of oxygen, or saturated with N_2O to promote some reactions) of a water-soluble polymer is the most common way to form hydrogels in the micrometer or submicrometer range. The gel

Table 2 Radiochemical yield of primary products of water radiolysis [45]

Transients	G #(number/100 eV)	G (10^{-7} mol J^{-1})
OH	2.75	2.9
H	0.65	0.68
e^-_{solv}	2.65	2.8
H_2	0.45	0.47
H_2O_2	0.70	0.74

particles result from the coupling of polymer radicals that were directly or indirectly produced from the polymer chain by the high-energy radiation. Most of the energy is absorbed by the water. The ionization of water molecules is followed by formation of reactive species. Therefore, irradiation of an aqueous solution leads to a great number of transients from water (e.g., OH radicals, H radicals, solvated electrons, hydrogen peroxide) that can react with the polymer. The content of the formed transients can be expressed in their radiochemical yields (G values, Table 2) (see [45]):

The mechanism of formation of a polymeric network is shown by the two following examples:

- Cross-linking of poly(acrylic acid) (PAA) (in Ar-saturated solution under acid conditions, pH 2) [27]:

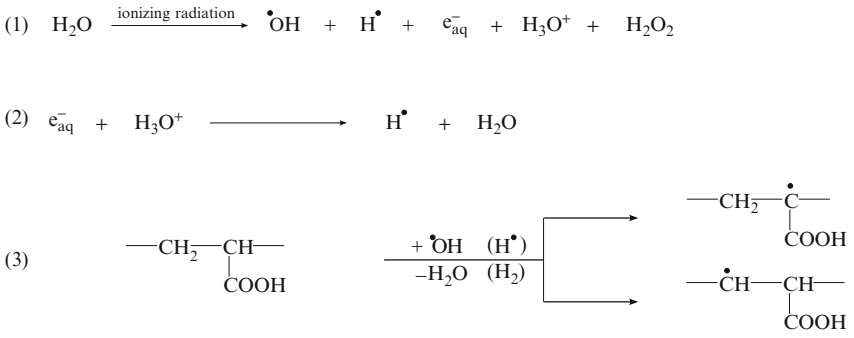

- Cross-linking of PVME (in N_2O saturated solution) [37]:

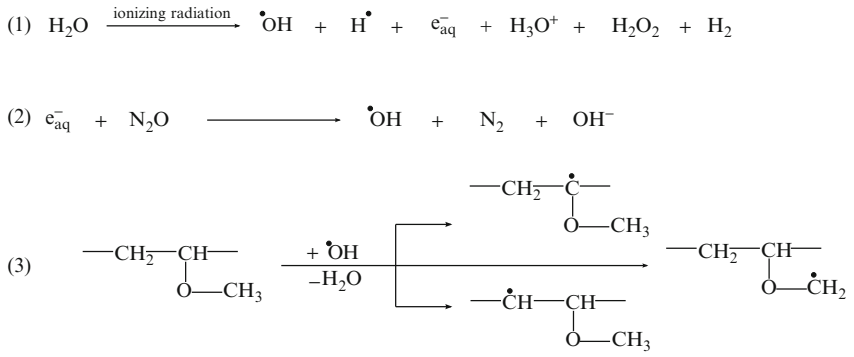

2.3 Radiation Sources and Techniques

As high-energy radiation, γ-rays (electromagnetic radiation emitted by a radioactive isotope, mostly ^{60}Co) or electron beams (electron accelerator of low energies, 0.1–3 MeV; or high-energy electron accelerator, 10 MeV) are available. Table 3 shows a comparison of both techniques.

γ-Irradiation: Mostly, the isotope ^{60}Co is used as radiation source.^{60}Co is formed in atomic reactors under the bombardment with neutrons: $^{59}_{27}\mathrm{Co} + {}^{1}_{0}\mathrm{n} \rightarrow {}^{60}_{27}\mathrm{Co} + \gamma$. A typical dose rate is 2 kGy h^{-1}. The dose is controlled by the exposure time and measured with a dosimeter.

Electron accelerator: To generate electrons of high energy it is necessary to accelerate the electrons leaving a cathode. Typical parameters are described for the example of an ELV-2 (Budker Institute of Nuclear Physics, Novosibirsk, Russia): The accelerator in a LINAC (linear accelerator) is working in the energy range from 0.6 to 1.5 MeV. The maximum beam current and beam power are 25 mA and 20 kW, respectively. The dimensions of the beam extraction windows (50-μm titanium foil) are 980 mm in length and 75 mm in width. Typically, applied experimental parameters for hydrogel synthesis are 1.5 MeV and 4 mA. The dose is regulated by the exposure time and is measured with a dosimeter.

Several research institutes use other electron-beam facilities with lower accelerator voltages (e.g., ANDREA 1 at Fraunhofer Institute for Electron Beam and Plasma Technology, Dresden, Germany). The accelerator voltage is in the range 90–120 kV. This results in smaller penetration depths (10–80 μm). Again, the applied radiation dose can be adjusted to several hundred kiloGrays at different dose rates by changing the beam current (e.g., 2–20 mA) and the exposure time.

Table 3 Comparison of electron beam and γ-irradiation

Radiation	Electron beam	γ-irradiation
Source	Electron accelerator	Radioactive isotopes (mostly ^{60}Co)
Depth of penetration	Millimeter range or less, in dependence of acceleration voltage (penetration profile!)	Centimeter range
Reaction time	1–2 min	Several hours
Critical process conditions	Variation in cross-linking density, gradient of cross-linking density, heating effects	Long reaction time, diffusion of oxygen must be prevented
Advantages	Short reaction time, beam focusing, pulse irradiation	Homogeneously cross-linked samples, no restrictions regarding dimension

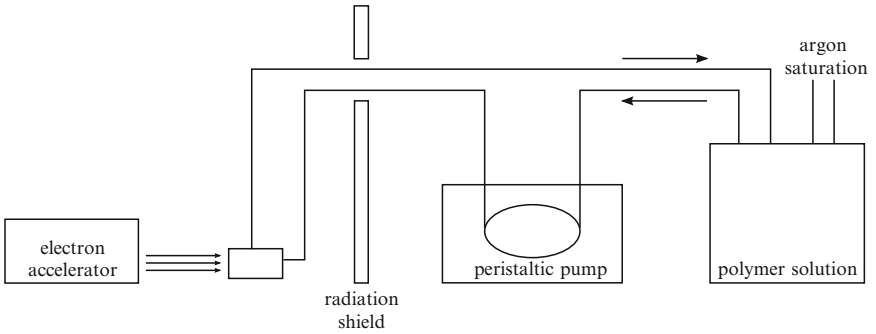

Fig. 1 Irradiation setup for pulse radiolysis consisting of a solution reservoir, a peristaltic pump, and a quartz irradiation cell. Prior and during irradiation, the polymer solution is continuously saturated with argon

Pulse irradiation (Fig. 1): In 1966, Henglein [21] studied the reaction kinetics of different radicals and low molecular weight compounds in water under the influence of an impulse of energy-rich electrons. The method of irradiation with short pulses of electrons was applied to investigation of chemical reactions in an aqueous solution of PEO [6]. The method of pulse irradiation is useful for studying processes at a high-energy irradiation by combination with analytical methods (e.g., investigation of changes in chemical structures by spectroscopic methods, monitoring changes in molecular weights and dimensions by light scattering). On the other hand, the method of pulse irradiation is useful for the synthesis of nanogels, e.g., by intramolecular cross-linking of polymer molecules with high molecular weights [4, 39, 47, 49]. The term nanogel is used for intramolecularly cross-linked polymers. For intermolecularly cross-linked gels in the range of several 100 nm, the term microgel is used. The polymer is dissolved in water and the solution, flowing through a quartz irradiation cell, is pulse-irradiated with electrons of several MeV generated by a linear accelerator. Typically experimental conditions are: pulse frequency 5.0 Hz; pulse duration 3 µs; flow rate 5.0 mL s^{-1}; and effective cell volume 1 mL [50].

For special purposes, a combination of γ- and electron irradiation can be useful: For polymer molecules with low molecular weight it is possible to increase M by irradiation with a low dose of γ-rays, followed by further electron beam irradiation to perform intermolecular cross-linking.

2.4 Advantages of Radiation Cross-Linking

In comparison with other laboratories techniques in polymer chemistry, radiochemical synthesis seems to be a large-scaled experiment, expensive, and exotic. But this is only partially true. There exist industrial facilities like electron accelerators and

γ-plants, and some of these radiation sources are operated by research institutes. The radiochemical approach has some advantages. In general, the outstanding features of radiochemical cross-linking processes are:

- Easy process control by simple on and off switching of the cross-linking reaction
- Degree of cross-linking is correlated to the applied dose
- No necessity to add any initiators, cross-linkers, etc.
- Possibility of joining hydrogel formation and sterilization in one technological step, which is advantageous for hydrogels in medical applications
- Possibility to obtain gel particles of different dimension and different structure by changing the parameters of the irradiation process.

3 Examples

Ionizing radiation is an alternative way (compared to classical initiation methods) to synthesize microgels. In general two different approaches can be used:

1. Initiating the cross-linking polymerization of monomers by radiation
2. Inducing the cross-linking of polymer chains in the absence of monomers or required cross-linker molecules

A striking advantage of the second approach is that no unreacted monomers remain in the microgel structure, which is an essential requirement for biomedical applications. Therefore, only examples of polymer cross-linking will be discussed here.

Depending on the polymer concentration and on the dose rate, two different cross-linking reactions can take place: intermolecular or intramolecular cross-linking (Fig. 2). If the average number of radicals per single chain is low, intermolecular recombination occurs. By increasing the dose rate, the number of radicals per chain is increased as well. The irradiation of dilute polymer solutions therefore leads to intramolecular cross-linking because the macromolecules are separated and radical recombination only occurs internally. By contrast, irradiation of polymer solutions at medium or high concentration mainly results in intermolecular cross-links.

3.1 Intramolecular Cross-linking

The cross-linking of individual macromolecules by intramolecular junctions results in microgels of typical sizes smaller than 0.1 μm (submicrometer range). Microgels obtained by intramolecular cross-linking are often referred as nanogels. Since single macromolecules are internally cross-linked, such nanogels are frozen polymer coils. Depending on the molecular weight, the size, and the architecture of the starting polymers, nanogels with various dimensions, including very small structures, can be synthesized.

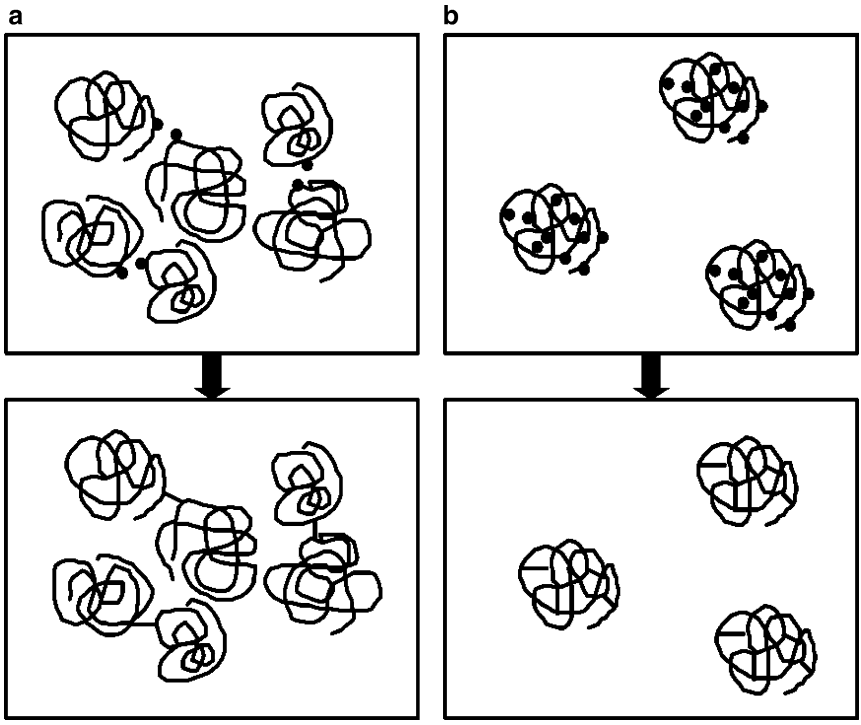

Fig. 2 Influence of the dose rate and the polymer concentration on the structures obtained by irradiation: (**a**) intermolecular cross-linking at medium concentrations and low dose rates, and (**b**) intramolecular cross-linking at low concentrations and high dose pulses. (Reprinted from [41], copyright 2009, with permission of Elsevier)

In principle, intramolecular cross-linking can be performed chemically by reactive groups present in the polymer chains. One way is the preparation of polymers containing pendant vinyl groups that can be cross-linked by a suitable initiator. Another possibility is the synthesis of polymers with functional groups (e.g., –OH, –COOH). By choosing a suitable bifunctional cross-linking agent, these functional groups can be cross-linked to obtain nano- or microgels. For example, poly(vinyl alcohol) nanogels were synthesized with glutaraldehyde as cross-linker [7]. Even at very low polymer concentrations, additional intermolecular cross-linking could not be avoided completely. An increase in the molecular weight with increasing glutaraldehyde concentration indicated that at most two chains were linked together, followed by further intermolecular cross-linking.

Using ionizing radiation for intramolecular cross-linking of individual polymers, the synthesis can be performed in the absence of additional initiators, cross-linkers, or additives. For this approach, a pure aqueous solution of the polymer is exposed to a short intense pulse of ionizing electron beam radiation (typically a few microseconds, see Sect. 2.3, Fig. 1). During the exposure many radicals are generated simultaneously along each polymer chain. The intramolecular recombination of these

radicals leads to the formation of nano- or microgels. This approach was first tested on poly(vinyl alcohol) to demonstrate that the radical recombination mainly occurs within a single polymer coil [49]. Doses ranging from 2 to 11 kGy were applied to the diluted poly(vinyl alcohol) solutions. For low doses, the molecular weight remained nearly constant, whereas for higher doses a slight increase in molecular weight was observed. This indicates that a fraction of initially formed macroradicals also recombined intermolecular. However, based on kinetic studies, it could be concluded that the yield of the intramolecular cross-linking is more than 99%.

The pulse radiolysis technique was further applied to PVP [47]. Up to doses of 5 kGy, the molecular weight remained constant, indicating a very low contribution of intermolecular cross-linking. Surprisingly, the radius of gyration decreased with increasing radiation dose. Evidently, the intramolecular cross-linking is associated with a shrinking of the dimensions. The introduction of internal chemical bonds leads to a higher segment density and therefore to less drained structures.

For PAA nanogels, a decrease in the molecular weight could be observed for low radiation doses [27, 50]. In addition to intermolecular recombination, polymer radicals can undergo competing reactions like chain scission. It has been shown for polyelectrolytes that scission is the dominating reaction over a broad pH range. Repulsive forces between charged polyelectrolyte chains reduce the probability that two radicals reach each other for recombination. Only in the acidic range (below pH 3) does cross-linking dominate over chain scission because of suppressed dissociation. However, for low total doses, chain scission still dominates over internal cross-linking and the molecular weight decreases. At higher doses, chain scission also occurs but intramolecular cross-links are formed more quickly and therefore prevent a significant decrease in the molecular weight. Generated chain fragments remain linked to the nanogel structure at a few other points. This means that nanogels, in general, should exhibit an enhanced resistance against degradation, as demonstrated in Fig. 3. For a linear polymer the formation of peroxyl radicals along the chain easily leads to the degradation in short fragments. If the same number of chain breaks occurs in a nanogel, no fragmentation is caused because the chain segments are still linked together at a number of other points.

To verify this assumption, aqueous solutions of linear PAA chains and PAA nanogels were irradiated in the presence of oxygen [27]. Under these conditions no cross-linking takes place for PAA [48]. The changes in the molecular weight and in the radius of gyration show clear differences for the linear and the nanogel PAA. Linear PAA degrades very easily even at low radiation doses, resulting in decreasing molecular weight and radius. Meanwhile, M_w and R_g of the nanogel PAA remain constant within the whole dose range. Therefore, it could be concluded that PAA nanogels are much more resistant to free-radical-induced degradation than the parent linear macromolecules.

The approach of intramolecular cross-linking was further extended to temperature-sensitive polymers. PVME nanogels were obtained by irradiation of dilute PVME solutions by a pulsed electron beam [41]. The M_w of these nanogels is independent of the radiation dose (above 2 kGy). The phase transition temperature T_c of PVME is slightly affected by the cross-linking reaction. With increasing radiation

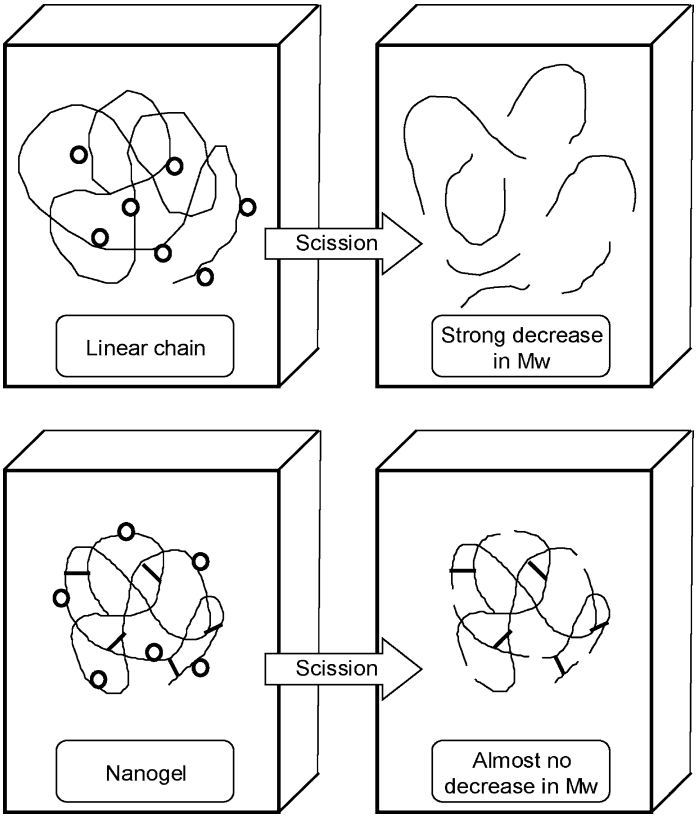

Fig. 3 Influence of free-radical-induced chain scission on linear chains and nanogels in the presence of oxygen. *Circles* denote a scission-initiating peroxyl radical. (Reprinted with permission from [27], copyright 2009 American Chemical Society)

dose, T_c is shifted to lower values indicating an influence of the formed internal cross-links. These additional chemical bonds raise the hydrophobicity of PVME and reduce the required thermal energy for hydrogen-bond breakage. Since the number of additional bonds per nanogel is relatively small, the decrease in T_c is not very pronounced.

A very well known biocompatible polymer with various applications in food and clinical fields is gelatin. The irradiation of gelatin aqueous solutions with γ-rays leads to nanometer-sized gelatin particles [17]. The resulting particles exhibit high molecular weight with a hydrodynamic radius of around 10 nm. These highly packed structures grant high stability against temperature so that the sol–gel transition of gelatin can be avoided. Strictly speaking, the nanogelatin is not synthesized solely by intramolecular cross-linking of single gelatin chains. Because gelatin aggregates are always present in aqueous solutions, intermolecular cross-linking also occurs.

A clear advantage of intramolecular cross-linking by high energy irradiation is the possibility of synthesizing gels or particles in the nanometer range without any additives. For biomedical applications, such particles can fulfill the requirements of biosafety as well as exhibit high stability, as shown in degradation studies. Furthermore, the molecular weight and the dimension of nanogels can easily be adjusted by adjusting the molecular weight of the parent polymers.

3.2 Intermolecular Cross-linking

The irradiation of dilute polymer solutions leads to the formation of radicals along the polymer chains. Intra- or intermolecular recombination results in nanogels (as discussed in Sect. 3.1) or microgels, which cause the solution to become turbid even at low radiation doses. Intensive studies (both experimental and theoretical) on poly(vinyl alcohol) indicate that at the initial state of the irradiation, small branched polymers are formed via intermolecular cross-linking, regardless of the polymer concentration [43, 53, 54]. Applying high doses, the initially formed branched molecules undergo further intramolecular cross-linking to microgels (see Fig. 4). In general, the approach of intermolecular cross-linking of different polymer chains is always combined with intramolecular cross-linking inside the desired microgels. A key feature of this strategy is the possibility of fixing pre-build structural formations, e.g., micellar structures or interpolymer complexes.

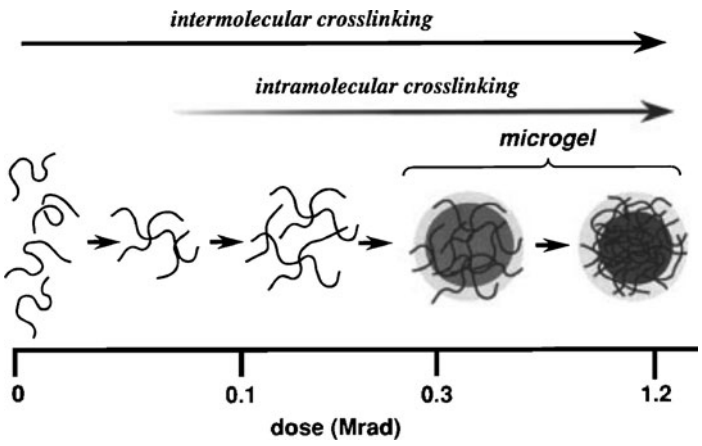

Fig. 4 Microgel formation during γ-ray irradiation. (Reprinted with permission from [53], copyright 2009 American Chemical Society)

3.2.1 Particles

The most popular way to synthesize microgel particles is via emulsion polymerization. Each micelle acts as a separate microreactor, preventing macrogelation during the reaction. Another way to obtain microgel particles is the irradiation of phase-separated polymer solutions (Fig. 5). Phase separation can be achieved by heating (for temperature-sensitive polymers) or mixing with non-solvents.

For PVME, the phase separation can be induced directly during the radiation process. Depending on the applied dose, the temperature of the solution increases. By choosing appropriate experimental parameters, the radiation can be performed above the phase transition temperature and the structure of the collapsed polymer chains will be fixed. The combination of cryo-preparation and field emission scanning electron microscopy (FESEM) allows the investigation of microgel particles at different swelling states (e.g., the swollen state at 25°C and the shrunken state above T_c). In particular, the microgels are immersed rapidly into liquid ethane (cooled to approximately −196°C) to avoid ice crystal formation, followed by freeze-drying at −80°C. As a result, the inner structure (e.g., porosity) can be characterized. Compared to conventional scanning electron microscopy (SEM), FESEM provides narrower probing beams at low as well as high electron energy, resulting in both improved spatial resolution and minimized sample charging and damage.

In Fig. 6 FESEM pictures of PVME particles in the swollen and shrunken state are shown [4]. Globular particles with diameters in the range of 250–600 nm can be obtained by static electron beam irradiation (in petri dishes) starting from a 4 g L^{-1} PVME solution. The resultant particles exhibit a sponge-like structure in the swollen state. The outer shell of the particles is highly porous. The sponge-like porous structure remains when the particles shrink. A higher radiation dose results in more dense particles with smaller average sizes (250–450 nm), which turn into very compact structures in the shrunken state while retaining their size.

Using pulse irradiation in a closed-loop system (see Fig. 1) for the synthesis of PVME particles, the irradiation can performed at lower PVME concentrations (0.1–0.5 g L^{-1}). The cross-linking density of the microgel particles increases with increasing dose, resulting in lower swelling degrees in the swollen state and therefore smaller diameters. In the shrunken state, the average radii are independent of the applied dose (see Fig. 7).

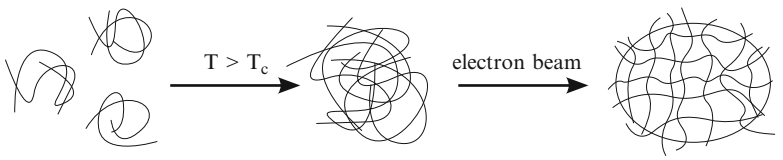

Fig. 5 Synthesis of PVME particles by irradiation of phase-separated solutions. Above the phase transition temperature T_c, the polymer chains collapse to globular aggregates. The collapsed structures are fixed by electron beam irradiation to yield temperature-sensitive microgel particles

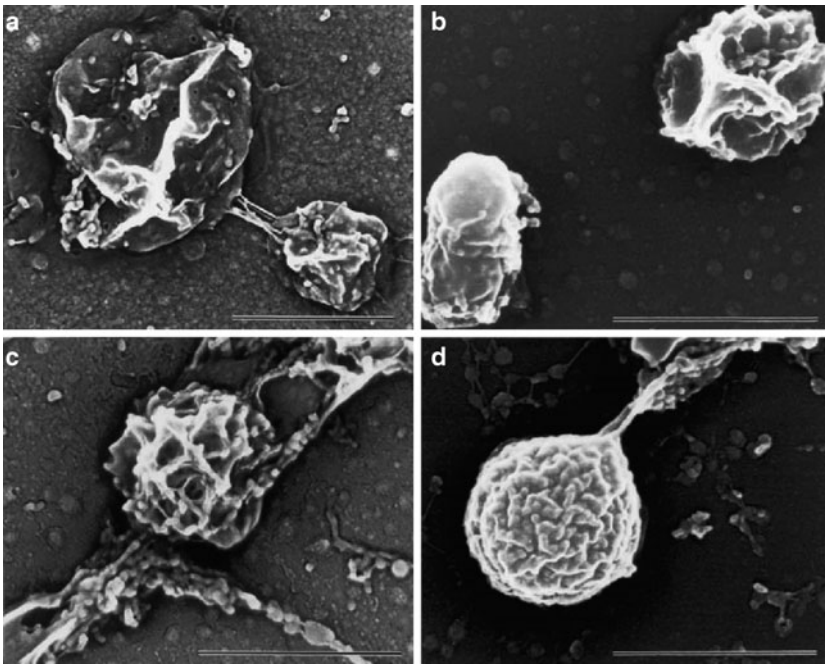

Fig. 6 SEM images of PVME particles after heat-induced phase separation followed by static electron beam irradiation with 20 kGy (*left*) and 80 kGy (*right*): (**a**,**b**) swollen state, and (**c**,**d**) shrunken state. *Scale bars*: 500 nm. (Reprinted from [4], copyright 2009, with permission of Elsevier)

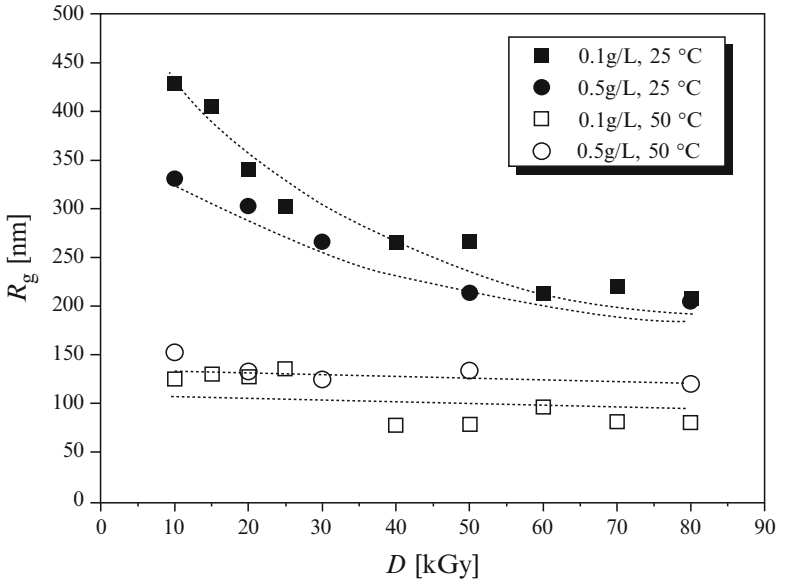

Fig. 7 Dose dependence of the radius of gyration R_g in the swollen (25°C) and shrunken (50°C) state of PVME microgel particles synthesized by pulsed electron beam irradiation above the phase transition temperature

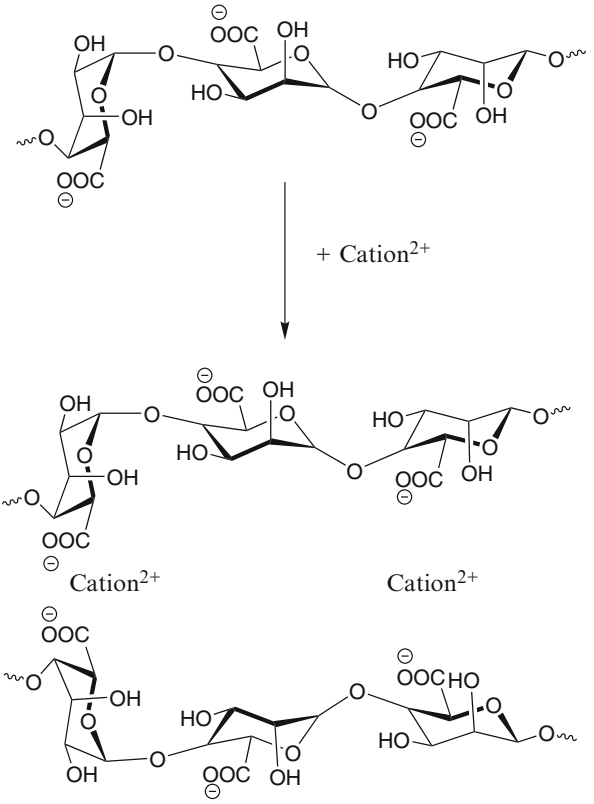

Fig. 8 Ionotrope gelation of alginate by divalent cations

Polymeric microgel particles can further be obtained by the alginate technique. Alginate is an anionic, hydrophilic, and biocompatible natural polysaccharide. The structural composition is that of a linear copolymer of β-D-mannuronic acid and α-L-guluronic acid units. Due to the presence of carboxyl groups, alginate is a negatively charged polyelectrolyte in neutral or basic solutions. In aqueous solution containing divalent or trivalent cations, alginate forms gels (Fig. 8) caused by the attachment and coordination of the metal cations into intermolecular (interchain) cavities. By dropping an alginate solution into an calcium chloride solution, the calcium ions diffuse into the alginate droplets and the alginate chains become cross-linked. The spherical shape of the droplets will be fixed. The droplets can be filled with reactive components or polymers simply by dissolving these molecules in the alginate solution prior immersing it into the calcium chloride solution.

Applying this technique, calcium cross-linked alginate spheres can be used as targets for the radiation cross-linking of PVME to obtain PVME microgel particles [46]. The dimension of the PVME particles is defined by the droplet size of the alginate beads. For the synthesis, PVME is incorporated into alginate beads

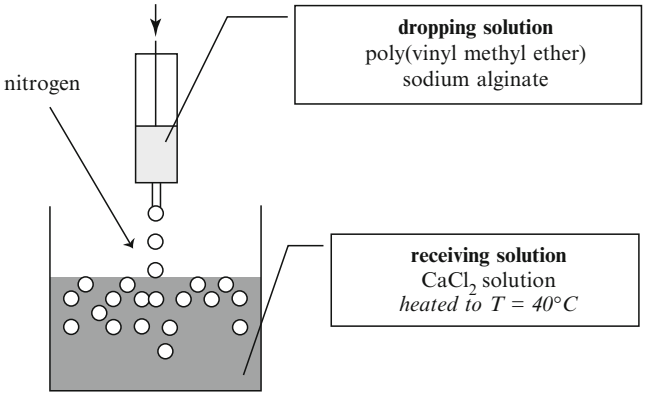

Fig. 9 Alginate technique for synthesis of gel beads ranging from 10^2 to 10^3 µm. An aqueous solution containing PVME and alginate is dropped into a calcium chloride solution to form gel beads. (Reproduced from [46], copyright Wiley-VCH, reproduced with permission)

as demonstrated in Fig. 9. A solution containing PVME and sodium alginate is injected into aqueous calcium chloride solution heated to 40°C to avoid PVME diffusion. The calcium ions cross-link the alginate by complexation and globular PVME–alginate beads are formed, which can be irradiated. After irradiation, the alginate shell is removed by flushing with ethylene diamine tetraacetate (EDTA). The resulting gel beads are in the range of 10^2–10^3µm in the dry state and exhibit temperature-sensitive behavior.

The phase separation of polymer solutions can also be used to cross-link unsaturated polyesters with so-called reactive diluents like styrene. Macroscopically, both components are compatible in a limited concentration range, depending on the polyester composition. On the microscopic level, the polyester is only partially swollen by styrene so that the concentration of styrene inside the polyester coils is lower than in its surrounding by an order of magnitude. Therefore, by starting the reaction, the partially cross-linked polyester coils phase-separate and form microgel structures. Due to diffusion limits, the initiation of the reaction with chemical initiators mainly occurs in the styrene-rich phase. Such an effect can be avoided by radiation initiation that is homogenous throughout the system. Depending on the radiation doses, liquid phases or bulk gels can be obtained. In the latter case, the liquid part can be separated [33].

A very interesting strategy is the synthesis of poly(acrylamide) (PAAm)-based superabsorbent microgel particles by electron beam irradiation in the solid state [1]. In this case, the cross-linking is achieved as a direct effect of radiation, creating radicals mainly localized on the main chains. The random recombination of these radicals results in chemical bonds between the chains and causes an increase in the molecular weight. SEM pictures of non-irradiated and irradiated PAAm show that the non-irradiated PAAm lost its particle shape (starting material: PAAm powder with about 0.3 mm particle size) and formed a highly porous film (Fig. 10a).

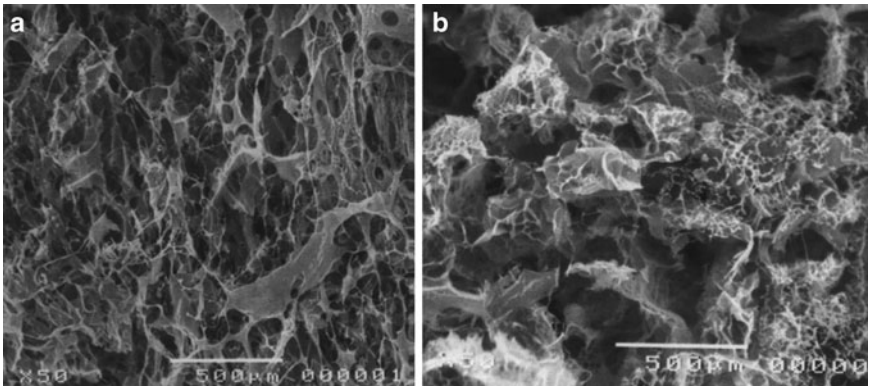

Fig. 10 SEM pictures of (**a**) non-irradiated PAAm, and (**b**) PAAm irradiated in the solid state. SEM pictures were taken of freeze-dried samples. (Reprinted from [1], copyright 2009, with permission of Elsevier)

By irradiation the initial particles are fixed and prevented from dissolving in water showing distinct aggregated particles in the SEM pictures (Fig. 10b). Compared to commercial superabsorbents the swelling ratios of the solid state irradiated PAAm based microgels are acceptable. The swelling equilibrium is reached after 3–10 min depending on the cross-linking density.

3.2.2 Micelles

The cross-linking of micellar structures is a very recent strategy for the preparation of nano- and micrometer-sized particles. Block copolymers (e.g., diblock or triblock copolymers) can self-assemble in aqueous solution and be cross-linked either chemically or by radiation. One example of the latter is the cross-linking of diblock copolymers consisting of poly(isoprene) (PI) and PAA by γ-ray irradiation of an aqueous solution [28]. PAA acts as a hydrophilic block and is also classified as the radiation cross-linking polymer, though chain scission also occurs during the radiation process. The radicals mainly react with the shell of the micelles (PAA) because most of the energy is absorbed by the surrounding water. Thus, the γ-irradiation induces inhomogeneous cross-linking due to chain scission, and intermolecular cross-linking at the same time. A schematic illustration of the reaction is shown in Fig. 11. The size of the initial micelles is reduced during the radiation and decreases linearly with increasing radiation dose. While the radius of the PI core remains constant over the whole dose range, only the thickness of the shell consisting of PAA decreases due to intermolecular cross-linking. Since PI can be removed by ozonolysis, nanocapsules can be obtained by this synthetic route [25].

Very well known commercially available block copolymers showing micellar behavior are polymers of the Pluronic type. Pluronic-type copolymers are symmetric triblock copolymers with the central block of hydrophobic poly(propylene

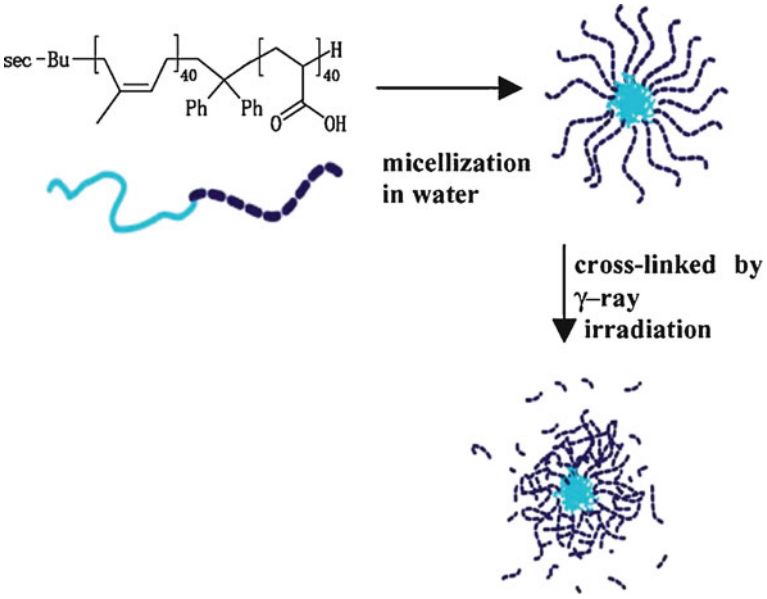

Fig. 11 Irradiation of micelles consisting of PI and PAA to obtain core–shell nanogels. (Reprinted from [28], copyright 2009, with permission of Elsevier)

oxide) (PPO) sandwiched between blocks of the more hydrophilic PEO. Due to their amphiphilic properties, these polymers exist in aqueous solution in the form of single chains, micelles, or physical gels depending on the concentration and the temperature. Electron beam irradiation of Pluronic F127 (BASF product with average composition EO_{100}–PO_{65}–EO_{100}) in the micellar state leads to an increase in the molecular weight [51]. As can be seen in Fig. 12 Pluronic F127 can be irradiated in the regions A (single macromolecules) or B (micelles).

In both cases M_w increases exponentially with the radiation dose (see Fig. 13). Applying high radiation doses, a three-dimensional network is formed that is considered to be composed of regularly arranged micellar structures. This means that cross-linking not only occurs within the micelles. More likely, different micelles are cross-linked intermolecularly finally building a bulk gel. The gelation doses are lower for Pluronic F127 solution with lower concentrations.

The comparison of Ar- and N_2O-saturated solutions of the same concentrations (10%) revealed that the irradiation of N_2O-saturated Pluronic F127 solutions results in higher M_w at lower radiation doses (see mechanism of cross-linking in N_2O saturated solutions in Sect. 2.2).

The irradiation of micellar solutions effects the phase behavior and the critical micelle concentration (CMC). Because radiation sterilization of biopharmaceutical products is a common routine it is important to investigate the influence of radiation on surfactants that are widely used in the pharmaceutical industry for formulations as wetting agents, emulsifiers, or solubilizers. In particular, in drug formulations

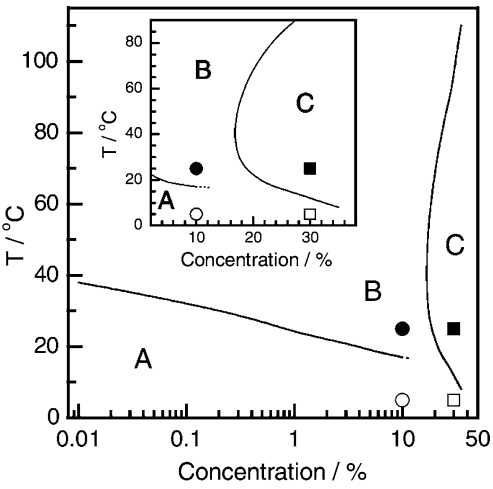

Fig. 12 Phase diagram of aqueous solution of Pluronic F127: *A* single macromolecules, *B* micelles, *C* physical gels. The phase transitions, especially A/B are not sharp and occur within some range of temperature and concentration. *Points* denote experimental conditions applied for irradiation. (Reproduced from [51], copyright Wiley-VCH, reproduced with permission)

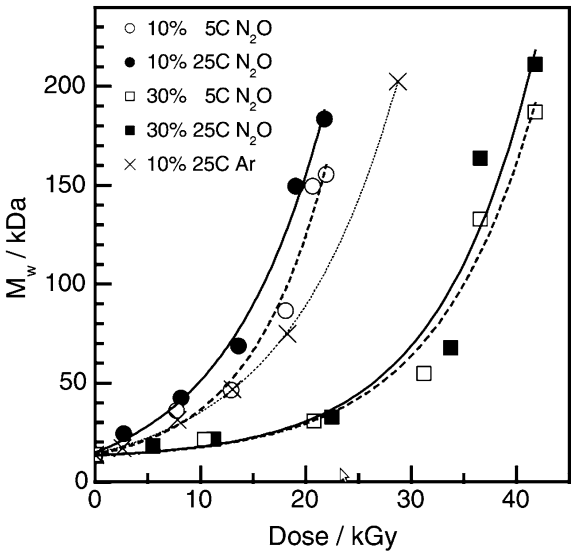

Fig. 13 Molecular weight as a function of the applied radiation dose for Pluronic F127 after irradiation of oxygen-free aqueous solutions (Ar- and N_2O-saturated) at different concentrations (10% and 30%) and temperatures (5°C and 25°C). Experimental values correspond to the points in the phase diagram (see Fig. 12). (Reproduced from [51], copyright Wiley-VCH, reproduced with permission)

and surfactant–polymer systems it is necessary to estimate how the functions of surfactants might be affected. Triton X-100 (octoxynol 9) is a commercially available surfactant used as solvent detergent in numerous pharmaceutical applications. Irradiation with γ-rays above the CMC causes cross-linking of the micelles, as shown by

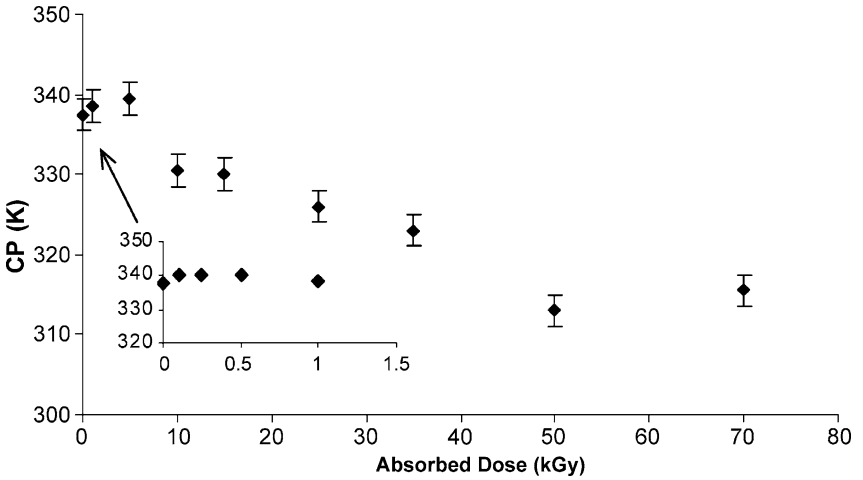

Fig. 14 Effect of γ-radiation on the phase behavior of micellar solutions of Triton X-100 (1 wt%): cloud point (*CP*) variations as a function of the absorbed dose. (Reprinted from [52], copyright 2009, with permission of Elsevier)

cloud point (CP) measurements [52]. For low radiation doses no significant changes in the CP occur, whereas for higher doses the decrease in CP is roughly linear (Fig. 14). CP variations are closely related to changes in the surfactant structure. The decrease in CP with increasing radiation dose can be related to an increase in the occurrence of cross-linking reactions. As a result, an effective increase of the hydrophobic portion of the cross-linked species increases the surfactant efficiency. The essential function of Triton X-100, reducing protein surface adsorption, is not affected by the cross-linking.

3.2.3 Complexes

Synthetic and natural polymers are able to interact with each other by secondary binding forces such as hydrogen bonds, Coulombic forces, or hydrophobic interactions. These interactions lead to the formation of intermolecular polymer complexes. Polyelectrolyte and hydrogen-bonding complexes have gained much attention in recent years due to their applications as biomaterials or in the field of wastewater treatment. However, the instability of interpolymer complexes when subjected to external conditions (e.g., pH, temperature, ionic strength) limits their application potential. Chemical methods have been developed to stabilize the structure of the complexes that involve the use of surfactants or cross-linkers. Very often the polymer structure has to be modified in order to promote the cross-linking. Thus, fixation with high energy irradiation in the absence of any of the mentioned substances is a promising alternative.

The first investigation on structural fixation of interpolymer complexes was carried out on Kollidon PVP 90F (BASF, $M_w = 1.2 \times 10^6$ g mol^{-1}) and oligomeric PAA ($M_w = 890$ g mol^{-1}) [22]. Spontaneous complexation involving a polyacid only occurs below a certain pH value (pH_{crit}), where the protonation level of the carboxyl groups of the polyacid chains is sufficient. pH_{crit} depends on the molecular weight of the polymers as well as on the stoichiometric ratio of the complexation partners. For PVP and PAA, pH_{crit} is in the range of 3.7–4.5 so the complexation was carried out at pH 3.4. The association process of PVP and PAA follows a dynamic behavior at a timescale of minutes to hours, as could be proven by light scattering experiments. Therefore, irradiation for structural fixation has to performed in a equilibrium state and not directly after mixing.

The cross-linking of the structures by irradiation occurs via intracomplex radical recombination and can be followed by static light scattering. As a result of complexation and further cross-linking, a more compact structure of the interacting macromolecules arises. This corresponds to the same effect as for intramolecular cross-linking of single polymer chains as discussed in Sect. 3.1. The formation of intercomplex bonds is expressed as an increase in the molecular weight (Fig. 15, left). M_w was determined at pH 10 because at such condition all polyacid chains are ionized and do not form complexes with PVP. If the radiation did not result in the formation of covalent bonds, M_w would present the values of the unirradiated sample. It can be seen in Fig. 15 that M_w of the cross-linked complexes is significantly lower than for the intramolecular cross-linked PVP. This arises from the typical effect accompanying the synthesis of nanogels from single polymer chains by pulse radiolysis, that intermolecular cross-linking cannot be totally eliminated. Furthermore, the chain scission that also occurs during radiation does not appear in the case of pure PVP. For PVP–PAA complexes it causes the weaker increase in M_w because PAA-derived radicals show a higher tendency to induce degradation than radicals of neutral polymers like PVP. The differences in M_w values therefore clearly show that complexes can in fact be internally cross-linked by pulse radiolysis.

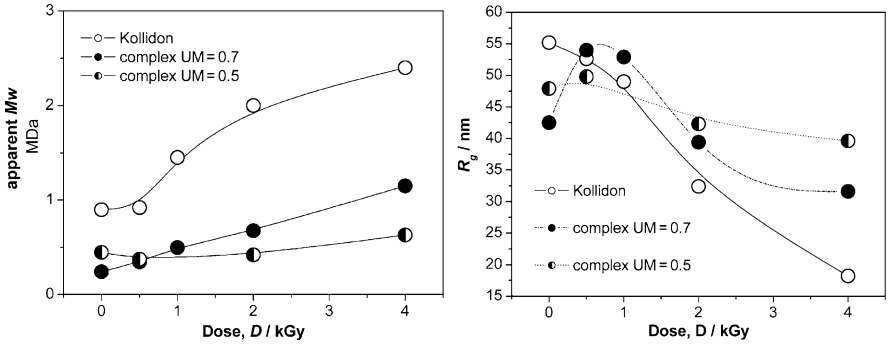

Fig. 15 Pulse irradiation of PVP (Kollidon) and PVP–PAA complexes at different unit molar ratios (UM = [PAA] / ([PAA] + [PVP])) of carboxylic groups. Measurements were conducted at pH 10. *Left*: Molecular weight as a function of the radiation dose. *Right*: Radius of gyration as a function of the radiation dose. (Reprinted from [22], copyright 2009, with permission of Elsevier)

Due to the introduction of covalent bonds between the chain segments, the structures become more compact and the diffusion of segments is limited. With increasing radiation dose, the size of the structures decreases, but the decrease in the size of the cross-linked complex is rather weak compared to that/marginparok? of the nanogel obtained from single polymer PVP (Fig. 15, right). Because polymer complexes are already compact structures before irradiation, their size decreases only slightly upon irradiation, whereas stronger contraction occurs upon irradiation of coils.

The cross-linking of PVP–PAA complexes is influenced by the molecular weight of PAA. A higher M_w of PAA results in higher M_w values of the cross-linked complexes compared to those obtained with low M_w PAA.

4 Characterization and Application of Radiation Cross-Linked Particles

The key feature of radiation cross-linked micro- or nanogels is that their synthesis can be carried out additive-free, meaning that no surfactants, cross-linkers, or monomers are needed. This offers a broad range of applications, especially in the field of biomaterials or biomedicine where a high purity is essential. In general, there is no difference in the characterization of radiation cross-linked structures or microgels obtained, for example, by emulsion polymerization. Typical methods for characterization are dynamic and static light scattering (DLS and SLS), viscosimetry, and various microscopy techniques. Beside the characterization of cross-linked microgels, the characterization of the radiation process is very important in order to decide whether cross-linking or degradation is the dominating reaction. Furthermore, the dose dependence of the resultant molecular weights and sizes need to be investigated for optimization and control. This section will focus on the characterization of the radiation reaction in relation to microgel structure. In Sect. 4.2 examples of applications of radiation cross-linked microgels will be discussed.

4.1 Characterization

A characteristic parameter in radiation cross-linking is the gelation dose D_g (see Sect. 2.1). Above D_g insoluble networks are formed, so-called bulk or "wall-to-wall" gels. D_g depends on the polymer concentration and the irradiation temperature. With decreasing polymer concentration, the value of D_g decreases to a minimum. The irradiation of diluted polymer solutions does not result in macroscopic networks, but leads to the formation of branched molecules or microgels, depending on the radiation dose. Figure 16 summarizes the radiation process.

By irradiating diluted PVME solution with low radiation doses, a strong increase in the molecular weight is observed [40]. The structural changes of the PVME

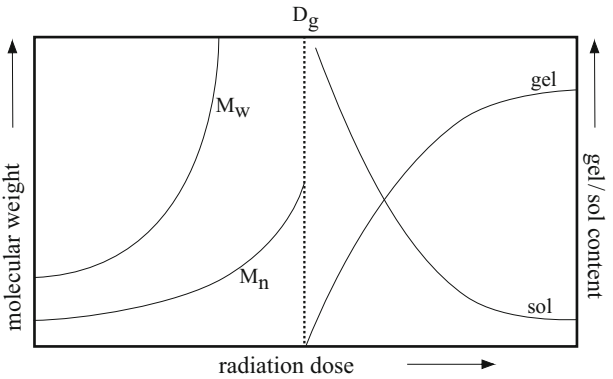

Fig. 16 Structural changes during irradiation. Below the gelation dose D_g, an increasing of the molecular weight occurs. M_w becomes infinite at D_g. Above D_g, the formation of macroscopic networks starts (gel content > 0)

molecules can be analyzed by size-exclusion chromatography in combination with static light scattering and viscosity detectors. This offers the possibility of branching analysis in terms of the branching parameters (contraction factors). For doses above 1.0 kGy, the radiation leads to a strong decrease in the branching parameter g' ($[\eta]_{branched}$ / $[\eta]_{linear}$, Fig. 17, bottom) indicating the formation of branched molecules that are highly contracted. The plot of $\log[\eta]$ against $\log M_w$ (Fig. 17, top) shows that for doses above 1.5 kGy a deviation from linear behavior occurs. In this range, almost linear polymers are formed. At higher doses, this behavior is influenced by the irradiation due to the formation of branched molecules. At radiation with higher doses (above 5 kGy), the intramolecular cross-linking becomes more pronounced and insoluble molecules (nano- or microgels) are formed [34].

Characterization of the radiation process of PVME solutions showed that the desired structures can be synthesized depending on radiation dose and polymer concentration. The concentration dependence results from the different distances between/marginparok? polymer molecules in solution. Whereas macroscopic cross-linking occurs above the overlap concentration, soluble structures (branched polymers or microgels) are formed in dilute solutions. Since PVME is a temperature-sensitive polymer, the solution temperature strongly influences the radiation process because phase-separated structures can be fixed by irradiation (as discussed in Sect. 3.2.1). Furthermore, the radiation temperature also influences the heterogenity of bulk gels that exhibit porous structures when irradiated above the phase transition temperature. As a result, very fast swelling kinetics can be observed. A scheme of the radiation process for PVME is given in Fig. 18.

Combined SLS and DLS studies on phase-separated PVME solution before and after irradiation enable the structural changes of the molecules to be followed. PVME does not show the coil to globule transition of single polymer chains, as known for poly(*N*-isopropyl acrylamide) [40]. Below the phase transition temperature, PVME associates exist in equilibrium with single PVME chains. Therefore,

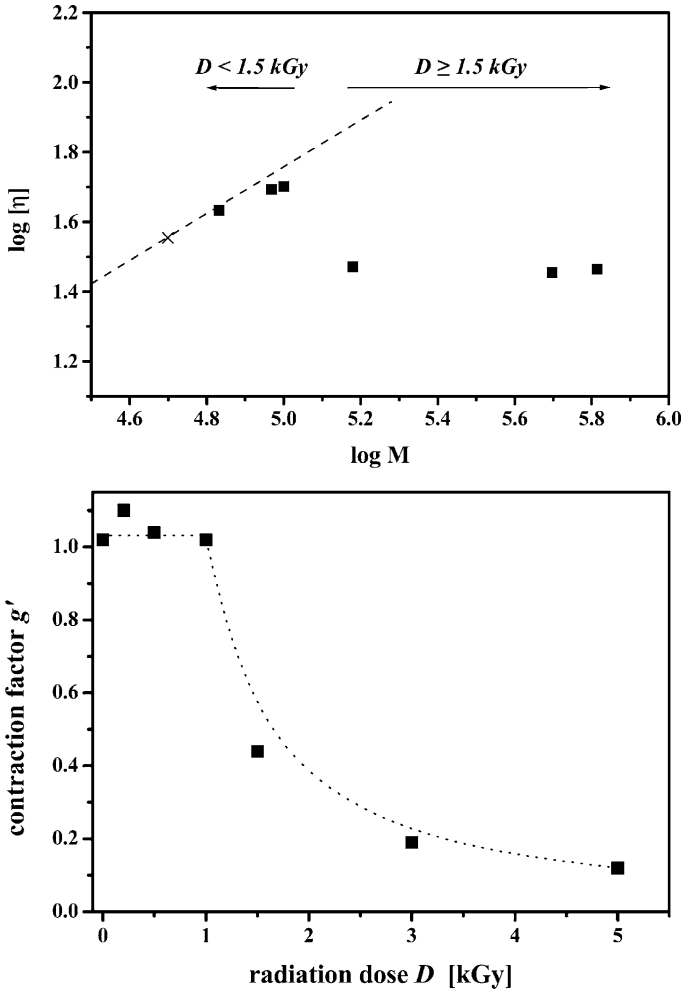

Fig. 17 Radiation of dilute PVME solutions. *Top*: Effect of γ-irradiation on M_w and viscosity $[\eta]$ in comparison with the Kuhn–Mark–Houwink relationship (*dashed line*) of non-irradiated PVME (*cross*). *Bottom*: Dependence of the viscosity branching parameter g′ on radiation dose. (Reprinted with permission from [34], copyright 2009 American Chemical Society)

two diffusion coefficients can be determined with DLS (Fig. 19 inset). Above the phase transition, the associates and the single chains collapse to compact structures that show the scattering functions of soft spheres. The irradiation of these structures results in globular PVME microgel particles. The temperature dependence of the hydrodynamic radius R_h is shown in Fig. 19. In the swollen state (below T_c), a bimodal size distribution can be observed, which indicates that sol molecules are still present in the solution. Above T_c, the particles are shrunken and exhibit a very narrow size distribution around 30–40 nm corresponding to cross-linked collapsed

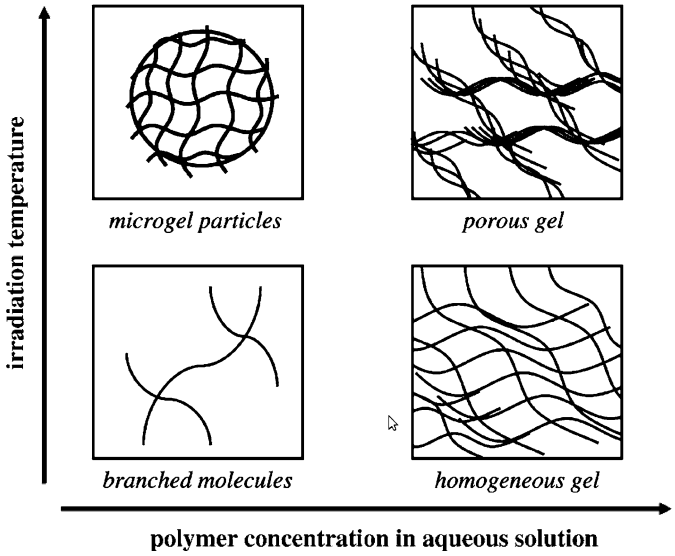

Fig. 18 Gel structures resulting from irradiation of temperature-sensitive PVME, showing the dependence on cross-linking parameters (polymer concentration and temperature during irradiation). (Reprinted from [40], copyright 2009, with permission of Elsevier)

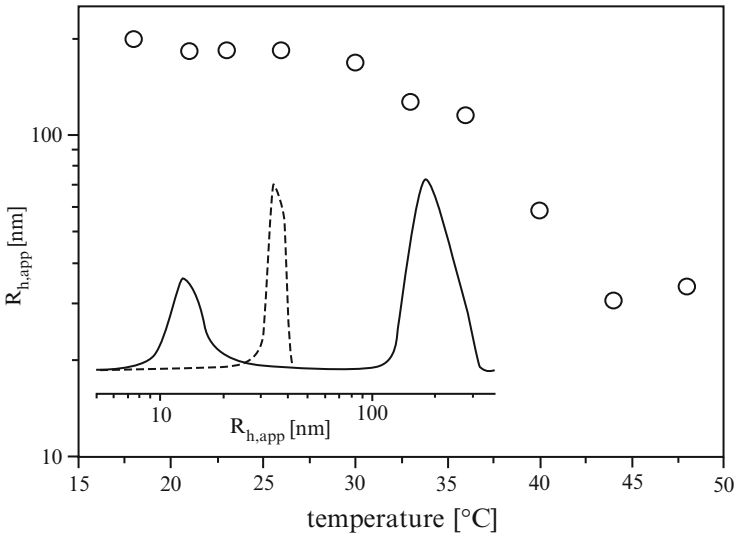

Fig. 19 Temperature dependence of the hydrodynamic radius $R_{h,app}$ of PVME microgel at a scattering angle of 90°. *Inset*: Particle size distribution of PVME microgels below (*solid line*) and above (*dashed line*) the phase transition temperature. (Reprinted from [40], copyright 2009, with permission of Elsevier)

PVME associates. No separate peak for sol molecules appears. Mainly, the sol molecules collapse to bigger aggregates and their size corresponds to that of the cross-linked particles. Single collapsed PVME chains would exhibit small sizes that cannot be seen with the used DLS setup [4].

4.2 Application

Most applications of radiation cross-linked polymers can be found for bulk gels, e.g., wound dressings based on radiation cross-linked gels are produced on a large scale [2, 38]. Furthermore, nanocomposite gels or nanocomposites can be produced by incorporation of particles into radiation cross-linked matrix polymers. Thus, γ-irradiation of an aqueous solution of dextran, gelatin, and glycidyl methacrylate in the presence of drug-loaded microspheres results in hybrid hydrogel scaffolds with good tissue biocompatibility [14].

Enzymes can also be entrapped in polymeric networks either by physical entrapment, chemical bonding or electrostatic attraction. Physical entrapment is very simple because it only involves dissolving the enzyme and subsequent irradiation to yield hydrophilic gels with entrapped enzymes of high reactivity and low leakage [23].

In general, microgels obtained by radiation methods can be used in various applications in the same way as conventional synthesized systems, e.g., as drug delivery templates, for encapsulation, or as microreactors [29, 30]. PAAm for example can be used as template material to synthesize hollow cadmium selenide nanospheres [24], and PVP can be used for the incorporation of ferromagnetic nanoparticles to obtain magnetic hydrogel microspheres [13].

Two examples of the application of radiation cross-linked microgels will be discussed in detail, covering the very challenging field of conducting polymers and a qualification study of microgel particles as diet supplements.

Conductive polymers have received increasing interest in the last decade due to their potential applications. The synthesis of molecular conductors, for example, is a field of intensive research with the purpose of producing objects in the nanometer scale. Therefore, control of the morphology of conducting polymers is very challenging for the production of molecular wires (nanowires) or tubes. Appropriate templates for the confined polymerization of conductive polymers are required to give them a controlled shape and dimension.

As an example, thermosensitive PVME microgels can be used as template and stabilizer for the synthesis of composite polypyrrole (PPy) particles [32]. The PVME microgels were obtained by electron beam irradiation above the phase transition temperature as described in Sect. 3.2.1 [3, 4]. Pyrrole (Py) was polymerized by oxidative polymerization with ferric chloride in the presence of the PVME microgels in water/ethanol mixtures as reaction medium. For comparison, the synthesis was also carried out in the presence of uncross-linked PVME.

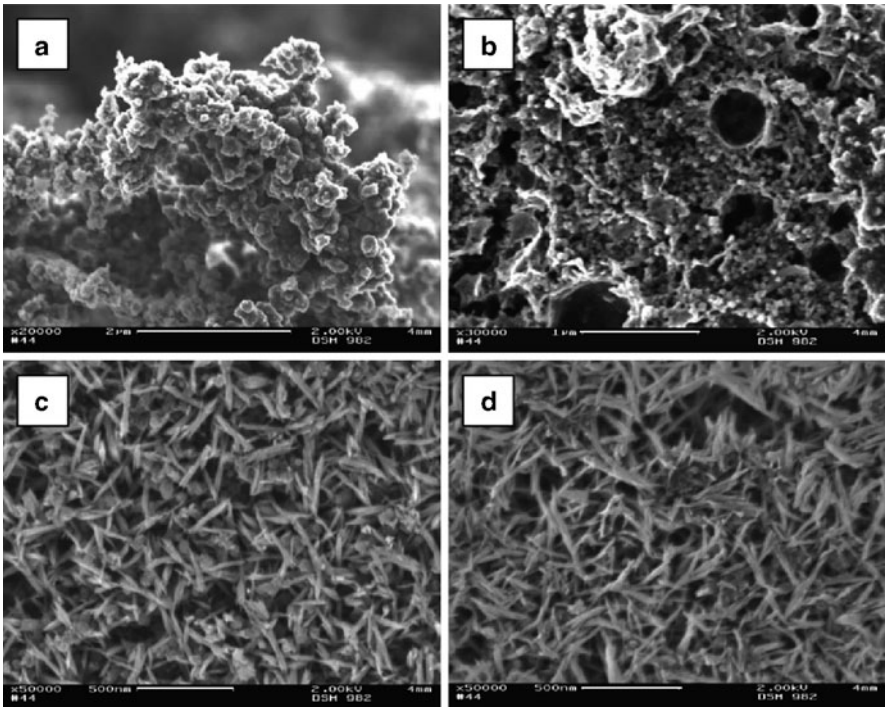

Fig. 20 SEM images of PPy particles obtained by oxidative polymerization in 50:50 water/ethanol mixture. The synthesis was carried out in the absence of PVME (**a**) or in the presence of PVME microgels (**b**–**d**) obtained by electron beam irradiation. The ratio of Py to PVME was varied: (**b**) 1:1; (**c**) 1:2; and (**d**) 1:3. *Scale bars*: (**a**) 2 µm; (**b**) 1 µm; (**c**,**d**) 500 nm. (Reprinted from [32], copyright 2009, with permission of Elsevier)

SEM investigations show that the morphology of the obtained particles depends on whether uncross-linked PVME and PVME microgels are used. In the case of uncross-linked PVME, small spherical particles in the range of 50–100 nm are formed. If Py is polymerized in water without any stabilizer (without PVME) the particles exhibit a cauliflower-like structure and the dispersion is unstable (Fig. 20a).

Using cross-linked PVME microgels, the dispersion is stable and the morphology of the PPy particles changes from spherical to needle-like, depending on the Py concentration (Fig. 20b–d). At low Py concentrations, mainly spherical particles are present. By increasing the Py amount, a needle-like morphology becomes dominant. However, when the ethanol content in the reaction is decreased the PPy particle morphology becomes spherical.

Since Py monomer is hardly soluble in water it will penetrate into the PVME microgel particle interior. FESEM studies pointed out that in the swollen state PVME microgel particles have a sponge-like structure and a porous shell, which provide corresponding membrane permeability (see Fig. 7). Subsequent addition of the oxidant starts the polymerization and the PPy particles are formed inside the PVME microgel network, resulting in a granular morphology.

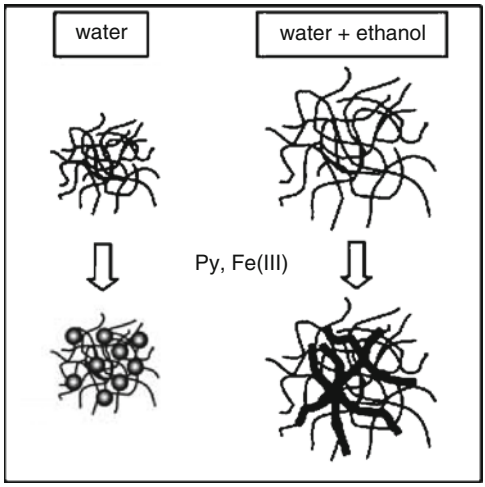

Fig. 21 Ppy particle morphology after polymerization in the presence of PVME microgels in water or water/ethanol mixtures. (Reprinted from [32], copyright 2009, with permission of Elsevier)

In water/ethanol mixtures, the PVME microgel network expands and the pores become larger. Additionally, the polymerization rate of Py is much slower than in pure aqueous solution. Both effects provide suitable conditions for PPy to self-assemble. As a result PPy needles are formed. If the Py content is increased, larger needles can be obtained. A presentation of the Py polymerization in the presence of PVME particles in water or water/ethanol mixtures is given in Fig. 21.

It is obvious that the pore size of the PVME microgel particles as well as the polymerization rate (defined by the solvent) have a significant influence on the PPy particle morphology. Since the pore size of PVME can be easily changed by the radiation dose or the radiation temperature, desired PPy dimensions can be synthesized. Furthermore, due to the temperature sensitivity of PVME, the pore size can also be influenced by the temperature of the reaction medium. These facts allow the controlled synthesis of PPy fibrils.

A second example of the application of radiation cross-linked microgels is a diet supplement based on modified chitosan and PVP [16]. Chitosan is currently the main ingredient of numerous commercially available dietary supplements that are advertised as having a body weight reduction effect based on trapping dietary fat in the digestive tract in a way that prevents fat absorption. Therefore, chitosan is expected to partially prevent a body weight increase caused by a fat-rich diet. The results of numerous studies on animals and humans are not consistent, but/marginparok? some recent experiments have indicated that the fat binding depends on the (M_w) of the chitosan used [15]. It seems that the application of low molecular weight chitosan ($\sim 2.5–5 \times 10^4\,g\,mol^{-1}$) to diet additives efficiently contributes to the fat binding. Additionally, PVP microgels are promising substances for dietary products as they can swell in the stomach and thus inducing a feeling of satiety. Using PVP microgels can counterbalance the effect of an increased food uptake, which is often observed by addition of chitosan. PVP as a nontoxic

biocompatible polymer exhibiting high hydrophilicity and high swelling ratios can absorb hydrophilic food components, and move along the digestive tract without being destroyed.

The chitosan/PVP supplement used in diet studies was composed of γ-radiation cross-linked PVP microgels and γ-radiation degraded chitosan. Both components are easily obtainable by solvent-, additive-, and waste-free radiation processing. PVP microgels were synthesized by γ-irradiation of pure vinyl pyrrolidone monomer followed by grinding and fractionation in 0.25–0.5 mm microgels. Chitosan was irradiated in the solid state, causing degradation. The final diet supplement was obtained by mixing both components in a 1:1 ratio, and was added to the diet of selected groups of animals at the 4% (by weight) level.

After 10 weeks of fat- and cholesterol-rich diet, animals fed with the chitosan/PVP supplement showed a significantly reduced liver weight increase. Furthermore, the presence of the microgel indeed showed an hunger-reducing effect. At the low microgel content used in this study it was just enough to compensate the chitosan-induced hunger effect evidenced in previous works.

For the in vitro application of polymers and microgels, ionizing radiation is an efficient tool for their synthesis. Chitosan can be degraded in a controlled way and the target molecular weight can be reached by selection of the appropriate radiation dose. The irradiation of vinyl pyrrolidone is a convenient way to synthesize microgels that exhibit uniform sizes after grinding and fractionation.

References

1. Abd El-Rehim HA (2005) Swelling of radiation crosslinked acrylamide-based microgels and their potential applications. Radiat Phys Chem 74(2):111–117
2. Ajji Z, Mirjalili G, Alkhatab A, Dada H (2008) Use of electron beam for the production of hydrogel dressings. Radiat Phys Chem 77(2):200–202
3. Arndt KF, Schmidt T, Menge H (2001) Poly(vinyl methyl ether) hydrogel formed by high energy irradiation. Macromol Symp 164:313–322
4. Arndt KF, Schmidt T, Reichelt R (2001) Thermo-sensitive poly(methyl vinyl ether) micro-gel formed by high energy radiation. Polymer 42(16):6785–6791
5. Arndt KF, Richter A, Mönch I (2009) Synthesis of stimuli-sensitive hydrogels in the μm and sub-μm range by radiation techniques and their application. In: Barbucci R (ed) Hydrogels: biological properties and applications. Springer, Berlin, Heidelberg, pp. 121–140
6. Borgward U, Schnabel W, Henglein A (1969) Determination of rate constants of combination of polyethylene oxide radicals in aqueous solution by pulse radiolysis. Makromol Chem 127:176–184
7. Brasch U, Burchard W (1996) Preparation and solution properties of microhydrogels from poly(vinyl alcohol). Macromol Chem Phys 197(1):223–235
8. Burkert S, Schmidt T, Gohs U, Dorschner H, Arndt KF (2007) Cross-linking of poly(*N*-vinyl pyrrolidone) films by electron beam irradiation. Radiat Phys Chem 76(8–9):1324–1328
9. Chapiro A (1962) Radiation chemistry of polymeric systems. Interscience, New York
10. Charlesby A (1960) Atomic radiation and polymers: radiation effects in materials. Pergamon Press, Oxford
11. Charlesby A, Alexander P (1955) Reticulation of polymers in aqueous solution by γ-rays. J Chim Phys Phys-Chim Biol 52:699–709

12. Charlesby A, Pinner SH (1959) Analysis of the solubility behaviour of irradiated polyethylene and other polymers. Proc R Soc Lond A 249(1258):367–386
13. Chen J, Yang LM, Liu YF, Ding GW, Pei Y, Li J, Hua GF, Huang J (2005) Preparation and characterization of magnetic targeted drug controlled-release hydrogel microspheres. Macromol Symp 225:71–80
14. Chen FM, Zhao YM, Sun HH, Jin T, Wang QT, Zhou W, Wu ZF, Jin Y (2007) Novel glycidyl methacrylated dextran (dex-gma)/gelatin hydrogel scaffolds containing microspheres loaded with bone morphogenetic proteins: formulation and characteristics. J Control Release 118(1):65–77
15. Czechowska-Biskup R, Rokita B, Ulanski P, Rosiak JM (2005) Radiation-induced and sonochemical degradation of chitosan as a way to increase its fat-binding capacity. Nucl Instrum Methods Phys Res B 236:383–390
16. Czechowska-Biskup R, Ulanski P, Olejnik AK, Nowicka G, Panczenko-Kresowska B, Rosiak JM (2007) Diet supplement based on radiation-modified chitosan and radiation-synthesized polyvinylpyrrolidone microgels: influence on the liver weight in rats fed a fat- and cholesterol-rich diet. J Appl Polym Sci 105(1):169–176
17. Furusawa K, Terao K, Nagasawa N, Yoshii F, Kubota K, Dobashi T (2004) Nanometer-sized gelatin particles prepared by means of gamma-ray irradiation. Colloid Polym Sci 283(2): 229–233
18. Gerlach G, Arndt KF (eds) (2009) Hydrogel sensors and actuators: engineering and technology. Springer, Berlin
19. Gottlieb R, Kaiser C, Gohs U, Arndt KF (2007) Temperature sensitive hydrogels based on hydroxypropylcellulose by high energy irradiation. Macromol Symp 254:361–369
20. Hegewald J, Schmidt T, Eichhorn KJ, Kretschmer K, Kuckling D, Arndt KF (2006) Electron beam irradiation of poly(vinyl methyl ether) films. 2. temperature-dependent swelling behavior. Langmuir 22(11):5152–5159
21. Henglein A (1966) Pulse radiolytic investigations of reactions of hydrated electrons and free radicals. Allgem Prakt Chem 17:295–301
22. Henke A, Kadlubowski S, Ulanski P, Rosiak JM, Arndt KF (2005) Radiation-induced crosslinking of polyvinylpyrrolidone–poly(acrylic acid) complexes. Nucl Instrum Methods Phys Res B 236:391–398
23. Hoffman AS (1981) A review of the use of radiation plus chemical and biochemical processing treatments to prepare novel biomaterials. Radiat Phys Chem 18(1–2):323–342
24. Hu Y, Chen JF, Chen WM, Ning JQ (2004) Preparation of hollow CdSe nanospheres. Mater Lett 58(22–23):2911–2913
25. Huang H, Remsen EE, Kowalewski T, Wooley KL (1999) Nanocages derived from shell crosslinked micelle templates. J Am Chem Soc 121(15):3805–3806
26. Janik I, Kasprzak E, Al-Zier A, Rosiak JM (2003) Radiation crosslinking and scission parameters for poly(vinyl methyl ether) in aqueous solution. Nucl Instrum Methods Phys Res B 208:374–379
27. Kadlubowski S, Grobelny J, Olejniczak W, Cichomski M, Ulanski P (2003) Pulses of fast electrons as a tool to synthesize poly(acrylic acid) nanogels. intramolecular cross-linking of linear polymer chains in additive-free aqueous solution. Macromolecules 36(7):2484–2492
28. Narita T, Terao K, Dobashi T, Nagasawa N, Yoshii F (2004) Preparation and characterization of core–shell nanoparticles hardened by gamma-ray. Colloid Surf B 38(3–4):187–190
29. Nayak S, Lyon LA (2005) Soft nanotechnology with soft nanoparticles. Angew Chem Int Ed Engl 44(47):7686–7708
30. Oh JK, Drumright R, Siegwart DJ, Matyjaszewski K (2008) The development of microgels/nanogels for drug delivery applications. Prog Polym Sci 33(4):448–477
31. Perera MCS, Hill DJT (1999) Radiation chemical yields: G values. In: Brandrup J, Immergut EH, Grulke EA (eds) Polymer handbook. Wiley Interscience, New York, p 481
32. Pich A, Lu Y, Adler HJP, Schmidt T, Arndt KF (2002) Dispersion polymerization of pyrrole in the presence of poly(vinyl methyl ether) microgels. Polymer 43(21):5723–5729
33. Pucic I, Ranogajec F (2003) Phase separation during radiation crosslinking of unsaturated polyester resin. Radiat Phys Chem 67(3–4):415–419

34. Querner C, Schmidt T, Arndt KF (2004) Characterization of structural changes of poly(vinyl methyl ether) gamma-irradiated in diluted aqueous solutions. Langmuir 20(7):2883–2889
35. Richter A, Paschew G, Klatt S, Lienig J, Arndt KF, Adler HJP (2008) Review on hydrogel-based pH sensors and microsensors. Sensors 8(1):561–581
36. Rosiak JM (1998) Gel/sol analysis of irradiated polymers. Radiat Phys Chem 51(1):13–17
37. Rosiak JM (2007) Nano- and microgels of poly(vinyl methyl ether) obtained by radiation techniques. Eurasian Chem Tech J 9:1–31
38. Rosiak JM, Rucinska-Reybas A, Pekala W (1989) Method of manufacturing of hydrogel dressings. US Patent 4 871 490
39. Sabharwal S, Mohan H, Bhardwaj YK, Majali AB (1999) Radiation induced crosslinking of poly(vinyl methylether) in aqueous solutions. Radiat Phys Chem 54(6):643–653
40. Schmidt T, Querner C, Arndt KF (2003) Characterization methods for radiation crosslinked poly(vinyl methyl ether) hydrogels. Nucl Instrum Methods Phys Res B 208:331–335
41. Schmidt T, Janik I, Kadlubowski S, Ulanski P, Rosiak JM, Reichelt R, Arndt KF (2005) Pulsed electron beam irradiation of dilute aqueous poly(vinyl methyl ether) solutions. Polymer 46(23):9908–9918
42. Schmidt T, Mönch JI, Arndt KF (2006) Temperature-sensitive hydrogel pattern by electron-beam lithography. Macromol Mater Eng 291(7):755–761
43. Schmitz KS, Wang BL, Kokufuta E (2001) Mechanism of microgel formation via cross-linking of polymers in their dilute solutions: mathematical explanation with computer simulations. Macromolecules 34(23):8370–8377
44. Schnabel W, Borgward U (1969) Crosslinking of poly(ethylene oxide) in solution by ^{60}Co-gamma-rays. Makromol Chem 123(1):73–79
45. Schwarz HA (1981) Free-radicals generated by radiolysis of aqueous-solutions. J Chem Educ 58(2):101–105
46. Theiss D, Schmidt T, Arndt KF (2004) Temperature-sensitive poly(vinyl methyl ether) hydrogel beads. Macromol Symp 210:465–474
47. Ulanski P, Rosiak JM (1999) The use of radiation technique in the synthesis of polymeric nanogels. Nucl Instrum Methods Phys Res B 151(1–4):356–360
48. Ulanski P, Bothe E, Hildenbrand K, Rosiak JM, von Sonntag C (1996) Hydroxyl-radical-induced reactions of poly(acrylic acid): a pulse radiolysis, EPR and product study. 2. oxygenated aqueous solutions. J Chem Soc Perkin Trans 2 (1):23–28
49. Ulanski P, Janik I, Rosiak JM (1998) Radiation formation of polymeric nanogels. Radiat Phys Chem 52:289–294
50. Ulanski P, Kadlubowski S, Rosiak JM (2002) Synthesis of poly(acrylic acid) nanogels by preparative pulse radiolysis. Radiat Phys Chem 63(3–6):533–537
51. Ulanski P, Pawlowska W, Kadlubowski S, Henke A, Gottlieb R, Arndt KF, Bromberg L, Hatton TA, Rosiak JM (2006) Synthesis of hydrogels by radiation-induced cross-linking of Pluronic® F127 in N_20-saturated aqueous solution. Polym Adv Technol 17(9–10):804–813
52. Valdes-Diaz G, Rodriguez-Calvo S, Perez-Gramatges A, Rapado-Paneque A, Fernandez-Lima FA, Ponciano CR, da Silveira EF (2007) Effects of gamma radiation on phase behaviour and critical micelle concentration of Triton X-100 aqueous solutions. J Colloid Interface Sci 311(1):253–261
53. Wang BL, Mukataka S, Kodama M, Kokufuta E (1997) Viscometric and light scattering studies on microgel formation by gamma-ray irradiation to aqueous oxygen-free solutions of poly(vinyl alcohol). Langmuir 13(23):6108–6114
54. Wang BL, Kodama M, Mukataka S, Kokufuta E (1998) On the intermolecular crosslinking of PVA chains in an aqueous solution by gamma-ray irradiation. Polym Gels Netw 6(1):71–81

Adv Polym Sci (2010) 234: 129–163
DOI:10.1007/12_2010_71

Published online: 28 May 2010

Microgels as Nanoreactors: Applications in Catalysis

Nicole Welsch, Matthias Ballauff, and Yan Lu

Abstract We review recent work on the use of "smart" microgel particles as "nanoreactors" for the immobilization of metal nanoparticles as well as enzymes. A general feature of the microgel systems under consideration is their ability to react to external stimuli such as the pH or temperature of the system. Special emphasis is given to our recent research work on thermosensitive core–shell microgel particles composed of a polystyrene core and a crosslinked poly(*N*-isopropylacrylamide) shell. Work done on these core–shell systems is compared to developments in the investigation of similar systems. Recently, it has been shown that these core–shell microgels can be used as "nanoreactors" for the immobilization of metal nanoparticles. The metal nanocomposite particles exhibit a "smart" catalytic behavior inasmuch as the catalytic activity of nanoparticles can be modulated through the volume transition that takes place within the thermosensitive shell of the carrier system. Moreover, microgel particles can work as efficient carrier systems for the immobilization of enzymes. The dependence of the enzymatic activity on temperature can also be manipulated by the temperature-dependent swelling behavior of the microgel. Thus, the microgel particles present an excellent "active" carrier system for applications in catalysis.

Keywords Catalysis · Enzyme · Metal nanoparticles · Microgels · Thermosensitive

Contents

N. Welsch, M. Ballauff, and Y. Lu (✉)
F-I2 Soft Matter and Functional Materials, Helmholtz-Zentrum Berlin für Materialien und Energie GmbH, Hahn-Meitner-Platz 1, 14109 Berlin, Germany
email: nicole.welsch@helmholtz-berlin.de; matthias.ballauff@helmholtz-berlin.de; yan.lu@helmholtz-berlin.de

1 Introduction

Nanoparticles consisting of noble metals have recently attracted much attention because such particles exhibit properties differing strongly from the properties of the bulk metal [1, 2]. Thus, such nanoparticles are interesting for their application as catalysts [3–5], sensors [6, 7], and in electronics. However, the metallic nanoparticles must be stabilized in solution to prevent aggregation. In principle, suitable carrier systems, such as microgels [8–11], dendrimers [12, 13], block copolymer micelles [14], and latex particles [15, 16], may be used as a "nanoreactors" in which the metal nanoparticles can be immobilized and used for the purpose at hand.

Microgels have several important advantages over other systems, namely, stability, ease of synthesis, good control over particle size, and easy functionalization to provide stimulus-responsive behavior (e.g., change in volume in response to a change in pH, ionic strength or temperature) [9]. In recent years, it has become clear that this kind of material holds great promise for nanotechnology [17]. Moreover, microgel-stabilized metal nanoparticles can in many aspects be viewed upon as "quasi-homogeneous" catalysts that combine the advantages of both homogeneous and heterogeneous catalysts, such as high activity and easy separation for reuse. The use of microgel particles as reactors for the deposition of functional materials in nanoparticle forms has thus opened new and exciting possibilities for the introduction of additional functionalities. Thus, these metal composite particles present a typical example of "mesotechnology" [18].

In a similar way, enzymes can be immobilized in colloidal microgel particles and used for technical applications [19]. A problem often encountered when trying to immobilize proteins and enzyme on solid substrates is denaturation (see the discussion of this point in [20]). This process is accompanied by a loss of enzymatic activity, and denaturation presents one of the main obstacles for the technical use of biomolecules. Some time ago, we demonstrated that spherical polyelectrolyte brushes (SPB) (i.e., colloidal particles onto which long polyelectrolyte chains are grafted) are excellent carriers of proteins [21]. The secondary structure of immobilized proteins as well as their enzymatic activity is largely preserved on the SPBs [22]. More recently, we have tried to use microgels as active carrier particles for the immobilization of enzymes. The enzymatic activity of β-D-glucosidase adsorbed on a suitable core–shell microgel is increased by a factor of more than three [23].

Here, we review the use of microgel particles as reactors for the immobilization of catalytically active metal nanoparticles or enzymes. The composite particles of microgels and the metal nanoparticles can be used for catalysis in aqueous media, that is, under very mild conditions [24–28]. Thus, the composite systems allow us to do "green chemistry" [29] and conduct chemical reactions in a very efficient way.

2 Microgels as Carrier Systems for Metal Nanoparticles

2.1 Synthesis of Microgel–Metal Composite Particles

Recently, aqueous microgels have become an important subdivision of polymer colloids, and numerous synthetic microgel systems have been developed [30]. Most of the microgel particles operating in aqueous media are based on poly(*N*-isopropylacrylamide) (PNIPA) [31], poly(*N*-vinylcaprolactam) (PVCL) [32, 33], or other water-soluble polymers [34–36]. In aqueous media, PNIPA exhibits a lower critical solution temperature (LCST) at about 32°C, which is close to the physiological temperature [37–39]. Below the LCST, the polymer chains are soluble in water due to formation of hydrogen bonds between the water molecules and the amide side-chains. When the temperature increases, the polymer undergoes a volume phase transition. Water is expelled from the microgel interior, thus causing a drastic decrease in volume above the LCST of the polymer. PNIPA microgels, which are submicron-sized crosslinked latex particles, are usually prepared by free-radical precipitation polymerization and have a high surface-to-volume ratio.

Microgels can be tailored to carry functional groups able to interact with metal ions, which are the precursors of metal nanoparticles. In this way, microgel particles can be loaded with metal precursors, which are subsequently reduced inside the microgels to produce metal nanoparticles. Antonietti et al. were the first to employ microgels as "exotemplates" for the preparation of metal nanoparticles [40, 41]. They prepared polystyrene-based microgels by microemulsion polymerization and then fully sulfonated them by treatment with concentrated sulfuric acid. The sulfonated microgels were soluble in water and could be conveniently loaded with gold ions, which were subsequently reduced, thus forming the microgel-stabilized colloids.

Subsequently, Biffis [42] reported the preparation of microgel-stabilized palladium colloids using a novel strategy based on the synthesis of microgels by radical solution copolymerization of suitable functional monomers containing sulfonic acid groups. These microgels can be conveniently loaded with Pd^{2+} ions, which are subsequently reduced. The resulting metal colloids (10–20 nm diameter) can be precipitated from the reaction mixture and redispersed in suitable solvents. Furthermore, metal nanoclusters with controlled particle size have been prepared in the presence of microgels containing tertiary amino or pyridyl functionalities, which can form stable complexes with Pd(II) species [8]. It has been demonstrated that such microgels can be used as stabilizers for metal nanoclusters in which the size of the nanoclusters can be chosen through the degree of crosslinking of the microgels. For example, the average size of Pd nanoclusters was decreased from 9 to 3 nm by increasing the concentration of crosslinker (ethylene dimethacrylate) from 5 to 20 mol%.

Recently, Zhang and Kumacheva [43] introduced poly(*N*-isopropyl acrylamide-acrylic acid-2-hydroxyethyl acrylate) [poly(NIPA-AAc-HEA)] microgel particles

crosslinked with *N*,*N*′-methylene bisacrylamide (BIS) as carrier systems for nanoparticles. They showed that semiconductors, metal, and magnetic nanoparticles with predetermined size, polydispersity, optical, and magnetic properties can be successfully synthesized using polymer microgels as a template. This may have promising applications in catalysis, biolabeling, and chemical and biological separation. Silver nanoparticles (AgNPs; ca 3 nm in diameter) have been incorporated into microgels, which presented well-defined surface plasmon resonance at 411 nm. In microspheres with a lower concentration of AgNPs (or smaller particle size), the absorption peak broadened due to the "intrinsic size effect" in metal nanoparticles [44]. Moreover, hybrid fluorescent microgels can be prepared via photoactivated synthesis of AgNPs in the PNIPA microgels [9]. The presence of carboxylic groups in the microgel structure leads to an effective uptake of Ag^+ ions and controlled nucleation and growth of very small nanoclusters. Additionally, the polymeric network protected the silver nanoclusters from interaction with photoluminescence quenchers in bulk dispersion. These fluorescent microgels are highly interesting candidates for the fabrication of colloidal crystals or sensor applications.

Suzuki and Kawaguchi [45, 46] have reported novel thermosensitive hybrid core–shell particles via in situ Au or Ag/Au nanoparticle formation using thermosensitive core–shell particles as a template. They found that the color of the hybrid microgels, originating from interparticle interactions between the nanoparticles, changes according to the swelling/deswelling property of the thermosensitive microgel.

Moreover, temperature-sensitive PVCL-based microgels have also been used as template for the deposition of metal nanoparticles. Pich et al. [47] reported the deposition of AgNPs into such microgel containers. It has been demonstrated that hybrid particles with different AgNP amounts can be prepared. Hybrid particles are sensitive to temperature and swelling, and collapse processes are reversible. Incorporation of AgNPs leads to shrinkage of the microgel template due to the partial immobilization of polymer chains on the microgel surface. As a consequence, gradual loss of temperature sensitivity is observed. Nevertheless, despite the high AgNP content, the hybrid microgels were colloidally stable and no aggregation was observed, even after several months of storage. Similarly, catalytically active AuNPs have been also embedded into such microgel particles [48]. Compared to pure AuNPs, hybrid microgels at similar conditions reduce the activation energy of the reduction process by a factor of two. This indicates that localization of AuNPs within the microgel template prevents their aggregation. Therefore, a high catalytic activity can be preserved for different reaction conditions. Additionally, the polymeric template provides a suitable environment for better mass transfer in the present system that improves the catalyst efficiency.

Armes et al. [49] have reported the use of pH-responsive microgels based solely on 2-(diethylamino)ethyl methacrylate (DEA) as colloidal templates for the in situ synthesis of Pt nanoparticles (PtNPs). The swollen microgels can be used as nanoreactors: efficient impregnation with PtNPs can be achieved by incorporating precursor platinum compounds, followed by metal reduction. Addition of platinic acid, H_2PtCl_6, to the latex particles causes the protonation of the tertiary amine

groups, leading to microgel formation. However, the divalent $PtCl_6^{2-}$ anions act as an ionic crosslinker for the protonated amine groups, which causes microgel deswelling. The equilibrium between these two opposing effects determines the final size of the microgels after H_2PtCl_6 complexation. Both the metal-salt-loaded microgel and the metal-nanoparticle-loaded latex particles possess a well-defined equilibrium structure with characteristics that are independent of the synthesis method. The dimensions of the PtNP-loaded microgels were similar to those of the microgel precursor prior to H_2PtCl_6 complexation, suggesting that, even at high metal loadings, the PtNPs have no significant effect on the dimensions of the deswollen latex.

Up to now, we have discussed that the formation of metal nanoparticles can be carried out in situ, that is in the presence of microgel templates. Electrostatic interaction between the positively charged Au nanorods (Au-NRs) and the negatively charged microgels has been also employed as the driving force to immobilize Au-NRs on the microgel [50]. Hellweg et al. [51] demonstrated that by modification of Au-NRs with polyelectrolyte layers, a negatively charged thermosensitive PNIPA microgel can be homogeneously covered with Au-NRs. The optical properties of Au-NRs were applied to monitor the thermoresponsive behavior of PNIPA microgels. More recently, Kumacheva et al. [52] found that the strong binding forces between Au-NRs and polyacryamide microgels is another driving force for loading microgels with NRs.

Recently, core–shell type microgels, which contain a hydrophobic core and a hydrophilic thermosensitive shell, have become attractive for scientists because such systems can combine the properties characteristic of both the core and the shell [53]. We have prepared core–shell microgel particles consisting of a poly(styrene) core onto which a shell of poly(*N*-isopropylacrylamide) (PS–PNIPA) has been affixed in a seeded emulsion polymerization [54–56]. In this case, the ends of the crosslinked PNIPA chains are fixed to a solid core, which defines a solid boundary of the network. In this respect, these core–shell latex particles present crosslinked polymer brushes on defined spherical surfaces. The solvent quality can be changed from good solvent conditions at room temperature to poor solvent conditions at a temperature

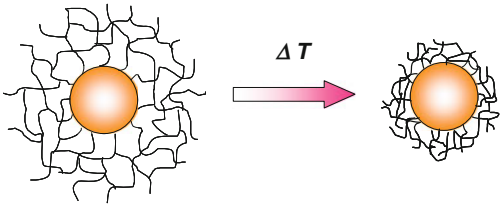

Fig. 1 Volume transition in thermosensitive core–shell particles. The thermosensitive PNIPA networks are affixed to the surface of the core particles, and thus provide one boundary of the network. The solvent (water) is taken up by the network at low temperature, but is expelled when the shell undergoes a volume transition at 32°C

above 32°C (see Fig. 1) [57, 58]. This transition behavior of thermosensitive core–shell particles has also been observed by cryo-TEM [55]. Figure 2 shows the cryo-TEM images for core–shell microgel particles quenched from room temperature and from 45°C. Obviously, vitrification must be much faster than the relaxation time characterizing the shrinking kinetics of the particles. From Fig. 2, it can be clearly seen that the thermosensitive shell of the particles are considerably shrunken when the sample was quenched from 45°C, which is accord with the results from dynamic light scattering (DLS) measurements. Moreover, the shell has been compacted by this shrinking process and provides a tight envelope for the core.

Recently, we have successfully used these thermosensitive core–shell microgel particles as templates for the deposition of metal nanoparticles (Ag, Au, Pd, Pt, and Rh) [29, 59, 60]. The reduction to metallic nanoparticles in the presence of microgel particles was done at room temperature via the addition of $NaBH_4$ and could be followed optically by the color change of the suspensions, as shown in Fig. 3. The immobilization of metal nanoparticles might be due to the strong localization of

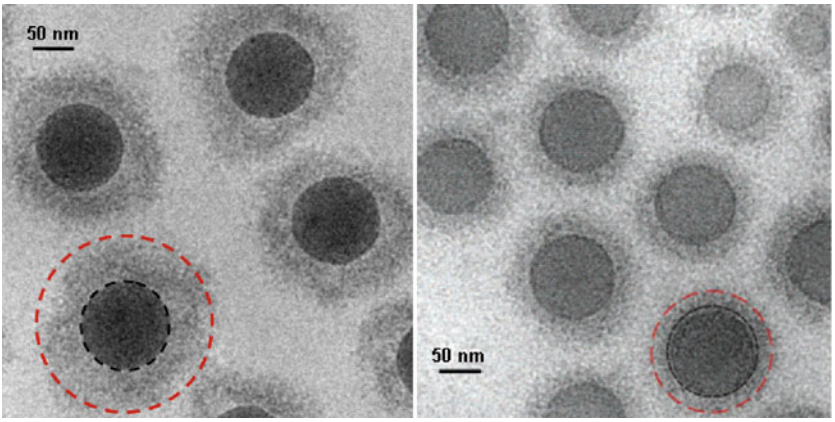

Fig. 2 Cryo-TEM images of PS–PNIPA core–shell particles. The sample was kept at 23°C (*left*) and 45°C (*right*) before vitrification [55]. The *circle around the core* marks the core radius determined by dynamic light scattering (DLS) in solution. The *circle around the entire particle* gives the hydrodynamic radius R_h of the core–shell particles as determined by DLS

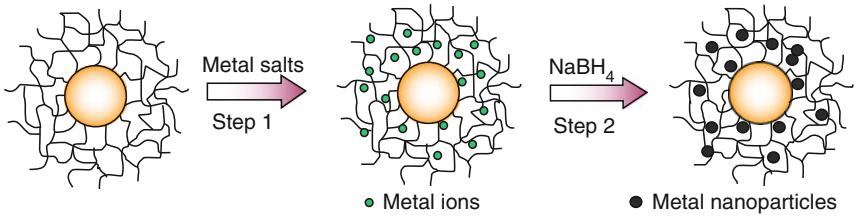

Fig. 3 Formation of metal nanoparticles in the PS–PNIPA core–shell system. The crosslinked PNIPA chains absorb metal ions (*step 1*) which are reduced to produce corresponding metal nanoparticles immobilized in the thermosensitive network (*step 2*)

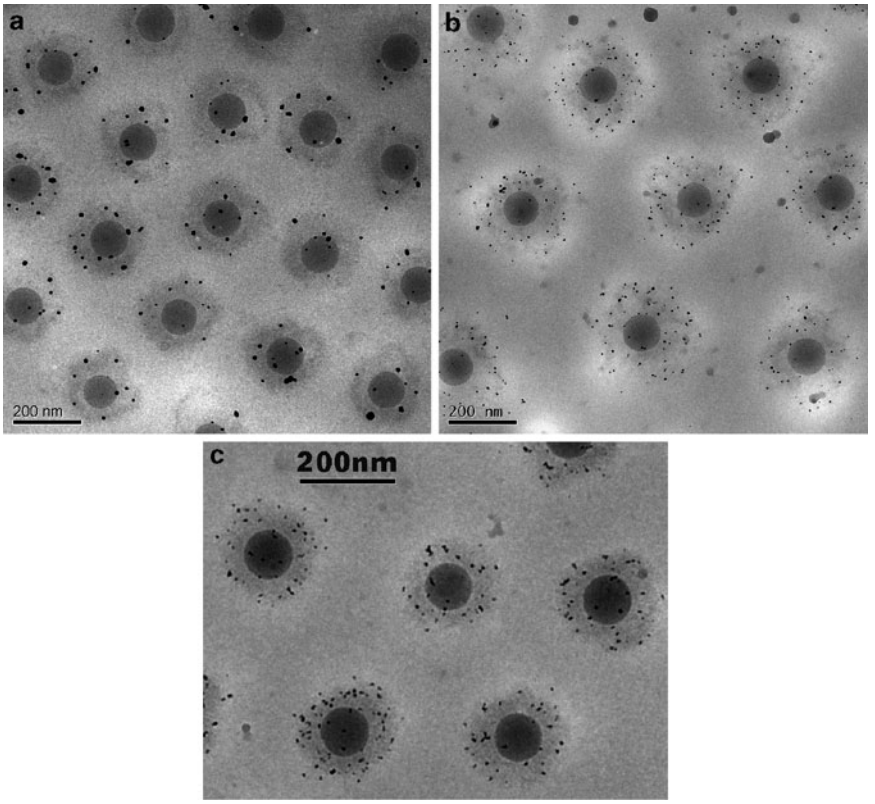

Fig. 4 Cryo-TEM images of negatively charged microgel particles embedded with different metal nanoparticles: (**a**) with Ag ($d = 8.5 \pm 1.5$ nm), (**b**) with Au ($d = 2.0 \pm 0.5$ nm), and (**c**) with Pd ($d = 3.8 \pm 0.6$ nm) nanoparticles. Small black dots are metal nanoparticles. [62]

the metalate ions within the network, most probably caused by a complexation of the metalate ions by the nitrogen atoms of the PNIPA [52, 61]. Both negatively charged and positively charged microgel particles can be used as the template. Their charges are introduced by the anionic initiator ($K_2S_2O_8$) and cationic initiator (V50), respectively, and not by anionic or cationic comonomers. Figures 4 and 5 display the cryo-TEM images of different metal nanoparticles embedded in microgel particles with negative charge and positive charge, respectively. In the cryo-TEM images, the dark spherical area indicates the PS core whereas the light corona around the dark core represents the PNIPA shell of the particles. The metal nanoparticles are seen as small black dots. It is evident that most of the metal nanoparticles are homogeneously immobilized inside the PNIPA networks affixed to the surface of the core particles. The analysis of cryo-TEM images revealed that the size of metal nanoparticles is different. This may be due to the difference of the complexation of the metal ions with the functional groups of the microgels. Furthermore, Figs. 4 and 5 show another important point: all particles are a well-defined distance from their

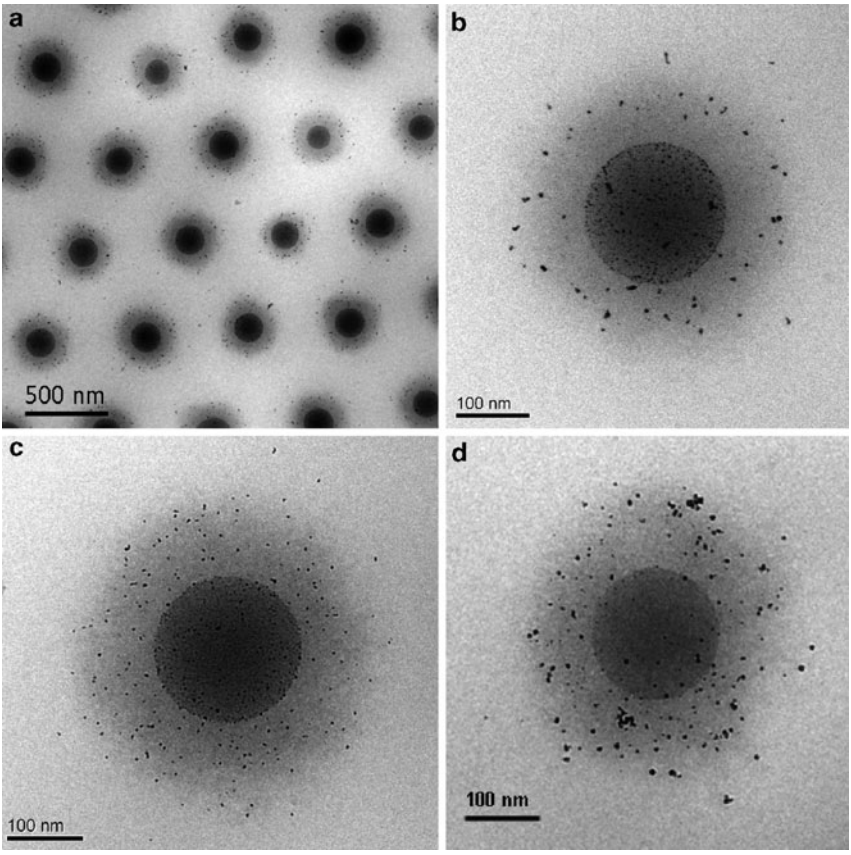

Fig. 5 Cryo-TEM images of Au (**a**, **b**) ($d = 4.8 \pm 1.2$ nm), Pt (**c**) ($d = 2.8 \pm 1.3$ nm), and Rh (**d**) ($d = 4.5 \pm 1.5$ nm) nanocomposite particles embedded in positively charged microgel particles. *Small black dots* are metal nanoparticles. [29]

neighboring particles. This is due to the electrostatic repulsion that originates from the charges affixed to the core particles. These charges keep the entire suspension stable, even above the volume transition where the steric repulsion between the particles breaks down. This point becomes important when considering the catalytic activity of the composite particles above the volume transition [55].

Moreover, AgNPs have been embedded into thermosensitive PNIPA networks with different crosslinking densities [60]. As shown in Fig. 6, the AgNPs are located mostly at the edge of corona instead of near the dark PS core when Ag nanocomposites are prepared by higher crosslinked PS–PNIPA particles. In the case of higher crosslinking densities, smaller Ag particles are generated in the system. This becomes obvious when comparing the size of the particles for the different systems: when 2.5, 5, and 10 mol% BIS are used for crosslinking, the diameters of the AgNP are 8.5 nm ($\pm$1.5 nm), 7.3 nm ($\pm$1.5 nm), and 6.5 nm ($\pm$1.0 nm), respectively.

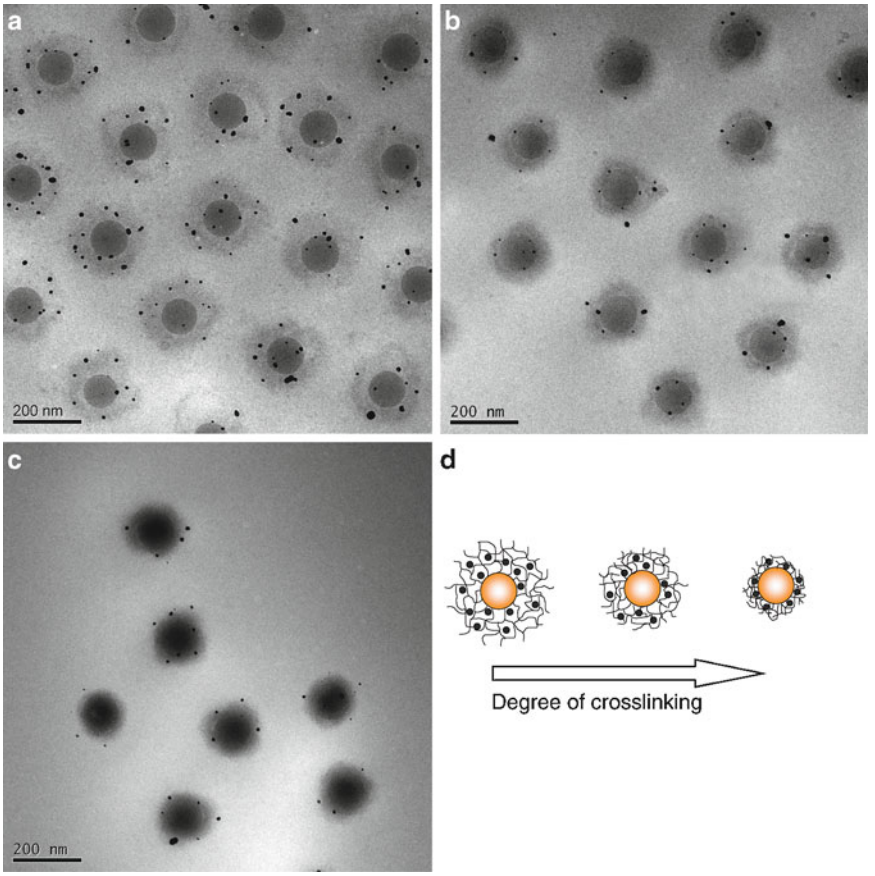

Fig. 6 Cryo-TEM images of the silver nanocomposite particles prepared using PS–PNIPA particles with different crosslinker content: (**a**) KPS1–Ag (2.5 mol% BIS), (**b**) KPS2–Ag (5 mol% BIS), and (**c**) KPS3–Ag (10 mol% BIS). (**d**) Influence of degree of crosslinking on the morphology of silver composite particles [60]

This could be due to the possible limitation of the growth of AgNPs in the densely crosslinked network. Moreover, since the amount of Ag embedded into the network is the same, smaller but more AgNPs are generated with the increase in crosslinking density. This is accord with the results reported recently by Ma et al. [63]. They prepared well-dispersed AgNPs within poly(NIPA-*co*-AAc) microgel particles that were synthesized with different crosslinking densities. The average diameter of the synthesized AgNPs decreases from 18 to 6 nm, when the crosslinking density of the microgel increases from 4.5 to 15 wt%. The interactions between the microgel particles and the incorporated AgNPs were investigated by XPS, which revealed the charge-transfer from the carbonyl groups of the microgel particles to the AgNPs.

Investigations by DLS measurements of composite particles indicated that the original thermosensitive properties of the PNIPA network are not suppressed by the incorporation of metal particles into the network. That is, the shrinking and re-swelling of microgel is not hampered by the incorporation of metal nanoparticles into the network. The metal composite particles show similar volume transition temperature as the carrier particle at 32°C, which is in excellent agreement with previous findings on these systems as shown in Fig. 7 [64, 65]. This indicates

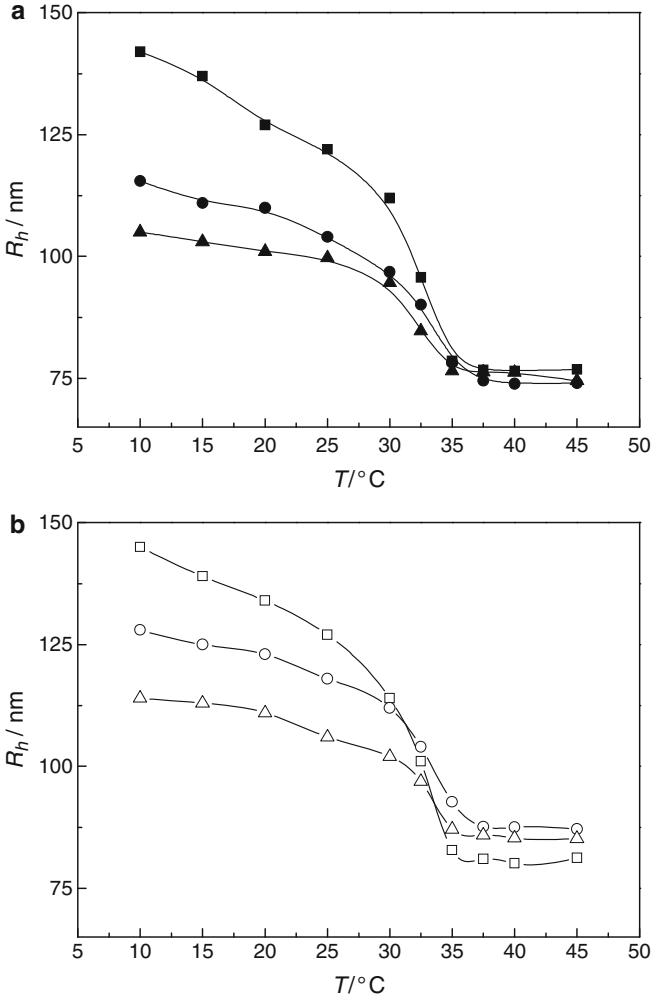

Fig. 7 Hydrodynamic radii versus temperature for (**a**) PS–PNIPA particles: *solid squares* KPS1 (2.5 mol% BIS), *solid circles* KPS2 (5 mol% BIS), and *solid triangles* KPS3 (10 mol% BIS); and (**b**) PS–PNIPA–metal composite particles: *open squares* KPS1–Ag, *open circles* KPS2–Ag, and *open triangles* KPS3–Ag [60]

that metal nanoparticles do not disturb the volume transition within the network. Moreover, with the increase of crosslinker content in the system, the transition temperature of the carrier systems remains constant. However, the degree of shrinking of the network with temperature decreases, as expected for a network with a higher crosslinking density.

2.2 Applications of Microgel–Metal Nanocomposites in Catalysis

Soluble metal nanoparticles in the size range 1–10 nm ("metal nanoclusters") are highly active catalysts. Generally, metal nanoclusters are grown from metal atom precursors in the presence of a stabilizer able to interact with the nanocluster surface, thus preventing agglomeration and controlling its growth to a definite, possibly predetermined size. Often, nanoparticles are stabilized by alkyl chains attached through thiol bonds to the surface of the metal [66]. However, the strong interaction of the thiol group with the surface of the nanoparticles may alter the catalytic properties of the metal profoundly. The same problem can occur when immobilizing the nanoparticles on solid substrates. Moreover, the concept of green chemistry has become a top priority for the catalysis industry, i.e., low temperature, easy removal of the catalyst, and low leaching of heavy metal into the product [67, 68]. This requires a carrier system that should allow separation by, e.g., filtration. The carrier system should have a long-term stability, be easy to handle, and prevent the metallic nanoparticles from coagulating. Moreover, no stabilizing agent should be induced that might alter or block the surface of the nanoparticles. The carrier systems should also be sufficiently stable during recycling of the catalyst.

Recently, microgel-stabilized, size-controlled metal nanoclusters have found promising applications in the field of catalysis. In particular, microgel systems can work as "active carriers" for the metal nanoparticles, which allows us to modulate the catalytic activity of nanoparticles by a thermodynamic transition that takes place within the carrier system [24, 69]. The principle is shown in Fig. 8: Metallic

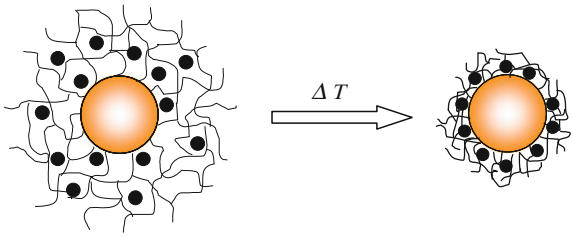

Fig. 8 Composite particles consisting of thermosensitive core–shell particles in which metallic nanoparticles are embedded. *Left*: The composite particles are suspended in water, which swells the thermosensitive network attached to the surface of the core particles. In this state, the reagents can diffuse freely to the nanoparticles, which act as catalysts. *Right*: At higher temperatures ($T > 32°C$) the network shrinks and the catalytic activity of the nanoparticles is strongly diminished

nanoparticles embedded in such a network are fully accessible by the reactants at low temperature. Above the transition, however, the marked shrinking of the network is followed by a concomitant slowing down of the diffusion of the reactants within the network. Thus, the rate of reactions catalyzed by the nanoparticles is slowed down considerably. In this way, the network acts as a "nanoreactor" that can be opened or closed to a certain extent.

2.2.1 Catalytic Activity for Reduction of 4-Nitrophenol

For a model reaction of catalysis of microgel-based metal nanoparticles, we chose the reduction of 4-nitrophenol by an excess of $NaBH_4$, which is one of the most refractory pollutants that can occur in industrial wastewaters [70, 71]. The reduction of 4-nitrophenol to 4-aminophenol is of industrial importance because 4-aminophenol is a commercially important intermediate for the manufacture of analgesic and antipyretic drugs. Moreover, reduction of 4-nitrophenol is a very useful reaction for investigating catalytic activities because it has a strong absorption band at 400 nm at high pH, whereas the resulting 4-aminophenol is transparent in the visible range.

The kinetics of 4-nitrophenol reduction in presence of microgel–metal nanocomposite particles was studied by UV/Vis spectroscopy. Figure 9 shows the UV spectra for the reduction of 4-nitrophenol measured at different times. For a typical measurement, successive decrease of peak intensity at 400 nm with time can be utilized to obtain the rate constant [59, 72, 73]. This peak is attributed due to the presence of 4-nitrophenate ions in the system. The formation of 4-nitrophenate ions

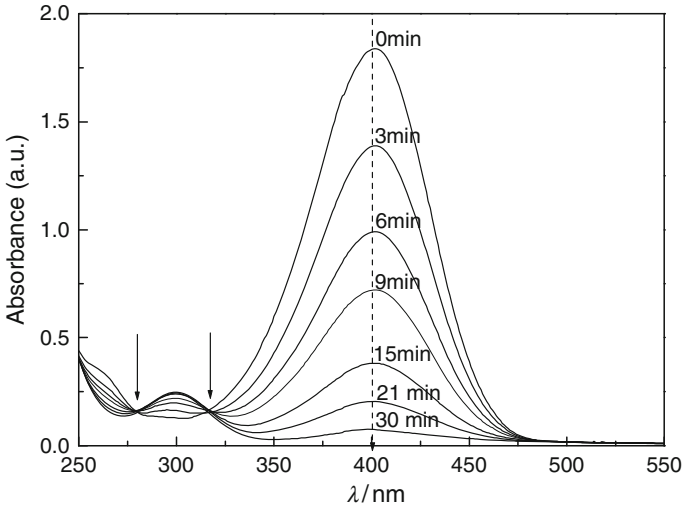

Fig. 9 UV spectra of solutions of 4-nitrophenol measured at different times *t* indicated in the graph [60]

takes place immediately after addition of $NaBH_4$ to the system. After addition of metal nanocomposite particles it was found that the peak height at 400 nm gradually decreases with time. With gradual decrease in peak height at 400 nm a new peak appears at 290 nm. Moreover, two isosbestic points can be observed in the UV spectra, which indicates that in the catalytic reduction reaction the conversion of 4-nitrophenol to 4-aminophenol is in equal molar ratio [70]. The conversion of the process can be directly read off these curves inasmuch as the ratio of the concentration c_t of the 4-nitrophenol at time t to its value c_0 at $t = 0$ is directly given by the ratio of the respective absorbances A/A_0.

We assumed that reduction rates were independent of the concentration of $NaBH_4$ because of its much higher concentration compared to 4-nitrophenol. The apparent rate constant, k_{app}, was found to be proportional to the surface S of the metal nanoparticles present in the system [72]:

$$-\frac{\mathrm{d}c_t}{\mathrm{d}t} = k_{app}c_t = k_1 S c_t, \tag{1}$$

where c_t is the concentration of 4-nitrophenol at time t, and k_1 is the rate constant normalized to S, which is the surface area normalized to the unit volume of the system.

Figure 10 shows the values of the apparent rate constant k_{app} as a function of theoretical specific surface area of metal nanoparticles immobilized in different carrier systems. As shown in Fig. 10, a strictly linear relationship between k_{app} and the surface of the metal nanoparticles can be observed. Figure 10 demonstrates that Pt and Pd nanoparticles exhibit higher catalytic activity than AgNPs. Table 1

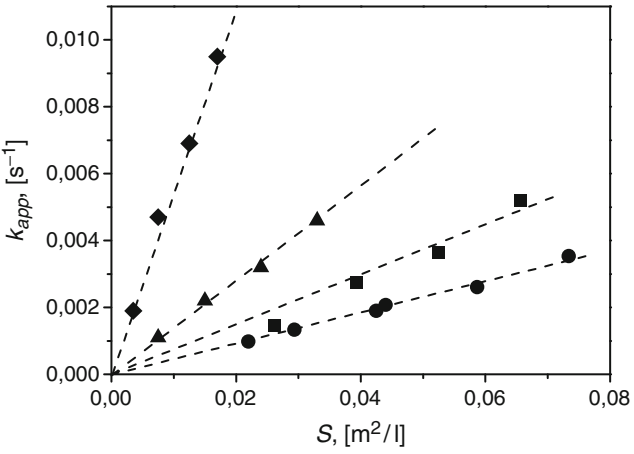

Fig. 10 Rate constant k_{app} as function of the surface area S of metal nanoparticles normalized to the unit volume of the system: *squares* SPB–Ag composite particles, *circles* microgel–Ag composite particles, *triangles* microgel–Pd composite particles, and *diamonds* SPB–Pt composite particles [72]. $T = 20°C$, [4-nitrophenol] $= 0.1\,\mathrm{mmol\,L^{-1}}$, [$NaBH_4$] $= 10\,\mathrm{mmol\,L^{-1}}$ [24]

Table 1 Catalytic activity of metal nanoparticles for the reduction reaction of 4-nitrophenol

Sample	Carrier system	Metal	D^a (nm)	k_1^b ($s^{-1}\,m^{-2}\,L$)
[60]	PS–PNIPA core–shell microgel	Ag	8.5 ± 1.5	5.02×10^{-2}
[24]	PS–PNIPA core–shell microgel	Pd	3.8 ± 0.6	1.01×10^{-1}
[74]	Anionic polyelectrolyte brush (SPB)	Ag	3 ± 1.2	7.81×10^{-2}
[75]	Highly branched polymer brush	Ag	7.5 ± 2	7.27×10^{-2}
[70]	PVA polymer	Ag	~ 25	3.78×10^{-7}
[71]	PVA/PS–PEGMA composite hydrogel	Ag	35 ± 5	7.80×10^{-5}
[71]	PVA hydrogel	Ag	45 ± 5	7.31×10^{-5}
[72]	Cationic polyelectrolyte brush (SPB)	Pt	2.1 ± 0.4	0.55
[24]	Cationic polyelectrolyte brush (SPB)	Pd	2.4 ± 0.5	1.5
[26]	Cationic polyelectrolyte brush (SPB)	Au	1.25 ± 0.25	0.31

[a]*D*iameter of the metal nanoparticles measured from cryo-TEM images
[b]Rate constant normalized to the surface of the particles in the system (1)

summarizes the rate constants of all systems shown in Fig. 10 together with some other reported systems. Rate constants are normalized to the surface area of the nanoparticles per unit volume. First of all, it is interesting to note that both for Ag and Pd composite particles, the catalytic activity of metal nanoparticles immobilized in the polyelectrolyte brush system is higher than that of the microgel system. This can be explained by the diffusion speed of reactant molecules to metal nanoparticles encapsulated in both carrier systems. For the microgel system, the metal nanoparticles are immobilized in the crosslinked PNIPA shell, thus reactant molecules need a longer time to reach the catalytic active center. In the case of polyelectrolyte reactant, molecules can diffuse in latex particles and reach metal nanoparticles more quickly because of its open structure. Secondly, in comparison with other metal composite particles (Au, Pt, Pd) prepared by similar carrier systems, the catalytic activity is Pd > Pt > Au > Ag. This result is also in accord with the results reported by Pal et al. [76] and needs further elucidation.

We now turn to the influences of the temperature on k_{app}. Figure 11 gives a typical curve for the influence of temperature on the rate constant k_{app} of the catalytic reaction, which does not follow a typical Arrhenius-type dependence on temperature. When the reaction temperature is low, the PNIPA network is swollen. In this case, metal nanoparticles that have been embedded in the network can be accessed by the reactants of the catalytic reduction. So, the rate constant k_{app} will exhibit a linear relationship of ln k_{app} with T^{-1}.

However, when the temperature increases further, the PNIPA network shrinks markedly, followed by a concomitant slowing down of the diffusion of reactants within the network. This in turn will lower the rate of reaction catalyzed by the metal nanoparticles. It is obvious that the increase of k_{app} by the raise of temperature is overcompensated by the diffusional barrier. Hence, the reaction rate must reach its minimum at the transition temperature. If the increase of temperature continues, the PNIPA network will not shrink any more and the density within the network stays constant. Now, the strong increase of k_{app} with T will be predominant and the

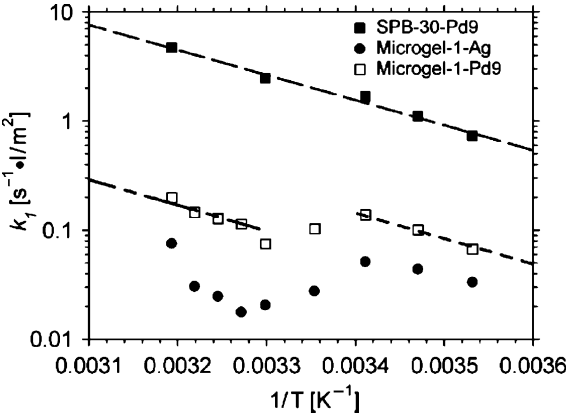

Fig. 11 Dependence of the rate constant k_1 on the temperature T for different systems: Arrhenius plot of k_1 measured in the presence of the composite particles SPB-30-Pd9 (*filled squares*, [Pd composites] $= 0.00063\,\mathrm{g\,L^{-1}}$). In the case of the Microgel-1-Pd9 system (*open squares*, [Pd composites] $= 0.00128\,\mathrm{g\,L^{-1}}$), we obtained an *S*-curve that is similar to that of silver nanoparticles (*filled circles*, data taken from [59], [Ag composites] $= 0.0063\,\mathrm{g\,L^{-1}}$). The concentrations of the reactants were [4-nitrophenol] $= 0.1\,\mathrm{mmol\,L^{-1}}$ and [$NaBH_4$] $= 10\,\mathrm{mmol\,L^{-1}}$ [24]

reaction rate will rise again. This demonstrates that the volume transition within a thermosensitive network can be used as a switch. Fig. 11 shows that the catalytic activity of the metallic nanoparticles can be tuned down by more than one order of magnitude. In the case of a SPB-based metallic system (i.e., the SPB-30-Pd9 system), the rate constant k_{app} is fully described by a conventional Arrhenius expression because SPB particles are not thermosensitive. The *S*-curve seen in the Arrhenius plot in Fig. 11 must hence be due solely to the diffusional barrier for the reactants if the network is shrinking with increasing temperature.

However, as shown in Fig. 12, with the increase of crosslinking density in the microgel carrier system this *S*-curve- type of catalytic activity is less pronounced. This can be explained as follows: The shrinking of the PNIPA network becomes less pronounced (see Fig. 7). For the highly crosslinked system, the influence of the diffusional barrier caused by the shrinking of the network on the rate constant will be not so strong as that for systems with lower crosslinking density. In the limiting case of a high crosslinking density, the shrinking of the network in the shell of the particles will become marginal. In this case, the composite particles will exhibit the conventional Arrhenius behavior of k_{app}.

In the meantime, this phenomenon has also been observed by other groups for thermosensitive polymer-based metal nanoparticles [77, 78]. Pich et al. have used microgel particles based on the copolymer of *N*-vinylcaprolactam (VCL) and acetoacetoxyethyl methacrylate (AAEM) (PVCL/PAAEM) as the carrier system for the deposition of metal nanoparticles. The microgels were first modified with poly(3,4-ethylenedioxythiophene) (PEDOT) nanorods through an in situ oxidative polymerization process. Microgels with PEDOT nanorods in the shell were then used for the

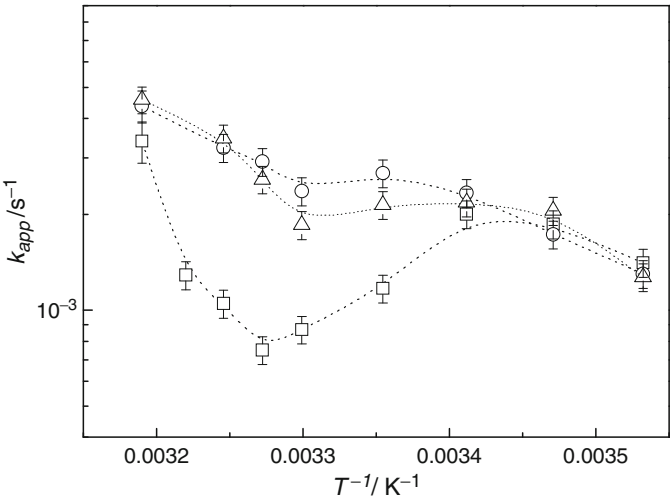

Fig. 12 Arrhenius plot of the reaction rate $k(T)$ measured in the presence of PS–PNIPA–Ag composite particles at different temperatures: *squares* KPS1–Ag (2.5 mol% BIS), *triangles* KPS2–Ag (5 mol% BIS), and *circles* KPS3–Ag (10 mol% BIS). The concentrations of the reactants are: composite particles, $S = 0.042\,m^2\,L^{-1}$; [4-nitrophenol] $= 0.1\,mmol\,L^{-1}$; [$NaBH_4$] $= 10\,mmol\,L^{-1}$. The *broken lines* are guides for the eye [60]

deposition of AuNPs. It has been demonstrated that the obtained hybrid microgels are effective catalysts for 4-nitrophenol reduction. The reaction speed of composite particles can be adjusted by varying the temperature in nonlinear order. Zhao et al. [79] have observed similar behavior for the metal nanoparticles protected by a double stimuli-sensitive diblock copolymer, poly(*N*-isopropylacrylamide)-*block*-poly(4-vinylpyridine) (PNIPAM-*b*-P4VP). They found that the nanocomposites possess pH and thermosensitivity, which can be utilized to modulate the catalytic properties of both bimetallic and monometallic nanocomposites.

2.2.2 Catalytic Activity for Oxidation of Alcohols

The oxidation of alcohols to the corresponding aldehydes or ketones is an important reaction in organic synthesis [80–82]. This catalytic reaction can be carried out at aerobic conditions and the conversions of the reaction can be checked by gas chromatography (GC). It is important to note that water is almost the only solvent currently deemed suitable for the industrial application of this catalytic process, because it avoids the hazards associated with the use of oxidizable organic solvents under oxygen pressure. Recently, Uozumi et al. [83] have reported the aerobic oxidation in water of various alcohols by using amphiphilic PS–PEG (polyethylene glycol) resin-supported Pt nanoparticles as catalyst. Biffs et al. [84] have studied the catalytic activity of microgel-stabilized Au nanoclusters in the aerobic oxidation

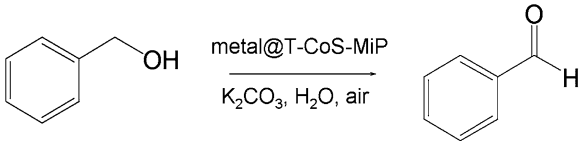

Fig. 13 Test reaction (oxidation of benzyl alcohol to benzaldehyde) used for the analysis of the catalytic activity of microgel–metal nanocomposite particles. All runs were done at room temperature

of benzylic and aliphatic alcohols in water under mild conditions (50–70°C, 1–3 atm O_2). More recently, we have demonstrated that SPB-stabilized Au–Pt nanoalloy particles are excellent catalysts for the oxidation of alcohols to aldehydes or ketones [28].

Metal nanoparticles embedded in thermosensitive core–shell microgel particles can also work efficiently as catalyst for this reaction. Figure 13 shows the oxidation reaction of benzyl alcohol to benzaldehyde in aqueous media by using microgel–metal nanocomposite particles as catalyst. All reactions were carried out at room temperature using aerobic conditions. It is worth noting that the reaction conditions are very mild and no phase transfer catalyst is needed. It has been found that microgel–metal nanocomposites efficiently catalyze the aerobic oxidation of benzyl alcohol at room temperature. No byproducts have been detected by GC after the reaction, and water is the only product formed besides the aldehyde.

The catalytic activity is expressed in turnover frequency, TOF = [amount of oxidation product formed (mmol)/amount of catalyst (mmol)] h^{-1}. The activities of microgel–metal nanocomposite particles have been also compared to the activities seen in other systems containing metal nanoparticles. The results are gathered in Table 2. In our study, we obtained TOF = 159.4 h^{-1} at 25°C and TOF = 2203 h^{-1} at 40°C for the oxidation of benzyl alcohol using microgel–Au nanocomposites as catalyst, which compares favorably to the systems reported in the literature. More recently, we have reported a high catalytic activity and selectivity of AuNPs immobilized in SPBs. Here, a TOF of 2976 h^{-1} for the oxidation of benzyl alcohol under similar conditions was reported [28]. This difference between the two carrier systems is certainly due to the different diffusion rate of the reactant molecules towards metal nanoparticles in both carrier systems. Moreover, it can be seen that Au composite particles show higher catalytic activities compared to Pt or Rh nanocomposites, which agrees well with the results obtained from SPB-stabilized metal nanoparticles.

Furthermore, it is reported that metal catalysts usually require a basic pH for sufficient activity for the aerobic oxidation of alcohols in water [85]. Thus, Biffis found that the productivity of the Au nanoclusters can be enhanced by running the reaction at basic pH (pH 9.9) in their system. However, further enhancement of the pH of the reaction solution was not possible, due to the precipitation of catalyst caused by the increased hydrophobicity of the microgel through deprotonation of the polymer-bound amino groups [84]. In our work, we tried to carry out the catalytic reaction

Table 2 Comparison of the catalytic activity for alcohol oxidation to the corresponding aldehyde in aqueous solution

Ref.	Catalyst	Alcohol	Reaction conditions			TOF (h^{-1})
			T (°C)	P (atm)	Gas	
[80]	Au/TiO_2	Benzyl alcohol	100	2	O_2	213
[82]	Microgel-stabilized Au ($d = 10 \pm 4$ nm)	1-Phenylethanol	100	1	O_2	Extremely low
[84]	Microgel-stabilized Au ($d = 2.5$ nm)	Benzyl alcohol	60	1.5	O_2	960
[85]	Au/PVP	4-Hydroxybenzyl alcohol	23	1	O_2	15
[29]	Au/core–shell microgel	Benzyl alcohol	25	1	Air	159.4
[29]	Pt/core–shell microgel	Benzyl alcohol	25	1	Air	81.4
[29]	Rh/core–shell microgel	Benzyl alcohol	25	1	Air	33.5
[29]	Au/core–shell microgel	Benzyl alcohol	40	1	Air	2203

with a decreased amount of K_2CO_3 in the system. It was found that the catalytic activity and selectivity of AuNPs were not altered when only 1 mmol K_2CO_3 instead of 3 mmol was used.

The influence of temperature on the catalytic activity of microgel-based metal nanocomposite particles has also been studied. It is known that the polarity of the gel changes with the volume phase transition of the microgel from hydrophilic to hydrophobic. As shown in Fig. 14, at low temperatures ($T < 32$°C) the network is swollen in water, and is hydrophilic. Above the volume transition ($T > 32$°C), the network becomes hydrophobic and can thus accumulate hydrophobic reactants. From this point of view, the catalytic activity of microgel–metal composite particles at high temperatures will be affected both by the volume transition of the microgel (as shown in Fig. 8) and by the change of polarity of the microgel (as shown in Fig. 14).

Figure 15 shows the influence of temperature on the catalytic activity in an Arrhenius plot of the TOFs. These data can be compared to data obtained for the reduction of 4-nitrophenol with an excess of $NaBH_4$ in presence of the metal nanocomposite particles. From Fig. 15, a nonlinear relationship between ln (TOF) and T^{-1} can be seen. The TOF increase more than exponentially with increased temperature. Only in the immediate vicinity a significantly smaller TOF is monitored.

In principle, there are two factors that will influence the catalytic activity: First, the collapsed PNIPA layer probably presents a higher steric barrier for benzyl alcohol molecules to diffuse from bulk aqueous dispersion to the surface of AuNPs, causing the reaction to slow down (as shown in Fig. 8). Second, with the increase of temperature, water-soluble hydrophilic PNIPA networks become oil-soluble and hydrophobic, which is favorable for the diffusion of hydrophobic benzyl alcohol onto the AuNP surface (as shown in Fig. 14). Thus, the catalytic activity of Au composite particles should increase with increasing temperature. Figure 15 demonstrates that the second effect prevails over most of the temperature range; the TOF value at 40°C

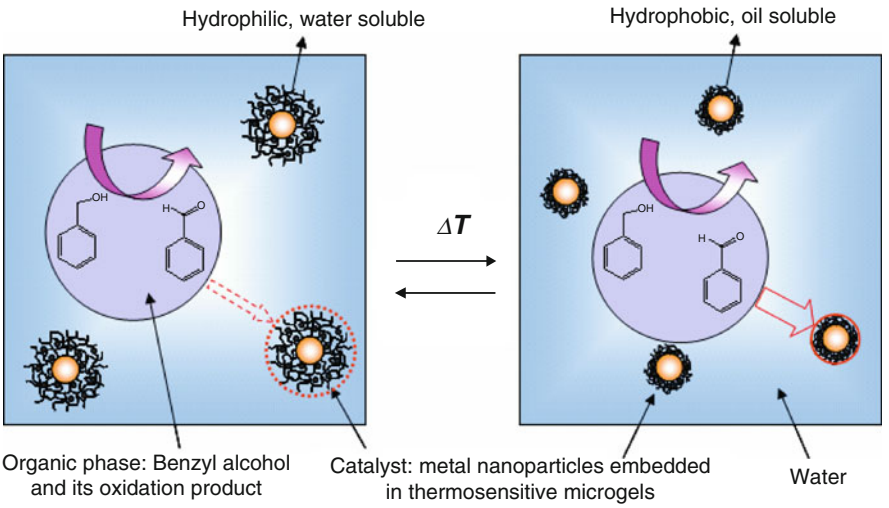

Fig. 14 Catalytic oxidation of benzyl alcohol in the presence of metal nanoparticles immobilized in thermosensitive core–shell microgels at different temperatures. At lower temperatures ($T < 32°C$) the microgel network is hydrophilic and swollen in water, whereas at high temperatures ($T > 32°C$), the network shrinks and becomes hydrophobic. Thus, microgel particles embedding the metal catalyst will move to the oil phase, which will be favorable for the uptake of hydrophobic benzyl alcohol into the metal–microgel composite. Therefore, the catalytic activity of the metal–microgel composites will be affected both by the volume transition and the polarity change of the microgel [29]

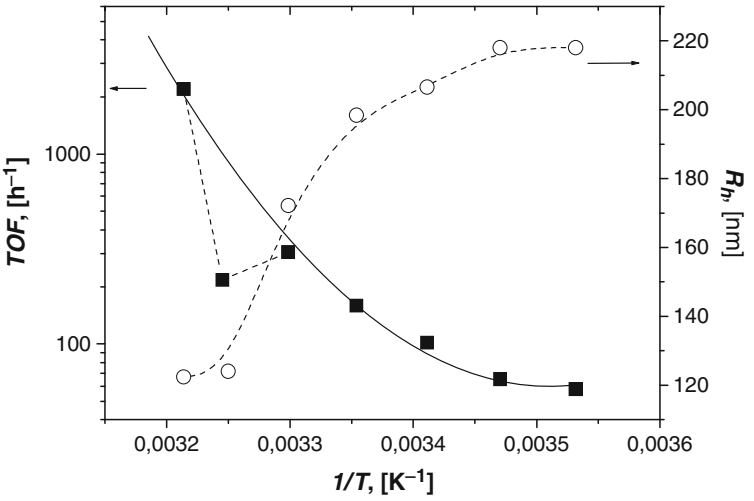

Fig. 15 TOF (*squares*) and hydrodynamic radius (*circles*) versus $1/T$ for the oxidation of benzyl alcohol in the presence of microgel–Au nanocomposite particles (1 atm air, 1 mmol K_2CO_3, [microgel–Au] $= 3.68 \times 10^{-5}$ mol L^{-1}). The *lines* are guides for the eye [29]

is much higher than the value following from conventional Arrhenius kinetics. This is different to the behavior that we found for the reduction reaction of 4-nitrophenol. The results demonstrate that the catalytic activity for the oxidation of benzyl alcohol is in general more sensitive to the change of polarity than the diffusional barrier brought about by the volume transition of the crosslinked PNIPA network. It needs to be pointed out that the selectivity of the reaction is lower when the reaction temperature is higher than 30°C. Under these conditions, benzoic acid has been detected as a byproduct by GC, which is accord with the phenomenon found by Hutchings [80] and Biffis [84].

2.2.3 Catalytic Application for Other Reactions

The Pd-catalyzed Heck [86, 87] and Suzuki [88, 89] reactions (cobalt nanospheres are also able to catalyze these reactions [90]) between aryl halides and alkenes or boronic acids, respectively, are well-established tools for C=C bond formation in organic synthesis [91, 92]. A convenient route for crosscoupling reactions involves reusable Pd nanoparticles that promote these reactions in organic solvents or in water [93, 94]. The handling of the nanoparticles, however, might impose problems during workup unless the particles are immobilized on suitable carriers. Biffis and Sperotto [95] have studied the application of microgel-stabilized metal nanoclusters as catalysts for different reactions and confirmed the enhanced catalytic activity of Pd nanoclusters in Heck reaction of activated aryl bromides, which is attributed to the smaller size of the metal nanoclusters. Moreover, in order to understand the mechanism of these reactions, they have compared the catalytic activity of microgel-stabilized Pd nanoclusters with that of the corresponding microgel–Pd(II) acetate complexes, precursors of the nanoclusters themselves, which were prepared in situ before reaction. They found that with activated or unactivated aryl bromides such as 4-bromoacetophenone or bromobenzene, the Pd nanocluster catalyst affords slightly higher yields than the corresponding Pd(II) precursor. The situation reverses when a deactivated aryl bromide such as 4-bromoanisole is the reagent. In this case, the unreduced Pd precursors are significantly more active than the corresponding nanoclusters. Finally, in the case of an activated chloride as the reagent, only the unreduced Pd precursors bound to microgel show significant activity. This can be explained by the reason that with activated or unactivated aryl bromides, oxidative addition of the aryl halide to the zerovalent metal is fast compared to its formation, and hence the metal nanoclusters appear to be more reactive. In contrast, oxidative addition is slower with deactivated aryl bromides, and in situ reduction probably leads to a higher dispersion of zerovalent Pd species and hence to higher activity. These observations demonstrate that the microgel-stabilized Pd nanoclusters act, in this case, mainly as a reservoir of Pd complexes, which are the true catalytically active species. This is accord with the results by Köhler for the Pd/C catalysts [96].

Li et al. [97] have synthesized Pd nanoparticles in the core of thermosensitive brush-grafted polymeric particles and used them for catalysis of aqueous biphasic hydrogenation of styrene. Thermoresponsive poly[methoxytri(ethylene

glycol) methacrylate] brushes were grown from initiator-functionalized core–shell crosslinked poly(*t*-butyl acrylate) (P*t*BA) particles via surface-initiated atom-transfer radical polymerization (ATRP). The supported Pd nanoparticles efficiently catalyzed hydrogenation of styrene in an aqueous/octane biphasic system. Kinetics studies showed that the catalytic activity of Pd nanoparticles was modulated by the phase transition of the thermosensitive brush layer, resulting in a non-Arrhenius dependence of the apparent initial rate constant, k_{app}, on temperature.

3 Microgels as Carrier Systems for Proteins and Enzymes

Microgel particles can be used not only as nanoreactors for the immobilization of catalytically active metal nanoparticles, but also for enzymes with high catalytic efficiency. In the last decade, immobilization of enzymes on suitable supports has become a central topic and there is a vast literature on this subject. In so far as biocatalysts are concerned, immobilization of enzymes is advantageous for commercial application due to convenience in handling, ease of separation of enzymes from the reaction mixture for reuse, low product cost, and possibly increased thermal and pH stability [98]. Enzymes can be also used as sensors as long as they retain their enzymatic activity [99, 100]. Therefore, an important requirement for protein or enzyme immobilization is that the matrix should provide a biocompatible and inert environment, i.e., it should not interfere with the native structure of the protein and thereby compromise its enzymatic activity. As most enzymes are water-soluble, they are usually immobilized into insoluble matrices. Very often, adsorption on flat surfaces is followed by a considerable flattening and deformation of proteins. Similar findings have been reported for proteins adsorbed onto the surface of colloidal particles. Hence, the surface of solid supports must be modified in a suitable way in order to prevent a direct contact with the immobilized protein [101]. Numerous protein- or enzyme-loaded microgels have been synthesized and investigated. Microgels composed of acrylamide and methylene bisacrylamide [102], dextrans grafted with methacrylates, PEG-methacrylates, and PLGA-PEG-methacrylates have all been synthesized and used to encapsulate proteins [103].

3.1 Control of Protein Adsorption

In general, the adsorption of protein on microgel could be driven by hydrophobic or/and by electrostatic interaction [104, 105]. However, it has been recognized that the adsorption of protein on the charged surface of microgel particles is particularly complicated and in need of further elucidation [106, 107]. Moreover, protein adsorption onto the surface of microgel particles causes the surface to be environed by protein. Therefore, the surface properties may change with an increase in the degree of surface coverage by protein. This gives an opportunity to modulate the final characteristics of the microgel after loading protein. Until now, a lot of research work has

been done to better understand the mechanisms controlling the adsorption process. In particular, both the changes in the microgel's pore size (its "porosity") and changes in its hydrophobicity above the transition temperature should be considered.

Kawaguchi et al. [108] found that the extent of adsorption of protein is decided by the hydrophilicity of the microgel surface. Since changes in temperature change not only the swellability of the microgel but also the hydrophilicity of the surface, the adsorbability of proteins on the PNIPA microgels is temperature-dependent. PNIPA microgels favor the adsorption of protein (human γ-globulin) when the thermosensitive surface of microgel becomes hydrophobic above the LCST. Moreover, proteins once adsorbed on the microgels at a high temperature could be desorbed more or less by lowering the temperature to below LCST.

Grabstain and Bianco-Peled [109] have studied the binding of proteins [bovine serum albumin (BSA), ovalbumin, and lysozyme] to PNIPA microgels to understand the relationship between the binding characteristics and the physical properties of the proteins. The experiments were conducted both below (25°C) and above (37°C) the volume phase transition temperature of the microgels, T_c. All binding isotherms could be well fitted to either the Langmuir adsorption isotherm or a linear adsorption isotherm. It is found that although microgel particles contain a larger amount of protein below T_c, the concentration of the protein within it is higher above T_c. This indicates that there are two coexisting binding routes for protein adsorption: penetration into the polymeric network, and adsorption on the surface of the particle. Further investigations show that although a sorption mechanism was dominant below T_c, surface adsorption was more important above it. Below T_c the binding increases with a decrease in the protein molecular weight. On the other hand, no significant difference in the bound protein amounts was observed above the T_c.

Pichot et al. [110] have investigated the physicochemical parameters ruling the immobilization of oligonucleotides (ODNs) onto aminated PNIPA microgel particles (either covalent or by physical adsorption). They showed that the adsorption of ODNs onto positively charged particles was mainly governed by electrostatic interactions. At low pH, when the microgel was positively charged by protonation of the amine groups, adsorption was maximum, and the ODN adsorbed amount decreased with increasing pH. Adsorption was also reduced by increasing the ionic strength of the buffer. The covalent immobilization took place in a basic pH (> 9) to avoid physical adsorption and to allow the best reactivity possible of the particle-borne amino groups. Ionic strength had a great effect on the amount of probe immobilized onto the PNIPA particles. Li et al. [111] investigated whether DNA–microgel conjugates were compatible with the enzymatic reactions that are commonly used for manipulations of DNA in the design of DNA-based bioassays or biosensors. They demonstrated that DNA ODNs can be covalently coupled to microgels and that DNA molecules on microgels can still be manipulated by DNA-processing enzymes such as T4 DNA ligase and phi29 DNA polymerase.

Huo et al. [112] studied the binding of protein to a charged microgel and the influence of protein on the physical appearance and structural peculiarities of the microgel. For this purpose, pH- and temperature-sensitive poly(*N*-isopropylacrylamide-*co*-acrylic acid) [P(NIPA-*co*-AAc)] microgels with various

contents of acrylic acid (AAc) and crosslinker were synthesized. The microgels exhibited affinity of binding BSA with increase of AAc contents. The temperature and the pH in suspension dominated the binding amounts of BSA due to three competing interactions, i.e., hydrophobic, electrostatic and hydrogen bonding. The maximum adsorption was observed at around pH 4.0, whereas both low pH and basic conditions induced the rather low adsorption. In addition, AFM images showed that the microgel particles underwent bridging aggregation by loading BSA. The resultant BSA–microgel particles became more hydrophobic after loading BSA. Importantly, the adsorption of BSA onto P(NIPA-*co*-AAc) microgel was found to alter the swelling/deswelling behavior of the resultant microgel suspensions. With an increase in BSA concentration, the volume phase transition temperature of BSA–microgel particles shifted to a lower temperature.

Gold nanoparticles are excellent candidates for bioconjugation. They are biocompatible and can readily bind to a range of biomolecules such as amino acids [113], proteins, enzymes [114], and DNA [115] and they expose large surface areas for immobilization of biomolecules. Tong et al. [116] have tried to immobilize AuNPs into microgel particles with PNIPA core and polyethyleneimine (PEI) shell via complexation between AuNPs and the amine groups on the surface of the microgel particles. It was found that the AuNPs bound to microgel particles can act as excellent supports for the immobilization of the enzymes horseradish peroxidase (HRP) and urease. The enzymes conjugated on the nano Au/microgel particles show enhanced biocatalytic activity, especially at lower enzyme concentrations. This could be due to the fact that nano Au/microgel particles can accumulate both substrates and enzymes on their surface and thus increase the local concentration of enzyme and substrate. In addition, the HRP on microgel particles also exhibits higher storage stability.

PEG is well known to provide resistance to protein adsorption [117, 118]. Thus, Gan and Lyon [119] tried to incorporate PEG chains into the thermoresponsive PNIPA microgels to minimize nonspecific interactions of the particles with biological environments. A reduced adsorption of BSA on the particle surface was observed as a result of incorporation of PEG chains into the particles, especially when the PEG chains were located in the shell of the particles. This effect is most pronounced when the PNIPA is phase-separated above the LCST, which indicates that the PEG side-chains may stretch outward from the particle surface as the particles collapse at temperatures above the transition temperature. Similar effects are also observed for particles where the PEG chains are localized in the particle core, which is then surrounded by a PNIPA shell. These results suggest that the PEG grafts can penetrate the PNIPA shell when it is in its phase-separated state.

The use of microgels as biodetecting microlenses is a new and interesting concept. Thus, Nayak and Lyon [120] synthesized complex core–shell microgel nanoparticles that bind to a protein through both native protein–ligand interactions as well as through steric sieving. The core is predominantly composed of PNIPA with AAc as a minor component (10 mol%). The acid groups are used for attaching biotin to the nanoparticles by carbodiimide coupling. These biotinylated hydrogel core nanoparticles are coated with a shell that contains the cleavable crosslinker

N,N'-(1,2-dihydroxyethylene) bisacrylamide (DHEA). At the initial crosslink density, the pore size of the shell is too small to allow avidin molecules to pass through to the core where they bind biotin. Upon chemical cleavage of the crosslinks, the pore size increases enough to allow avidin to pass through and bind biotin. Such nanoparticles could find applications in protein separation processes in which the shell essentially behaves as a molecular-weight-cutoff membrane to eliminate the binding of macromolecules and assemblies that are larger than the protein of interest. Furthermore, hydrogel microlenses can be prepared via Columbic assembly of these biotinylated P(NIPA-*co*-AAc) microgel particles onto a silane-modified glass substrate [121]. Arrays containing biotinylated P(NIPA-*co*-AAc) microgels have been used to detect multivalent binding of both avidin and polyclonal anti-biotin. Protein binding can be determined by monitoring the optical properties of the microlenses using a brightfield optical microscopy technique. The microlens method is shown to be very specific for the target protein, with no detectable interference from nonspecific protein binding.

The most common method for engineering acid sensitivity in microgels is through the incorporation of cationic groups, which become protonated at acidic pH and cause hydrogel swelling. However, for protein delivery, it would be preferable to develop acid-sensitive hydrogels that were neutral, thus avoiding the potential toxicity of polycations and the complications of electrostatic interaction with proteins. Fréchet et al. [122] synthesized a new acetal crosslinker with *p*-methoxy substituent, which can be used to prepare acid-sensitive, acetal-crosslinked, protein-loaded hydrogels and microgels. At acidic pHs, the pore size of the acetal-crosslinked hydrogels increases due to the hydrolysis of the acetal, and entrapped protein diffuse out, whereas at neutral pH the crosslinker remains largely intact, and the release of entrapped protein is significantly slower.

More recently, we have demonstrated that thermosensitive core–shell PS–PNIPA microgels can serve as superior carriers for the adsorption of β-D-glucosidase. The adsorption capacity of the microgel particles was determined by investigating the efficiency of immobilization at different enzyme concentrations at 4°C (Fig. 16). Hence, β-D-glucosidase is adsorbed onto this microgel below the LCST. At the chosen conditions, up to 620 mg β-D-glucosidase per gram microgel could be adsorbed. This indicates that strong interactions between both species exist, even in the swollen state of PNIPA. The adsorption behavior of β-D-glucosidase can be described by a Langmuir-type model:

$$\frac{\tau_{\mathrm{ads}}}{\tau_{\mathrm{ads,M}}} = \frac{Kc_{\mathrm{sol}}}{1 + Kc_{\mathrm{sol}}}, \tag{2}$$

where $\tau_{\mathrm{ads}}/\tau_{\mathrm{ads,M}}$ denotes the fraction of adsorption sites occupied as the function of the enzyme concentrations in solution c_{sol} and $\tau_{\mathrm{ads,M}}$ is the maximum binding capacity. K was determined to be $0.08 \pm 0.03\,\mathrm{mL\,mg^{-1}}$ and $\tau_{\mathrm{ads,M}}$ $1400 \pm 300\,\mathrm{mg\,g^{-1}}$ microgel by fitting the experimental data using (2), as shown in Fig. 16. This high capacity demonstrates that enzyme molecules penetrate deeply into the network. Furthermore, it could be confirmed that, at given adsorption conditions, no

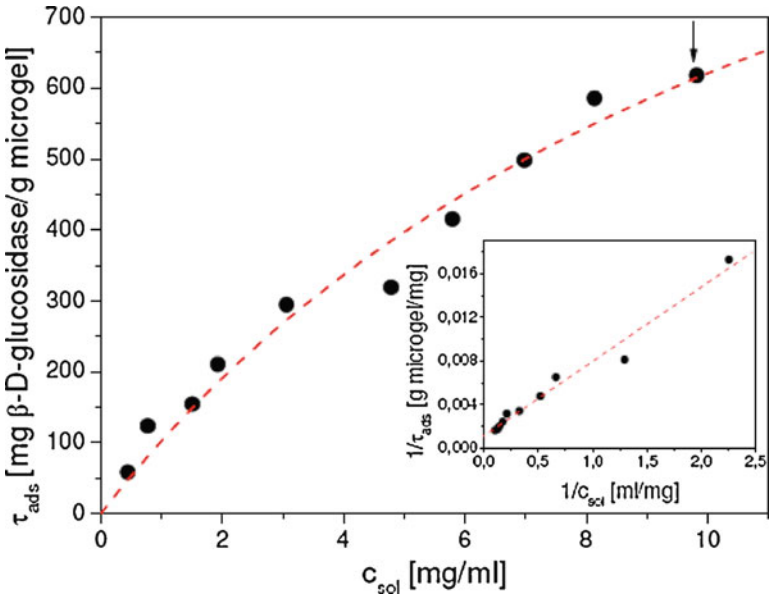

Fig. 16 The adsorbed amount of β-d-glucosidase per gram microgel τ_{ads} is plotted versus the concentration of free enzyme c_{sol} in solution. The *dashed line* represents the fit of the experimental data by (2). The *arrow* marks the amount of entrapped enzyme used for kinetic investigation (620 mg β-D-glucosidase per gram microgel). The inset displays the data as a linear Langmuir plot. The adsorption was conducted at 4°C in 10 mM MOPS buffer solution (pH 7.2) and with a microgel concentration of 1 wt%. The immobilized enzymes do not prevent the microgel from shrinking at temperatures above the LCST [23]

leakage of β-D-glucosidase occurs. Since the isoelectric point of the isozyme of β-D-glucosidase from almonds is 4.4, the enzyme is negatively charged at the chosen adsorption conditions. PS–PNIPA microgel is also weakly negatively charged due to the sulfate groups that were introduced into the polymer by the initiator $K_2S_2O_8$. This results in an overall repulsion between particles and enzyme. Thus, the main driving forces for immobilization are the formation of hydrogen bonds between the backbone of the enzyme and the amide side chains of the microgel, as well as hydrophobic bonding [123].

3.2 Modulation of Enzyme Activity with Temperature

Microgel particles have been demonstrated to be good substrates for the immobilization of enzymes, which retain their catalytic efficiency [124]. However, the design of a carrier system in which the catalytic efficiency can be regulated by some extrinsic stimulation such as temperature, pH, ion intensity, or magnetism remains a challenge. Very recently, Liu et al. [125] have reported the introduction of glutathione

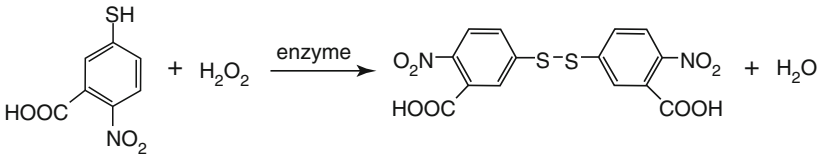

Fig. 17 Determination of glutathione peroxidase activity using TNB and H_2O_2 as substrates [125]

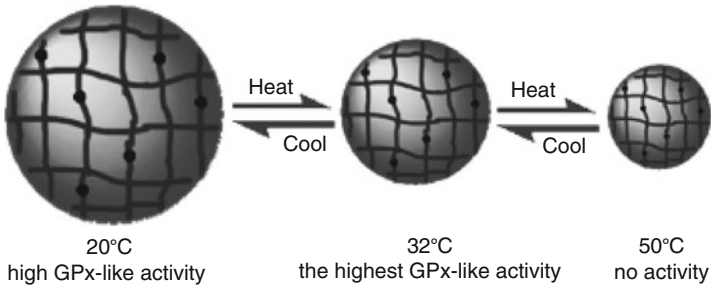

Fig. 18 Change in the activity and size of the microgel catalyst with temperature [125]

peroxidase (GPx) active sites into the temperature-responsive PNIPA scaffolds. A tellurium-containing compound, bis(3-acryloyloxypropyl)-telluride, was copolymerized with PNIPA and functionalized as a GPx-like catalytic center. The reduction of cumene hydroperoxide (CUOOH) by 3-carboxyl-4-nitrobenzenethiol (TNB) was used to evaluate the GPx-like activity of the microgel catalyst (as shown in Fig. 17). By combining the binding ability endowed from micropores of functional microgels and the catalytic moiety tellurium, this new microgel catalyst exhibits high GPx-like catalytic activity with the typical saturation kinetics behavior of a real catalyst. More importantly, the catalytic efficiency of this microgel enzyme model displays obvious temperature-responsive characteristics, as shown in Fig. 18. The catalytic activity of the microgel can be turned on and off reversibly by changing the temperature. Below 32°C the catalytic activity increases slowly with increasing temperature and reaches the highest catalytic activity at 32°C. When the temperature goes up further the catalytic activity goes down sharply and is almost lost above 50°C. This phenomenon might be caused by the change in the pore size of the microgel networks, together with the change in the hydrophobicity of the core by altering the temperature. The smaller pore size means that it is more difficult for substrates to enter the core to approach the catalytic site, thus resulting in the dramatic decrease in catalytic efficiency. This demonstrates that the changes in pore size and hydrophobicity of the microgel, which are induced by the change in temperature, play key roles in regulating the enzyme activity.

Our group has demonstrated that the catalytic properties of immobilized enzymes can be manipulated by the temperature-dependent swelling behavior of the microgel. The hydrolytic activity of adsorbed and native β-D-glucosidase was determined as a function of temperature. Desorption of immobilized enzyme upon

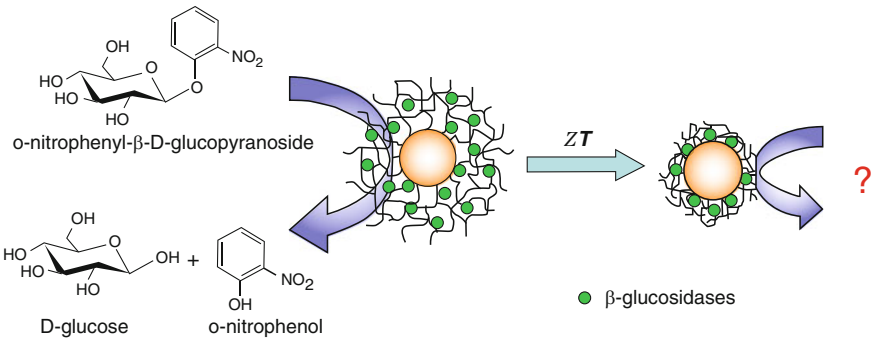

Fig. 19 Reactions used for testing the activity of enzymes (β-D-glucosidase) immobilized in the thermosensitive core–shell microgel template at different temperatures. Enzymatic hydrolysis of the substrate oNPG produces d-glucose and *o*-nitrophenol. The concentration of the resulting *o*-nitrophenol can be monitored photometrically

temperature increase can be excluded because higher adsorption capacities above the LCST are observed in general [126]. As depicted in Fig. 19, *o*-nitrophenyl-β-D-glucopyranoside (oNPG) was chosen as substrate. The enzymatic activity was evaluated in terms of Michaelis–Menten kinetics [127]:

$$v = \frac{v_{\max}[\mathrm{S}]}{K_\mathrm{m} + [\mathrm{S}]} = \frac{k_\mathrm{cat}[\mathrm{E}]_\mathrm{tot}[\mathrm{S}]}{K_\mathrm{m} + [\mathrm{S}]}, \tag{3}$$

where [S] is the substrate concentration, $v_{\max}$ is the maximum rate attained at infinite concentration of substrate, K_m is the Michaelis–Menten constant, $[\mathrm{E}]_\mathrm{tot}$ is the total enzyme concentration and k_cat is the turnover number.

Figure 20a displays the resulting rates v and k_cat for the native and adsorbed β-D-glucosidase at 20°C and 40°C. Table 3 summarizes the respective kinetic parameters. The values for the free enzyme at 20°C are comparable to data obtained in preceding studies [128], whereas the immobilization of β-D-glucosidase onto PS–PNIPA microgels results in a remarkable enhancement of the hydrolytic activity by a factor of 3.2–3.5. In order to elucidate this effect further, we investigated the catalytic rate for native and adsorbed β-D-glucosidase between 12°C and 60°C. The values of k_cat that were evaluated from Michaelis–Menten kinetics were plotted according to the Arrhenius equation. Figure 20b displays the Arrhenius plots for native and entrapped β-D-glucosidase. These experiments unambiguously show that for the whole temperature range, k_cat of the adsorbed β-D-glucosidase exceeds that of the native enzyme. Moreover, as is obvious from Fig. 20b, adsorption of the enzyme leads to a slowing down of the catalytic rate at temperatures where the volume transition of PNIPA occurs. Moreover, above the LCST, a smaller activation energy for the catalyzed reaction is observed compared to that for the free enzyme. Both phenomena can be attributed to the volume phase transition of the PS–PNIPA polymer at 32°C, where the hydrodynamic radius of the carrier shrinks by about 40 nm. Therefore,the reduction of the pore sizes of the PNIPA network must lead

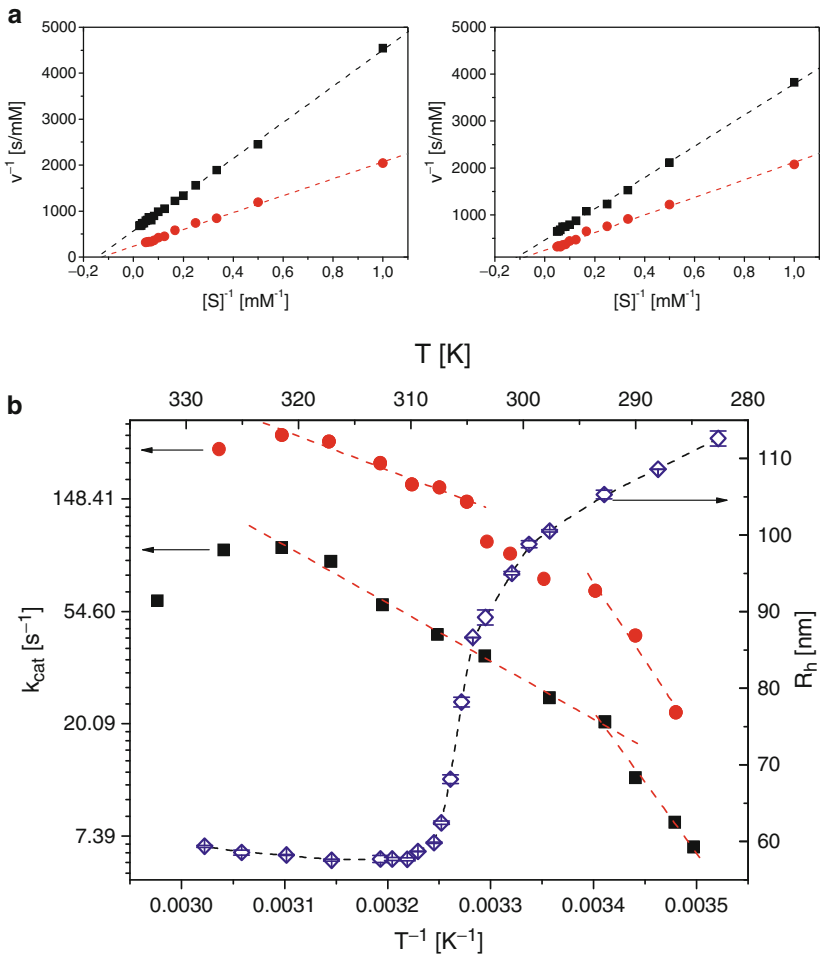

Fig. 20 (**a**) Lineweaver–Burk plots for the hydrolysis of oNPG catalyzed by immobilized (*circles*, 620 mg enzyme per gram microgel) and native β-D-glucosidase (*squares*) at 20°C (*left*) and 40°C (*right*) in MOPS buffer (pH 7.2). (**b**) Arrhenius plots of native (*squares*) and immobilized (*circles*) β-D-glucosidase (620 mg enzyme per gram microgel) in MOPS buffer solution (pH 7.2). The turnover number k_{cat} for each temperature was determined by performing a whole Michaelis–Menten curve according to Fig. 20a. The enzyme concentration was between 0.005 and 0.01 g L^{-1} (native enzyme) and 0.0035–0.01 g L^{-1} (immobilized enzyme), respectively, and the substrate concentration varied between 1.0 and 20.0 mM. The *dashed lines* are linear fits of the experimental data according to the Arrhenius equation to determine the activation energies of the rate-limiting steps of the reaction. In addition, the swelling curve (*diamonds*) of the carrier particles is plotted [23]

to a slowing of the diffusion of oNPG. This increase of the diffusional barrier is followed by a slight decrease of k_{cat}. When the temperature decreases further, the density within the network is constant and the linear relationship between ln k_{cat} and T^{-1} is recovered again. The lower activation energy (E_a) above the LCST indicates

Table 3 Kinetic parameters of native and immobilized β-D-glucosidase at 20°C and 40°C [23]

Enzyme	Temperature (°C)	K_m (mM)	k_{cat}[a] (s^{-1})
Free	20	6.8 ± 1	20.4
Free	40	6.8 ± 1	57.8
Immobilized	20	9.4 ± 1	65.5
Immobilized	40	11.3 ± 1	204.2

[a]Related to β-D-glucosidase in its dimeric form with a molecular weight of 135 kD

that diffusional limitations affect the catalytic rate in the shrunken state of the microgel. Analogous catalytic results were obtained when metal nanoparticles were embedded within microgel particles [59].

Thus, the results shown here demonstrate that thermosensitive microgel particles can serve as superior carriers for the adsorption of enzymes in which the activity of adsorbed enzymes are preserved. The catalytic activity of adsorbed β-D-glucosidase from almonds is increased by a factor of more than three. Moreover, the catalytic properties of immobilized enzymes can be manipulated by the volume transition of the microgel. Hence, such microgels present a novel class of "active" nanoreactors for biocatalysis.

4 Conclusion

All results reviewed herein demonstrate that the microgel particles may serve as "nanoreactors" for the immobilization of catalytically active nanostructures, namely for metal nanoparticles and enzymes. In both cases, the resulting composites particles are stable against coagulation and can be easily handled. Moreover, the catalytic activity of metal nanoparticles can be modulated through the volume transition that takes place within the thermosensitive microgel carrier system. Similar behavior has been also observed for the temperature dependence of enzymatic activity. Thus, the microgel particles present an "active" carrier system for applications in catalysis.

Acknowledgments Financial support by the Deutsche Forschungsgemeinschaft, Schwerpunkt "Hydrogele" and by the Sonderforschungsbereich 481, Bayreuth, is gratefully acknowledged.

References

1. Burda C, Chen X, Narayanan R, El-Sayed MA (2005) Chemistry and properties of nanocrystals of different shapes. Chem Rev 105:1025–1102
2. Ferrando R, Jellinek J, Johnston RL (2008) Nanoalloys: from theory to applications of alloy clusters and nanoparticles. Chem Rev 108:845–910
3. Campbell CT, Parker SC, Starr DE (2002) The effect of size-dependent nanoparticle energetics on catalyst sintering. Science 298:811–814

4. Ge J, Huynh T, Hu Y, Yin Y (2008) Hierarchical magnetite/silica nanoassemblies as magnetically recoverable catalyst support. Nano Lett 8:931–934
5. Chauhan BPS, Rathore JS, Chauhan M, Krawicz A (2003) Synthesis of polysiloxane stabilized palladium colloids and evidence of their participation in silaesterification reactions. J Am Chem Soc 125:2876–2877
6. Frederix F, Friedt J, Choi K, Laureyn W, Campitelli A, Mondelaers D, Maes G, Borghs G (2003) Biosensing based on light absorption of nanoscaled gold and silver particles. Anal Chem 75:6894–6900
7. Tokareva I, Minko S, Fendler JH, Hutter E (2004) Nanosensors based on responsive polymer brushes and gold nanoparticle enhanced transmission surface plasmon resonance spectroscopy. J Am Chem Soc 126:15950–15951
8. Biffis A, Orlandi N, Corain B (2003) Microgel-stabilised metal nanoclusters: size control by microgel nanomorphology. Adv Mater 15:1551–1555
9. Zhang J, Xu S, Kumacheva E (2005) Photogeneration of fluorescent silver nanoclusters in polymer microgels. Adv Mater 17:2336–2340
10. Wong JE, Gaharwar AK, Müller-Schulte D, Bahadur D, Richtering W (2008) Dual-stimuli responsive PNIPAM microgel achieved via layer-by-layer assembly: magnetic and thermoresponsive. J Colloid Interface Sci 324:47–54
11. Kuang M, Wang D, Bao HB, Gao MY, Möhwald H, Jiang M (2002) Fabrication of multicolor-encoded microspheres by tagging semiconductor nanocrystals to hydrogel spheres. Adv Mater 17:267–270
12. Scott RWJ, Wilson OM, Crooks RM (2005) Synthesis, characterization, and applications of dendrimer-encapsulated nanoparticles. J Phys Chem B 109:692–704
13. Esumi K, Isono R, Yoshimura T (2004) Preparation of PAMAM- and PPI-metal (silver, platinum, and palladium) nanocomposites and their catalytic activities for reduction of 4-nitrophenol. Langmuir 20:237–243
14. Xu H, Xu J, Zhu Y, Liu H, Liu S (2006) In situ formation of silver nanoparticles with tunable spatial distribution at the poly(*N*-isopropylacrylamide) corona of unimolecular micelles. Macromolecules 39:8451–8455
15. Sun Q, Deng Y (2005) Encapsulation of polystyrene latex with temperature-responsive poly(*N*-isopropylacrylamide) via a self-assembling approach and the adsorption behaviors therein. Langmuir 21:5812–5816
16. 6 Cen L, Neoh KG, Kang ET (2005) Gold nanocrystal formation on viologen-functionalized polymeric nanospheres. Adv Mater 17:1656–1661
17. Nayak S, Lyon LA (2005) Soft nanotechnology with soft nanoparticles. Angew Chem Int Ed Engl 44:7686–7708
18. Antonietti M, Ozin GA (2004) Promises and problems of mesoscale materials chemistry or why meso? Chem Eur J 10:29–41
19. Kawaguchi H (2000) Functional polymer microspheres. Prog Polym Sci 25:1171–1210
20. Czeslik C (2004) Factors ruling protein adsorption. Z Phys Chem 218:771–801
21. Wittemann A, Haupt B, Ballauff M (2003) Adsorption of proteins on spherical polyelectrolyte brushes in aqueous solution. Phys Chem Chem Phys 5:1671–1677
22. Wittemann A, Ballauff M (2006) Interaction of proteins with linear polyelectrolytes and spherical polyelectrolyte brushes in aqueous solution. Phys Chem Chem Phys 8:5269–5275
23. Welsch N, Wittemann A, Ballauff M (2009) J Phys Chem B 113:16039–16045
24. Mei Y, Lu Y, Polzer F, Ballauff M, Drechsler M (2007) Catalytic activity of palladium nanoparticles encapsulated in spherical polyelectrolyte brushes and core–shell microgels. Chem Mater 19:1062–1069
25. Sharma G, Mei Y, Lu Y, Ballauff M, Irrgang T, Proch S, Kempe R (2007) Spherical polyelectrolyte brushes as carriers for platinum nanoparticles in heterogeneous hydrogenation reactions. J Catal 246:10–14
26. Schrinner M, Polzer F, Mei Y, Lu Y, Haupt B, Ballauff M, Göldel A, Drechsler M, Preussner J, Glatzel U (2007) Mechanism of the formation of amorphous gold nanoparticles within spherical polyelectrolyte brushes. Macromol Chem Phys 208:1542–1547

27. Malysheva YB, Gushchin AV, Mei Y, Lu Y, Ballauff M, Proch S, Kempe R (2008) C–C coupling reaction of triphenylbismuth(V) derivatives and olefins in the presence of palladium nanoparticles immobilized in spherical polyelectrolyte brushes. Eur J Inorg Chem 3:379–383
28. Schrinner M, Proch S, Mei Y, Kempe R, Miyajima N, Ballauff M (2008) Spherical polyelectrolyte brushes: synthesis, characterization and application for the oxidation of alcohols. Adv Mater 20:1928–1933
29. Lu Y, Proch S, Schrinner M, Drechsler M, Kempe R, Ballauff M (2009) Thermosensitive core–shell microgel as a "nanoreactor" for catalytic active metal nanoparticles. J Mater Chem 19:3955–3961
30. Park TG, Hoffman AS (1994) Estimation of temperature-dependent pore size in poly(*N*-isopropylacrylamide) hydrogel beads. Biotechnol Prog 10:82–86
31. Pelton R (2000) Temperature-sensitive aqueous microgels. Adv Colloid Interface Sci 85:1–33
32. Peng SF, Wu C (2000) Poly(*N*-vinylcaprolactam) microgels and its related composites. Macromol Symp 159:179–186
33. Boyko V, Pich A, Lu Y, Richter S, Arndt KF, Adler HJ (2003) Thermo-sensitive poly(*N*-vinylcaprolactam-*co*-acetoacetoxyethyl methacrylate) microgels: I. synthesis and characterization. Polymer 44:7821–7827
34. Bromberg L, Temchenko M, Hatton TA (2002) Dually responsive microgels from polyether-modified poly(acrylic acid): swelling and drug loading. Langmuir 18:4944–4952
35. Eichenbaum GM, Kisetr PF, Shah D, Meuer WP, Needham D, Simon SA (2000) Alkali earth metal binding properties of ionic microgels. Macromolecules 33:4087–4093
36. Amalvy JI, Wanless EJ, Li Y, Michailidou V, Armes SP, Duccini Y (2004) Synthesis and characterization of novel pH-responsive microgels based on tertiary amine methacrylates. Langmuir 20:8992–8999
37. Schild HG (1992) Poly(*N*-isopropylacrylamide): experiment, theory and application. Prog Polym Sci 17:163–249
38. Wu C, Wang X (1998) Globule-to-coil transition of a single homopolymer chain in solution. Phys Rev Lett 80:4092–4094
39. Hellweg T, Dewhurst CD, Eimer W, Kratz K (2004) PNIPAM-*co*-polystyrene core–shell microgels: structure, swelling behaviour and crystallisation. Langmuir 20:4330–4335
40. Antonietti M, Groehn F, Hartmann J, Bronstein L (1997) Nonclassical shapes of noble-metal colloids by synthesis in microgel nanoreactors. Angew Chem Int Ed Engl 36:2080–2083
41. Whilton NT, Berton B, Bronstein L, Henze H, Antonietti M (1999) Organized functionalization of mesoporous silica supports using prefabricated metal-polymer modules. Adv Mater 11:1014–1018
42. Biffis A (2001) Functionalised microgels: novel stabilisers for catalytically active metal colloids. J Mol Catal A Chem 165:303–307
43. Zhang J, Xu S, Kumacheva E (2004) Polymer microgels: reactors for semiconductor, metal, and magnetic nanoparticles. J Am Chem Soc 126:7908–7914
44. Mulvaney P (1996) Surface plasmon spectroscopy of nanosized metal particles. Langmuir 12:788–800
45. Suzuki D, Kawaguchi H (2005) Gold nanoparticle localization at the core surface by using thermosensitive core-shell particles as a template. Langmuir 21:12016–12024
46. Suzuki D, Kawaguchi H (2006) Hybrid microgels with reversibly changeable multiple brilliant color. Langmuir 22:3818–3822
47. Pich A, Karak A, Lu Y, Ghosh A, Adler HJP (2006) Preparation of hybrid microgels functionalized by silver nanoparticles. Macromol Rapid Commun 27:344–350
48. Pich A, Karak A, Lu Y, Ghosh AK, Adler HJP (2006) Tuneable catalytic properties of hybrid microgels containing gold nanoparticles. J Nanosci Nanotechnol 6:3763–3769
49. Palioura D, Armes SP, Anastasiadis SH, Vamvakaki M (2007) Metal nanocrystals incorporated within pH-responsive microgel particles. Langmuir 23:5761–5768
50. Gorelikov I, Field LM, Kumacheva E (2004) Hybrid microgels photoresponsive in the near-IR spectral range. J Am Chem Soc 126:15938–15939
51. Karg M, Pastoriza-Santos I, Pérez-Juste J, Hellweg T, Liz-Marzán LM (2007) Small 7:1222–1229

52. Das M, Mordoukhovski L, Kumacheva E (2008) Sequestering gold nanorods by polymer microgels. Adv Mater 20:2371–2375
53. Pelton RH (1988) Polystyrene and polystyrene-butadiene latexes stabilized by poly(*N*-isopropylacrylamide). J Polym Sci 26:9–18
54. Dingenouts N, Norhausen Ch, Ballauff M (1998) Observation of the volume transition in thermosensitive core–shell latex particles by small-angle X-ray scattering. Macromolecules 31:8912–8917
55. Crassous J, Drechsler Y, Talmon Y, Ballauff M (2006) Langmuir 22:2403–2406
56. Lu Y, Wittemann A, Drechsler M, Ballauff M (2006) Preparation of poly(styrene)-poly(*N*-isopropylacrylamide) (PS–PNIPA) core–shell particles by photoemulsion polymerization. Macromol Rapid Commun 27:1137–1141
57. Ballauff M (2003) Nanoscopic polymer particles with a well-defined surface: synthesis, characterization, and properties. Macromol Chem Phys 204:220–234
58. Hellweg T, Dewhurst CD, Bruckner E, Kratz K, Eimer W (2000) Colloidal crystals made of poly(*N*-isopropylacrylamide) microgel particles. Colloid Polym Sci 278:972–978
59. Lu Y, Mei Y, Drechsler M, Ballauff M (2006) Thermosensitive core–shell particles as carriers for Ag nanoparticles: modulating the catalytic activity by a phase transition in networks. Angew Chem Int Ed Engl 45:813–816
60. Lu Y, Mei Y, Drechsler M, Ballauff M (2006) Thermosensitive colloid particles as carrier systems for metallic nanoparticles. J Phys Chem B 110:3930–3937
61. Frattini A, Pellegri N, Nicastro D, de Sanctis O (2005) Effect of amine groups in the synthesis of Ag nanoparticles using aminosilanes. Mater Chem Phys 94:148–152
62. Ballaff M, Lu Y (2007) "Smart" nanoparticles: preparation, characterization and applications. Polymer 48:1815–1823
63. Dong Y, Ma Y, Zhai T, Shen F, Zeng Y, Fu H, Yao J (2007) Silver nanoparticles stabilised by thermoresponsive microgel particles: synthesis and evidence of an electron donor–acceptor effect. Macromol Rapid Commun 28:2339–2345
64. Dingenouts N, Ballauff M (1998) Structural investigation of latexes by small-angle X-ray scattering in slit-collimation. Measurements and evaluation of data. Acta Polym 49:178–183
65. Seelenmeyer S, Deike I, Dingenouts N, Rosenfeldt S, Norhausen Ch, Ballauff M, Narayanan T (2000) Analysis of the volume transition in thermosensitive core–shell particles by synchrotron small-angle X-ray scattering. J Appl Crystallogr 33:574–576
66. Astruc D, Lu F, Aranzaes R (2005) Metallodendritic catalysis: major concepts and recent progress. Angew Chem Int Ed Engl 44:7852–7872
67. Anastas PT, Kirchhoff MM (2002) Origins, current status, and future challenges of green chemistry. Acc Chem Res 35:686–694
68. Hashmi ASK, Hutchings GJ (2006) Gold catalysis. Angew Chem Int Ed Engl 4:7896–7936
69. Lu Y, Yu M, Drechsler M, Ballauff M (2007) Ag nanocomposite particles: preparation, characerization and application. Macromol Symp 254:94–102
70. Pradhan N, Pal A, Pal T (2002) Silver nanoparticle catalyzed reduction of aromatic nitro compounds. Colloids Surf A Physicochem Eng Asp 196:247–257
71. Lu Y, Spyra P, Mei Y, Ballauff M, Pich A (2007) Composite hydrogels: robust carriers for catalytic nanoparticles. Macromol Chem Phys 208:254–261
72. Mei Y, Sharma G, Lu Y, Drechsler M, Ballauff M, Irrgang T, Kempe R (2005) High catalytic activity of platinum nanoparticles immobilized on spherical polyelectrolyte brushes. Langmuir 21:12229–12234
73. Antipov AA, Sukhorukov GB, Fedutik YA, Hartmann J, Giersig M, Moehwald H (2002) Fabrication of a novel type of metallized colloids and hollow capsules. Langmuir 18: 6687–6693
74. Lu Y, Mei Y, Schrinner M, Ballauff M, Mölle MW, Breu J (2007) In-situ formation of Ag nanoparticles in spherical polyacrylic acid brushes by UV irradiation. J Phys Chem C 111:7676–7681
75. Lu Y, Mei Y, Walker R, Ballauff M, Drechsler M (2006) 'Nano-tree'-type spherical polymer brush particles as templates for metallic nanoparticles. Polymer 47:4985–4995

76. Pradhan N, Pal A, Pal T (2001) Catalytic reduction of aromatic nitro compounds by coinage metal nanoparticles. Langmuir 17:1800–1802
77. Hain J, Schrinner M, Lu Y, Pich A (2008) Design of multicomponent microgels by selective deposition of nanomaterials. Small 4:2016–2024
78. Wang Y, Wei G, Wen F, Zhang X, Zhang W, Shi L (2008) Synthesis of gold nanoparticles stabilized with poly(*N*-isopropylacrylamide)-*co*-poly(4-vinyl pyridine) colloid and their application in responsive catalysis. J Mol Catal A Chem 280:1–6
79. Zhao D, Chen X, Liu Y, Wu C, Ma R, An Y, Shi L (2009) Thermosensitive and pH-sensitive Au–Pd bimetallic nanocomposites. J Colloid Interface Sci 331:104–112
80. Enache DI, Edwards JK, Landon P, Solsona-Espriu B, Carley AF, Herzing AA, Watanabe M, Kiely CJ, Knight DW, Hutchings GJ (2006) Solvent-free oxidation of primary alcohols to aldehydes using Au-Pd/TiO2 catalysts. Science 311:362–365
81. Uozumi Y, Nakao R (2003) Catalytic oxidation of alcohols in water under atmospheric oxygen by use of an amphiphilic resin-dispersion of a nanopalladium catalyst. Angew Chem Int Ed Engl 42:204–207
82. Biffis A, Minati L (2005) Efficient aerobic oxidation of alcohols in water catalysed by microgel-stabilised metal nanoclusters. J Catal 236:405–409
83. Yamada YMA, Arakawa T, Hocke H, Uozumi Y (2007) Catalyst for aerobic oxidation of alcohols in water. Angew Chem Int Ed Engl 46:704–706
84. Biffis A, Cunial S, Spontoni P, Prati L (2007) Microgel-stabilized gold nanoclusters: powerful "quasi-homogeneous" catalysts for the aerobic oxidation of alcohols in water. J Catal 251:1–6
85. Tsunoyama H, Sakurai H, Negishi Y, Tsukuda T (2005) Size-specific catalytic activity of polymer-stabilized gold nanoclusters in aerobic alcohol oxidation in water. J Am Chem Soc 127:9374–9375
86. Heck RF, Nolley JP (1972) Palladium-catalyzed vinylic hydrogen substitution reactions with aryl, benzyl, and styryl halides. J Org Chem 37:2320–2322
87. Heck RF (1979) Palladium-catalyzed reactions of organic halides with olefins. Acc Chem Res 12:146–151
88. Miyaura N, Suzuki A (1995) Palladium-catalyzed cross-coupling reactions of organoboron compounds. Chem Rev 95:2457–2483
89. Beletskaya IP, Cheprakov AV (2000) Heck reaction as a sharpening stone of palladium catalysis. Chem Rev 100:3009–3366
90. Zhou P, Li Y, Sun P, Zhou J, Bao J (2007) A novel Heck reaction catalyzed by Co hollow nanospheres in ligand-free condition. Chem Commun 1418–1420
91. Phan NTS, Van Der Sluys M, Jones CW (2006) On the nature of the active species in palladium catalyzed Mizoroki-Heck and Suzuki-Miyaura couplings – homogeneous or heterogeneous catalysis, a critical review. Adv Synth Catal 348:609–679
92. Astruc D (2007) Palladium nanoparticles as efficient green homogeneous and heterogeneous carbon-carbon coupling pre-catalysts: a unifying view. Inorg Chem 46:1884–1894
93. Reetz MT, Breinbauer R, Wanninger K (1996) Suzuki and Heck reactions catalyzed by preformed palladium clusters and palladium/nickel bimetallic clusters. Tetrahedron Lett 37:4499–4502
94. Klingelhofer S, Heitz W, Greiner A, Oestreich S, Fçrster S, Antonietti M (1997) Preparation of palladium colloids in block copolymer micelles and their use for the catalysis of the Heck reaction. J Am Chem Soc 119:10116–10120
95. Biffis A, Sperotto E (2003) Microgel-stabilized metal nanoclusters: improved solid-state stability and catalytic activity in Suzuki couplings. Langmuir 19:9548–9550
96. Köhler K, Heidenreich RG, Krauter JGE, Pietsch J (2002) Highly active palladium/activated carbon catalysts for Heck reactions: correlation of activity, catalyst properties, and Pd leaching. Chem Eur J 8:622–631
97. Li D, Dunlap JR, Zhao B (2008) Thermosensitive water-dispersible hairy particle-supported Pd nanoparticles for catalysis of hydrogenation in an aqueous/organic biphasic system. Langmuir 24:5911–5918
98. Tischer W, Wedekind F (1999) Immobilized enzymes: methods and applications. Top Curr Chem 95–126

99. Su S, Ali MM, Filipe CDM, Li Y, Pelton R (2008) Microgel-based inks for paper-supported biosensing applications. Biomacromolecules 9:935–941
100. Pelton RH, Chibante P (1986) Preparation of aqueous latices with *N*-isopropylacrylamide. Colloids Surf 20:247–256
101. Lu Y, Wittemann A, Ballauff M (2009) Supramolecular structures generated by spherical polyelectrolyte brushes and their application in catalysis. Macromol Rapid Commun 30: 806–815
102. Retama JR, Lopez-Ruiz B, Lopez-Cabarcos E (2003) Microstructural modifications induced by the entrapped glucose oxidase in cross-linked polyacrylamide microgels used as glucose sensors. Biomaterials 24:2965–2973
103. Lu S, Anseth KS (2000) Release behavior of high molecular weight solutes from poly(ethylene glycol)-based degradable networks. Macromolecules 33:2509–2515
104. Hu T, Gao J, Auweter H, Iden R, Lueddecke E, Wu C (2002) Adsorption of gelatins on surfactant-free PS nanoparticles. Polymer 43:5545–5550
105. Alvarez C, Bertorello H, Strumla M (1996) Polymer 37:3715–3719
106. Taniguchi T, Duracher D, Delair T, Elaissari A, Pichot C (2003) Adsorption/desorption behavior and covalent grafting of an antibody onto cationic amino-functionalized poly(styrene-*N*-isopropylacrylamide) core–shell latex particles. Colloids Surf B Biointerfaces 29:53–65
107. Chacon D, Hsieh YL, Kurth MJ, Krochta JM (2000) Swelling and protein absorption/desorption of thermo-sensitive lactitol-based polyether polyol (LPEP) hydrogels. Polymer 41:8257–8262
108. Kawaguchi H, Fujimoto K, Mizuhara Y (1992) Hydrogel microspheres III Temperature-dependent adsorption of proteins on poly-*N*-isopropylacryamide hydrogel microspheres. Colloid Polym Sci 270:53–57
109. Grabstain V, Bianco-Peled H (2003) Mechanisms controlling the temperature-dependent binding of proteins to poly(*N*-isopropylacrylamide) microgels. Biotechnol Prog 19: 1728–1733
110. Delair T, Meunier F, Elaissari A, Charles MH, Pichot C (1999) Amino-containing cationic latex-oligodeoxyribonucleotide conjugates: application to diagnostic test sensitivity enhancement. Colloids Surf A Physicochem Eng Asp 153:341–353
111. Ali MM, Su S, Filipe CDM, Pelton R, Li Y (2007) Enzymatic manipulations of DNA oligonucleotides on microgel: towards development of DNA–microgel bioassays. Chem Commun 4459–4461
112. Huo D, Li Y, Qian Q, Kobayashi T (2006) Temperature-pH sensitivity of bovine serum albumin protein-microgels based on cross-linked poly(*N*-isopropylacrylamide-*co*-acrylic acid). Colloids Surf B Biointerfaces 50:36–42
113. Huang YF, Lin YW, Chang HT (2006) Growth of various Au–Ag nanocomposites from gold seeds in amino acid solutions. Nanotechnology 17:4885–4894
114. Abdelhady HG, Allen S, Ebbens SJ, Madden C, Patel N, Roberts CJ, Zhang JX (2005) Towards nanoscale metrology for biomolecular imaging by atomic force microscopy. Nanotechnology 16:966–973
115. Alivisatos AP, Peng X, Wilson TE, Loweth CL, Bruchez MPJ, Schultz PG (1996) Organization of 'nanocrystal molecules' using DNA. Nature 382:609–611
116. Xu J, Zeng F, Wu S, Liu X, Hou C, Tong Z (2007) Gold nanoparticles bound on microgel particles and their application as an enzyme support. Nanotechnology 18:265704–265712
117. Graham NB, Zulfiqar M, Nwachuku NE, Rashid A (1989) Interaction of poly(ethylene oxide) with solvents: 2. Water-poly(ethylene glycol). Polymer 30:528–533
118. Graham NB, Zulfiqar M, Nwachuku NE, Rashid A (1990) Interaction of poly(ethylene oxide) with solvents: 4. Interaction of water with poly(ethylene oxide) crosslinked hydrogels. Polymer 31:909–916
119. Gan D, Lyon LA (2002) Synthesis and protein adsorption resistance of PEG-modified poly(*N*-isopropylacrylamide) core/shell microgels. Macromolecules 35:9634–9639
120. Nayak S, Lyon LA (2004) Ligand-functionalized core/shell microgels with permselective shells. Angew Chem Int Ed Engl 43:6706–6709

121. Kim J, Nayak S, Lyon LA (2005) Bioresponsive hydrogel microlenses. J Am Chem Soc 127:9588–9592
122. Murthy N, Thng YX, Schuck S, Xu MC, Fréchet JMJ (2002) A novel strategy for encapsulation and release of proteins: hydrogels and microgels with acid-labile acetal cross-linkers. J Am Chem Soc 124:12398–12399
123. Lindman S (2007) Systematic investigation of the adsorption of HSA to *N*-isopropylacrylamide/*N-tert*-butylacrylamide copolymer nanoparticles. Effects of particle size and hydrophobicity. Nano Lett 7:914–920
124. Wang QG, Yang ZM, Wang L, Ma ML, Xu B (2007) D-glucosamine-based supramolecular hydrogels to improve wound healing. Chem Commun 1032–1034
125. Huang X, Yin Y, Tang Y, Bai X, Zhang Z, Xu J, Liu J, Shen J (2009) Smart microgel catalyst with modulatory glutathione peroxidase activity. Soft Matter 5:1905–1911
126. Shamim N, Liang H, Hidajat K, Uddin MS (2008) Adsorption, desorption, and conformational changes of lysozyme from thermosensitive nanomagneetic particles. J Colloid Interface Sci 320:15–21
127. Copeland RA (2000) Enzymes – a practical introduction to structure, mechanism, and data analysis, 2nd edn. Wiley-VCH, New York
128. Henzler K, Haupt B, Ballauff M (2008) Enzymatic activity of immobilized enzyme determined by isothermal titration calorimetry. Anal Biochem 378:184–189

Index